Particulate organic carbon dynamics along the land–ocean aquatic continuum

Submitted by Jo Snöälv to the University of Exeter
as a thesis for the degree of
Doctor of Philosophy in Physical Geography
In June 2019

I certify that all material in this thesis which is not my own work has been identified and that no material has previously been submitted and approved for the award of a degree by this or any other University.

Signature: …………………………………………………………..

Abstract

The anthropogenic and natural input and transport of particulate organic carbon (POC) into and along stream systems from land to ocean is not yet well described (Regnier et al, 2013). Accelerated soil erosion due to changes in land use (e.g. expansion and intensification of agriculture) contribute to POC transport from land to ocean, while artificial damming of river systems, such as hydropower, trap the suspended particulate fractions and contribute to limnic storage in reservoirs. These perturbations on the landscape impact the volumes, transport and fate of suspended organic material. While mainly geomorphic processes control erosion and deposition of inorganic sediments, the mobility and transformation of POC is further subject to within-catchment stabilisation processes, sequestration by burial into sediments, and microbial fermentation which contribute to the vertical emission of potent greenhouse gases like CO_2 and CH_4. These sources, sinks and transformations of POC along the land-ocean aquatic continuum (LOAC) are dynamic and depend on input, transport, and deposition of suspended organic materials. Particulate organic carbon dynamics has been studied broadly in the past, both in freshwater systems, estuaries and oceans. However, its role in the global carbon cycle has been highlighted especially in recent years due to the lack of quantifiable pathways of POC sequestration, transport and mineralisation in freshwater systems. This project studied POC in two contexts: 1) POC transport and fate in a tropical reservoir was modelled and measured, and 2) the effects of flocculation on riverine DOM was measured by experiments.

In the first study, erosion rates were calculated from fallout radionuclides (FRN) in a highly perturbed and largely deforested tropical catchment in Brazil. The results from these field observations were used to quantify soil erosion and sedimentation in the catchment. The results also validated modelled output with Revised Universal Soil Loss Equation (RUSLE) which was used to model soil erosion for the whole catchment. The contribution of allochthonous organic carbon from catchment soils into the reservoir was then quantified.

The second study utilized the same field site, and addressed the relative inputs of allochthonous and autochthonous POC into the reservoir. Physical and chemical protection of organo-mineral aggregates and flocs determine the fate of catchment-derived POC. This second part of the study investigated whether

allochthonous POC derived from terrestrial soils was more important than autochthonous POC (e.g. from macrophytes, biofilms and algae) for limnic storage in post-flooding sediments of a tropical reservoir. POC was calculated from C inventories of reservoir sediment cores collected along the delta–reservoir gradient and linked to organic matter content by loss on ignition (LOI). POC sources were determined by analysis of carbon-nitrogen ratio (C/N). Finally a POC budget was calculated for the post-flooding reservoir sediments.

The third part of this project investigated flocculation dynamics of riverine organic matter in the LOAC. Flocculation experiments were undertaken to determine the effects of three treatments with coagulants on water DOM quality from eight streams draining a rural landscape with headwaters in Exmoor, UK. Through flocculation experiments stream samples were reacted with added clay and salt standards which simulated three flocculation boundaries along the LOAC. The three treatments were T1: increased input of minerogenic coagulants, such as clay, by soil erosion into streams, T2: saline mixing at the estuarine boundary, and T3: a mixture of salt and clay representing soil erosion at the estuarine boundary. Residual DOM quality by each treatment was analysed by mass spectrometry, UV-Vis absorbance and synchronous fluorescence. The results showed preferential removal of humic-like components in residual DOM and the efficiency of the chosen coagulant standards, which demonstrated the dynamics of chemical change in riverine organic matter along the LOAC.

Acknowledgements

List of contents

List of figures

List of software

Software mainly used to interpret results were RStudio 1.1.453, Inkscape 0.92.3, MS Excel 2016, MS Paint, QGIS 2.18.1, Krita 3.2.1, Matlab R2018a, Gimp 2.10.4, IBM SPSS Statistics 25.

List of abbreviations

POC	particulate organic carbon
DOC	dissolved organic carbon
DIC	dissolved inorganic carbon
PIC	particulate inorganic carbon
SOM	soil organic matter
LOAC	land-ocean aquatic continuum
POM	particulate organic matter
DOM	dissolved organic matter

Chapter 1. Introduction

The biogeochemical cycle of carbon composes multiple fluxes of carbon species between C pools of the biosphere, geosphere, pedosphere, hydrosphere and atmosphere. These natural exchanges of organic and inorganic carbon species have been perturbed by human impact, by for instance the release of fossil fuels into the atmosphere (IPCC, 2013). While carbon is stored in its inorganic and organic forms in terrestrial soils, bedrock, vegetation and the ocean, potent greenhouse gases such as carbon dioxide (CO_2), methane (CH_4) and nitrous oxide (N_2O) have increased rapidly in the atmosphere since the industrial revolution to levels unprecedented in the last 800 000 years (IPCC, 2013). These greenhouse gases absorb and radiate energy and contribute to global warming and climate change. Examples of natural emissions of greenhouse gases occur due to mineralisation and fermentation of decaying organic matter by microbes, CO_2 evasion from supersaturated waters, and fires. Anthropogenic sources contribute with emissions from for instance burning of fossil fuels, cement production, deforestation and land use change (Le Quéré et al, 2013). Part of this land use change perturbs the lateral transport of C from land to ocean. This is represented in Figure 1, as erosion from soils to rivers, or the freshwater transport of total dissolved and particulate suspended matter (sediment, organic matter and total dissolved solids, among other aquatic species) containing C. This project aims to investigate the nature of particulate organic carbon (POC) and its sources, transformation processes, and sinks along the land–ocean aquatic continuum (LOAC). A brief introduction to the various pathways and turnover of this carbon pool are presented in this section.
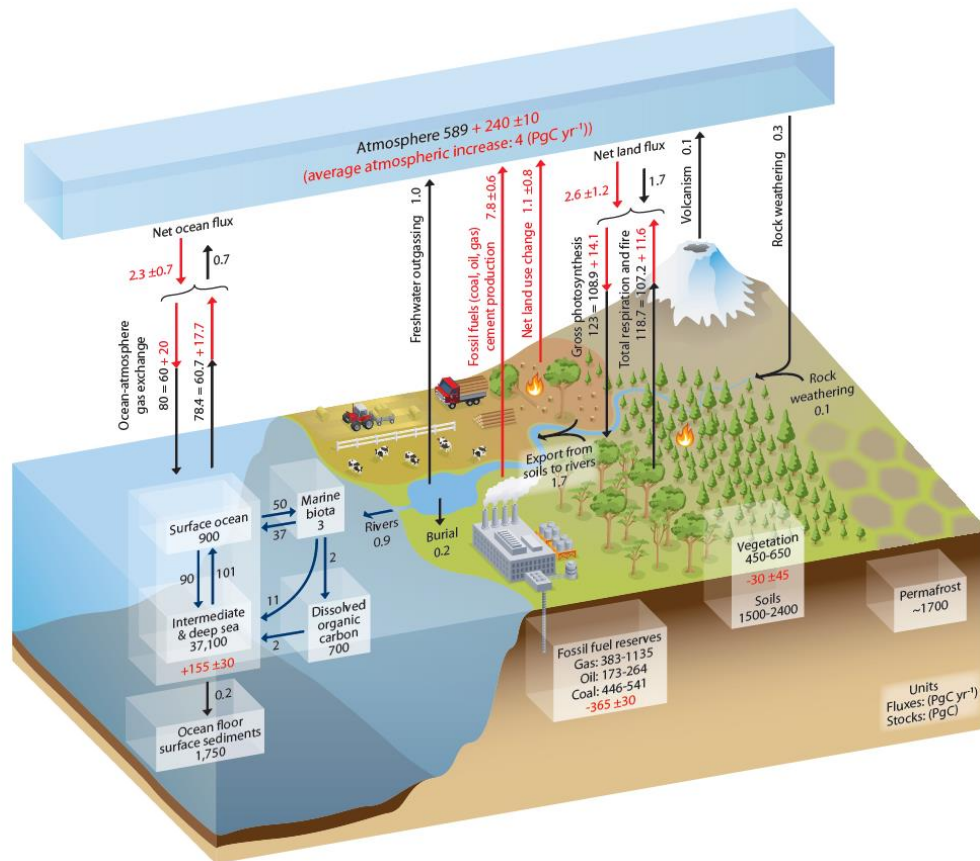
Figure 1 Schematic model showing the pathways of carbon on Earth's surface. From IPCC report, 2013.

1.1 POC dynamics along the LOAC

The land–ocean aquatic continuum (LOAC) is the drainage network of watercourses with the ability to transport chemical species, including various forms of carbon (e.g. DOC, DIC, POC), from sources on land to the estuaries and oceans (Regnier, 2013). This freshwater transport of carbon composes one of the important pathways in the carbon cycle (Hope et al, 1994). Freshwater ecosystems therefore are concluded to serve as dynamic conduits of carbon transport and transformation, rather than acting as neutral pipelines of lateral carbon transport from land to ocean (Cole et al., 2007; Tranvik et al, 2009; Aufdenkempe et al, 2011). Only a few years ago the riverine pipeline transport model in global carbon budgets neglected in-stream sources, sinks and transformation processes of carbon species (ICPP, 2007) such as net primary production (NPP), heterotrophic microbial mineralisation, photolytic oxidation,

organic carbon burial, etc., but recently several studies have contributed to a more dynamic picture of the lateral carbon transport in freshwater drainage systems (e.g. Cole et al, 2007; Battin et al, 2009; Raymond et al, 2012; Regnier et al, 2013; Kirschbaum et al, 2019).

POC consists of a dynamic organic carbon pool of varying mineralisability, which is provided into the aquatic environment from several sources of organic matter (Porcal et al, 2009; Petrone et al, 2011). The nature of the POC determines its reactivity in the water column, which partly controls its pool size and turnover in the LOAC together with other parameters, e.g. hydrology, geology of the drained landscape, geochemistry, vegetation and litterfall, solar irradiation (further discussed in 2.5). The natural processes which conserve and transform organic matter are important for the final carbon load that reach the oceans (Trumbore et al, 1992; Raymond et al, 2004). While vertical C fluxes readily exchange greenhouse gases (GHG) across the terrestrial–atmospheric boundary, lateral C fluxes are influenced by geomorphic boundaries of catchment characteristics on all scales in the landscape. The lateral transport of carbon follows the downstream direction through the water film of the LOAC (Regnier et al, 2013). This implicates that carbon ages and transforms throughout the downstream gradient, and that vertical sources of C become increasingly complicated while mixing of organic matter occurs beyond headwaters. In the humid tropics, Mayorga et al (2005) reported that while riverine bulk organic matter could be up to thousands of years old, the main contributor to CO_2 outgassing composed organic matter contemporary in age, reducing the main source of outgassing to a small reactive part of total organic matter transported in watercourses. While outgassing from the Amazon basin has been attributed to 470 Tg C year^{-1} (Richey et al, 2002), it has been estimated that c. 32.7×10^{12} g C year^{-1} (DOC: 2.7 x 10^{13} g year^{-1}; POC: 0.5 x 10^{13} g year^{-1}) is released into the costal sea of the Atlantic Ocean from the Amazon River system (Moreira-Turcq et al, 2003).

Hydrological factors are closely related to riverine transport of total suspended sediments and particulate organic carbon in equatorial rivers, e.g. by increasing the amount of erosion of river banks that contain plant litter and soil organic carbon (Seyler et al, 2006). In a study of tropical rivers in Venezuela a positive linear relationship was found between increased concentrations of DOC

and the chromophoric properties of DOM, which corroborates that qualitative properties of riverine organic carbon in the tropics are coupled to riverine discharge patterns (Yamashita et al, 2010). Humankind impacts the geomorphology of the landscape directly through erosion and indirectly through the carbon transport through the LOAC. When natural drainage areas are perturbed by anthropogenic impact, e.g. through change of land use or damming of reservoirs, the carbon cycle is influenced (Tranvik et al, 2009). For instance, increased agricultural land use can lead to more tillage and water erosion with accelerated carbon loads into river systems (Regnier et al, 2013), and the constructions of manmade reservoirs become sites of vertical greenhouse gas emissions as well as sites of sequestration through burial of carbon rich sediments due to the artificial catchment acting as a sediment trap in the landscape (Maavara et al, 2017).

To distinguish the fluxes of the natural biogeochemical cycle of carbon from the perturbed cycle, it is important to understand the magnitude of fluxes between the carbon pools and where perturbation influences the natural cycle. Lateral carbon transport in the LOAC is a well-known pathway for carbon, something that was described as a mixture of perturbed and natural transport already decades ago by Meybeck (1982) as: "Effect of man's activities are generally not taken into account or are indirectly estimated". Yet the impact of anthropogenic perturbation on this part of the carbon cycle is still under debate (Regnier et al, 2013).

1.2 Research problem

In relation to DOC, POC comprises a small fraction of TOC in the water column. Wetzel (1984) reported an average POC:DOC ratio of 1:10 in rivers, while other studies which have used models to estimate average fluxes of POC and DOC suggest that the contributions of these carbon species to the worlds surface oceans are of similar values, for instance studies like Li et al (2017) who reported DOC (0.24 Pg year^{-1}) and POC (0.24 Pg year^{-1}) indicate that the average overall contribution of DOC and POC is in principle equal. However, the heterogeneity of world rivers affect the individual contribution from each river system, where river POC:DOC ratios compose the result of various environmental factors such

as climate, geology, vegetation. Observations of varying POC:DOC ratios have been found for different aquatic systems. For example, in subtropical to tropical regions, higher ratios have been reported, e.g. 5.8 in the Godavari river in India (Balakrishna et al, 2006), and 4.1-17.7 for the extensive Paraná River in South Central America, which flows through various climate regions from its headwaters to the SW Atlantic (Depetris & Kempe, 1993). In temperate regions such as the the UK, Pawson et al (2012) have similarly reported POC:DOC ratios of 1.01-4.00 from blanket peat in the catchment of River Ashop in the English Peak District; the results of their study suggested that POC fluxes in riverine systems are not only controlled by upstream POC erosion but are also influenced by in-stream POC dynamics within the aquatic continuum. Properties such as stream order, trophic state, environmental setting and climate all contribute to the variation in POC:DOC ratios of these highly diverse aquatic systems.

Fractional size and chemical composition plays a role in protecting OC from mineralisation at different degrees by physical and chemical stabilization, allows POC to transform by e.g. complexation, coagulation, flocculation and photooxidation, and consequently the higher density of POC reduces its transport distance compared to the dissolved phase of organic carbon in freshwaters which increases its probability to accumulate in sedimentation basins, and contribute to limnic storage of organic carbon. This has impact on emissions of greenhouse gas concentrations from the terrestrial environment to the atmosphere and OC burial in sediment stores. POC forms an important part of the dynamic global carbon cycle, yet its origin and fate in the LOAC is not yet fully understood.

1.3 Aims

This project aims to increase process understanding of the fate of POC in the LOAC. The main research questions to be investigated include 1) explaining the influence of anthropogenic impact on carbon export (by land use induced soil erosion and hydrological traps in the form of dams) and the subsequent effect on the fate of POC in freshwaters, and 2) clarifying flocculation dynamics of stream waters draining perturbed landscapes and how physicochemical parameters constrain this process. The results from aims 1) and 2) will be used as validation data for case studies on POC export from soils to freshwaters in the LOAC.

Chapter 2. Background

This section introduces the environment of POC studies. Findings on characteristics and transport of POC along the land-ocean aquatic continuum by previous studies are presented to summarize current understanding of the significance of POC in the carbon cycle and its relevance to climate change. At the end of this chapter the aims and hypotheses of this project are presented.

2.1 What is POC?

The precise definition of POC is subject to debate. Ittekot & Laane (1991) and Delu et al (2013) for example define POC in terms of the living and biologically active organic carbon, such as plankton and microbes, along with the non-living POC which comprises decaying organic matter. Ittekot & Laane (1991) also described the labile fraction of particulate organic matter (POM) that can be subjected to mineralisation, and the refractory or recalcitrant fraction which, due to its non-reactivity, has the potential of being transported along the LOAC and reaching the estuaries and the oceans.

Other definitions of POC focus on size where, in numerous studies, POM and POC are considered to be the filtered organic matter and associated C that will not pass a 0.45 μm pore size filter (Schlesinger & Melack, 1981; Koelmans & Prevo, 2002; Adams et al, 2015; Delu et al, 2013), without any upper maximum size defined. Similarly, dissolved organic carbon/matter (DOC/DOM) compose the soluble fraction which includes soil humic substances, polysaccharides, and polypeptides (Schlesinger & Melack, 1981) that pass a 0.45 μm filter (Trumbore et al, 1992; Bisutti et al, 2004). Chemical characteristics and sources have also been considered: in the natural ecosystem POC and POM derive from various organic sources and may compose plant litter from terrestrial and aquatic sources, algae and biofilms, and soil organic matter (SOM) (Hope et al, 1994).

In this work POC and POM are defined by the often used >0.45 μm fraction of organic carbon, with varying recalcitrance. While in some literature POC and POM are considered equivalent organic species, in this study POC is strictly defined as organic carbon, and similarly POM is considered particulate organic matter which may compose various organic compounds.

21

2.2 Importance of POC in the C cycle

2.2.1 Carbon in the dynamic riverine pipeline model

Carbon in running freshwater mainly compose the particulate organic carbon (POC), dissolved organic carbon (DOC) fractions, and dissolved inorganic carbon (DIC) (Hope et al, 1994). Kirschbaum et al (2019) estimated that the total amount of carbon reaching the oceans compose the following annual fluxes: DIC (450 MtC year^{-1}), DOC (200 MtC year^{-1}) and POC (250 MtC year^{-1}). Of the organic components, DOC is readily transported in the water column, while POC is important because it has greater potential to be stored in the sediments of watercourses (Thurman, 1985). It has been suggested that POC make up 0.5–0.6% of the riverine suspended sediment that reaches the oceans (Ittekot & Lane, 1991). In world rivers concentrations of POC have been reported in the range 0.5–40% of total suspended matter (TSM) (g L^{-1}) and negatively correlated with suspended matter and positively correlated with stream discharge (Meybeck, 1982). However, due to the ecological and geomorphological variety of riverine systems globally, when it comes to modelling POC concentrations, the average world river, in terms of water quality and suspended matter load, is ill-suited to be used as a baseline reference (Meybeck & Helmer, 1989).

Cole et al (2007) introduced a dynamic riverine carbon transport model (Figure 2), in which considerations were taken to include CO_2 evasion and carbon storage in freshwater sediments through burial. In their model, Cole et al (2007) estimated that at least 1.9 Pg C year^{-1} enters the riverine environment from land and from this, estimates of carbon being returned to the atmosphere or stored in sediments roughly results in 1 Pg C year^{-1}. From available data, Cole et al (2007) also estimated that the CO_2 evasion from manmade reservoirs amount to double that the natural emissions (0.28 Pg C year^{-1}), noting that emissions from many small reservoirs are still occluded from available datasets. Despite its simplicity, the dynamic riverine pipeline model composes a "boundless carbon cycle" and highlights that in-stream processes of freshwater systems need to be considered when it comes to mitigating the perturbed carbon cycle and its impact on climate change (Battin et al, 2009). Another flux from freshwaters to the atmosphere compose the outgassing respired from secondary production by heterotrophs (about 1.2 Pg C year^{-1}), when this additional flux was inputted into the dynamic river pipeline model increased net ecosystem production and carbon input into

freshwaters amounting to 2.7 Pg C year^{-1} was required to balance the budget (Battin et al, 2009).
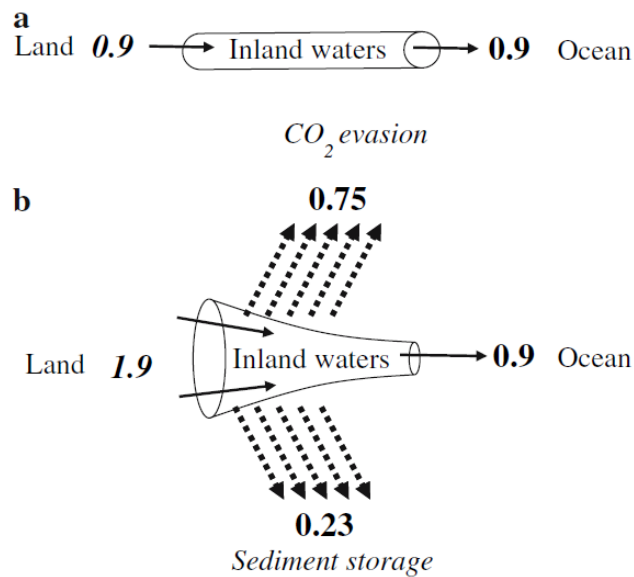
Figure 2 Cole et al (2007) compared the previous pipeline-only model (a), to a preferred revised riverine pipeline model for carbon export (b) in the LOAC, including outgassing and sediment burial. From Cole et al (2007).

Similar to the studies mentioned above, Aufdenkempe et al (2011) discussed how rivers comprise a dynamic pathway of carbon in the terrestrial delivery of carbon from land to ocean. They concluded that 1) the quantities of net ecosystem production (NEP) of carbon is delivered, transported and processed by river systems, 2) that burial of carbon in continental sediments is one order of magnitude higher than in oceanic sediments, and that 3) weathering of minerogenic species from the continental landscape promotes acidification of the coastal environment. Their dynamic riverine carbon transport model is based on data from Battin et al (2009) and includes more high-latitude freshwater data on CO_2 evasion and C sequestration through burial, which results in changed numbers for these fluxes compared with the equivalent transport model by Cole et al (2007). Aufdenkempe et al (2011) also found that the anthropogenic impact on watersheds lead to increased rates of weathering of minerogenic material. They discussed the potential of the formation of organic-inorganic complexes and

23

the carbon imprint this leaves in different riverine environments, which is dependent on climate and human perturbation.

Richey et al (2002) estimated an average CO_2 evasion from wetlands in the Amazon basin of 0.5 Gt C year^{-1}. Extrapolating from this to all areas covered by humid tropical forest globally, they estimated a global CO_2 evasion flux of 0.9 Gt C year^{-1}. In their study, the source of the exported DIC was assumed to constitute mineralised organic matter from upstream sources, indicating the role of rivers as hydrological transport conduits of organic matter, with in-stream transformation (e.g. microbial mineralisation and fermentation) and outgassing of inorganic carbon products. From data on inland water surface area, pCO_2 and gas transfer velocity, Raymond et al (2013) estimated that carbon dioxide evasion from freshwater amounts to 2.1 Pg C yr^{-1} and that, of this, rivers contribute 1.8±0.25 Pg yr^{-1} while still water bodies (including reservoirs) contribute roughly 0.32 Pg C yr^{-1}. The combined CO_2 evasion flux amounts to 2.1 Pg C year^{-1}, which is higher than previous studies have shown. In their study supersaturation of CO_2 in watercourses was frequent, the median values for pCO_2 exceeded atmospheric values for 95% of the observations, and pCO_2 showed positive correlation with TOC concentrations and inverse relationship with lake size. Raymond et al (2013) highlighted potential problems that can arise when modelling pCO_2, including overestimations that can occur in systems with varying concentrations of organic acids, as pCO_2 is a calculated value from pH and alkalinity. Another potent greenhouse gas that is emitted from the LOAC is methane (CH_4). About 25% of the apparent terrestrial GHG sink is linked to CH_4 emissions from inland freshwaters, which indicates a smaller total GHG land sink than previously considered (Bastviken et al, 2011). CH_4 enters the atmosphere through numerous pathways of different emission rates, for instance through ebullition which is highly sporadic, via diffusion from the water column which is less episodic, and transport through emergent aquatic plants. Bastviken et al (2011) highlighted the need to incorporate this sink of DIC and subsequent source of CH_4 into future studies on terrestrial GHG emissions from freshwaters.

Historical anthropogenic impact has altered the global carbon cycle, mainly in terms of carbon export from soils into rivers (Stallard, 1998). Regnier et al (2013) found that the magnitude of this impact might amount to as much as 1 Pg C year^{-1}, since the industrial revolution. This anthropogenic impact on lateral

carbon fluxes composes change of land use, such as deforestation, intensified cultivation and degradation of soils. The realisation that freshwaters not only transport chemical species but that there are in-stream processes influencing the properties of these species is well-known, but has been highlighted in recent years, due to the increasing awareness of its importance to the sources and sinks of greenhouse gases. The carbon fluxes and pools in schematic models of the riverine pipeline model (Cole et al, 2007) have been improved with updated numbers in recent years, which successively has acknowledged more detail for each process (e.g. Tranvik et al, 2009; Aufdenkampe et al, 2011; Regnier et al, 2013; Kirschbaum et al, 2019). Available data is insufficient to investigate the carbon cycle with respect to different soil types and types of inland and coastal waters, and therefore future studies will contribute to more robust databases and improved estimates. The land net GHG sink might be smaller than previously thought, as improved numbers on inland water emissions of CO_2 and CH_4 are included in the budgets (Bastviken et al, 2011). As the carbon cycle has a main influence on the Earth's global energy budget, it is of general concern to identify the various constraints that control carbon fluxes in the environment and to promote sampling campaigns to validate carbon budget models (Raymond et al, 2013). While erosion modelling is becoming a more common practice, extensive field experiments are still necessary to obtain reasonable time-series data (Lal, 2005), which would serve as validation data for existing Earth system models and increase the reliability of the results from these.

The input of global POC to the coastal oceans has been modelled from datasets. For instance, Beusen et al (2005) reported a global average POC flux of 226 Tg year^{-1}. A re-estimation by Li et a (2017) who reported a value of modelled POC export from riverine discharge into the ocean amounting to 0.24 Pg year^{-1}, included in a revised number of the total amount of C exported from land to ocean by discharge of 1.06 Pg year^{-1}. In comparison, Kandasamy & Nath (2016) estimated global mean riverine POC export of 203 Tg C year^{-1} (*sd*=41) after 1990.

2.2.2 Human perturbations on the LOAC and C cycle

The human impact on the C cycle along the LOAC is dominated by land use change (LUC) and the construction of dams and reservoirs. Regnier et al (2013)

estimated that an increase of carbon flux into inland waters of 1.0 Pg C year^{-1} could be attributed to human perturbation, out of which, after mineralisation and sequestration processes along the LOAC, c. 0.1 Pg C year^{-1} reaches the open ocean. Most of this additional C input into the aquatic system can be connected to soil sources (further discussed in 2.4.1).

The number of manmade reservoirs and dams has been increasing worldwide over the course of human history, summing to over 45,000 dams worldwide by year 2000 (WCD, 2000). Reservoirs comprise artificial sediment traps that influence the natural carbon transport along the LOAC (Tranvik et al, 2009). The artificial control on water flow, residence time and storage affect the natural water cycle, water quality and transport of chemical species (e.g. nutrients and trace metals) for the influenced drainage area. The global surface area taken up by hydroelectric reservoirs amount to 3.4×10^5 km^2 (Barros et al, 2011) but the magnitude of vertical emission of carbon from these artificial water bodies has been sparsely investigated. Existing flux estimations of CO_2 and CH_4 amount 48 Tg C and 3 Tg C per year respectively, which deliver 4% of the worldwide total carbon emissions from terrestrial water bodies, and 16% carbon emissions of all manmade dams (other purpose-built reservoirs) (Barros et al, 2011). Despite these numbers being rather modest, they imply that energy obtained from hydropower is not carbon neutral, and that these fluxes must be considered when evaluating hydropower energy as an alternative to fossil fuels. Greenhouse gas emissions from reservoirs are constrained partly by dam age and by geographic location, e.g. emissions from tropical regions such as the Amazon are greater than from other regions (Barros et al, 2011). The effect of carbon sequestration through sediment accumulation and burial can lead to less net mineralisation rates and greenhouse gas emissions, if environmental parameters change, for instance a decrease in temperature leading to slower reaction rates (Gudasz et al, 2010), and subsequently reservoirs in colder regions can act as net sinks of carbon while reservoirs located in warmer climatic regions might act as net sources (Mendonça et al, 2012). Accumulation of organic carbon in reservoir sediments comprise c. 75% material of allochthonous origin (Maavara et al, 2017). Land use change such as agricultural practices that increases soil erosion contribute to relocating this allochthonous carbon into human made dams. By adding trapping efficiency of reservoirs and dams to their model, Beusen et al

(2005) estimated that the average global input of POC from the continents to coastal oceans was reduced to 197 Tg year^{-1}, compared to their estimated natural input of 226 Tg year^{-1}. This highlights some of the importance of POC in the C cycle, as it functions as a readily sequestered carbon species in depositional environments.

2.3 Sources of POC

Previous studies have divided freshwater organic carbon in the LOAC into three pools, based on the original source: 1) terrestrial (allochthonous), 2) in-situ NPP (autochthonous), and 3) anthropogenic sources (Thurman, 1985). Because human perturbation affect both allochthonous and autochthonous sources, for this work, anthropogenic sources have been considered as integrated parts and thus only allochthonous and autochthonous POC have been considered.

2.3.1 Soil organic carbon (SOC) – a terrestrial source of potential POC

POC from the terrestrial environment comprise carbon compounds from different sources, e.g. soil organic carbon (SOC) from soils; litterfall from vegetation; petrogenic organic carbon from weathered carbonates in the rock cycle; black carbon (BC) consisting of wholly or partially combusted organic matter (e.g. from forest fires), soot particles, aerosols, and other organic complexes; other anthropogenic sources like fertilizers and pesticides (Bianchi, 2011). Of the main terrestrial C pools, the phytomass pool holds 26.0% and soils 74.0% of the total terrestrial C pool (Scharlemann et al, 2014). The C pool of land plants amount to 560 Pg, with a dynamic yearly exchange of 60 Pg between land vegetation and the atmosphere (Lal, 2003). The exchange of these pools with the atmosphere are highly dependent on land use, vegetation and climate. Even though litterfall plays a role as a direct allochthonous source of POC in the LOAC, most litterfall components are either readily decomposed in the aquatic column or fall to the ground and subsequently become part of the organic soil horizon where it is decomposed and transformed into soil organic matter. This work is primarily focused on soil derived POC, and more emphasis in this literature review will be given to this source of POC in the LOAC.

2.3.1.1 Soil organic carbon – global inventories

Soils contain the largest pool of terrestrial carbon (Stockmann et al, 2013; Doetterl et al, 2015), which amounts to about 1500 Pg C (Scharlemann et al, 2014). Batjes et al (2014) similarly reported total C stocks of 2157–2293 Pg for the upper 1 m of global soil, out of which 1462–1548 Pg compose SOC. Soils store ca. 75% of the terrestrial total organic carbon (TOC) (Edmondson et al, 2015), a store that compose the largest OC pool on land (Jobbagy & Jackson, 2000). Several studies on the global and regional distribution of carbon stocks and latitudinal spread have utilized spatial soil databases, including:

- Köchy et al (2015) calculated a global mean SOC value 2476 Pg for the top 100 cm of the soil column from Harmonized World Soil Database (HWSD);
- Batjes (2005) utilized Soil and Terrain Database (SOTER)[1] for estimating total SOC of Brazilian soils (65.9–67.5 Pg C);
- Jobbagy & Jackson (2000) estimated a global mean SOC of 1502 Pg for the top 100 cm from National Soil Characterisation Database (NSCD)[2] and World Inventory of Soil Emission Potential Database (WISE)[3] among others.

Other older databases include the Soil Map of the World (SMW)[4] and Harmonized continental SOTER-derived database SOTWIS. Among the available databases HSWD version 1.2 (FAO) compiles one of the most detailed datasets available on soil characteristics and properties (Figure 3) (Köchy et al, 2015). Being an aggregation of existing global soil information on regional and national scale, HSWD composes 15,000 different soil units combined in a harmonized structure that uses standard classification (FAO)[5].

---

[1] Developed by ISRIC World Soil Information and Food and Agricultural Organization (FAO)
[2] Developed by U.S. Department of Agriculture (USDA)
[3] Developed by International Soil Reference and Information Centre
[4] Food and Agricultural Organization (FAO)
[5] http://www.fao.org/soils-portal/soil-survey/soil-maps-and-databases/harmonized-world-soil-database-v12/en/
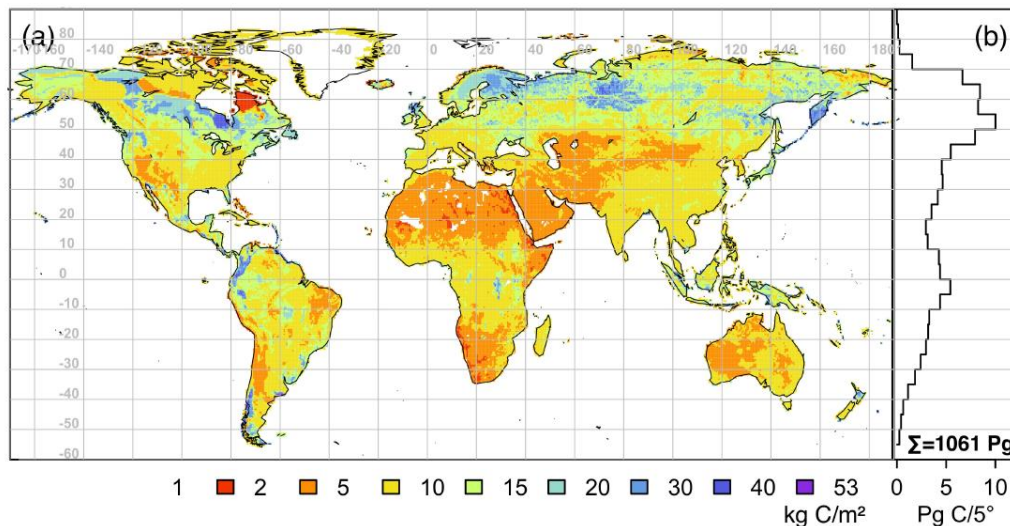
Figure 3 Map showing a) global SOC stocks for the top 1 m and b) mass for every 5-degree latitudinal band, of terrestrial soils, derived from Harmonized World Soil Database v.1.1-adjusted. From Köchy et al (2015).

2.3.1.2 Soil organic carbon – characteristics and quality

The carbon content in soils originate from a range of sources, where the main source of SOC derive from the local vegetation (Schlesinger, 1984). Litterfall, roots, microbial biomass and fungi constitute the main sources of SOC, which is subject to translocation in the soil profile. The main SOC mass appears in the upper A horizon, onto which litterfall accumulates. Erosive agents like water and wind preferentially erode this upper low-density OC-concentrated soil layer and deposit SOC-rich sediment at sites of accumulation, e.g. in geomorphological depressions in the landscape, for instance as accumulated sediment in lakes (Lal, 2005), in colluvium at footslopes of hills and in alluvium of floodplains and wetlands (Aufdenkampe et al, 2011).

Fulvic acids, humic acids and humins percolate through the soil column from top soils but with depth carbonic acid commonly becomes increasingly important for the soil solution in gradually more minerogenic subsoils (Schlesinger, 1997). Large parts of the abundant dissolved organic matter are mineralised or stabilized in the soil profile, while only a part is drained into local watercourses (Kaiser & Kalbitz, 2012), e.g. leaching composes the main transport of soil-derived DOC into the LOAC (Lal, 2003). Humic substances (HS) comprise microbially processed organic matter (Stockmann et al, 2013) and are

reactive aggregates with pH- and salinity-dependent sorptive properties (Millour & Gagné, 2012). The solubility of humic substances increase at higher pH and are present as either long chains or coiled molecules at high and low pH respectively, with correspondingly low and high ionic strength (Schäfer et al, 2000). As a result, these properties increase and decrease the mobility of humic substances in soil solution.

The turnover for organic carbon in soils ranges from 3 years to thousands of years, for fresh, readily decomposed plant litter and recalcitrant humus, respectively (Schlesinger, 2013). Carvalhais et al (2014) estimated a global mean residence time of $23\pm^{7}_{4}$ years that was calculated through a simple relationship between plant and soil storage of OC and gross primary production (GPP). However, the heterogeneity of soils, vegetation and climate makes it difficult to estimate a representative turnover time for specific sites without validating field measurements.

Carbon mineralisation in soils is inhibited by stabilization, the interaction (binding and occlusion) of organic matter with the minerogenic fraction, which increases carbon storage in soils and reduces GHG emissions (Saidy et al, 2012). Chemical stabilization, through intermolecular binding mechanics between organic matter (OM) and mineral surfaces, renders OM unavailable as consumable substrates for microorganisms, while physical stabilization preserves intra-aggregate OM found in-between minerogenic particles (Guggenberger & Kaiser, 2003). Organic matter that is adsorbed to mineral surfaces (e.g. by ligand exchange, cation bridging, ion exchange, van der Waals interaction etc.) comprise a large part of the stabilized SOM pool and adsorption is affected by pH and ionic strength (Feng et al, 2005).

SOC aggregates are stabilized by inorganic, organomineral or organic binding agents (Tisdall & Oades, 1982). Inorganic agents comprise for instance sesquioxides and oxy-/hydroxides containing multivalent cations such as aluminium (Al^{3+}) and iron (Fe^{2+} and Fe^{3+}) which form water-stable aggregates, while clay-based aggregates are water-soluble and less stable (Tisdall & Oades, 1982). Soil aggregates that are redistributed through erosion by water are prone to physical breakdown, which releases the organic carbon that was previously trapped within the aggregate and renders it available for mineralisation or oxidation. Six et al (2002) defined SOC within soil aggregates of sizes >53 μm as

not occluded or unprotected, while SOC occluded within the <53 µm fraction was considered protected. Mikutta et al (2007), who investigated the effects of binding mechanisms of organic matter to mineral surfaces, found that the adsorption capacity of the organic matter controls its degradation. For instance, biomineralisation of organic matter is controlled by desorbability, itself being dependent on solution chemistry, binding forces at the mineral surfaces and the reactivity of these, where increased pH levels promote desorption. The recalcitrant lignin-derived DOM fraction has more sorption and desorption potential than the labile DOM fraction, which readily leads to accumulation of the former in soils (Kaiser & Guggenberger, 2000). Wang et al (2014) investigated the burial efficiency in colluvial soils by stable isotopes and found that soil organic matter is more stable in colluvial deposits compared with SOC present at the equivalent soil depth in uphill soils at reference sites. Soil redistribution into colluvium amount to about 50–80% (Wang et al, 2010), which progressively buries SOC in the process. Eroded SOC is subject to mineralisation and atmospheric evasion, re-deposition in terrestrial sediments such as colluvium, or exported from the watershed (Wang et al, 2014).

While many previous studies assume that top soil and subsoil layers respond similarly to disruptions with the mere difference that subsoils are less concentrated in organic carbon, Salomé et al (2010) found that disturbed (sieved) subsoils can undergo up to 75% increased mineralisation, and that priming effects are restrained to top soil layers (where fresh organic matter is readily introduced compared to sparsely in subsoil layers). The priming effect occurs when the rate of mineralisation in old SOC is affected by input of fresh organic matter (Kuzyakov, 2002). Salomé et al (2010) suggested that the main factor controlling OM degradability and mineralisation is the substrate availability to exoenzymes of decomposers. Since priming is regulated by organic matter input (e.g. litterfall, root exudates) to top soil layers, accumulation of soil organic matter dominates in subsoils. This conclusion contradicts the findings of Fontaine et al (2007) who reported that the SOC stability in the soil profile mainly is controlled by priming. Rumpel & Kögel-Knabner (2011) emphasized the importance of accounting for subsoil carbon stocks in the global carbon cycle and that stabilisation of organic matter by occlusion into mineral protected aggregates differ in top soil (where biological processes might dominate) compared to subsoil

(where physical processes like compaction may be more important for the protection and occlusion of organic matter). Soil properties such as texture, temperature, and biological activity differ in different types of soils and therefore these parameters also need to be interpreted when studying soil organic carbon storage and its fluxes. Jobbagy & Jackson (2000) suggested that plant functional types contribute to regulating SOC with depth in the soil profile. In their study, they found that mean SOC concentrations in the upper 20 cm of the first 100 cm soil depth were 33% for shrublands, 42% for grasslands and 50% for forest, and that relative SOC depth distribution in soils on a global scale was more linked to vegetation than climate, however climate showed a stronger relationship with absolute concentrations of SOC.

2.3.2 Aquatic sources of POC

Aquatic autochthonous organic matter is mainly produced by algae and macrophytes (Bertilsson & Jones, 2003), which both photosynthetically fix carbon in watercourses. During growth, these provide dissolved organic matter of low molecular weight (LMW) to the water column (Bertilsson & Jones, 2003). Growth of phytoplankton is highly dependent on the availability of nutrients in the watershed, e.g. nitrogen, phosphorous (Silva et al, 2014). Organic polymers of phytoplankton compose mainly proteins, sugars and lipids; organic matter which upon cell death can be utilized by heterotrophs or be transformed by chemical processes (Bertilsson & Jones, 2003). Biofilms contribute to the biomass of watercourses and compose stationary colonies of microorganisms that have attached to any submerged surface with suitable habitat conditions (Fischer, 2003). Part of this OM pool includes transparent exopolymer particles (TEP) (de Vicente et al, 2009), which are sticky gel-like acidic polysaccharides that promote aggregation of particles (e.g. mineral grains and organic species) in the water column (Passow, 2002). TEP are products with high carbon contents formed from phytoplankton DOM exudates. Their sticky nature acts as matrices of aggregation of non-adhesive particulates, and to a degree provides surface areas for microbial growth, which can contribute to production of particulate organic matter and carbon in the water column, by for instance flocculation and POC production through biomass growth.

2.4 Input and transport of POC in the LOAC

Figure 4 illustrates the transport and dynamics of POC in the LOAC that is influenced by sources (section 2.4), imports (section 2.4), mineralisation pathways (section 2.5), transformation reactions (section 2.5), sediment burial (section 2.6) and exports (section 2.6). Whilst DOC is readily transported as a solute in waters of the LOAC, POC is influenced by gravitational settling in the water column dependent on stream discharge, which can disrupt its lateral transfer along the LOAC (Battin et al, 2008).
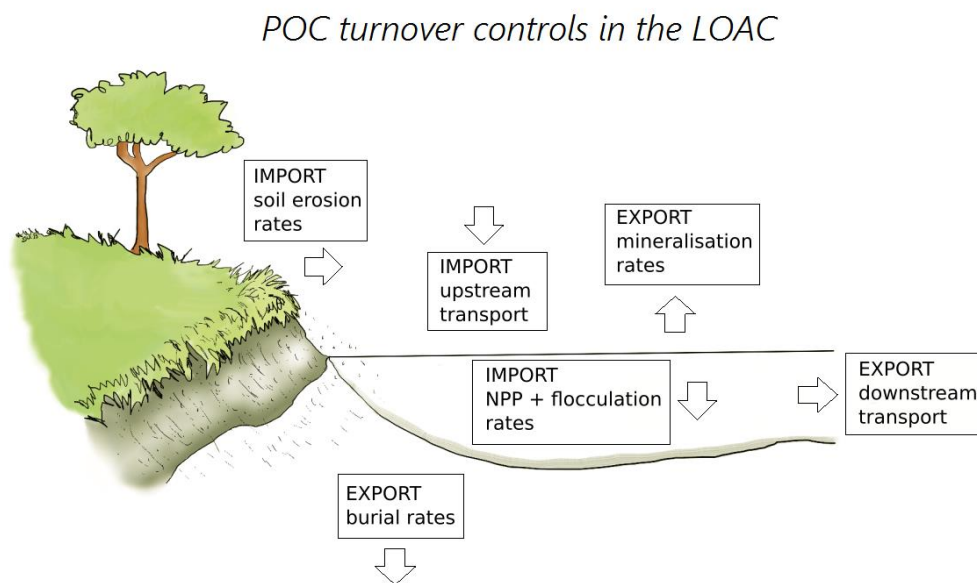
Figure 4 Basic imports and exports of organic matter into and out of a watercourse within the LOAC.

2.4.1 Soil erosion

Soil erosion is the displacement process of soil particles from the site of formation to depositional environments in the landscape (Figure 5) (Lal, 2003). Common weathering processes are connected to temperature and moisture content of soils, as well as biochemical action (Starr et al, 2000). Geological soil erosion can be divided into water erosion, e.g. rain-drop splash/interrill, sheet, gully, mass movement, and rill erosion where runoff erodes the soil surface and transport particles downstream, and wind erosion that has the ability to displace fine soil particles both uphill and downhill (Blanco & Lal, 2008; Segura et al, 2014). Where

water channels cut through the soil layers more collapse-like bank erosion can occur, e.g. in stream channels.

Relative to soil formation rates, soil erosion is often a rapid destructive process (Paroissien et al., 2014), comprising the detachment and movement of soil particles by erosive agents. Global gross water erosion of soils can amount up to 75 Gigatonnes (Gt), with 15–20 Gt being delivered to watercourses (Lal, 2003). It has also been reported that on a global scale soil erosion by water affects 1094 mega-hectares (Mha) and wind erosion affects 549 Mha, with areas of 751 Mha and 296 being critically degraded by water and wind erosion respectively (Lal, 2003). Acceleration of natural soil erosion has been induced by human activities in the form of e.g. agricultural practices, deforestation, and overgrazing (Ritchie & McHenry, 1990; Porto et al, 2012). This mobilized soil is the effect of degradation and downwasting of a valuable resource that can further cause problems downstream when sediment is deposited in fields, floodplains and lakes and dams (Zapata et al, 2003). Since soil erosion impact both the sustainability of agriculture in managed lands and environmental conservation of protected areas, quantification of soil erosion is a primary step towards soil conservation (Gaspar et al, 2013), and as part of effective environmental management to control soil degradation in productive landscapes there is the need to quantify soil erosion and deposition rates (Porto et al, 2012; Gaspar et al, 2013). Reliable data on soil erosion is sparse in many regions globally despite the general acceptance that net soil loss from the landscape composes a major problem (Zapata, 2003). Although soil erosion is a primary cause of input of carbon into the LOAC, only 5–25% of eroded soil matter is transported to the ocean (Aufdenkampe et al, 2011). Most of the soil is redistributed as sediment in colluvium, alluvium or lake sediment, where it stores carbon by burial.

34
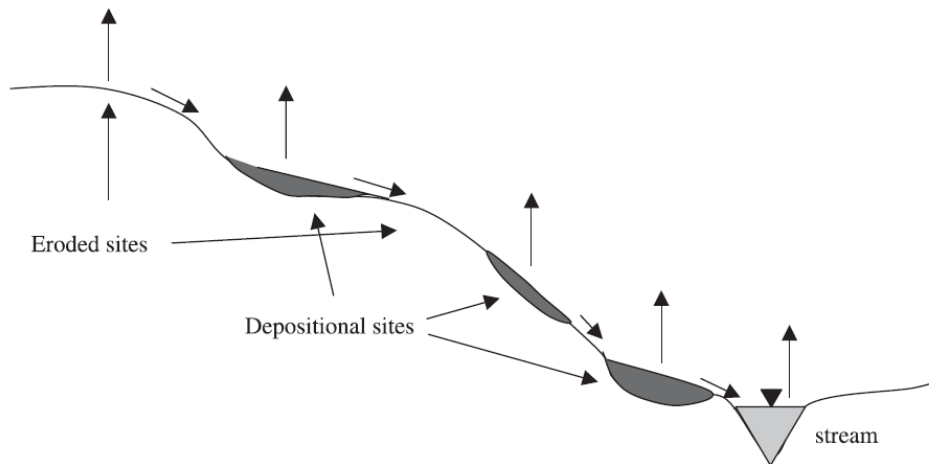
Figure 5 Typical stepwise redistribution patterns of soil organic carbon in the eroding landscape, with subsequent SOC mineralisation leading to greenhouse gas emissions. From Lal (2003).

2.4.2 SOC erosion – a source or sink of GHG?

Whether soil erosion creates a net source or sink of carbon at the terrestrial–atmospheric interface has been widely debated (e.g. Stallard, 1998; Lal, 2005; Van Oost et al., 2007; Berhe et al., 2007). Recent estimates show likely SOC losses of 25–50% when natural vegetation is converted into cropland (Scharlemann et al, 2014). Lal (2005) emphasized that the soil–atmospheric carbon flux depends on scale and perspective; soil erosion is a process divided into four stages: detachment, transport, redistribution, deposition – all of which need their own unique mass balance models – and combined, these make up a realistic total mass balance model for general SOC erosion. Organic carbon burial on land has been suggested to amount up to 10^{15} g C year^{-1} (Stallard, 1998), but the minerogenic and organic heterogeneity of soils, and the wide range of ongoing physicochemical processes that vary spatiotemporally in these, make modelling of the contribution of greenhouse emissions by soil respiration complex (Fang et al, 1999). Van Oost et al (2007) estimated a global sink of up to 0.12 Pg C year^{-1} in agricultural soils, accounting for long-term soil redistribution by tillage, water and wind erosion. Agricultural practices can decrease carbon residence time in a soil profile by increased top soil erosion (Quinton et al, 2010), attributed to increased physical aggregate breakdown that exposes intra-aggregate organic carbon which then becomes available to decomposers and subsequent net

respiration, and contribute to physical redistribution of soil organic carbon. Six et al (1998) studied the influence of tillage practices on different types of particulate organic matter (POM) fractions (free light fraction, and intra-aggregate particulate organic matter) and concluded that while physically protected organic matter is released by tillage (leading to regular aggregate breakdown and subsequent exposure of previously protected SOC), the turnover of the labile (unprotected) free light fraction is influenced by other factors such as soil temperature and moisture. For instance, a field study on arable fields by van Hemelryck et al (2010) showed that mineralisation rates were controlled by porosity, moisture and temperature of the studied soils, with most prominent CO_2-efflux over a time span of weeks after a soil redistribution event by erosion. Poirier et al (2005) found that the chemical composition differs between aggregate-bound and free SOM fractions, and that the order of reactivity corresponds to SOM fractions with increased physical protection in mineral aggregates, namely free>intra-aggregate>organomineral.

For comparison, the 2013 report by Intergovernmental Panel on Climate Change (IPCC, 2013) accounted for 1.7 Pg (Gt) C $year^{-1}$ being exported from soils to the aquatic system annually. As discussed above, only c. 0.9 Pg C $year^{-1}$ reaches the coastal ocean, while the rest goes into limnic storage or is mineralised.

2.4.3 Riverine POC fluxes

Other studies have modelled global riverine POC fluxes (Beusen et al, 2005; Kandasamy & Nath, 2016; Li et al, 2017). Li et al (2017) based their model on published data up to 2015 and suggested that the largest riverine POC fluxes were present at latitudinal bands 30–60ºN, with modelled continental scale fluxes of POC (0.24 Pg), DOC (0.24 Pg), DIC (0.41 Pg) and PIC (0.17 Pg). Kirschbaum et al (2019) arrived at similar numbers for the riverine carbon fluxes (Figure 6) and added more detail to the riverine pipeline model introduced by Cole et al (2007). As POC is mainly derived from soil organic carbon stocks, soil erosion is one of the key contributors to riverine POC, however the fate of the majority of remobilized soil particles remain on land in terrestrial and freshwater storage.
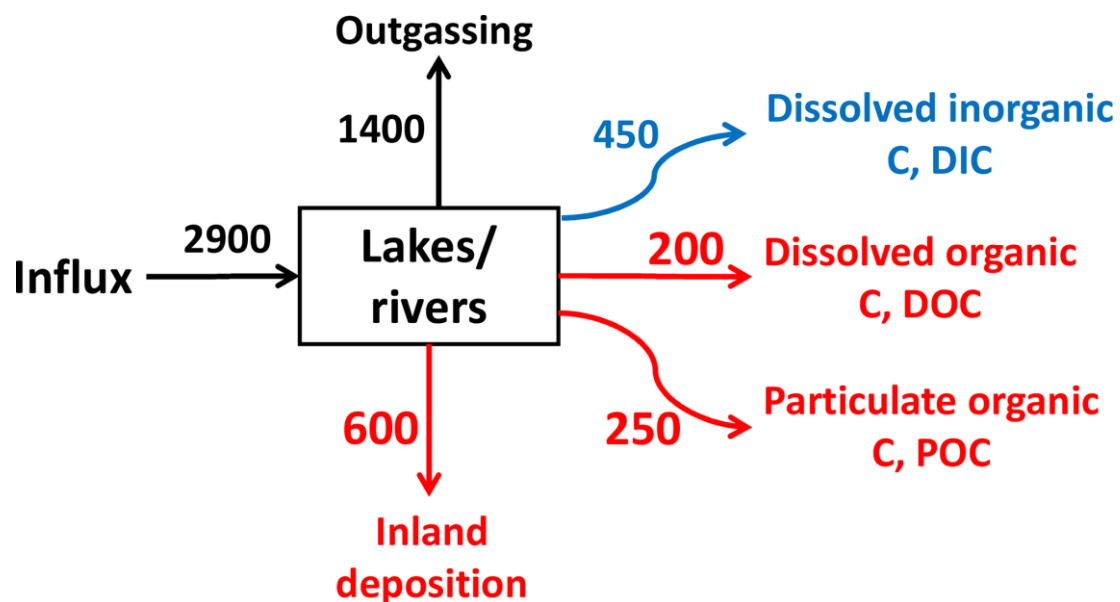
Figure 6 A more detailed riverine pipeline model of primary carbon fluxes (MtC year^{-1}). From Kirschbaum et al, 2019.

Main sinks of POC in the water column comprise physical breakage of POC into the dissolved phase, mineralisation, transformation processes, such as photooxidation, and sediment burial, which will be discussed below.

2.5 Transformation dynamics of POC in the LOAC

2.5.1 Carbon species in the LOAC

Three main sources account for the occurrence of riverine POC: 1) OM from terrestrial and aquatic NPP, 2) aged SOC input from subsoils, and 3) fossil or kerogen OM from sedimentary rocks (Blair & Aller, 2012). Physicochemical characteristics of organic matter that influence its reactivity in the environment compose e.g. molecular weight, aromaticity, functional groups (Pullin et al, 2004). Soil derived POC that enters the aquatic continuum vary in qualitative properties (e.g. age, state of decomposition, aromaticity, solubility, ionic strength etc.) which affect its capacity to be mineralised or oxidised in the water column. Fresh litterfall from the canopy (often considered labile POC) is readily decomposed compared to organo-mineral aggregate-bound POC (considered stabilized and recalcitrant) and therefore, along with geology and climate, erosion and weathering processes which deliver top soil and subsoil POC into watercourses, play a role in the input and fate of POC along the LOAC. Furthermore, the transport capacity of POC in the aquatic continuum will depend on the size, density and chemistry of the POC.

In for instance stratified watercourses these properties affect the turnover time of POC above the hypolimnion, which will reduce oxidation of POC and subsequently increase the input into limnic carbon storage. In relation to identifying labile and recalcitrant soil organic matter, Adams et al (2015) investigated riverine PO^{14}C from rural low erosion rate catchments in the United Kingdom and found that top soil erosion is a major contributor of POC into river systems. However, the apparent ^{14}C-ages obtained in their study represent POC from a range of mixed upstream sources which characterize both aquatic POC inputs from top soils, due to surface soil erosion, and material from subsoils, where bank erosion has been prominent. In their global study, Marwick et al (2014) found that riverine DOC in general is of younger age than POC. An increase in age of riverine POC corresponded with increased sediment loads (Marwick et al, 2014), which is in line with a soil derived origin.

DOM composes a mixture of aliphatic and aromatic organic compounds that, depending on residence time in the water column and exposure rates, have been transformed by decay processes (Stedmon et al, 2003). While fulvic acids commonly compose aliphatic organic compounds and carboxyl groups, humic acids contain more aromatic groups e.g. methoxyls and phenolics (Aitkenhead et al, 2003). DOC contributes to the staining of surface waters, so called "browning" (Köhler et al, 2013), which is typically found in surface waters with low alkalinity and arise from the solution of woody tissue debris and/or soil organic matter (Bratby, 2006). In natural waters humic substances (HS) comprise 30–50% of total organic matter (Thurman et al, 1982) and the potential interaction with other aqueous species can be substantial due to humic substances acting as polyelectrolytes that decrease the electrostatic repulsion between colloids in the water column, which allows for POC aggradation through processes like coagulation, complexation and flocculation.

The nature of the carbon compounds which enter the aquatic environment is of significance as it either provides a nutrient proxy for net primary production (NPP) or serves to acidify the water column (Sun et al, 2015). The terrestrial sources of aquatic POC primarily derive from litterfall and soil organic carbon (SOC), while lacustrine sources compose e.g. in-stream growth of biomass in watercourses, which make use of available dissolved organic and inorganic

carbon (DOC and DIC), and flocculation products from the processes that transform DOC into POC.

2.5.2 Water chemistry and quality

Sources of dissolved aquatic substances in natural surface waters compose rock weathering, input from terrestrial organic matter, and atmospheric deposition (Meybeck & Helmer, 1989) and the resulting water quality is a product of interactions between aquatic species from each of these sources together with present conditions of e.g. geology, climate, aquatic biota (Manahan, 2001). Anthropogenic impact that influence natural water chemistry is often pollution, such as dispersion of agricultural pesticides, wastewater drainage, and acid mine drainage (Neubecker et al, 1983). Especially in non-buffered systems, such as freshwaters in environments of alkaline rock type, acidification of freshwaters can contribute to flocculation processes and increase the burial rate of organic sediments.

One of the challenges in measuring the chemistry of streams transporting aquatic species from land to ocean is to identify baseline geochemistry from natural imprint on the water quality from the input of pollutants from anthropogenic sources (Meybeck & Helmer, 1989). Metals can be defined as three size fractions in the aquatic environment: dissolved (<1 kDa), colloidal (1 kDa–0.45 μm), and particulate (>0.45 μm) which exhibit generally decreasing mobility and bioavailability respectively (Nystrand et al, 2012). In the freshwater environment metals are commonly present in the form of complexes with humic and fulvic acids because of the high complexing capacity of these organic compounds with metal cations (Niessner et al, 1998). The properties of metals in complexed and ionic forms differ and therefore humic substances control the geochemical dispersion and bioavailability of metals in the aquatic system (Neubecker et al, 1983). The composition of humic substances determine their complexing capacity and therefore the geochemical imprint is an artefact of the HS properties. Thurman et al (1985) found that high-molecular weight (HMW) fraction of aquatic humic matter likely is colloidal and only comprise 5-10% of the total aquatic load.

2.5.3 Transformation of OC in the water column

Processes that transform organic carbon in the aquatic system can either reduce or produce POM and POC. In freshwaters, abiotic photochemical flocculation has the potential to remove DOM of terrestrial origin from the dissolved phase before reaching the estuarine environment (Helms et al, 2012). For instance, flocculation of allochthonous DOC can produce POC that is subject to sequestration into lake and reservoir sediments (von Wachenfeldt & Tranvik, 2008), which contributes to OC burial. On the other hand, degradation processes such as photo-dissolution transforms aquatic POC into the dissolved species of carbon. Transformation processes of OM in the aquatic environment affect the local ecosystem functions (Porcal et al, 2009), as DOM play a role in controlling surface water characteristics e.g. light attenuation, substrate availability for NPP, and metal complexation (Mulholland, 2003, pg.140). Flocs can also influence water quality through physical, chemical and biological functions (Droppo et al, 1997), e.g. through the ability to bind to aquatic species, such as contaminants, and transport them along the LOAC.

2.5.3.1 Coagulation

Coagulation is the irreversible process where colloids aggregate due to charge neutralization (Atkins & de Paula, 2005) by reducing the repulsion potential of electrical double layers in colloids (Matilainen et al, 2010). Particles between 10^{-3}–1 µm are colloids, which do not settle under gravity due to Brownian motion, and in urban waters comprise e.g. fine silts, clay particles, bacteria, viruses (Manahan, 2001; Scholz 2016) and in natural waters e.g. humic substances, mono- and multivalent ions, micro-organisms, metals and carbonates (Schäfer et al, 2000). Organic colloids can amount to 20% of the dissolved aquatic species in rivers (Hope et al, 1994). Colloid stability in suspension is directly influenced by the sign and degree of surface charge (Koopal, 2005). In a stable suspension the surface charge of colloids is balanced by solution counter-ions of opposite charge (Dukhin, 2006). Adsorption and precipitation occur when ions are removed from a solution to accumulate on a solid to form either two-dimensional or three-dimensional structures, respectively (Goldberg, 2004). Coagulation is the process where the electrical charge in the suspension is changed by the introduction of e.g. chemical coagulants (multivalent ions or colloids) of an

opposite charge to that of the particles in suspension; commonly, the greater the valence is, the greater the coagulation effect becomes in the suspension (Scholz, 2016). The main types of coagulation mechanisms are adsorption with subsequent destabilization, a typically fast process (0.1–1s), and sweep coagulation (3–17s), which are effective at different alkalinities and turbidity (Scholz, 2016). Adsorption induces particle destabilization by either charge neutralisation or interparticle bridging (Edzwald et al, 1974). Sweep coagulation results in the colloid settling inside a metal hydroxide precipitate (Edzwald et al, 1974; Schloz, 2016), while double layer compression is an effect of the increased concentrations of counter-ions in e.g. saline environments, where the degree of compression is determined by the valence; colloidal destabilization increases with ionic strength (Edzwald et al, 1974). Similarly, Ramos & McBride (1996) found that reactions which increased the surface charge (negative or positive) contributed to dispersion and charge neutralization promoted flocculation effects. Organic compounds of neutral charge can also provide sites of attachment (Larsen et al, 2009).

The behaviour of colloids present at close proximities of each other (<1 µm) can also be influenced by van der Waals forces (Scholz, 2016 pg. 41). A higher electrokinetic potential, or zeta potential, will keep the colloid suspension stable (in general >25, either negative or positive), while destabilisation occurs at lower zeta potential. The pH level also influences coagulation processes, for instance oxidation by dissolved oxygen (DO) will occur at pH levels >8.5 (Schloz, 2016).

Cationic and anionic polyelectrolytes, which are long-chained polymers that produce ions of positive and negative charges when dissolved, can be used as coagulants to remove colloids of opposite charges respectively (Scholz, 2016), however charge neutralization by electrolytes is not the only coagulation and agglomeration process (Bratby, 2006).

2.5.3.2 Clay particles in suspension

The commonly net negative charge of inorganic clay particles influence the behaviour of these in the water column, in particular for freshwaters which lack saline ions where this net negative charge leads to stable suspensions in which coagulation is prevented, either by charge balance through the mutual repulsion

between hydrophobic colloids or by the attraction of (hydrophilic) colloids to counter-charged ions in the solution itself (Edzwald et al, 1974; Scholz 2016 pg. 40–41). The common reason for a net negative charge of clay particles is due to isomorphous substitution, where cations of a higher positive charge have been replaced in the crystal lattice by cations of lower positive charge, e.g. Si^{4+} by Al^{+3} etc. (Scholz, 2016 pg. 41). The inorganic particle acts as an electrode in the solution, in which electrostatic attraction influences the behaviour of particle and counter-ions. Edzwald et al (1974) used three clay standards (kaolinite, illite and montmorillonite), to perform coagulation experiments in artificial seawater mixtures and found that for all clay standards higher ionic strength of the seawater standard increased coagulation rates in the suspensions. Their experiment included a field study where they found that upstream sediments retain a higher stability factor (α), indicating that upstream sediment are less stable than downstream and estuarine sediments.

2.5.3.3 Flocculation

Flocculation is the process where particle cohesion forms larger aggregates from smaller ones and the process can be reversible. It is affected by collision efficiency through steps of transport and attachment (Dukhin et al, 2006). Electrochemical flocculation happens due to increased concentrations of dissolved ions in the water column (van Olphen, 1964), where high valence cations, such as Ca^{2+} and Mg^{2+} which are common in clay minerals, rather than monovalent cations, are the more important ions in the process (Tsai et al, 1987; Droppo & Ongley, 1994; Ramos & McBride, 1996) and can form agglomerates together with negatively charged organic matter. Since produced organic flocs retain higher density and achieve higher settling velocities (Tsai et al, 1987), these are more prone to sink and accumulate on the lakebed, which subsequently removes this fraction of organic matter from the water column and mineralisation processes further downstream.

Microflocs (<125 µm) often consist of stable organomineral complexes and serve as building blocks for larger but less stable macroflocs (3–4 mm) that are more sensitive to physical breakdown, with a maximum size constrained by turbulent shear in the water column (Eisma, 1986). Verney et al (2009) also reported that maximum floc size is highly dependent on intensity of turbulence

and found that in their estuarine samples maximum floc size was attained in systems with concentrations of suspended particulates >9.1 g L^{-1}. In a study by Droppo & Ongley (1994) the parameters that showed the strongest relationship with floc size were suspended solids, POC and bacterial colonies, while pH, conductivity and major ions were less important.

Collisions between particles despite the existence of intermolecular repulsive forces can be induced by Brownian motion (perikinetic flocculation) (Edzwald et al, 1974) or hydrodynamic effects, like turbulence (or fluid shear) (Stechemesser, 2005; Scholz, 2016), known as shear or orthokinetic flocculation (Gregory, 1981).

The physicochemical and biological nature of flocs is connected to their structure and composition, which further alters their mode of transport and settling behaviour as sediment particles (Droppo et al, 1997). A study on light-dependent flocculation by von Wachenfeldt et al (2008) showed positive correlation between the DOC concentration and the sedimentation rates of allochthonous organic carbon in a boreal lake, leading to significant DOC losses in the water column. The increased sediment load contributes to carbon sequestration by burial, and therefore flocculation not only removes organic carbon from the DOC pool and transfers it into the POC pool, but also influences both the mineralisation rates (and subsequently the local evasion of CO_2 and CH_4) and the net storage through burial in basins with sediment accumulation.

Neto et al (2006) showed that the biochemistry of flocs is mainly determined by input of litterfall from local catchment vegetation together with diagenesis. In a study by Helms et al (2012) organic matter with carbohydrate properties showed low photochemical transformation and flocculation potential, while produced flocs showed more aliphatic properties compared with the residual dissolved fraction.

2.5.3.4 Photochemical transformation of organic matter in the water column

Solar radiation contributes to photodegradation of DOC in the water column, which in the process produces building blocks for POC formation (substrates for microbial growth) or oxidizes DOC into DIC through photomineralisation (Porcal et al, 2015). Kieber et al (2006) found that high-energy UV light is most effective

for DOC and POC degradation, while photosynthetically active radiation, or photosynthetically available radiation, (PAR) has a lower effect.

Molot & Dillon (1997) described the effect of solar radiation on DOC of different ages in the water column of a peatland stream; suggesting that recently eroded DOC (which has just entered a stream system) is more susceptible to photodecay than aged DOC that has been in suspension in the water column over a longer period of time. This was also one of the suggested conclusions in a study by von Wachenfeldt et al (2008), who through a light-mediated flocculation experiment found that up to 25–60% DOC loss accounted for produced POC in water from a mire outlet compared with a corresponding experiment with lake water (8–22%). This suggests that the labile fraction is being readily transformed upon entering a watercourse, while the recalcitrant organic matter remains as suspended matter in the water column.

Photodissolution also contributes to the breakdown of POC and deliver this carbon into the DOC pool (Estapa & Mayer, 2010, Pisani et al, 2011). Photoproducts may be reactive and subjected to metabolism, and therefore contribute to the DIC pool after mineralisation by microbial activity (Estapa et al, 2010). Pisani et al (2011) conducted time series experiments on POC samples by exposing flocs to artificial irradiation, and observed that most contribution to chromophoric DOM (cDOM; the fraction absorbing UV and visible light) came from the photodissolution of terrestrial humic-like species rather than protein-like species, and that the concentrations of both dissolved nitrogen and soluble phosphorous increased in the process, implicating that photodissolution not only transforms POC into DOC but also releases nutrients important for the biological food supply. Through flocculation experiments Asmala et al (2014) simulated estuarine mixing and found that both quantitative and qualitative properties of the remaining DOC (post-flocculation) changed significantly in terms of molecular weight, cDOM, fluorescence, and iron content, in boreal freshwater DOC samples subjected to saline conditions. Vähätalo et al (2008) performed long-term incubation experiments where they exposed water DOC samples to solar irradiation (459 days) and microbial mineralisation (898 days) and found that both processes were able to completely mineralise metabolically unavailable allochthonous DOC derived from wetlands, if the residence time of this DOC in surface waters is sufficiently long.

In a case study in Alaska, Cory et al (2015) found that increased light absorbance and attenuation due to photodissolution and subsequent production of cDOM in the top layers of the water column was connected to thermal stratification, concluding that important controls on photodegradation rates in this system was UV irradiation intensity and residence time of cDOM in the upper water column. Since both stratification and residence times were influenced by turbulence in the water column, stream flow affected photo-dissolution rates. Porcal et al (2015) found that temperature is a main controlling factor for photochemical degradation, i.e. at lower temperatures the DOC–DIC transformation dominates while DOC–POC transformation dominates at higher temperatures. Mayer et al (2006) found temperature and light limitation (intensity) to be the main constraining factors of photodegradation, while Pisani et al (2011) found that fluorescence characteristics of mainly terrestrial humic-like components, and to a lesser degree protein-like components, increased with exposure in released DOC from degraded floc samples.

Photoirradiation experiments conducted by Pullin et al (2004) showed that while the irradiation reduced HMW-OM, formed LMW-OM compounds such as carboxylic acids contributed to adsorbed DOM onto goethite mineral with reduced UV-Vis absorptivity.

2.5.3.5 Fate of flocs in the LOAC

From headwaters to estuary, different environments in the LOAC promote and reduce transformation processes. Climatic conditions, geochemistry (lithology, soils), vegetation, all influence the water chemistry of the LOAC.

In the estuarine environment, saline mixing promotes aggregation of DOC (Ertel et al, 1991). In their experimental study, Verney et al (2009) found that flocculation in estuarine systems appeared to be more dependent on the properties of the suspended sediment and initial OM content, rather than salinity. Similarly, Forsgren et al (1996) studied the aggregation of iron, phosphorous and DOC in saline environments and found that <10% of DOC aggregated, mainly the high molecular weight fraction. Ertel et al (1991) found that the C/N ratio of flocs formed due to saline mixing was higher for flocs formed by OM in filtered samples, than for OM adsorbed onto existing particulates in non-filtered samples, which indicates that different OM species were removed by the two different

processes studied. Repeta et al (2002) found that while humic acids for freshwater and seawater are clearly separated by properties of C-isotopic composition, C/N ratios, adsorption potential in UV-light, and molecular structure, the bulk chemical properties of high molecular weight (HMW) DOM (>1kDa) from freshwater and seawater were indistinguishable, suggesting that biogeochemical cycling of these compounds are comparable in different aquatic environments from freshwater to sea.

Several studies have investigated the nature of suspended sediment loads in rivers with emphasis on controls on organic floc production (Droppo & Ongley, 1994), but it has been emphasized that further studies are needed in this area (Neto et al, 2006), to identify the fate of particulate phase of OM produced from these processes. Especially interesting is identifying sections along the LOAC where riverine OM is affected by naturally occurring coagulants and where POC is prone to form, which affects downstream C burial and mineralisation pathways.

Transformation processes of organic matter and their residual effects in the LOAC are poorly understood (Sleighter & Hatcher, 2008). While coagulation science has roots in the water treatment industry and numerous chemically produced coagulants have been studied for their residual effects on freshwater, understanding natural agglomeration processes in the LOAC can contribute with insights regarding C pathways and fate – both natural and anthropogenic. As flocs change the hydrodynamic conditions for suspended particle transport (Droppo et al, 1998), increased POC loads into the riverine system due to changed land use practices can affect the resulting OC burial and GHG emission downstream. Because the characteristics of natural OM in the LOAC have impact on molecular to global scale processes (Kim et al, 2003), there is a need to study effects of flocculation to identify selective sorption of more or less recalcitrant carbon species, to elucidate fractionation of OM components along the LOAC, which can have implications for aquatic biota downstream and in the ocean, and to determine the effects of different natural flocculation boundaries on riverine OM.

2.6 Fate of POC

2.6.1 Sediment records

Inputs of carbon into lakes consist mainly of the dissolved species (DOC, DIC) while particulate phases (POC, PIC) occur with lower concentrations – differences of their relative concentrations in surface waters and fate vary with climate, geochemical characteristics of the landscape, and land use (Hope et al, 1994; Tranvik et al, 2009). Sedimentation of organic matter in natural low energy environments, such as freshwater lakes, deltas, floodplains and brackish estuaries, contribute to deposits of POC. Manmade reservoirs compose artificial lakes that similar to natural lakes can hold semi-permanent limnic storage of organic matter over the lifetime of the reservoir. Lake and reservoir sediment compose accumulated material from terrestrial and aquatic sources. If resuspension is sparse, annual sediment layers that accumulate on the reservoir floor compose minerogenic material previously eroded from soils of the catchment (Figure 7). The volume of post-flooding sediment reveals the net deposit of accumulated material from soil erosion, and exhibits net storage of accumulated POC.

The chemistry of surface sediments is influenced by diagenetic effects (Callender et al, 2000) which constrains the mineralisation and oxidation reactions. The sediment accumulation rate is also important for the preservation of settling material – faster burial of sediments limits the exposure time of substrates to depth-specific microbial metabolism and oxidation reactions. Another complication is hiatus in the sediment record. This can be important in manmade reservoirs where resuspension during events such as dam discharge is likely to impact the sedimentation, by for instance physical disturbances such as stream turbulence, oxygenation and temperature changes due to controlled alteration of the water table.
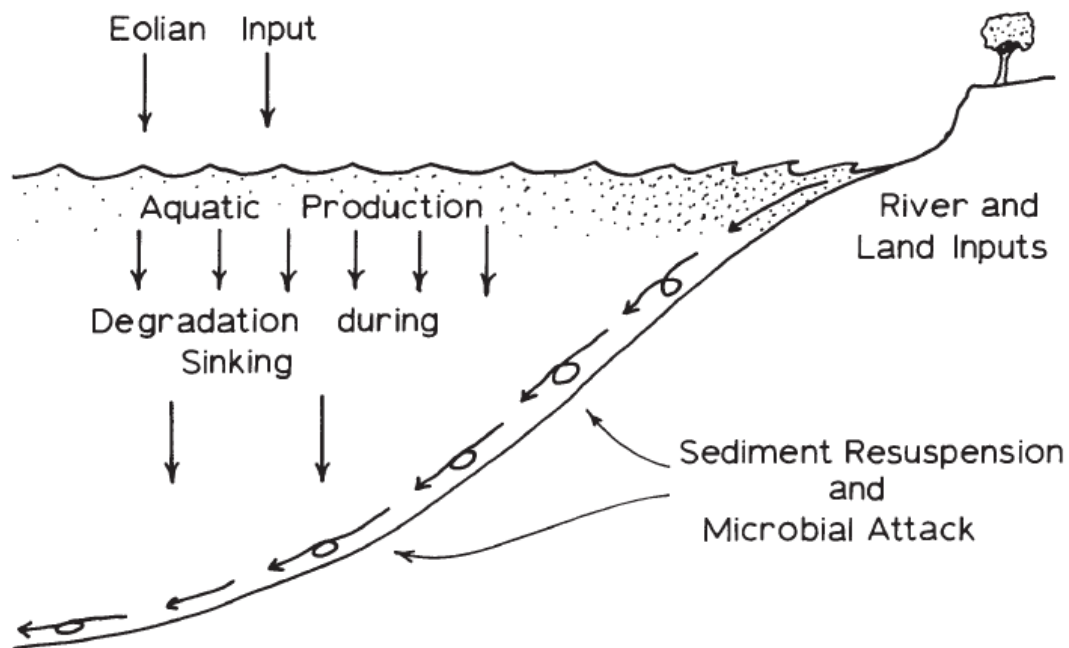
*Figure 7 Sources of organic matter into lacustrine sediments. From Engel &
Macko, 1993.*

2.6.2 Early diagenesis of lacustrine sediments

On a geological time scale, many early diagenetic processes in surface
sediments are considered fast processes occurring within 1000 years of particle
deposition (Engel & Macko, 1993). The selective transformation, decomposition
and reworking of reactive organic matter that is water-soluble and readily
available for microbial consumption (e.g. proteins and carbohydrates), leads to
sediment profiles showing relatively increased concentrations of non-reactive
recalcitrant components of organic matter (e.g. humic substances and lipids) with
sediment depth (Meyers & Ishiwatari, 1993). During the reworking process
synthesized products further become part of the sediment biomass, either as new
reactive substrates for consumption or as recalcitrant persisting artefacts (Meyers
& Ishiwatari, 1993).

2.6.3 Vertical and lateral limnic OC exports

OC burial is the process where carbon is sequestered into semi-permanent
sediment storage. Burial of organic carbon composes one of the terrestrial C
sinks, with main pathways being the settling of aquatic biota at sites of

48

accumulation, deposition of litterfall and minerogenic particles, and POC production from the DOC pool (de Vicente et al, 2009). Sobek et al (2009), found that OC burial efficiency mainly is influenced by the input of allochthonous organic matter into limnic sediments together with the degree of oxygenation. In their study, Sobek et al (2009) found that as much as 66% of the allochthonous sediment input is buried into lakebed sediments (while mineralisation processes produce CO_2 and CH_4 which evades to the atmosphere) concluding that the main drivers determining the proportion which is buried compose a product of environmental conditions (e.g. trophic state of the catchment, temperature, oxygenation) along with the qualitative characteristics of the inputted organic carbon itself, and residence time in the particular part of the water column that is affected by these factors. The volumes of carbon burial in freshwater bodies exceed burial in oceanic environments by one order of magnitude globally (Aufdenkempe et al, 2011). Better understanding of this pathway would improve estimates of the global organic carbon sink on land.

About 0.2–1.6 Pg C is buried in freshwater sediments annually and Regnier et al (2013) estimated that out of this roughly 20% comprise autochthonous carbon. In a study by Cole et al (2007) carbon burial was equivalent to 0.2 Pg C year^{-1}, while at least 0.8 Pg C year^{-1} is released through CO_2 evasion. Raymond et al (2013) estimated that CO_2 evasion from freshwater amount to 2.1 Pg C yr^{-1}, and that out of this, rivers contribute 1.8±0.25 Pg yr^{-1} while still water bodies (including reservoirs) contribute roughly 0.32 Pg C yr^{-1}.

2.6.4 Organic matter quality and sources

One way to distinguish the quality and sources of particulate organic matter in soil and sediments is the use of geochemical bulk parameters such as carbon-nitrogen ratios (Meyers & Ishiwatari, 1993). C/N ratios of organic matter is commonly preserved in lake sediments despite early diagenetic effects in the sediment column (Meyers, 1994). C/N ratios for algae and aquatic macrophytes that lack cellulose range between 4–10, while terrestrial vascular plants with supportive cellulose walls show C/N values >20 (Meyers & Ishiwatari, 1993; Meyers, 1994). These differences in C/N have often been interpreted in conjunction with C-isotopes, to distinguish terrestrial and limnic sources of organic matter (Figure 8).

49
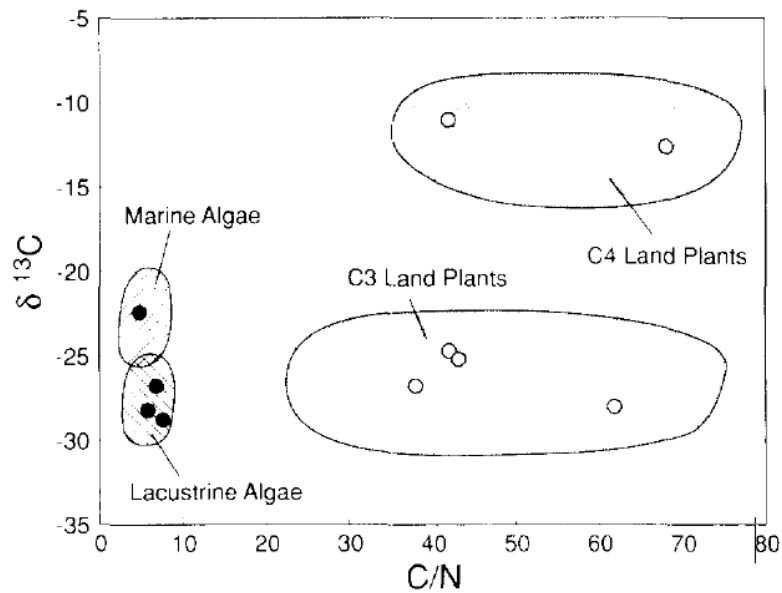
Figure 8 C/N ratios interpreted in conjunction with C-isotopic values of various organic matter sources (Meyers, 1994).

Lake sediments with contributing sources of plant litter from both vascular and non-vascular plants show typical C/N ratios of 13–14 (Meyers & Ishiwatari, 1993). In soils, C/N ratios depend on the degradation state of organic matter which has been subject to biogeochemical processing (e.g. biomineralisation) which has altered the stoichiometric relationship between macronutrients in SOM (Tipping et al, 2016). For instance, fresh plant litter typically has higher C/N-ratios than humic acids (Schlesinger, 2013). The method is a useful qualitative tool to determine sources of organic matter in aquatic sediments. For instance, at their study sites in Upper Paraná River basin, South Eastern Brazil, Albuquerque & Mozeto (1997) observed higher C/N ratios in riverine POM (6.5–11) compared to lacustrine POM (3.5–5.9), indicating the presence of refractory autochthonous organic matter in the river water compared to allochthonous organic matter in lakes. The C/N ratio further showed seasonal variation, connected to increased flow and transport of suspended sediment, which suggested a possible change in quality of suspended particulate matter throughout the hydrologic year.

There are a number of other specific molecular biomarkers used for tracing sources and discrimination of organic matter in sediments, such as stable isotopes, lignin polymers, *n*-alkanes, lipids and branched glycerol dialkyl glycerol

tetraethers (GDGT) among others. The use of stable isotopes has been widely implemented to determine the sources and mixing of organic matter in aquatic systems (Schindler Wildhaber et al, 2012). Isotopic composition of C in riverine organic matter can be used to determine the composition of POC, for instance to determine the relative contribution of C3 and C4 plants or to determine the fate of labile and refractory organic carbon. For example Nagao et al (2010) used stable isotopic composition together with lignin phenols to determine the composition of riverine POC from terrigenous origin, while in a study of isotopic composition of organic matter from the Amazon River system, Mayorga et al (2005) proposed that young riverine organic matter (less than five years old) compose a primary source for CO_2 outgassing in the tropics. In three tributaries of the vast Amazon River, Bouchez et al (2014) further utilized radioactive and stable carbon isotopes (^{14}C and ^{13}C) to determine the qualitative properties and sources of POC in sediments. In their study, it was determined that up to 10% of POC exported by the Amazon River may be rock-derived and that C3 plants contribute as a main terrestrial biospheric POC source. Furthermore, higher detail of organic matter sources can be achieved with compound specific stable isotope analysis (CSIA), e.g. with these methods Alewell et al (2015) quantified relative contributions of suspended sediments from agricultural and forested land use during various flow rates in a Swiss lowland river, showing the power of biomarkers in identifying sediment sources.

Other biomarkers are used especially to determine the original plant type, for instance phenolic compounds derived from lignin polymers are indicative of vascular plants and have been used to discriminate between sources of plant organic matter in sediments (Hu et al, 1999). In general, distinctive chain lengths of *n*-alkanes reveal the provenance of the plant matter, terrestrial or aquatic, and stable isotope analysis of *n*-alkanes can be used to distinguish organic matter from C3, C4 and CAM plants (Maioli et al, 2012).

Molecule specific lipid biomarkers have been extensively used to determine original sources of organic matter in sediments, for instance van Dongen et al (2008) analysed an array of molecular properties to discriminate the terrestrial and marine OM sources of estuarine sediment in the Siberian Arctic. Other studies have also made use of branched glycerol dialkyl glycerol tetraethers (GDGT) as complementary tracers to conventional biomarkers such

as stable carbon isotopes and carbon-nitrogen ratio (Kim et al, 2012). GDGT are thought to be products by heterotrophic bacteria found in anaerobic soil (Sinninghe Damsté et al, 2011) and can be used to trace terrigenous input into the aquatic POC pool (Lopes dos Santos & Vane, 2016). For instance in a study by Kim et al (2012) it was found that 70-80% of the riverine POC at Óbidos in the Amazon River originated from soil sources, emphasising the importance of erosion as a source of organic matter in the Amazon River.

Biomarkers are often interpreted with statistical modelling methods. For instance, Cooper et al (2015) utilized a Bayesian mixing model to interpret CSIA of long-chain leaf wax *n*-alkane biomarkers to determine sources of organic matter in stream bed sediment, while other studies have used mass balance mixing models to trace sediment-associated POC (e.g. Collins et al, 2009).

In this study, the method to determine qualitative properties of organic matter was limited to C/N ratio analysis.

2.7 Methods to determine erosion and sedimentation of soils and sediment

2.7.1 FRNs as soil erosion tracers

Fallout radionuclides (FRN) are radioactive isotopes that readily fix onto mineral surfaces and primarily follow the physical processes which relocate soil particles (Quine & Van Oost, 2007). Assuming that the distribution of FRN follow soil mobilization, these therefore serve as good indicators of erosion and deposition by water, wind and tillage (Mabit et al, 2008). Radioactivity measured in field samples are compared for unique sampling sites in eroding and depositional environments against a local reference site, which compose a sample from a non-disturbed setting where no net loss nor gain is observed (Gaspar et al, 2013). The FRN inventory at the time of sampling represents the net accumulation of tracer over the time from fallout deposition, including all processes that have contributed to the inventory in-between (Dercon et al, 2012).

The use of fallout radionuclides, such as ^{137}Cs, ^{210}Pb$_{ex}$, and ^{7}Be, as tracers of soil loss and sedimentation in both managed and non-managed landscapes allows for improved estimates on soil erosion over different spatiotemporal scales (Gaspar et al, 2013). In a field study in north-eastern Spain, using ^{137}Cs and

[210]Pb, Gaspar et al (2013) found that the highest soil losses occurred in mid-slope areas of cultivated fields, whilst the highest deposition occurred in depressions of tilled fields. Different radionuclides have different half-lives and elemental properties, which provide information relating to their respective dispersion and decay in the soil profile (Porto et al, 2012). While artificial ^{137}Cs and geogenic [210]Pb$_{ex}$ can be used to study past annual erosion rates dating back to ca 50 and 100 years respectively, cosmogenic [7]B has a shorter half-life ($t_{\frac{1}{2}}$=53 days) and provides short-term information up to only days–months into the past (Porto et al, 2012).

When using this methodology the following assumptions about the surficial FRN distribution in the landscape are 1) the atmospheric fallout has been relatively uniform across the terrestrial environment which is being used as a field site (Ritchie & McHenry, 1990; Dercon et al, 2012), that 2) the surface particles of FRN enriched soil layers will exhibit a steadily decaying radionuclide footprint regardless of redistribution, and therefore 3) erosion processes dilute or concentrate the radioisotope-bearing particles (Walling, 1998). Practical applications of FRN properties can be implemented when measuring soil erosion across a landscape; by using a set reference point with neither erosion nor deposition, sampling sites with erosion and deposition relative to the reference site can be identified (Figure 9) (Ritchie & McHenry, 1990; Rodway-Dyer & Walling, 2010). For instance, dated sediment profiles showing the concentrations of the radioactive isotope can be used to estimate sediment accumulation rates, former sediment horizons can be identified in a vertical soil profile, and erosion sites identified due to the correlation between radionuclide loss and erosion (Ritchie & McHenry, 1990). Lake sediments undergo both physical and chemical processes that lead to redistribution of radionuclides within the sediment column, e.g. bioturbation and mixing near the water–sediment boundary and porewater transport, e.g. diffusion (Appleby, 1998).
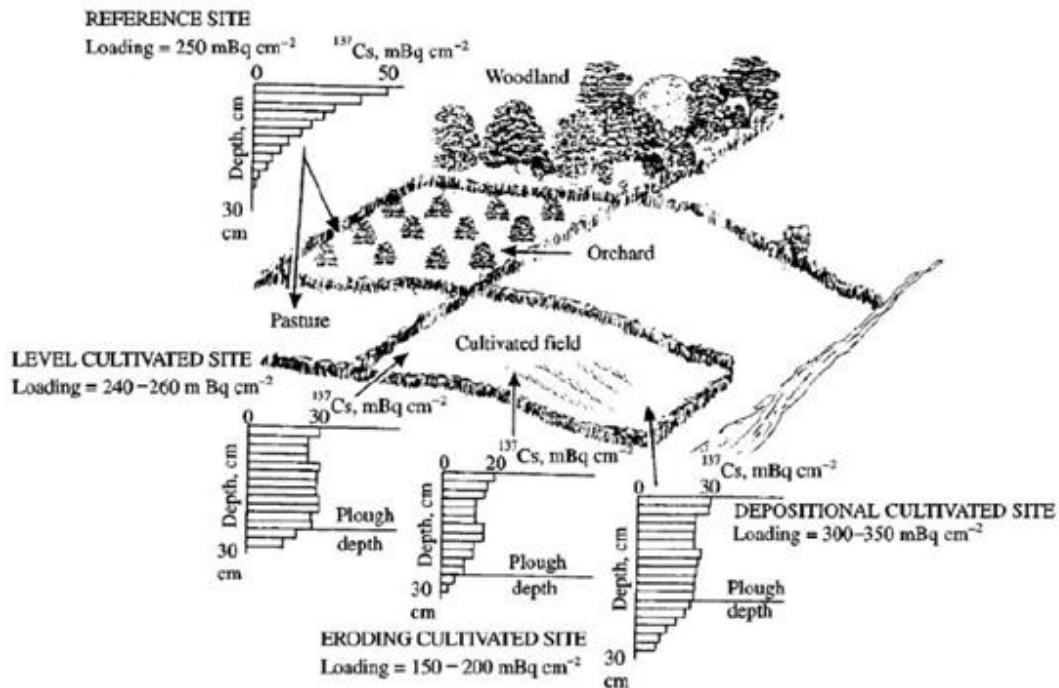
Figure 9 Illustration of ^{137}Cs distribution in the landscape with typical profiles of eroding, stable and depositional sites. From Walling & Quine (1991).

2.7.1.1 Caesium-137 (^{137}Cs)

Caesium (atomic number 55) is an alkali metal that readily forms ionic bonds with a 1+ charge with non-metals. The unstable radionuclide caesium-137 (^{137}Cs) with a half-life of 30.2 years readily adsorbs onto clay particles and absorbs to organic complexes after atmospheric deposition (fallout) and therefore exhibits limited movement in soils (Staunton & Roubaud, 1997). Caesium behaves similar to rubidium (Ru) and potassium (K) in the biosphere (Anke, 2004) and when it comes to adsorption to biological matter and has higher solubility in marine water than freshwater (Eisenbud & Gesell, 1997). Among the alkali metals Cs is the most electropositive and alkaline element (Guzmán et al, 2013), and among the isotopes only one, ^{133}Cs, occurs naturally in the environment (Anke, 2004). The element occurs with an average of only 0.65 ppm in the Earth's crust (Anke, 2004).

The isotope ^{137}Cs is a fission product from ^{137}I decay and is a man-made fallout radionuclide which does not appear naturally. It was released into the atmosphere during bomb tests in the period 1950–1970 (Nouira et al, 2003), and

54

in particular in the Northern Hemisphere from the Chernobyl accident in 1986 (Tang et al, 2006) and Fukushima (Teppei et al, 2011). Despite the Chernobyl incident, main fallout of ^{137}Cs occurred in years 1962–1964 (>50%), and 80% of deposition had occurred by 1964 (Quine & Van Oost, 2007). The radioactive fallout is considered uniform, and despite some delivery being through local dryfall in the vicinity of key sources, the main deposition is via rainfall precipitation (Ritchie & McHenry, 1990; Mabit et al, 2008; Dercon et al, 2012). The amount that sorbed by vegetation also plays some role in the concentration of ^{137}Cs on surface soils, since there is delay before this deposition is delivered to the soil surface (Ritchie & McHenry, 1990).

^{137}Cs serves as a useful tracer for physically relocated soil particles and has therefore been widely used for soil erosion measurements (Ritchie & McHenry, 1990; Quine, 1999). The ^{137}Cs radionuclide has successfully been used to study medium-term (up to c. 50 years) soil erosion rates in managed and non-cultivated soils in the past (Ritchie & McHenry, 2007). The ^{137}Cs method for measuring soil erosion is a straightforward method to identify the relocation of soil particles by physical processes. Random variation in ^{137}Cs concentrations in samples due to mixing is unavoidable and therefore the method is more robust with increasing reference and sample numbers (Zhang et al, 2015). As one of the most common radionuclides used within FRN research, ^{137}Cs has been used extensively in studies worldwide.

2.7.1.2 Lead-210 (^{210}Pb)

Lead (Pb) is a heavy metal with atomic number 82 and a mean abundance in Earth's crust of 14 ppm (Enghag, 2004). Six natural isotopes of Pb exist, of which three are stable and three are radioactive. Activity measurements of excess (unsupported) lead-210 (^{210}Pb$_{ex}$) with a half-life of 22.26 years in soil samples can be complementary to present-day ^{137}Cs studies, and will become important in the future in replacing the ^{137}Cs-method altogether as the man-made ^{137}Cs signal has decayed in the environment (Matishof, 2014). Especially in the Southern Hemisphere, where the fallout of ^{137}Cs has been less prominent, there is scope in using ^{210}Pb as a nuclear tracer (Mabit et al, 2008). The redistribution of ^{210}Pb$_{ex}$ in the landscape is, similar to the ^{137}Cs distribution, mainly connected

to physical relocation of soil particles, as it readily adsorbs to mineral surfaces as well as organic matter. The continuous fallout, however, provides $^{210}Pb_{ex}$ activity profiles in soil and sediment that are highest at the surface with declining activities with depth (Walling et al, 1995).

The fallout of ^{210}Pb from the atmosphere is relatively continuous due to its geogenic source and therefore the soil profiles obtained from undisturbed soils will show the highest activity of $^{210}Pb_{ex}$ near the surface (Figure 10). The in-situ component ^{210}Pb ("supported") derives from ^{222}Rn decay, which itself is a radioactive daughter of naturally occurring ^{226}Ra from the ^{238}U decay series (Appleby, 2008; Gaspar et al, 2013). This product is the supported ^{210}Pb that is in equilibrium with ^{226}Ra. As gaseous ^{222}Rn diffuse through the soil column, atmospheric fallout deposit ^{210}Pb onto surface soils. This atmospheric fallout decay product composes "unsupported" lead-210 ($^{210}Pb_{ex}$), which can be calculated as the difference of measured ^{210}Pb and ^{226}Ra (Zapata, 2003; Gaspar et al, 2013). Because the $^{210}Pb_{ex}$ inventory is continuously replaced, historic records of erosion rates up to ca 100 years are obtainable, compared with ^{137}Cs which fallout is associated with bomb tests in 1950–1960 (Gaspar et al, 2013).

Mabit et al (2014) describe assumptions about $^{210}Pb_{ex}$ behaviour that are important to consider when using this radionuclide as a tracer of soil and sediment redistribution – for instance it is assumed that $^{210}Pb_{ex}$ is readily deposited from the atmosphere over time and the radionuclide is fixed in the soil layer after fallout, there is no downward migration, and the concentrations of activity are not dependent on sediment or soil depth.

Potential disadvantages compose high analytical uncertainty along with very low activities in natural samples which might lead to measurements below the detection limit, however this has been shown to be controllable in several successful studies (Mabit et al, 2008).
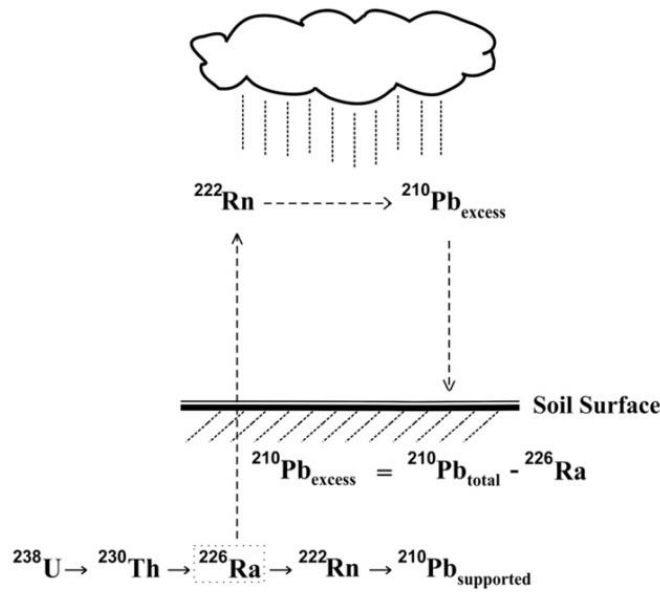
Fig. 1. Origin of geogenic ^{210}Pb and fallout ^{210}Pb (i.e. ^{210}Pb$_{ex}$).

Figure 10 Illustration of ^{210}Pb$_{ex}$ fallout, from Mabit et al (2014).

Even though ^{210}Pb$_{ex}$ has been used less than ^{137}Cs for soil erosion studies in the past, the interest for this radionuclide as a tracer is increasing (Porto et al, 2012), partly because compared to ^{137}Cs, for which the substantial fallout ended in the 1970's, the ^{210}Pb inventory is being continuously replenished in soils (Gaspar et al, 2013).

2.7.1.3 Advantages and disadvantages of FRN methods

There are a number of assumptions being made when using FRN methods to study soil redistribution. The radioactive fallout of ^{137}Cs is considered to have been uniform, and despite some delivery being through dryfall the main deposition is considered to be via rainfall precipitation (Ritchie & McHenry, 1990; Mabit et al, 2008). Some main advantages of the use of FRN as indicators of soil redistribution are the following:

1) quick and direct sampling campaigns of new areas without the need to establish long-term and costly monitoring programmes,

2) the samples obtained from the field can be readily measured for radionuclide activities that reveal the erosion and sedimentation history, without

the need to revisit the site under investigation (Zapata, 2003) with no need to install monitoring equipment (Porto et al, 2012),

3) ^{137}Cs measurements can be used to study records of erosion and deposition rates over the past 30–40 years, progressed as mean rates less susceptible to influence by erosion and deposition anomalies,

4) the field derived data from FRN studies can be used to validate erosion models,

5) the data represent all effects from erosive processes influencing soil redistribution (Nouria et al, 2003),

6) both erosion and deposition rates can be obtained, together calculated into a net flux of soil erosion.

Some limitations comprise the following:

1) FRN samples are obtained from point sampling and the quality of extrapolation is thus influenced by site and sample numbers (Zapata, 2003)

2) there is a need for equipment with sufficient analytical precision, which in cases can comprise an economic limitation (Zapata, 2003)

3) a number of different conversion models add to the uncertainty when estimating soil redistribution from FRN activity (Zapata, 2003)

4) the measurements provide mean soil redistribution rates for the past 30–40 years without high-resolution details of single anomalies within this time span (Zapata, 2003)

5) global standardisation of protocols for the technique are lacking (Zapata, 2003)

6) It is assumed that FRN follow the mobilization of soil particles, however some FRN might adsorb to organic matter which may then depend more on OM redistribution processes, e.g. chemical and biological (Gaspar et al, 2013). For instance microbial activity appears to contribute to the migration of radio-caesium in soils (Parsons & Foster, 2011).

Other limitations of the technique have been carefully described (Walling, 1998; Mabit et al, 2008), for instance, there is a simplification through the assumption of proportionality – i.e. for some conversion models it is assumed that if there is a certain decrease in percentage FRN, the same number will reflect the percentage soil loss since the fallout event. Since radionuclides readily adsorb to finer fractions there might be over- or underestimation of soil loss, if there is a

preferential particle size connected to the soil erosion process. Grain size therefore play an important role when it comes to selective mobilisation of FRNs. The adsorption capacity of FRNs in relation to grain size has been debated, e.g. He & Walling (1996) highlighted the problems with biased results which arise when analysing the mean grain size in connection with FRN activity, which from experimental results appears to be more closely related to specific surface area, and from analysis of natural samples seem to have higher absorbance to finer soil fractions. Effectively, the FRN redistribution in the landscape will be related to the selective erosion of sediment due to particle size. This fractionation would be connected to erosion processes which fractionate soil by particle size and therefore results in a dilution issue. However, this is less likely when soil aggregates of mixed particle sizes are eroded, for instance when mass movement cause episodic erosion.

2.7.1.4 FRN activities in South-eastern Brazil

Fallout of ^{137}Cs has been more prominent in the Northern Hemisphere than in the Southern Hemisphere and show higher concentrations in the environment around for instance centres of nuclear tests and the Chernobyl power plant (Tang et al, 2006; Dercon et al, 2012). Earlier studies have shown that the ^{137}Cs activities obtained in Brazilian soils of the Southern Hemisphere generally occur at levels c. 10 times lower compared to data from the Northern Hemisphere (Bacchi et al, 2000). The generally low activities of ^{137}Cs in the Southern Hemisphere cannot be overcome, however, analysis of complementary radionuclides, such as geogenic ^{210}Pb$_{ex}$, provides additional detail about the soil redistribution record at the site of investigation. Despite the relatively low activities of ^{137}Cs in soils of the Southern Hemisphere, in a long-term runoff monitoring study to evaluate the use of ^{137}Cs in Brazilian soils, Correchel et al (2006) found that where this radioisotope is detectable in soils it provides confident results. At their reference site (Campinas, SP, Brazil) 98% of the ^{137}Cs activity was concentrated to the upper 20 cm of the soil profiles and corresponded to an average inventory of 272±20 Bq m^{-2}. Similarly, Bacchi et al (2000) reported an average ^{137}Cs reference inventory of 422±14 Bq m^{-2} from five profiles in Piracicaba river basin, which has a climate classified as *Cwa* according to the Köppen classification system, representing a humid sub-tropical climate. Correchel et al (2005)

investigated the spatial variability of four reference sites in sub-tropical Piracicaba, Brazil, and reported total inventories of their reference sites were 314, 250, 253, and 242 Bq m^{-2}.

Few studies have reported the spatial variability of ^{137}Cs reference sites in South America, e.g. Correchel et al, 2005 found that the random spatial variability typically exceeded the systematic spatial variability, however the causes for this variability remain unidentified but were suggested to be influenced by "chemical, physical, mineralogical and biological differences" relating to adsorption dynamics in the tropical environment. Similarly, for sediments, Wilken et al (1986) studied estuarine sediment cores from Guanabara Bay in Brazil and found that while ^{137}Cs signal were measured under the detection limit (<0.8 mBq), ^{210}Pb$_{ex}$ could be successfully used to determine the average sedimentation rate (2 cm year^{-1}) in the bay.

2.7.1.5 Summary FRN

Nuclear tracers, such as fallout radionuclides (FRNs) like artificial caesium-137 (^{137}Cs) and geogenic excess lead-210 (^{210}Pb$_{ex}$), compose an alternative to models and monitoring schemes as these serve as useful tools for soil erosion studies that reveal the historical average erosion and deposition rates at a specific site (Zapata, 2003). Fallout radionuclides provide empirical spatial information on soil erosion and sedimentation that uniquely describes annual soil redistribution, which cannot be measured by other methods (Porto et al, 2012). Since the novel development in the 1960's, FRN methods have become well established and gained successful recognition as empirical techniques to measure soil erosion worldwide (Zapata et al, 2003).

2.7.2 Modelling surface erosion processes with soil erosion models

There are several techniques available to estimate soil erosion, each method being used for a specific research purpose (Zapata, 2003). Traditional monitoring techniques, with erosion plots and terrestrial laser scanning (TLS) techniques, which continuously or frequently measure a certain ground surface over a period of time, provide measurements of modern changes to the ground surface but are limited when it comes to investigating historical soil redistribution to the site

unless monitoring scheme has been long-term. These survey data lay ground for modelling approaches, which comprise predictive simulations that utilize interpretation and extrapolation methods. A number of existing soil erosion models are used to evaluate and determine conservation practices and land management today: for instance empirical models such as EPIC, USLE (including MUSLE, RUSLE (Renard et al., 1994)), WATEM, and physically-based Water Erosion Prediction Project (WEPP) (Nearing et al. 1989), EUROSEM (Morgan et al., 1998), ANSWERS (Beasley et al, 1980), and LISEM models (De Roo et al., 1996) among others. Databases with field data on e.g. topographic parameters, precipitation, satellite imagery, soil properties and geology, make it possible to model soil erosion at the catchment scale. Many models have been developed in the past century due to increased computer resources complemented by growing and increasingly accessible databases that provide digital resources on satellite imagery, DEM, precipitation, landscape characteristics and geology etc. (Pandey et al, 2016). Pandey et al (2016) suggested that a "desirable model" acquires universal acceptance when it fulfils the following criteria: it is reliable, robust, requires minimum data, and accounts for varying environmental inputs of land use, climate and conservation practices. The many approaches and motivations to determine soil erosion and landscape evolution have led to a range of models that are purpose specific and show variation in results. Different models are also dependent on the input data quality of each input factor (e.g. precipitation, topography, soil type, land management) used for that particular model, and due to their differences in complexity these are capable of delivering outputs of varying quality, scale, practical applicability (Pandey et al, 2016). While models comprise good alternatives for geographical areas which are inaccessible and remote, there is a need for field surveys in order to obtain validation data for these models (Porto et al, 2012) and to develop understanding of possibilities and limitations of these models. Over the past 20 years, fallout radionuclides (e.g. ^{137}Cs, ^{210}Pb$_{ex}$, and ^{7}Be) have been increasingly used as soil erosion traces in field studies of spatial soil redistribution (Gaspar et al, 2013). Monitoring enclosed erosion plots yield spatially limited results and only give gross soil loss without context to for instance sedimentation rates in nearby geomorphological depressions (Porto et al, 2012). Long-term monitoring schemes are necessary to achieve representative measurements of river

discharge and transported eroded material, to avoid bias due to extreme precipitation and, oppositely, the lack there of during dry seasons (Pandey et al, 2016). Physically based models are readily validated and calibrated by field measurements. Karydas et al (2014) described the spatiotemporal relationship between different erosion parameters and their recognized overlap (Figure 11).
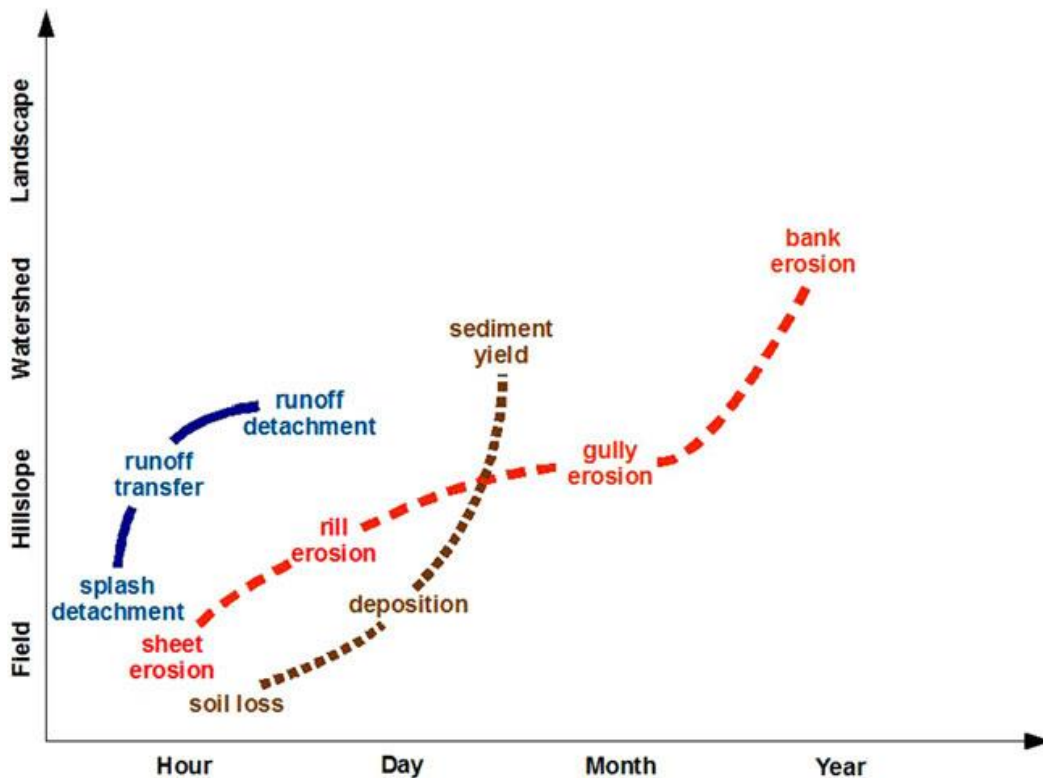
Figure 11 Spatiotemporal scale of overlapping erosion parameters. From Karydas et al (2014).

2.8 Summary of literature review

In this literature review an overview of the current understanding about POC transport and dynamics in the global carbon cycle has been introduced. The transportation processes are dependent on physical erosion and water retention time in catchments and streams. Transformation processes are complex and highly dependent on environmental factors such as biogeochemistry (water quality, biology) and physical processes (photodegradation, water discharge).

This literature review has identified the importance of POC in the carbon cycle, its sources, transformation processes, and related species of carbon. Although the literature on organic carbon is extensive, several authors have

emphasized the importance of further research in the field of POC research, in particular quantification of POC in the LOAC and on transformation dynamics. One of the gaps that exist in the field compose understanding of POC fate from various sources in the LOAC. How much SOC enters the LOAC from the terrestrial environment and what is the fate of this often mineral associated allochthonous POC – is it preserved in lake and reservoir sediments due to its recalcitrant properties or is it mineralised. Another research question is related to how flocculation processes change the DOC quality of streams along the LOAC.

In this work current research questions address the challenge of quantifying the mass export, transformation and quality of the riverine carbon load, which in turn affect in-stream sources and sinks of organic carbon; the understanding of how flocculation processes and rates are influenced by organic matter quality and coagulants present along the LOAC; and how anthropogenic impact influences soil erosion and the export of organic carbon from the terrestrial environment into the aquatic continuum.

2.9 Hypotheses

This project aims are to test the following hypotheses:

1. The fate of catchment-derived POC in the LOAC is determined by physical and chemical protection in soil aggregates and flocs. Therefore, stabilized soil-derived allochthonous POC composes the main source of buried OC in reservoir and lake sediments in catchments where soil erosion is prominent, whilst readily mineralised OC of autochthonous sources has a shorter turnover.
2. Clay and saline mixing are flocculation boundaries in the landscape which increase POC formation and removal of DOC in freshwaters. Therefore, increased erosion due land use change (LUC), e.g. increased agriculture, increases flocculation of riverine transported natural OC and removes OC from the dissolved phase.

These hypotheses are tested by the following studies:

2.9.1 Modelling and measuring terrestrial soil erosion input into a tropical freshwater reservoir, Brazil, with RUSLE and fallout radionuclides ^{137}Cs and [210]Pb

In this study, the spatial redistribution of soil particles from a catchment into a dammed reservoir was quantified. Soil organic carbon (SOC) compose an allochthonous input of POC into the LOAC and adequate methods to study erosion rates are essential to determine transport rates of this POC contribution into the aquatic system. An empirical soil erosion model, RUSLE, was tested for its suitability in this study catchment, which represents an increasingly common deforested Brazilian landscape. The model was validated by field observations of fallout radionuclides.

2.9.2 Importance of terrestrial particulate organic carbon (POC) for organic carbon burial in a tropical reservoir, Brazil

This study aims to quantify the relative distributions of POC from allochthonous and autochthonous sources in reservoir sediments (Figure 12). This was acquired by studying transport and settling rates of POC in a dammed catchment, along with analysis of chemical composition to determine POC provenance. Hypothetically, allochthonous mineral-associated POC remain stabilized while autochthonous in-stream derived POC to a higher degree is subject to mineralisation processes, therefore soil-derived POC should be the more important component for OC storage. At the end of this study, the importance of mineral-associated POC for OC burial in relation to in-stream sources of POC will be evaluated.
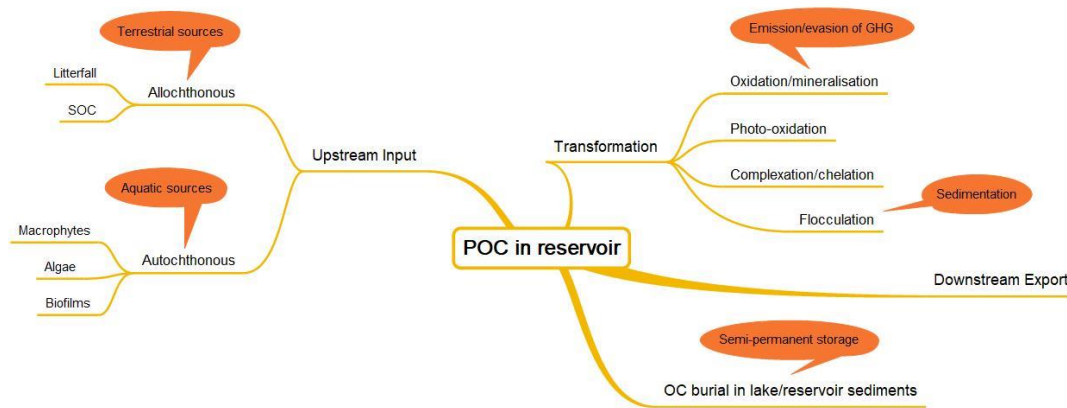
Figure 12 Simplified process diagram describing the fate of POC in a reservoir/lake system.

2.9.3 Flocculation boundaries in the landscape - an experimental study on transformation processes of organic matter in eight coastal moorland streams, UK

POC that forms in streams by transformation processes such as flocculation compose the fraction of organic carbon that can settle on lakebeds and contribute to sediment OC storage. In this study, processes which control flocculation rates of riverine organic matter were investigated to determine the impact of coagulants on dissolved organic matter in rural streams draining Exmoor. By experimental methods two flocculation boundaries in the landscape were simulated: scenario 1) depicts soil erosion input from agricultural activities by the addition of an inorganic clay standard, while scenario 2) compose saline mixing at the estuary by addition of an artificial sea salt standard. Finally a mixed scenario 3) clay and saline mixing which is plausible in the estuarine environment was simulated. The qualitative properties of residual DOM was investigated to determine which organic matter that is preferentially withdrawn from solution during flocculation processes. The importance of these flocculation boundaries on the formation of POC was qualitatively evaluated.

Chapter 3. Methods João Penido study, Brazil

This study focused on the transport of POC in a semi-closed tropical catchment impacted by human perturbation through land use change and damming. Transport of soil organic matter and associated POC was determined from soil erosion measurements by fallout radionuclides, which were also used to validate a soil erosion model, RUSLE, for its suitability in this type of landscape. The distribution and quality of POC in soils and sediments of the catchment were determined from physical properties and analysis of carbon and nitrogen, which could be used to evaluate the fate of POC in this tropical reservoir. Along with erosion and sedimentation rates, POC transport and fate could be interpreted. This chapter introduces the methods used to study POC transport and fate in João Penido reservoir catchment.

3.1 Field site João Penido reservoir, Minas Gerais, Brazil

João Penido reservoir (LAT: –21.675459, LONG: –43.394960) was constructed to provide a drinking water supply for the city Juiz de Fora in state Minas Gerais, Brazil (Figure 13). The watershed composes a minor drainage basin contributing to the 56,000 km^{-2} large Paraíba do Sul River watershed (Bucci et al, 2015: Pacheco et al, 2017). The reservoir composes a mesotrophic system with a medium level of water quality, which likely has been negatively affected by land use change in the watershed (Bucci et al, 2015). Catchment analysis showed that c. 17.7% of the total catchment area is forested and 4.0% compose deltaic areas. Deforested land is used for residential purposes (built-up areas compose 1.9% of the catchment land use) and grasslands (72.5% of the catchment) which are partly being used as pasture for cattle. Land in direct connection with the reservoir compose residential properties with a managed beachline and deforested shrubland exhibiting bank erosion (Figure 14).

Figure 13 Location of João Penido reservoir and catchment, Brazil.

The reservoir was built in 1934 and its sediments have accumulated on top of inundated soils over a period inclusive of the bomb tests in the 1960s, which provides radioactive caesium-137 (^{137}Cs) signals in the sediment column that can be used to calculate sediment accumulation rates. When the latter rates are combined with erosion rates calculated from ^{137}Cs signals in soils in the catchment, the overall local soil erosion rates for the reservoir catchment can be estimated. The organic carbon content and quality of the soils and sediments provide additional information about organic matter sources and decomposition states. The results can be used to express estimates of input and burial rates, C storage and turnover for POC in the reservoir sediments of João Penido.

Figure 14 Most of the catchment is deforested. View looking West towards the reservoir João Penido c. 100 m south of sampling location A.

3.1.1 Climate and vegetation

The Köppen classification system categorizes the region as *Cwa*, which composes a sub-tropical climate with two distinct seasons composed of dry winters in May–September and rainy hot summers in October–April (Bucci et al, 2015), with the hottest months having mean temperatures >22°C. The annual rainfall on a regional scale for south-eastern Brazil range between 1200–1600 mm year^{-1} (da Silva, 2004), and for Juiz de Fora, the city located closest to the study site at c. 3.8 km distance, the mean annual rainfall amounted to 1949 mm year^{-1} between 1979–2013, with a minimum and maximum ranging between 1347–2949 mm year^{-1} (Global Weather Data for SWAT). The vegetation of the watershed is mapped as semi-deciduous forest belonging to the Atlantic forest biome[6], however most of the catchment area comprises deforested grasslands. Atlantic forest composes a main hotspot for biodiversity conservation that has been reduced to less than 12% of its original extent of 1.5 million km^2 on the South American continent (Ribeiro et al, 2011). In Brazil, deforestation practices over the past 500 years have reduced the area of Brazilian Atlantic forest (Mata

---

[6] Mapa de Vegetacão do Brasil (1992)
http://mapas.mma.gov.br/mostratema.php?temas=vegetacao

Atlântica) to 7.6% of its original extent, historically replaced by plantations of sugarcane, coffee, cocoa, and eucalyptus, as well as pasture for livestock and the expanding infrastructure of urban areas, since the European colonization began in the 16th century (Colombo & Joly, 2010; Ribeiro et al, 2011). This history of land use change has not only led to severe habitat loss for indigenous species but also impacts the geomorphological landscape in areas where exposed soil which was previously stabilized by vegetation is readily degraded and lost through soil erosion.

3.1.2 Geology and soils

The lithology of the catchment comprises metamorphic rocks, such as Neoproterozoic schist and Rhyacian orthogneiss (CPRM 1:1M, 2018)[7]. The dominating soil type in the area is mapped as orthic ferralsol or ultisol (CPRM, 2016; DSMW 2003) (Figure 15), characterized by deep, highly weathered acid soil units that have undergone leaching and are mainly composed of SiO_2–Al_2O_3–Fe_2O_3–H_2O (Chesworth, 2008 pg.7). The solum of ferralsols are typically red or yellow colour due to the ferric state of iron (Fe) in minerals hematite and goethite, and kaolinite and gibbsite usually compose the main clay minerals in ferralsols (Chesworth, 2008 pg.7). Occurrences of mass movement of soil on the hillslopes were visible in the study area, which had caused scarring in the vegetation and provided unprotected patches of ground with higher erosion potential than protected soil covered by vegetation.

---

[7] URL: http://portal.onegeology.org/OnegeologyGlobal/
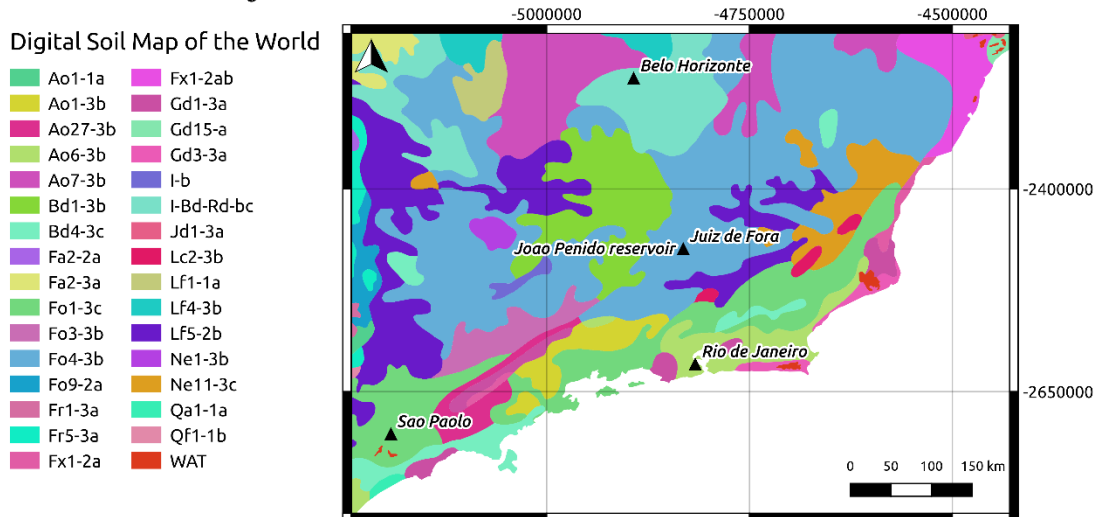
Figure 15 FAO soil unit classifications of the south-western region of Brazil, derived from Digital Soil Map of the World (DSMW, version 2.3, 2003). João Penido reservoir is located in a soil unit classified as Fo4-3b, orthic ferralsol. Source: Land and Water Development Division, FAO, Rome.

3.1.3 Terrain

The watershed covers an area of ca 772 km^2 and the elevation of the terrain ranges between ca 684–1061 m.a.s.l. (DEM analysis) with the main water body being located at ca 746 m.a.s.l. From DEM analysis catchment slope values could be calculated, ranging between 0–36.7 degrees with a mean of 10.8 degrees.

3.1.4 Catchment analysis by GIS and selection of sampling sites

By GIS-analysis several possible sites to study soil erosion were found in the study catchment. The basic criteria to find appropriate sampling sites for the fallout radionuclide study were the following: 1) non-forested soil that is subject to erosion due to rainfall erosivity, and 2) by categorisation of slope classes.

A total of 35 soil profile sites were studied at the three soil sampling locations (A, B, C) of this study, along with 20 reservoir sites selected for sediment core sampling (Figure 16). Sample sites were chosen to represent the range of topographic classes in the watershed, from floodplain and wetland sites to eroding hill sites.

70
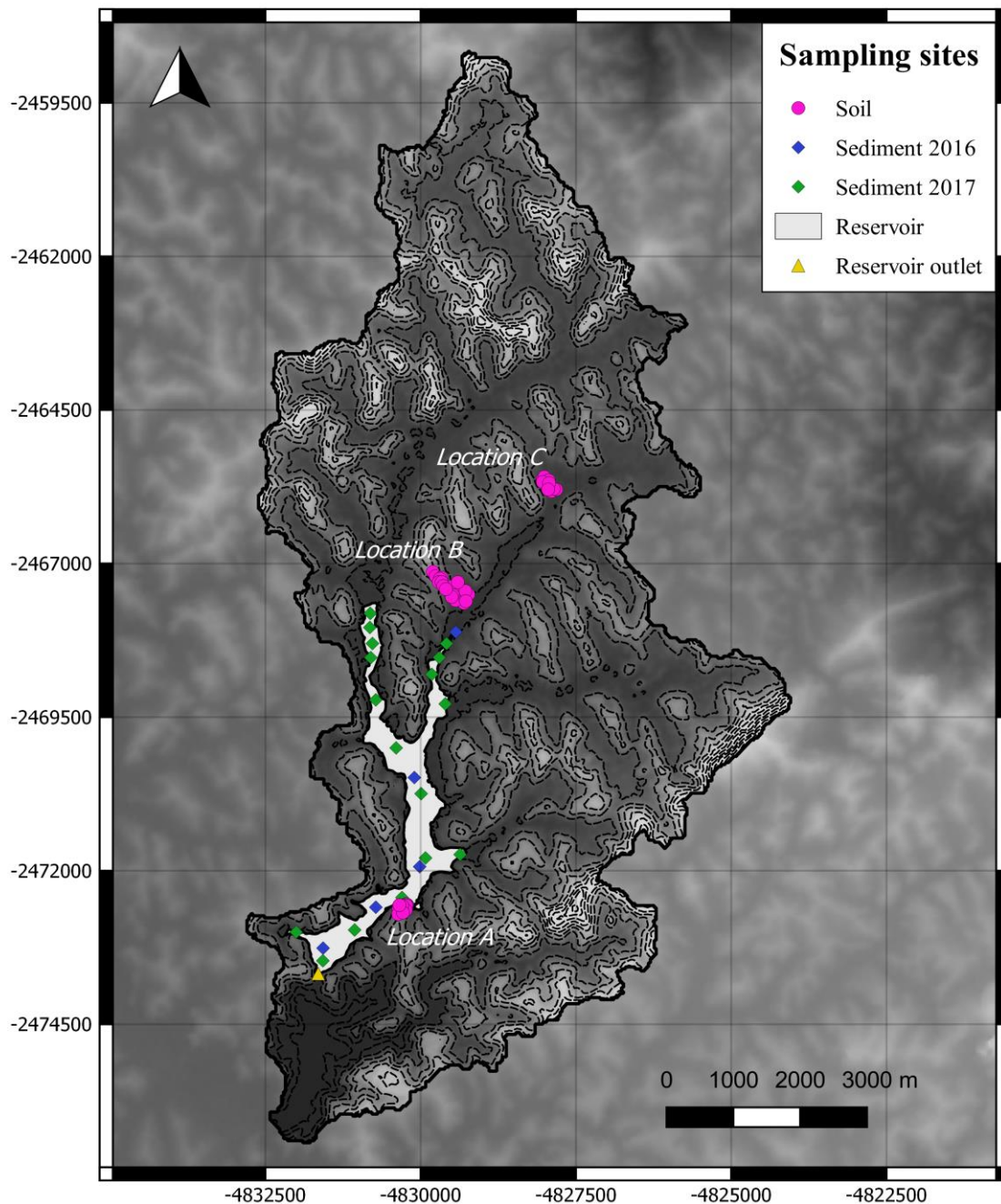
Figure 16 Soil sampling locations A, B, and C, and sediment sites of 2016 and 2017 sampling campaigns in João Penido watershed and reservoir. Elevation lines show 25 m contours. EPSG: 3857.

Figure 17 shows a slope map of the catchment divided into 4 classes: flat (0 degrees), near-flat (0–5 degrees), lightly undulating (5–20 degrees), moderate to strongly undulating (>20 degrees) (Table 1).
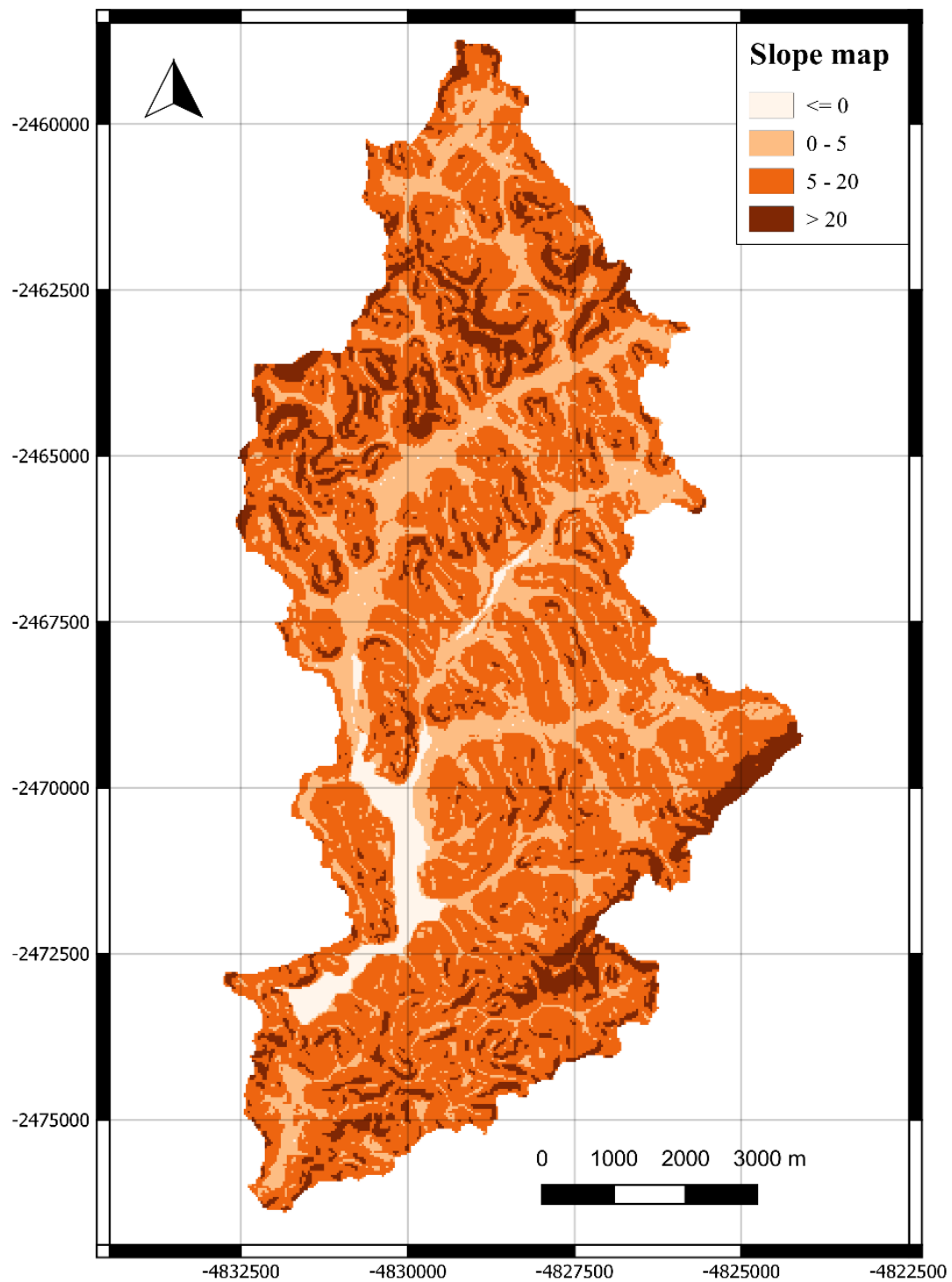
Figure 17 Slope analysis of the catchment of reservoir João Penido.

EPSG: 3857.

The sampling method chosen was stratified random sampling where sites were selected in each class by random point allocation with the built-in QGIS-tool *Random points inside polygons (variable) in QGIS*. Two topographic groups, areas subjected to 1) erosion and 2) deposition, were each further divided into three subclasses; erosion sites (>5 degrees) composed areas with flat, moderately undulating, and steep slope, and deposition sites (<5 degrees) were divided into seasonally drained sediments (colluvium), permanently waterlogged delta environment, and lakebed sediments (Table 1). The sites selected for FRN analysis compose downstream transects, which reflect the erosion from highest peak into the valley from the ridges between drainage sub basins (ridge transect), as well as from peak to the centre of drainage sub basins (through transect) (Figure 18, Figure 19). The number of sites comprise 22 profiles, summing up to 286 top soil samples for radionuclide analysis. The shrubland sites at location A were: JP2, JP4, JP7, JP11, JP15 (ridge) and JP8, JP9, JP13, JP14 (trough) (Figure 18); and for pasture sites at location B: JP22, JP24, JP36, JP35, JP34, JP32, JP30 (through) and JP17, JP18, JP19, JP20, JP21 (ridge) (Figure 19). Additionally, terrestrial sedimentation sites (colluvium) JP25, JP26 and JP28 at location B were sampled. For comparison 4 soil profiles from another site of pasture at sampling location C were investigated.

Sampling classes of soil and sediment sites

Groups	*Classes*
1) Erosion	A) Near-flat slope (<5 degrees)
	B) Moderate slope (5–20 degrees)
	C) Steep slope (>20 degrees)
2) Deposition	A) Seasonally drained sediments/colluvium (<5 degrees)
	B) Permanently waterlogged wetlands (0 degrees)
	C) Lakebed sediments (0 degrees)

Table 1 Groups of sampling areas and site classes for João Penido reservoir.
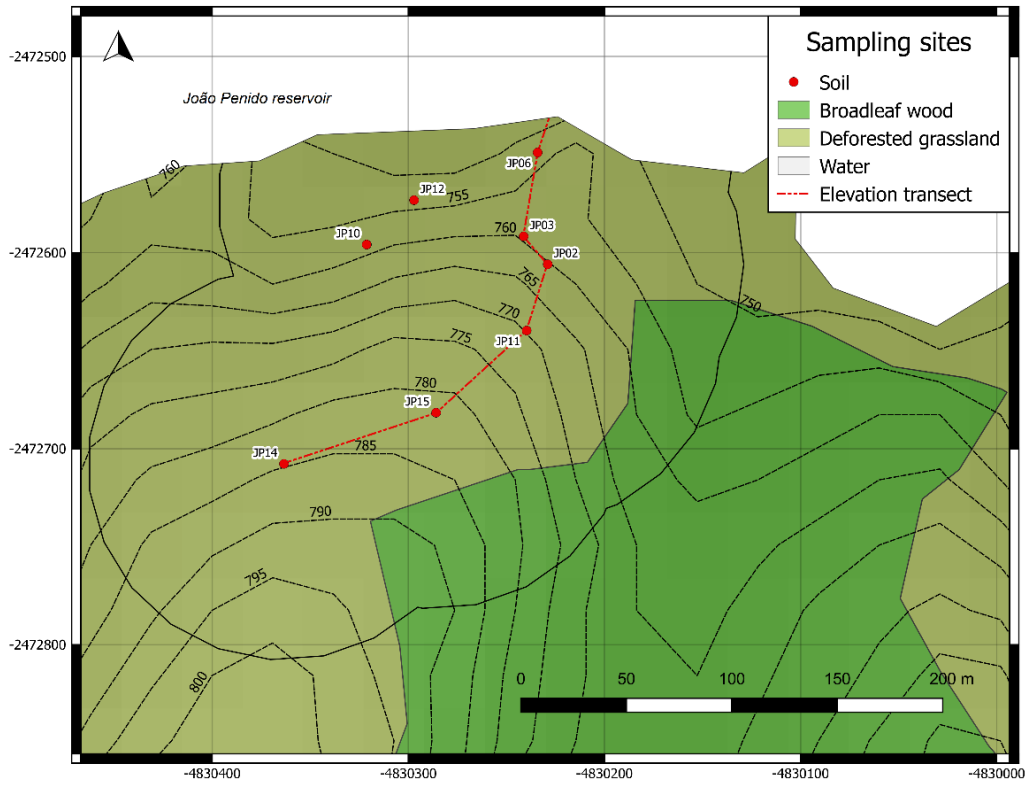
Figure 18 Location A sampling sites of shrublands.
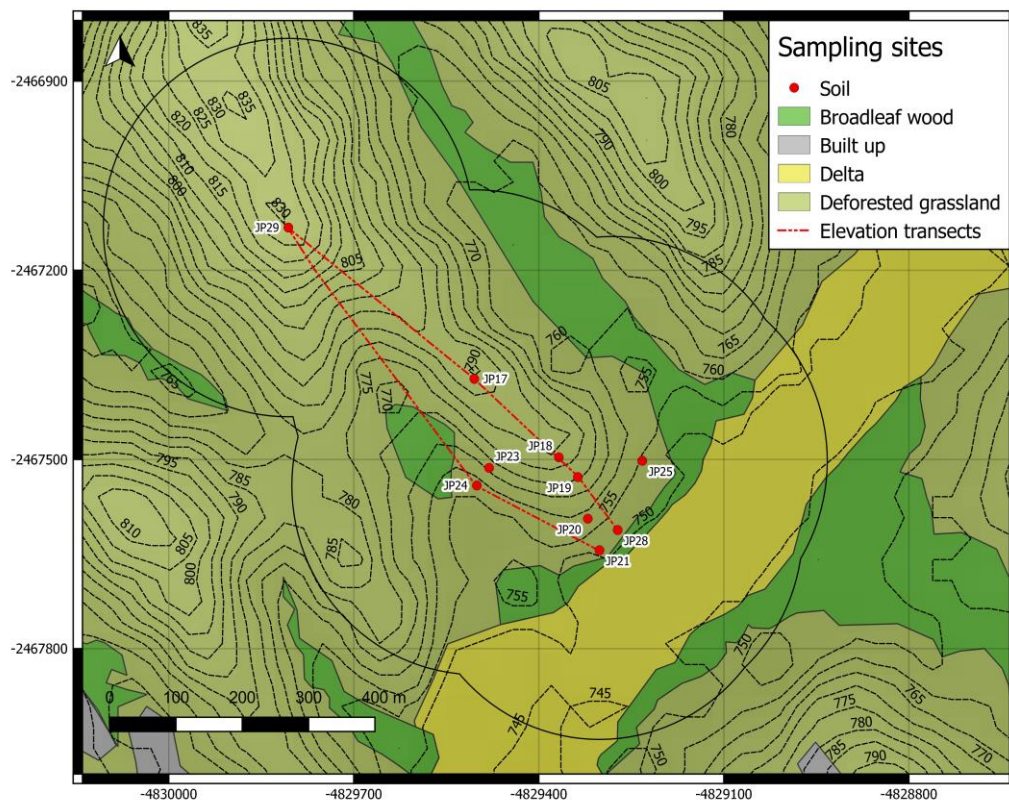
Figure 19 Location B sampling sites of pasture and colluvium.

Historical imagery (Google Earth Pro version 7.3.2) shows that soil sampling location B (pasture) was previously covered by forest, until it was deforested in years c. 1994–1995. Soil sampling location A (shrubland) appears to have been deforested before available imagery, which goes back to 1984.

3.2 Field sampling methods

Soil, sediment and water samples were collected during a field campaign in June 2016. Additional sediment cores were acquired in 2017.

3.2.1 Soil sampling

Sampling was conducted during the dry season in June 2016. A total of 560 soil samples from hand-dug pits were collected from the surface up to 80 cm depth. Custom-made samplers were used to obtain a vertical soil profile in 20 cm segments from which subsections were extracted by large spatula from every 2 cm sections in the top soils (<20 cm) and for subsoils (>20 cm) from every 5 cm section (Figure 20). Samples were stored in plastic zip-bags, after removal of larger particulates (e.g. stones, pebbles, roots). The samples were initially weighed, air dried and stored in room temperature before transport to University of Exeter laboratories, UK.

Figure 20 Soil survey and samplers.

3.2.2 Hydroacoustic sub bottom profiling

Sediment properties (e.g. thickness, texture and heterogeneity) and depth in lakes and reservoirs can be measured effectively with hydroacoustic survey methods, allowing for detailed lakebed analysis prior to field sampling of discrete sediment cores that provide spatially limited data, for instance when assessing contaminated watersheds (Anderson et al, 2013). Hydroacoustic measurements have been used to determine burial rates of OC in accumulation basins such as hydropower reservoirs through sub-bottom profiling (Figure 21), by investigation of post-flooding sediments that accumulate on top of pre-flood material (Mendonça et al, 2014). Since gases in sediment dilute backscatter signals, the precision of hydroacoustic techniques is limited where sediments and the water column have high gas content and, therefore, the approach is limited to watersheds that are mesotrophic or oligotrophic. However, the method is advantageous as a quick and non-invasive survey method, as hydroacoustic measurements provide physical sediment properties without any disturbance of the sediment column (Anderson & Pacheco, 2011).

Bathymetric survey lines were sampled in João Penido reservoir June 2016, with a parametric sub-bottom profiler (Innomar SES-2000) which detects

the lakebed at 100 kHz frequency. Transects were measured in lines zig-zagging across the reservoir surface along the entire length at a speed of 10 km h^{-1} (Fig). An onboard GPS receiver was used to geo-reference output data. Echograms were interpreted with Innomar ISE software (version 2.95). Sites of representative sedimentation in the reservoir were selected after visual inspection of these echograms.
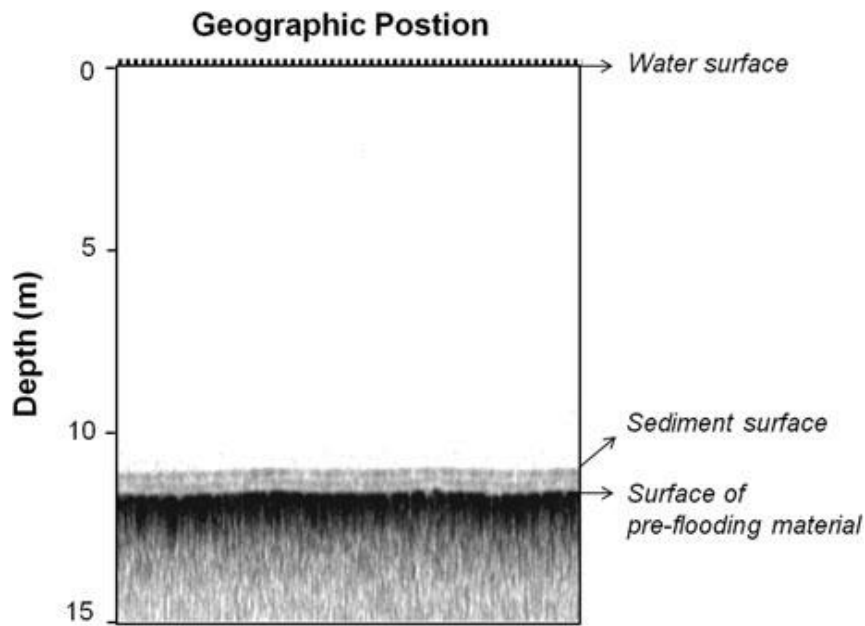
Figure 21 A typical sub-bottom profile sample. The distance between the sediment surface and the surface of the pre-flooding material gives the thickness of inputted sediment since damming, which can be used to calculate the volumes of post-flooding sediment. From Mendonça et al (2014).

The post-flooding layer composes a "fluffy" layer of sediment with high porosity and water content, and overlies pre-flood material, typically inundated catchment soils. This layer is representative of net deposition since the dam was created and contains trapped sediments that would otherwise have been transported downstream. Because of its porosity and low compaction, the surface layer is readily affected by resuspension, wave action and discharge from the reservoir outlet. Sampling of physical cores disturb the true post-flooding sediment surface and acquired cores might therefore suffer from some compaction. A comparison with acquired sub-bottom data help reveal the true thickness of these sediments in mesotrophic–oligotrophic systems. For João Penido reservoir, the method was

not sufficient to determine post-flooding sediment thickness, however it revealed the bathymetric trends and from the obtained survey lines, sediment core locations were selected for physical core sampling. The thickness of post-flooding sediment was then determined from these collected cores.

3.2.3 Sediment sampling

Reservoir sediment cores were retrieved from five selected locations in 2016 (Figure 22). Three field duplicate cores were retrieved at each sampling site with a gravity corer deployed by boat. The cores were subsampled by 2 cm sections, which were then weighed and air dried before transport and further analysis at University of Exeter. The lakebed sediment sampling sites were selected from initial studies of the sub-bottom profile of the reservoir. The sites were located at the delta outlet progressing towards the deepest sedimentation basin within the south-western part of the main water body, where sediment accumulation was considered regular. Additional sediment cores were sampled in 2017 (Figure 22). The reservoir outlet is located in the small bay south-west of SEDJP17. A total of 512 sediment subsamples were retrieved.
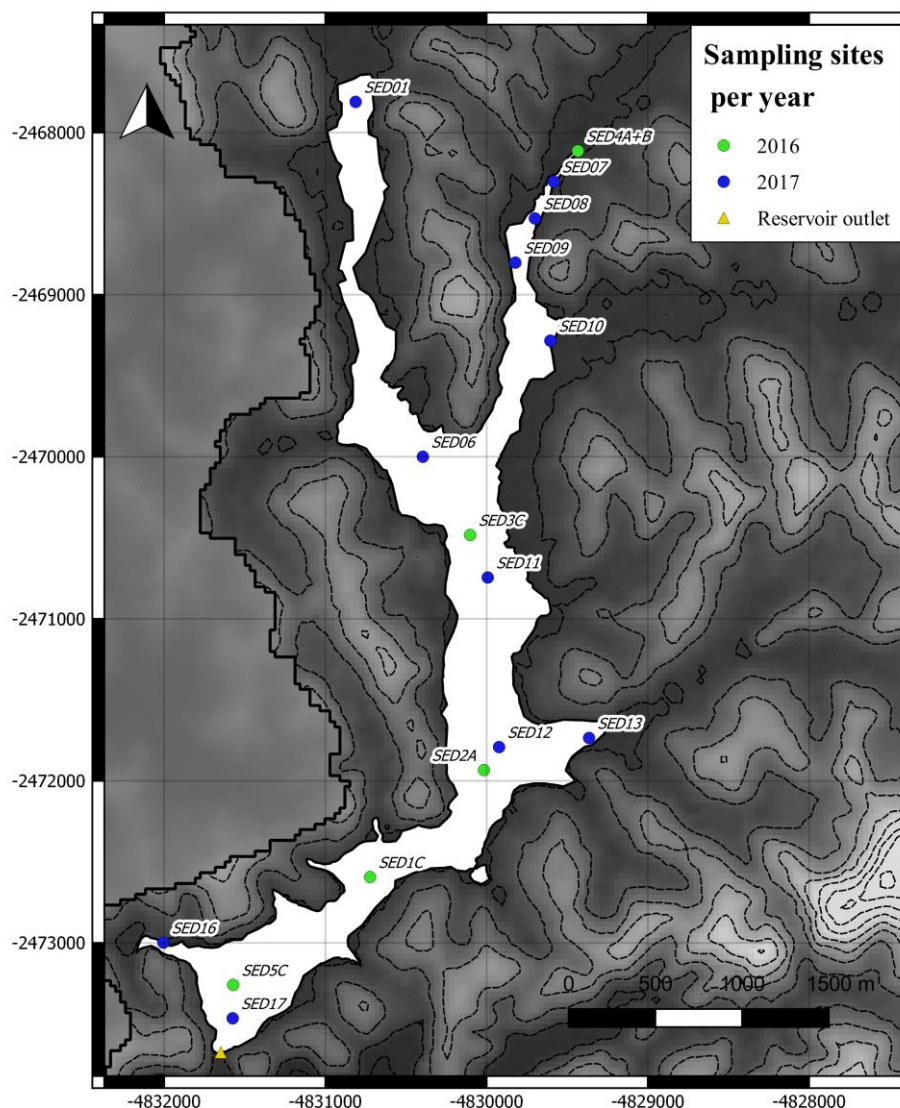
Figure 22 Sediment sites for sampling years 2016 and 2017.

3.3. Analytical methods

3.3.1 Bulk density, porosity and water content (WC%)

The particle density of minerogenic sediment particles is assumed to have a value of 2.65 g cm^{-3} (Avnimelech et al, 2001). In this study observations of the boundaries of low–high bulk density and the high–low bulk porosity between the post-flooding sediment overlying pre-flood material were used to determine the thickness of post-flooding sediment. Dry bulk density indirectly takes porosity into account and was determined by:

$$\rho_b = W_d/V_t$$

Where ρ_b is the bulk density, W_d is the dry weight, and V_t is the total volume. The OM density in samples was determined as the product of OM% and sample total bulk density. Bulk density was determined for soil and sediment samples, while porosity and water content was determined for sediment samples only, as soils showed varying field moisture.

3.3.2 Particle size analysis

Particle size analysis (PSA) was performed on the <2000 μm fractions of 3 sediment cores and 3 soil cores, totalling 90 samples. Along with manual sieving, an automatic dry shaker sieving system was used to separate fractions: >2000 μm, 2000–250 μm, 250–63 μm, and <63 μm. Larger mineral fractions and plant fragments such as roots in soils and wood artefacts in sediments, were discarded in the field.

3.3.3 Total Carbon, Total Nitrogen and C/N analysis

Total organic carbon and total nitrogen analysis and C/N ratio analysis was undertaken using a *ThermoScientific Flash 2000 Organic Elemental Analyzer.* C/N ratios were used to determine the provenance of organic matter in soils and sediments on duplicates of 100 sediment and 50 soil samples.

To determine the organic carbon content of the samples it is necessary to remove inorganic carbon from the samples. Different methods have been used to remove carbonates from soil and sediment samples as a pre-treatment for TOC analysis, for instance wet oxidation (Walkley-Black method) which consists of step-wise addition of acid washing. Dhillon et al (2015) evaluated two pre-treatment methods with HCl (acid addition and acid fumigation), and while their results were similar for both methods, greater accuracy and precision were reached with the acid fumigation pre-treatment. Therefore, acid fumigation was used as a pre-treatment for 24 hours on duplicate samples before C/N analysis.

The soil and sediment samples were subsampled to 15–20 mg into tin capsules on a Sartorius MC5 balance with 3-digit accuracy. Samples that required pre-treatment were initially weighed into silver capsules, treated for 24 hours by HCl acid fumigation in a desiccator and after pre-treatment

encapsulated into larger tin capsules. Between weighing and analysis, the samples were stored in a desiccator. Ethylenediaminetetraacetic acid (EDTA) standard (*BDH AnalaR*, assay 99.0%) was similarly weighed to 2.8–3.2 mg standards, three occurring at the beginning of each sample batch as initial control standards, and 2.5–3.5 mg control standards, occurring at every 10th sample slot as in-between-sample controls within the batch. Blanks (empty capsules) were run at the beginning and end of each batch, together with one empty slot at position 62. The calculated error derived from EDTA standards for TC analysis was 0.24%.

3.3.4 Fractionation by size and density

To understand the geochemical imprint of the aggregate-bound soil organic matter with respect to OM from other sources in the sediments, density fractionation was done on 15 soil and sediment samples. These samples were selected from four soil cores and four sediment cores, where 2 samples from the top layer (2–4 cm) and sub layers (18–20 cm) were selected from each core respectively. For two sediment cores, samples of sub bottom pre-flooding material were selected to determine the characteristics of soils underlying the post-flooding sediment. Two soil cores were from land used as pasture and two cores from non-managed shrubland. The sediment cores were from the deepest part of the reservoir and from a site in the central part of the main water body. Density separation of particles was done with sodium-polytungstate (SPT) (CAS#12141-67-2) with a density of 1.85 g cm^{-1} into a light fraction (LF) and heavy fraction (HF) for three size groups (2000>250 µm, 250>53 µm, 53 µm) previously separated by wet sieving, following the method by Six et al (1998) in Figure 23. The separated fractions were weighed and analysed for C/N, as described above.
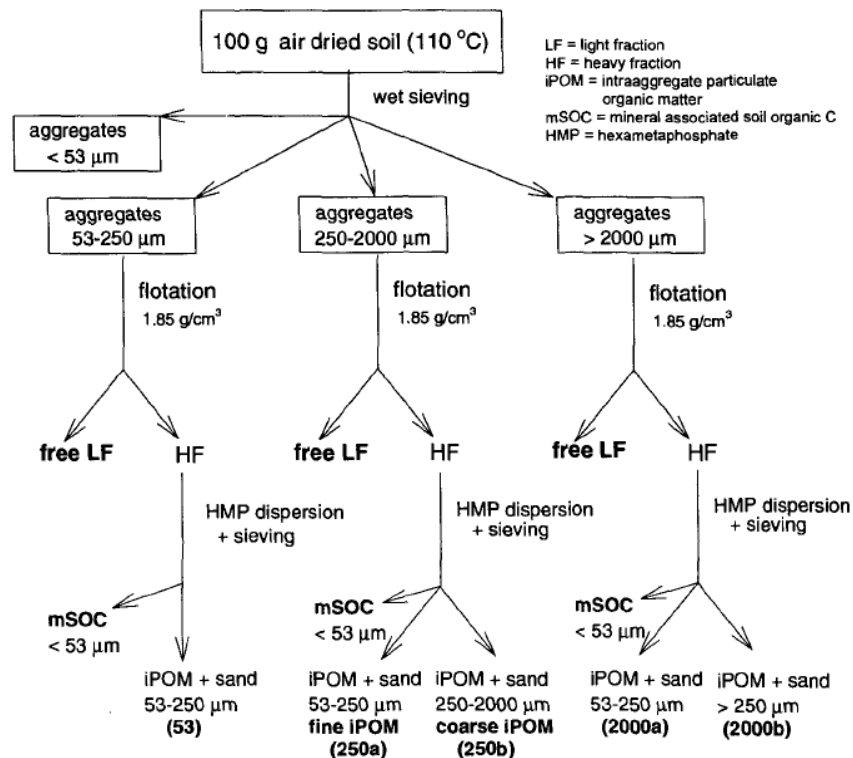
Figure 23 Wet-sieving and density fractionation method. From Six et al (1998).

3.3.5 Loss on ignition (LOI)

Loss on ignition (LOI) was done on 401 soil (*N*=219) and sediment (*N*=182) samples from the catchment slopes and the reservoir of João Penido watershed. The samples were oven-dried at 100°C in pre-weighed crucibles overnight, before initial sample weighing. The samples were then combusted at 550°C for 4 hours, before weighing to account for weight loss of the organic matter. The weight difference was noted on a 4-decimal balance. The carbonates were determined similarly by the gravimetric method after further combustion at 925°C for an additional (1) hour, for 305 of the samples. In a study by Pribyl (2010) it was concluded that a conversion factor of 58% assumed OC in OM (e.g. Brady et al, 1984) compose an overestimation, and should be reduced to 50%. In this study the relationship between OC from loss on ignition (LOI) analysis and C/N data from 115 samples were used to find a suitable conversion factor. By comparing the ratio of OC concentrations from C/N analysis and the OM content from LOI analysis, mean conversion factors of 25% (*N*=65, *sd*=0.11) for sediment samples and 20% (*N*=50, *sd*=0.07) for soil samples were found suitable (Figure 24). Very low sediment OC concentrations are common for the region and biome,

for instance Mendonça et al (2016) found average reservoir sediment OC concentrations of 1.2–3.1% in pelagic sediment and 1.8–2.5% for reservoir margin sites.

For this study the OC content derived from LOI data in soils and sediments was calculated according to:

$$SOC = cf \times SOM$$

Where the conversion factor *cf* was set to 20% and 25% for soil and sediment samples, respectively.

a)

b)
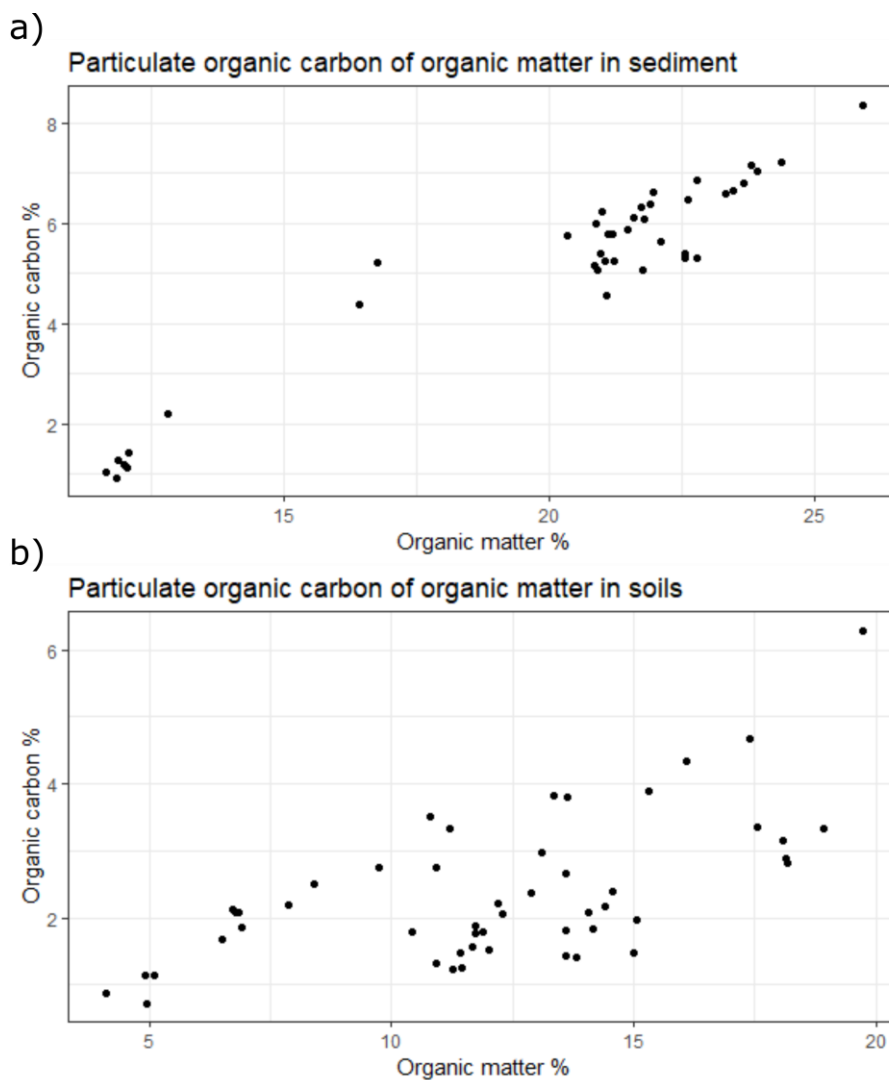
Figure 24 TOC% in (particulate) organic matter content of a) sediments and b) soils.

Figure 25 shows the sites of LOI samples of soil profiles dug on the hillslopes of João Penido at sampling locations A, B, and C. These concentrations of SOC were used to estimate a carbon budget for the terrestrial SOC in the catchment. The budget was used to estimate transport rates of soil derived POC from slopes to sites of deposition.
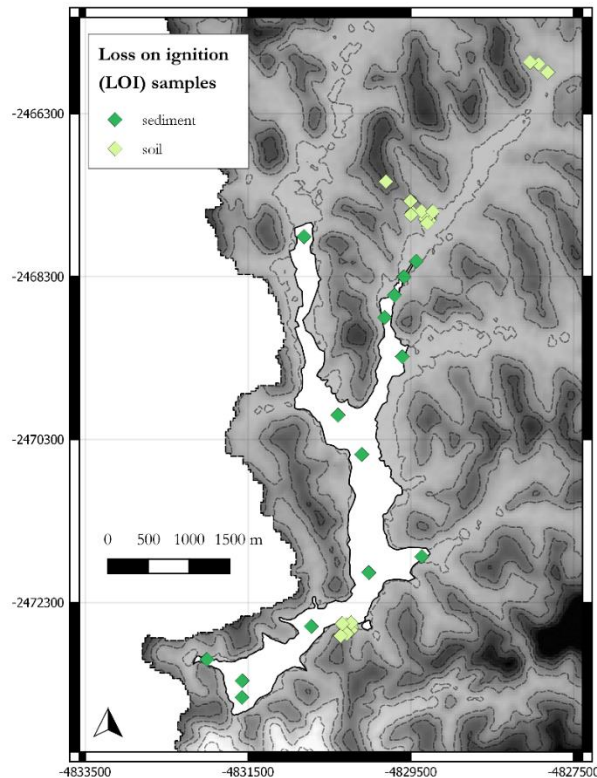
Figure 25 Sampling sites of loss on ignition (LOI) samples in João Penido catchment.

For interpretation purposes gap-filling was required for some reservoir sediment cores where POC% data was incomplete, the mean of values from the one sample directly above and the sample directly below this missing sample in the core profile were used for interpolation. This gap-filling data is clearly marked with bold font in the data tables, and SAR and OC burial values calculated from these artificially gap-filled data are marked with an asterisk (*).

Soil POC inventories POC_{inv} (g m^{-2}) were calculated for the <2 mm fraction according to the following modified equation (this study is not taking the rock fraction into account because the samples were sieved to <2 mm) from Berhe et al (2008):

$$POC_{inv} = \sum \Delta Z_i \times \rho \times (\%POC_i \times 100)$$

Where ΔZ_i is the depth increment in the profile, ρ is the bulk density (g/cm^3), %POC is the concentration of organic carbon in the <2mm fraction in each sample increment.

3.3.5.1 Sediment accumulation rates and organic carbon accumulation

The sediment accumulation rate (SAR) was estimated using 1) post-flooding sediment thickness and 2) fallout radionuclides. The first method was based on direct observations at each site where sediment cores were retrieved and it was possible to distinguish between pre- and post-flooding material. SAR determined from sediment thickness, where the sediment is assumed to have accumulated continuously over the period from reservoir completion (flooding) to sampling date, can only provide an average linear SAR value (cm year^{-1}). By using the radionuclide $^{210}Pb_{ex}$, the average SAR for each slice of sediment (2 cm thickness) can provide more in-depth information on how SAR has varied over time from flooding to sampling date, by using an appropriate conversion model. SAR rates from $^{210}Pb_{ex}$ conversion models give mass accumulation per area unit per year (kg m^{-2} year^{-1}).

3.3.5.2 Sediment accumulation rate from sediment thickness

The sediment thickness was determined by the presence of pre-flooding material with depth, SAR (cm year^{-1}) was then calculated by the following:

$$SAR = \frac{d}{t_r}$$

Where d is the depth of the pre-flooding material and t_r is the reservoir age, which was 82 years for the 2016 campaign and 83 years for the additional 2017 sediment core collection.

SAR was also calculated from ^{137}Cs and $^{210}Pb_{ex}$ activities and inventories of the sediment cores, using the CRS (3.3.7.18) and CIC models (3.3.7.19).

3.3.5.3 Organic carbon accumulation rates

The OC accumulation rate (g cm^{-2} year^{-1}) was calculated for sediment cores where OC data had been obtained, by the following adapted OC burial expression (Mendonça et al, 2015):

$$Burial_{OC} = \frac{m_C}{A}/t_r$$

Where m_C is the sum of C mass (g) in the post-flooding sediment samples down to the pre-flooding material, A is the sediment core surface area (2.8 x 10^{-3} m^2), and t_r is the reservoir age (defined in 3.3.5.2 Sediment accumulation rate from sediment thickness).

3.3.6 Fallout radionuclides (FRN) study in João Penido catchment

3.3.6.1 Measurement

Soil and sediment samples, that had been previously air- and oven-dried, ground, and sieved to <2 mm fraction, were stored in plastic containers with screw caps for radionuclide analysis. To obtain the $^{210}Pb_{ex}$ concentration, the sample containers were sealed with electric tape for a minimum of 21 days before measurement, to provide an isolated environment in which the gaseous ^{222}Rn decay product $^{210}Pb_{ex}$ would be preserved (Mabit et al, 2014). FRN activities were measured with shielded *ORTEC* coaxial high-purity germanium (HPGe) detectors with multi-channel buffers for γ-ray spectrometry. The sample weight ranged between 50–100 g for HPGe–detector soil samples, and between 2–7 g for smaller well–detector sediment samples. The counting time was set to 86400 s for all measurements.

The spectral photopeak for ^{137}Cs occurs at 662 keV, while the spectral photopeaks for ^{210}Pb and ^{226}Ra (or in fact its daughter ^{214}Pb (Mabit et al, 2014)) occur at 46.5 keV and 352 keV respectively. Gamma emissions of ^{137}Cs were measured on a total of 336 soil samples and 76 sediment samples, while photopeaks for $^{210}Pb_{ex}$ calculation were measured on 254 soil samples and 76 sediment samples. $^{210}Pb_{ex}$ was calculated as the difference between total ^{210}Pb and supported ^{210}Pb, according to:

$$^{210}\text{Pb}_{ex} = {}^{210}\text{Pb}_{tot} - {}^{210}\text{Pb}_{supp}$$

Where $^{210}\text{Pb}_{supp}$ is the ^{226}Ra-supported ^{210}Pb concentration of individual samples (Porto et al, 2014). Typically, ^{210}Pb is not in equilibrium with ^{226}Ra, due to upward diffusion and escape of ^{222}Rn in soils, a loss is normalized for by multiplying the activity of ^{226}Ra by a reduction factor (Porto et al, 2014). The reduction factor can be calculated from the ratio of $^{210}\text{Pb}_{tot}$ and ^{226}Ra activities from subsoil samples (assuming no addition of unsupported ^{210}Pb to subsoil). In this work, the reduction factor was calculated to a value of 0.8, which was used for all sample profiles in João Penido catchment.

In principal, the activities of the two radionuclides ^{210}Pb and ^{226}Ra are necessary to calculate the activity of $^{210}\text{Pb}_{ex}$ (Mabit et al, 2014), by simple subtraction of radionuclide activities:

$$^{210}\text{Pb}_{ex} = {}^{210}\text{Pb}_{tot} - {}^{226}\text{Ra}$$

The concentrations of each element were calculated separately before subtraction to achieve $^{210}\text{Pb}_{ex}$ concentrations. Photopeaks recorded by a multichannel buffer (MCB) were interpreted by ORTEC Maestro® software.

3.3.6.2 Activity calculation

The equation used to calculate the activity of a sample follows the expression (Mabit et al, 2014):

$$A = \frac{N \lambda t_c e^{\lambda t_0}}{\varepsilon I_y M t_c (1 - e^{\lambda t_c})}$$

where A is the concentration of activity (activity per mass) of the radionuclide (Bq kg^{-1}), N is the net peak area, λ is the decay constant (ln2/$t_{1/2}$)*, t_c is the counting time, t_0 is the difference in time between sampling and measurement (years), M is the mass of the sample (kg), ε is the absolute efficiency, and I_y is the gamma intensity or probability of emission. This equation can be simplified to:

$$A = \frac{N e^{\lambda t_0}}{\varepsilon I_y M t_c}$$

which is the equation used for the ¹³⁷Cs and ²¹⁰Pb_ex measurements in this study. Each calculated activity was corrected ("corrected activity") by the number of days between sampling and analysis.

3.3.6.3 Areal activity

The areal activity was calculated by the following equation:

$$A_S = \Sigma C_i \rho_i H_i$$

Where A_S has the unit (Bq m⁻²), and C_i is the activity of the ith sample depth increment (Bq kg⁻¹), ρ_i is the bulk density of the ith sample increment (kg m⁻³), and H_i is the depth of the ith sample increment (m).

3.3.6.4 Reference sites

Soil cores from reference sites should have the following characteristics: 1) a pronounced decreasing concentration of ¹³⁷Cs activity with increasing core depth, with 80–90% of the total activity present in the top 20 cm of soil, and 2) low coefficient of variation (<30%) (Mabit et al, 2014).

Reference inventories were derived for one chosen soil profile, the pasture site JP17, which was a site assumed to 1) undergo neither net erosion nor net deposition, 2) displayed a continuously decreasing ¹³⁷Cs inventory with depth and 3) had 80% of the total activity of ¹³⁷Cs in the top 20 cm of the sampled soil profile. For comparison, the reference value was compared with the average ¹³⁷Cs inventory from all measured profiles in each land use category, as an alternative reference inventory calculation, following a study by Aldana Jague et al (2016).

3.3.6.5 Inventory calculations

The redistribution of soil is calculated on the basis that an eroding site has an inventory lower than the reference site, whilst a site of sediment accumulation is characterised by higher inventories.

The inventory, $^{137}Cs_{inv}$, was calculated by:

$$^{137}Cs_{inv} = A \times \rho \times d$$

Where *A* is the concentration of activity (Bq kg^{-1}) in a sample, *ρ* is the soil bulk density (kg m^{-3}), and *d* is the depth (m) of the sample. The inventory is reported in units of Bq m^{-2}. The total inventory of the soil profile is the sum of the sample inventories of that profile. Inventories for $^{210}Pb_{ex}$ were calculated by the same procedure.

3.3.6.6 Quality control

Four main sources of error commonly influence the determined ^{137}Cs inventory for a site: 1) sampling technique, 2) pre–analytical sample fractionation, 3) quantifying randomness in radioactive decay, and 4) methods to determine the limit of detection (LOD) (Parsons & Foster, 2011).

In-house standards were used to determine detector efficiencies and potential instrumental drift. The in-house standards used in this study for detectors 1 and 16 (soil samples) and well-detector 11 (sediment), previously prepared from reference materials, are listed in Table 2.

Radionuclide standards

Radionuclide	Activity (Bq)	Standard ID	Weight (g)	Detector
^{137}Cs	6.75	SH2	50	1, 16
^{137}Cs	13.5	SH1	100	1, 16
^{210}Pb	423.904	CA13	100	1, 16
^{226}Ra	20.08	CA38	100	1, 16
^{137}Cs	0.79	SH4	5.8208	11
^{210}Pb	52.988	CA19	10.2	11
^{226}Ra	10.4	CA42	5.6	11

Table 2 In-house radionuclide standards used at University of Exeter laboratories.

3.3.6.7 Efficiency calibration

Various parameters need to be considered when determining the detector efficiency: counting geometry, sample matrix, detector type and properties,

among others (Mabit et al, 2014). The equation used to calculate the detector efficiency (%) is:

$$\varepsilon = N/(At_c I_y)$$

where ε is the absolute efficiency, N is the net peak area, A is the activity of the sample (Bq), t_c is the counting time (s), and I_y is the gamma intensity or probability of emission (Table 3) (Mabit et al, 2014).

Radionuclide properties

Radionuclide	Half-life (years)	Level energy, E_y (keV), photopeak	I_y, Probability of emission (photons decay^{-1})
^{137}Cs	30.17	661.66	0.85
^{210}Pb	22.26	46.539	0.0425
^{226}Ra	1600	352	

Table 3 Radionuclide properties.

Calibration of the detectors was done by direct calibration with prepared standards that had similar counting geometry (volume and area) and matrix to those of the samples, for each measured radionuclide (^{137}Cs, ^{210}Pb, ^{226}Ra) (Table 2). Detector efficiencies were determined from in-house standards for the three radionuclides and are summarized in Table 4.

Average detector efficiency (%)

	Radionuclide	In-house standard	Detector efficiency %
Detector 1	^{137}Cs	SH1	1.3
	^{210}Pb	CA13	0.2
	^{226}Ra	CA38	0.7
Detector 16	^{137}Cs	SH1	2.1
	^{210}Pb	CA13	0.3
	^{226}Ra	CA38	1.0
Well-detector 11	^{137}Cs	SH4	10.5
	^{210}Pb	CA19	1.2
	^{226}Ra	CA42	5.6

Table 4 Average detector efficiencies for detectors used in this study.

3.4.9.8 Uncertainties

Relative uncertainty was calculated using the quadratic sum of uncertainties of the input parameters N, ε, while assuming that the uncertainties of M, I_y were

sufficiently low to be neglected (IAEA, 2014). The background noise can be divided into two main sources: 1) internal signals from the material of the detector itself, and 2) external signatures from natural radioactivity of for instance radon and cosmic radiation (Mabit et al, 2014).

The lower limit of detection (LLD) can be calculated by:

$$LLD = 4.66 \frac{\sqrt{B}}{\varepsilon I_y \sqrt{T}}$$

Where B is the background count rate (counts s^{-1}), T is the counting time (s), ε is the absolute efficiency, and I_y is the gamma intensity or probability of emission for the radionuclide. This expression assumes a 95% degree of confidence to detect activity in excess of the background signal.

The minimum detection activity (MDA), also the concentration of activity in a sample mass, similarly corresponds to:

$$MDA = 4.66 \frac{\sqrt{B}}{\varepsilon I_y M \sqrt{T}}$$

where M, the mass of the sample, is added to the previous equation for LLD.

3.3.6.9 Measurement precision

Measurement precision depends on the activity of a sample, the detector efficiency and counting time (Owens et al, 1996). In this study, the method to determine measurement of precision followed:

$$M_e(\%) = 1.96 \frac{\sqrt{A}}{A} \times 100$$

Where A is the net area of the activity of the radionuclide and 1.96 representing the 95% confidence level. Average sample M_e for detectors is summarized in Table 5.

Sample M$_e$% per detector

	Radionuclide	Me%
Detector 1	^{137}Cs	8.40
	^{210}Pb	9.21
	^{226}Ra	5.20
Detector 16	^{137}Cs	8.11
	^{210}Pb	8.77
	^{226}Ra	5.99
Well-detector 11	^{137}Cs	8.47
	^{210}Pb	14.98
	^{226}Ra	7.32

Table 5 Average sample measurement precision (M$_e$%) per detector.

3.3.6.10 Conversion models for ^{137}Cs and ^{210}Pb$_{ex}$

Conversion models are used as mass balance calibration to provide rates of erosion and accumulation of sediments from radionuclide inventories, as radionuclide inventories alone only describe current distribution (Parsons & Foster, 2011). Conversion models that are applicable to ^{137}Cs in uncultivated soils and colluvium are the profile distribution model (PDM) and the diffusion and migration model (DMM) (Walling et al, 2002; Guzmán et al, 2013; Mabit et al, 2014). The theoretical conversion models used in this study are profile distribution model for uncultivated soils for ^{137}Cs inventories, and the diffusion and migration model for both ^{137}Cs and ^{210}Pb$_{ex}$ inventories in terrestrial soils and colluvium. For reservoir sediments the constant rate of supply (CRS) for ^{210}Pb$_{ex}$ was used (described 3.3.6.16). In any of the following conversions, it was assumed that the majority of ^{137}Cs fallout occurred in 1963 due to bomb testing, hence this is the only source accounted for in the interpretation of ^{137}Cs-data for Brazilian soils. It was also assumed that ^{210}Pb fallout is continuous over time, displaying a reference inventory that is in steady state balance (Mabit et al, 2014). Factors required for conversion models are summarized in Table 6.

Factors for conversion models

Model	Radionuclide	Variable	Parameter input	Unit
Profile distribution model	^{137}Cs	h_0	relaxation depth	kg m^{-2}
Diffusion and migration model	^{210}Pb$_{ex}$	D	diffusion coefficient	kg^2 m^{-4} year^{-1}
		H	relaxation mass depth	kg m^{-2}
		V	migration coefficient	kg m^{-2} year^{-1}

Table 6 Factors needed for conversion models used in this study.

3.3.6.11 Relaxation depth (h_0)

h_0 is the profile shape factor, commonly known as the relaxation depth, that describes the exponential decline of radionuclide concentration with depth in a soil or sediment profile. The deeper any radionuclide activity occurs, the higher the value for h_0 is. An exponential function fitted to radionuclide concentrations with depth using a least-squares curve, gives the depth of fallout radionuclide penetration into the soil profile at the reference site (Porto et al, 2001; Zapata, 2002). $h0$ was determined from linear regression of calculated values of mass depth and mass activity density. In this work, $h0$ for reference site JP17 was calculated to 95.2 kg m^{-2}, ignoring layers in the soil profile with no detectable ^{137}Cs activity.

3.3.6.12 Particle size correction factor (P_{cf})

P is the particle size correction factor that describes the grain size selectivity potential during erosion and sedimentation processes, to account for preferential adsorption of radionuclides to finer mineral fractions and the under- and overestimations of soil redistribution that occur due to the property of this radionuclide (Mabit et al, 2014). The difficulties of deriving the P factor arise from complicating factors such as the nature of soil type, behaviour of the studied radionuclide, preferential removal of fine fractions due to erosion process etc. The concept of P has been explained for the purpose of introducing this factor. In this study P was set to a constant of 1.

3.3.6.13 Diffusion coefficient (D) and downward migration rate (V)

The diffusion coefficient can be approximated from the depth distribution of radionuclide concentrations by the following expression (Walling et al, 2002):

$$D \approx \frac{(N_p - W_p)^2}{2(t - 1963)}$$

Where t is the year of soil collection, Np is the mass depth where the concentration of the measured radionuclide has been reduced to $1/e$ compared to its maximum concentration in the soil core (kg m^{-2}), and Wp is the mass depth

of the maximum radionuclide concentration (kg m^{-2}). D is commonly in the range of 20–50 (Zapata, 2002). Similarly, the downward migration rate (V) is approximated by (Walling et al, 2002):

$$V = \frac{W_p}{t - 1963}$$

V typically composes a number 0.2–1 (Zapata, 2002). For ^{137}Cs profiles D was calculated to 22.56 for JP17, while V was calculated to 1.08. For ^{210}Pb D was calculated to 0.88, and V was calculated to 0 (Table 7).

Diffusion coefficients and downward migration rate

Reference core	D ^{137}Cs	V ^{137}Cs	D ^{210}Pb$_{ex}$	V ^{210}Pb$_{ex}$
JP17	22.56	1.08	0.88	0

Table 7 Diffusion and migration constants for reference soil cores.

3.3.6.14 Profile distribution model (PDM)

The profile distribution model uses an exponential relationship for the vertical inventory of ^{137}Cs in an undisturbed soil profile, which is calculated by the following equation (Zhang, 1990; Rodway-Dyer et al, 2010):

$$A'(x) = A_{ref}(1 - e^{-\frac{x}{h_0}})$$

Where $A'(x)$ is the concentration ^{137}Cs above depth x (Bq m^{-2}), A_{ref} is the reference inventory of ^{137}Cs (Bq m^{-2}), x is the depth from the soil surface (kg m^{-2}), and h_0 is the profile shape coefficient or relaxation depth (kg m^{-2}). h_0 is calculated by least squares regression between the variables ln $A(x)$ and the cumulative mass depth (kg m^{-2}), as described in e.g. Porto et al (2001) and Martinez et al (2009).

For an eroding site, the following expression describes soil loss as a negative value (Porto et al, 2001; Walling et al, 2004):

$$Y = \frac{10}{(t-1963)P} \ln\left(1 - \frac{X}{100}\right) h_0$$

Where Y is the yearly soil loss (kg m^{-2} year^{-1}), t is the sampling year, P is the particle size correction factor, and h_0 is the relaxation depth (kg m^{-2}), and X is the percentage of reduction of total ^{137}Cs inventory (%) which is calculated by:

$$X = (A_{ref} \times A)/(A_{ref} \times 100)$$

Where A_{ref} is the reference inventory of ^{137}Cs (Bq m^{-2}), and A is the total ^{137}Cs inventory (Bq m^{-2}) for a sampling point.

For an accumulating site, the following equation describes deposition (Rodway–Dyer et al, 2010; 2013):

$$R' = \frac{A_{ex}}{\int_0^t A(0)(t')e^{-\lambda(t-t')}dt'} = \frac{A_u - A_{ref}}{\frac{1}{\int_S RdS}\int_S A_{ref}(1 - e^{-R/h_0})dS}$$

Where R' is the yearly increase of soil (kg m^{-2} year^{-1}), A_{ex} is A_u–A_{ref} (where A_u is the radionuclide inventory of the site of the soil core), $A(0)(t')$ is the concentration of ^{137}Cs activity in accumulated soil for the year t', λ is the decay constant for ^{137}Cs (0.023 year^{-1}), and S comprises the area of upslope erosion (m^2) (Porto et al, 2004; Rodway–Dyer et al, 2010).

3.3.6.15 Diffusion and migration model (DMM)

The diffusion and migration model was used to interpret ^{137}Cs and ^{210}Pb$_{ex}$ inventories in terrestrial soil and sediment samples. This model requires input parameters such as the diffusion coefficient (D) with a unit of kg^2 m^{-4} year^{-1}, the downward migration rate (V) with a unit of kg m^{-2} year^{-1}, and the relaxation depth (h_0) with the unit kg m^{-2}.

The radionuclide concentration at the soil surface can be approximated as (Walling et al, 2008):

$$C_u(t) \approx \frac{I(t)}{H} + \int_0^{t-1} \frac{I(t')e^{-R/H}}{\sqrt{D\pi(t-t')}}e^{-\frac{V^2(t-t')}{4D}-\lambda(t-t')}dt'$$

Where $I(t)$ is the yearly flux of deposited radionuclide (Bq m^{-2} year^{-1}).

For sites of erosion an erosion rate R can be determined from reduction of the radionuclide inventory $A_{ls}(t)$ (Bq m^{-2}), which is (A_{ref}–A_u), together with the surface soil concentration $C_u(t')$, according to:

$$\int_0^t PRC_u(t')e^{-\lambda(t-t')}\, dt' = A_{ls}(ts)$$

For sites of deposition, the deposition rate R' is estimated from concentrations of the measured radionuclide in sediment $C_d(t')$ by the excess inventory of the core $A_{ex}(t)$, by (Walling et al, 2008):

$$R' = \frac{A_{ex}}{\int_0^t C_d(t')e^{-\lambda(t-t')}dt'} = \frac{A_u - A_{ref}}{\int_0^t C_d(t')e^{-\lambda(t-t')}dt'}$$

Where radionuclide concentrations in deposited sediment $C_d(t')$ is determined from:

$$C_d(t') = \frac{1}{\int_S RdS}\int_S P'PC_u(t')RdS$$

3.3.6.16 Conversion models for $^{210}Pb_{ex}$ in reservoir sedimentation settings

Several conversion models have been developed specifically for $^{210}Pb_{ex}$ that are typically used for depositional settings, e.g. constant rate of supply (CRS) model, constant initial concentration (CIC) model, and constant flux and constant sedimentation (CFCS) (Appleby, 2001). In this study, outputs from the CRS and CIC models were compared. While the CIC model requires assumptions of constant initial concentrations at the sediment surface and that sedimentation rates are roughly proportional to ^{210}Pb fluxes, the CRS model only assumes constant supply rates but requires no assumption of proportional sedimentation, and therefore it can be used for less homogenic sedimentation settings (Wren et al, 2016). A list of input variables required for the two models is shown in Table 8.

Input variables used for CRS and CIC models

Variable	Description	Unit
$A(0)$	Activity $^{210}Pb_{ex}$ at top sediment	Bq kg^{-1}
$A(z)$	Activity $^{210}Pb_{ex}$ at depth z	Bq kg^{-1}
$I(z)$	Inventory $^{210}Pb_{ex}$ at depth z	Bq m^{-1}
λ_{Pb}	^{210}Pb decay constant 0.03114	s^{-1}
SAR	Sediment accumulation rate	kg m^{-2} yr^{-1}
t	Age	years
z	Depth	m

Table 8 List of variables for $^{210}Pb_{ex}$ conversion models for sedimentation.

3.3.6.17 ^{210}Pb fluxes

The Pb flux (Bq m^{-2} yr^{-1}) from atmosphere to sediment is calculated by (Appleby, 1998):

$$P = \lambda_{Pb} \, A(0)$$

where λ_{Pb} is the decay constant for ^{210}Pb and $A(0)$ represents the inventory of $^{210}Pb_{ex}$.

3.3.6.18 $^{210}Pb_{ex}$: CRS model

The constant rate of supply (CRS) model assumes that $^{210}Pb_{ex}$ fallout is continuous (Du & Walling, 2012) regardless of variations in sedimentation rates (Appleby, 2008). The CRS model used for $^{210}Pb_{ex}$ gives the sediment age by (Appleby, 1998):

$$t = \frac{1}{\lambda_{Pb}} ln \frac{A(0)}{A}$$

Where λ_{Pb} is the decay constant of $^{210}Pb_{ex}$, $A(0)$ is the core inventory of $^{210}Pb_{ex}$, and A is the sample inventory of $^{210}Pb_{ex}$ for the sample increment directly beneath the dated sample increment. The sediment accumulation rate (SAR) then becomes (Appleby & Oldfield, 1978):

$$SAR = \frac{\lambda_{Pb}I(z)}{A(z)}$$

Where λ_{Pb} is the ^{210}Pb decay constant, $I(z)$ is the inventory at depth z, and $A(z)$ is the activity of [210]Pb$_{ex}$ at depth z. The unit for SAR is kg m^{-2} year^{-1}.

Uncertainties of the CRS method compose under-estimation of inventories resulting in too old ^{210}Pb dates in sample above equilibrium depth, and the lack of accounting for any gaps in the sediment record (Appleby, 1998).

3.3.6.19 [210]Pb$_{ex}$: CIC model

The constant initial concentration (CIC) model assumes a constant supply of the radionuclide with deposited sediment particles and the input of ^{210}Pb varies with sedimentation rates (Appleby, 2008), i.e. there is no redistribution of sediment (Du et al, 2012). The equation (Appleby & Oldfield, 1983) assumes decreasing concentrations of [210]Pb$_{ex}$ activity with depth:

$$A(z) = A(0)e^{-\lambda_{Pb}t}$$

Where $A(z)$ is the activity of [210]Pb$_{ex}$ (Bq kg^{-1}) at depth z, $A(0)$ is the activity at the top sediment, λ_{Pb} is the Pb decay constant, and t is the age calculated as follows:

$$t = \frac{1}{\lambda_{Pb}} \ln\left(\frac{A(0)}{A(z)}\right)$$

The sedimentation rate is further calculated by (Angeli et al, 2016):

$$v = \frac{\lambda_{Pb}D}{\ln\left(\frac{(^{210}Pb_{ex})_t}{(^{210}Pb_{ex})_b}\right)}$$

Where v is the average sedimentation rate (cm year^{-1}), D is the core length of the sediment profile (cm), $(^{210}Pb_{ex})_b$ is the bottom sediment layer [210]Pb$_{ex}$ activity, and $(^{210}Pb_{ex})_t$ is the top sediment [210]Pb$_{ex}$ activity.

3.3.6.20 Data interpretation

The soil and colluvium radionuclide inventories were converted into erosion and sedimentation rates by conversion models PDM and DMM (described in sections 3.3.6.14 Profile distribution model (PDM) and 3.3.6.15 Diffusion and migration model (DMM)) with the Excel Add-In *radiocalc* (Walling et al, 2007) downloaded in 2018 from the Joint FAO/IAEA Programme website[8]. Results from CRS and CIC models (described in sections 3.3.6.18 and 3.3.6.19) were calculated in Microsoft Excel®. Software used for data interpretation and statistics were *RStudio 1.1.463, Microsoft Excel 2016* and *IBM SPSS Statistics 25.* For map production and raster statistics, *QGIS 2.18.27 Las Palmas* was used.

3.4 Modelling methods

Soil erosion and sediment volume were estimated by RUSLE model and GIS analysis. The methods used are described in this section.

3.4.1 Hydrological analysis

3.4.1.1 Preparation procedure hydrological analysis

Unidentified sinks or artificial depressions occur when contour lines from remote approach survey data is based on gridded input data[9]. Depressions occur due to e.g. low resolution of survey lines, which may cause error in hydrological modelling, as the digital topography is misinterpreted (Lindsay & Creed, 2005). However, newer DEM, e.g. SRTM in the 21st century, provide better depression accuracy than traditional survey lines, and is recommended for usage before the latter[10]. Lindsay & Creed (2005) investigated the impact of methods developed for removal of artificial depressions created in DEMs, finding that the methods least influencing terrain attributes were depression breaching and the impact reduction approach (IRA), the latter built-in within QGIS-packages *r.hydrodem* and the SAGA (System for Automated Geoscientific Analyses) tool *Fill Sinks (Wang & Liu)* with B-spline interpolation, which were used prior to further watershed analysis in GIS.

---

[8] http://www-naweb.iaea.org/nafa/swmn/models-tool-kits.html
[9] https://grasswiki.osgeo.org/wiki/Hydrological_Sciences
[10] https://grasswiki.osgeo.org/wiki/Hydrological_Sciences

3.4.1.2 Terrain analysis

A DEM was created from 30 m resolution Shuttle Radar Topography Mission data (*SRTM s22w044 1arc-second v3),* downloaded in 2016 from USGS Eros Data Center[11]. This DEM had a 30 m resolution and was carefully clipped to a smaller raster layer by delineation of HydroBASIN[12] (Lehner et al, 2013) shape files, covering the catchment in which João Penido reservoir is located. Slope was derived from the raster file by using the GRASS tool *r.slope* and ranged between 0–36.7 degrees, with a standard deviation of 6.8 degrees (Figure 26). The SRTM image was processed with the GRASS tool *r.watershed* to create sub basins. The input parameters were set to the following: minimum size of exterior watershed basin: 1000 (m), maximum length of surface flow, for USLE: 10 (m). The GRASS tool *r.to.vect* was used to build drainage basins of vector format. Selected drainage basins were then saved to create a vector shape-file that represented the whole catchment area for João Penido watershed. These selected features were merged by using the QGIS built-in geoprocessing tool *Dissolve*. The catchment properties derived from GIS-analysis are summarized in Table 9.

---

[11] https://earthexplorer.usgs.gov/, downloaded in 2016
[12] http://www.hydrosheds.org/page/hydrobasins
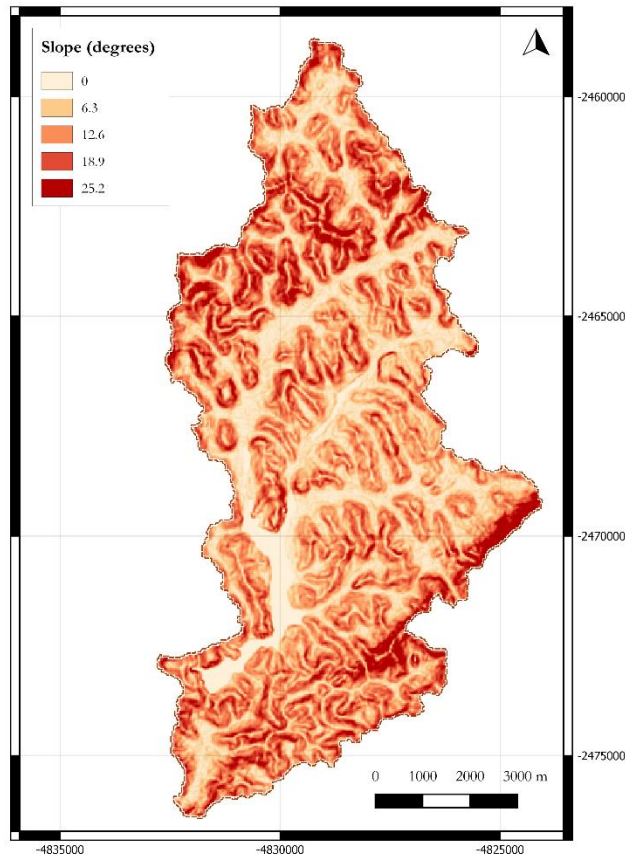
Figure 26 Slope of João Penido reservoir catchment. EPSG: 3857.

João Penido reservoir catchment properties from GIS-analysis

	Value	Unit
Catchment area	72.14	km^2
Reservoir surface area	3.72*	km^2
Range elevation	677–1061	m.a.s.l.
Average slope	10.8	degrees
*Bucci et al 2015		

Table 9 Basic catchment characteristics of João Penido reservoir, determined by GIS-analysis.

3.4.1.3 Topographic wetness index (TWI)

The topographic wetness index (*TWI*), also known as compound topographic index (*CTI*), is often used to determine the topographic control on hydrology (Sørensen et al, 2006). *TWI* is defined by:

$$TWI = \ln(\frac{\alpha}{\tan \beta})$$

101

where α is the upslope contributing catchment area (m^2) per unit width orthogonal to flow direction and *β* represent slope angle (Gessler et al, 1995; Pei et al, 2010). Practically, *TWI* is highly correlated with soil attributes (e.g. OM%, silt content, phosphorous). *TWI* was created for the João Penido catchment in QGIS, by the tool *SAGA Wetness Index* (Boehner et al, 2002) to determine likely areas of POC accumulation (Figure 27).
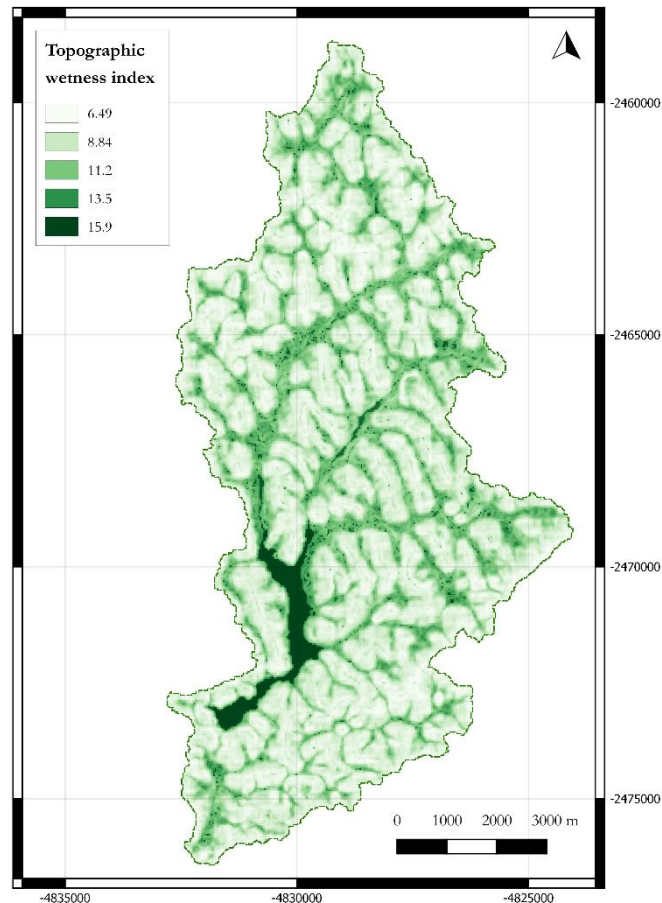
Figure 27 Compound topographic index (CTI) or Topographic wetness index (TWI) for João Penido catchment. EPSG: 3857.

3.4.2 RUSLE model

Revised Universal Soil Loss equation (RUSLE) is an upgraded empirical soil loss model based on the original Universal Soil Loss equation (USLE) model developed originally by United States Department of Agriculture (USDA), defined by the following equation with six factors:

$$A = RKLSCP$$

where A is the calculated yearly average soil loss (tonnes ha^{-1} year^{-1}), R is the annual rainfall erosivity factor, K is the soil erodibility factor, S is slope steepness, L is slope length, C is the vegetation cover and crop management factor, and P represents the specific erosion control practice. The RUSLE model has been successfully implemented in local to global scale studies. Together, L and S factors compose the topographic factor, LS, which can be derived from topographic data. Oliviera et al (2013) found that the topographic factor derived from digital elevation models (DEM) can also be calculated from shuttle radar topography mission (SRTM) data, which is the input dataset for this study. The LS and C factors compose the more important factors in the soil erosion model (Panagos et al, 2015) and on its own the combined LS factor can be used to evaluate potential sites of erosion, whilst the product of factors R, K, LS can be used to determine the natural potential of erosion (NEP) of an area. The spatial scale of RUSLE composes field–hillslope range (Terranova et al, 2009), although a number of studies have applied this model on a global scale (e.g. Yang et al, 2003; Naipal et al, 2015). The input data from database sources used in this work is summarized below (Table 10). Erosion rates were calculated in the unit tonnes ha^{-1} year^{-1}, to convert this value into kg m^2 year^{-1}, the value was divided by 10.

RUSLE input parameters

Type	Factor	Unit	Source
Rainfall erosivity	R	MJ mm ha^{-1} year^{-1}	Environmental Prediction (NCEP) Climate Forecast System Reanalysis (CFSR) (*Global Weather Data for SWAT*)
Soil erodibility	K	tonnnes ha h ha^{-1} MJ^{-1} mm^{-1}	1. Harmonized World Soil Database (HWSD), FAO 2. Observations from catchment soil profiles.
Length-slope	LS	dimensionless	Derived from 30 m resolution SRTM with SAGA tool *LS factor, field based*; method Desmet & Govers (1996).
Cover and management	C	dimensionless	1. GlobCover V2.3 (ESA) with literature C-values from Panagos et al (2015). 2. Digitized land cover map by Google Satellite data (2018) at scale 1:2000.
Support practices	P	dimensionless	Set to 1.

Table 10 RUSLE input factors and sources.

3.4.2.1 Rainfall erosivity factor (R)

The rainfall erosivity maps by Da Silva (2004) indicate an annual range of 6000–8000 MJ mm ha^{-1} year^{-1} in the SE region of Brazil, where the study catchment is located. Similarly, Oliveira et al (2013) approximated the same range of R factor for the region, of 6000–8000 MJ mm ha^{-1} year^{-1} (Figure 28).
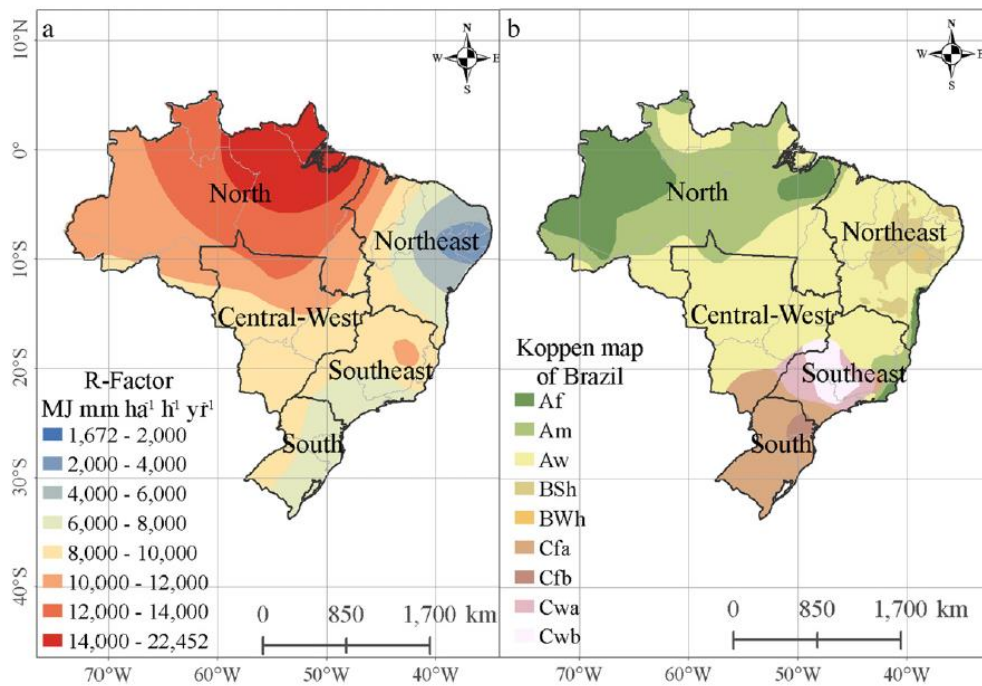
Figure 28 R-factor and Köppen map derived from Oliveira et al (2013) – the study catchment João Penido is located near the south-eastern coast, within in the R factor range of 6000–8000 (left) and within the Köppen climate class Cwa (right).

The expression to calculate the R factor by Renard & Freimund (1994) was used:

$$R = 0.0483 \times P^{1.610}$$

Where P is the annual average rainfall in mm year^{-1}, estimated from the database *PSD South America Daily Gridded Precipitation* (Liebmann & Allured, 2005), which temporal range is 1940–2012, obtained from South American Precipitation data provided by the NOAA/OAR/ESRL PSD, Boulder, Colorado, USA, from their Web site[13] (downloaded 2017-10-30). By plotting the values as a raster in GIS, the yearly average precipitation values for the raster pixel which incorporates the catchment area of João Penido, could be analysed by the QGIS plugin *Value Tool*. Data was extracted from the raster point (LAT, LONG: –4832176.366, –2471825.954) to calculate the annual average precipitation for an area that includes the João Penido catchment. The resulting annual average precipitation

---

[13] https://www.esrl.noaa.gov/psd/data/gridded/data.south_america_precip.html

105

(between 1940–2012) equalled 1540.69 mm year^{-1}, which gave an *R* factor value of 6548.90 MJ mm ha^{-1} year^{-1} which falls within the range of the above-mentioned studies on rainfall erosivity. Even though this *R* factor value is based on historical precipitation data, in this study it was assumed that it gave a realistic estimate of the general precipitation trend in this region.

3.4.2.2 Soil erodibility factor (*K*)

The soil erodibility factor could be derived from soil properties data. For this work the regional soil database (2005) "*A National Soil Profile Database for Brazil Available to International Scientists*", by Cooper et al (2005) was used[14], in conjunction with the *Digital Soil Map of the World* (DSMW) database by FAO. Extracted values from the attribute table of the FAO DSMW database[15] were used as input parameters in the *K* factor equation used (Table 11). In the João Penido watershed the dominating soil code was: DOMSOIL:fo and the FAO code: Fo4-3b, which corresponds to orthic ferralsol or ultisol.

João Penido soil properties

FAO code	sand % topsoil	silt % topsoil	clay % topsoil	OC % topsoil
fo4-3b	15.7	16.5	67.8	2.21

Table 11 Soil properties derived from FAO DSMW attribute table.

To calculate the K factor, the following equation from Stewart et al (1975) was used, as it is suitable for soils with a silt fraction <70% (Renard et al, 1978):

$$K = [2.1 \times 10^{-4}(12 - OM)M^{1.14} + 3.25(s - 2) + 2.5(p - 3)]/100$$

Where *M* is defined as (Wischmeier & Smith, 1978):

$$M = silt\% \times (100 - clay\%)$$

In the *K* factor equation above*, M* is the product of particle structure, based on clay, silt, and sand content, *p* is the permeability class, and *s* is the structure code. The value of *K* can be converted from U.S. customary units into S.I. units (Mg ha

---

[14] http://www.esalq.usp.br/gerd/

[15] http://webarchive.iiasa.ac.at/Research/LUC/External-World-soil-database/HTML/HWSD_Data.html?sb=4

h ha^{-1} MJ^{-1} mm^{-1} or t ha h ha^{-1} MJ^{-1} mm^{-1}) by multiplying it with a conversion factor 0.1317 (Wang et al, 2016). For this unit, hectares in the numerator and denominator are left shown to represent soil loss per unit area per unit EI (Foster et al, 1981). For João Penido reservoir, a permeability class of 3 (moderate) and structure code of 3 (medium–coarse and granular) were used after field observations (Renard et al, 1997; Table 3-3). The dominating soil type in João Penido catchment was orthic ferralsol (latosol) which has been identified with a typically low K value, e.g. Medeiros et al (2015) reported 0.0162 Mg ha h ha^{-1} MJ^{-1} mm^{-1} for this type of soil. Similarly, Beskow et al (2009) reported a value of 0.010 t ha h ha^{-1} MJ^{-1} mm^{-1} from a study by Silva (1997)[16].

       In S.I. units, the K factor for the FAO database soil covering the watershed of João Penido reservoir corresponded to: 0.0077 tonnes ha h ha^{-1} MJ^{-1} mm^{-1}. This value is similar to the K values found in another South American regional study of Uruguay catchments using USLE/RUSLE by Carrasco-Letelier & Beretta-Blanco (2017) who obtained 0.0073–0.0088 tonnes ha h ha^{-1} MJ^{-1} mm^{-1}, and a study by Galdino et al (2016) who found a K factor range of 0.0047–0.0551 tonnes ha h ha^{-1} MJ^{-1}mm^{-1} in cultivated pasturelands of Goiás State and the Federal District in central Brazil. Specifically, Galdino et al (2016) reported K factor values of 0.0145 and 0.0193 tonnes ha h ha^{-1} MJ^{-1}mm^{-1} exhibited by the two classes of ferralsols found in their study region. Similarly, da Cunha et al (2017) reported a K factor range 0.001–0.2122 tonnes ha h ha^{-1} MJ^{-1}mm^{-1}, however, these soils were not strict ferralsols.

       For comparison, the K factor was also calculated from observations of soil properties from field samples. Input data from field observations compose an average OM value of 13.09% (N=125) and grain size data from 26 samples with a mean of 3.71% silt and 96.28% sand in the upper 20 cm of the available soil profiles that were used (Table 12). Since clay was not separated from the <53 µm fraction in this study, it was set to zero in the observation based calculation of K. The resulting K value 0.0040 tonnes ha h ha^{-1} MJ^{-1} mm^{-1} was used in the RUSLE model.

---

[16] PhD Thesis.

João Penido soil properties (observations in the field)

	sand % topsoil	silt % topsoil	clay % topsoil	OC % topsoil
N	26	26	26	125
Mean	96.28	3.71	NA	13.09

Table 12 Soil properties to calculate soil erodibility factor from observations in João Penido catchment. Because the clay fraction (<0.002 mm) was not measured in this study, it was set to 0 in this calculation.

3.4.2.3 Length-slope factor (LS)

The *L* (slope length) and *S* (slope steepness) factors within the USLE equations are commonly combined and known as the *LS*-factor (Zhang et al, 2017). This parameter composes a dimensionless value that characterises the erosion effect of topography and numerous mathematical methods to calculate the *L* and *S* factors exist (Van Remortel et al, 2001). In this work, equations for *LS* are derived from Desmet & Govers (1996) that are implemented through the SAGA tool *LS-factor, field based*, where input composes the SRTM-derived DEM with *Rill/Interill Erosivity* set to 1. The resulting *LS*-factor map display dimensionless values ranging between 0.03–103.6, with a mean of 6.85 (Figure 29). To assess whether *LS*-factor values produced for the João Penido catchment were reasonable, these were compared to other studies using RUSLE/USLE in the South American region, e.g. Galdino et al (2016) who found a similar min–max range of 0–104 and a mean of 1.80 in their regional study of catchments with similar topography in central Brazil.
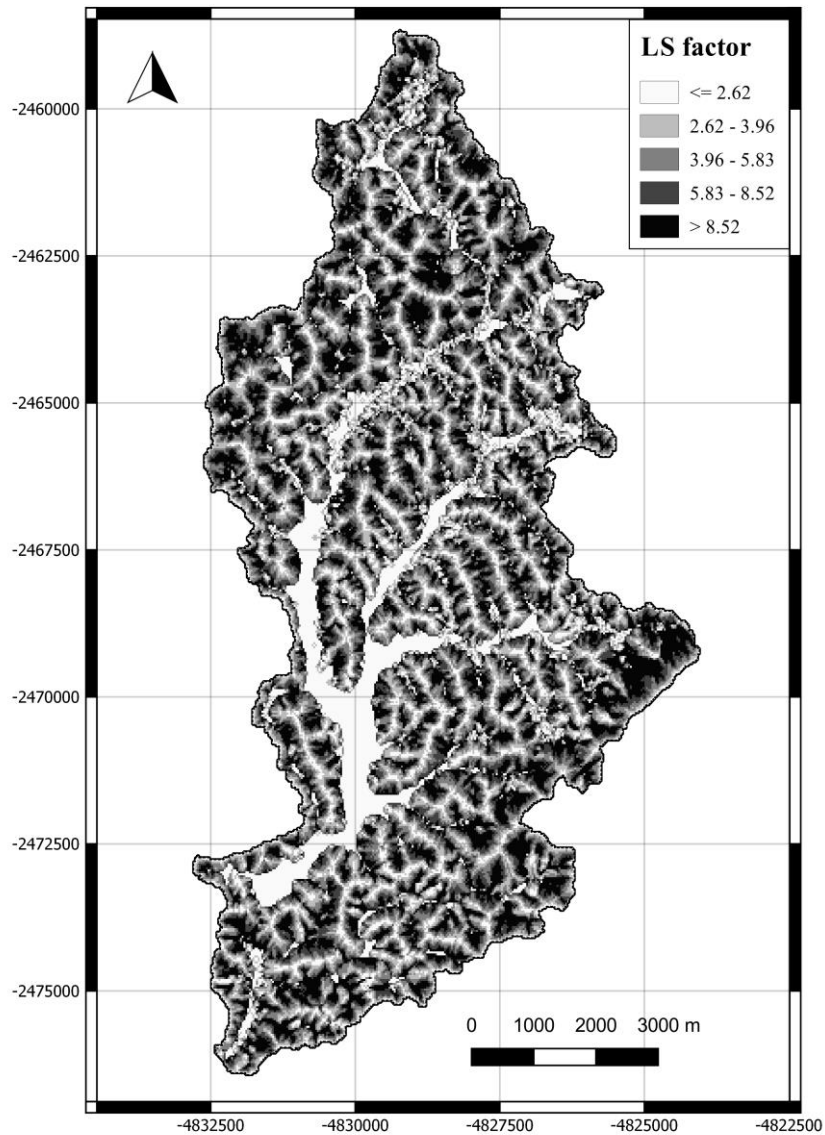
*Figure 29 LS-factor for João Penido watershed, method by Desmet & Govers
(1996) by SAGA tool LS-factor, field based. Classes are based on quantiles.
CRS: WGS84/Pseudo-Mercator. EPSG:*

3.4.2.4 NPE Map

The product of factors *R, K, LS* compose the natural potential of erosion (NPE)
of soils in the catchment, expressed in tonnes ha^{-1} $year^{-1}$. This is a value that
does not consider any influence of vegetation or management practices on the
soil.

3.4.2.5 Cover factor (C)

The cover and management (*C*) factor composes a dimensionless factor with values ranging between 0–1, that describes the influence of cultivated and natural vegetation cover on erosivity in the landscape (Kouli et al, 2008). It is one of the factors of soil erosion which can most readily be controlled by land owners to reduce soil erosion risk (Panagos et al, 2015). Satellite imagery can be used to derive vegetation cover, from indices such as Normalized Difference Vegetation Index (NDVI), which is a measure of the spectral reflectance of vegetation in the red and near-infrared regions and is helpful in determining vegetation cover using remote sensing data.

Literature *C*-values can also be assigned to existing database land cover maps which can serve as *C* factor input for the RUSLE equation, e.g. Panagos et al (2015) used the CORINE land cover map[17] for soil erosion modelling on European scale. In this study, *C* factor input for the study catchment were derived from 1) literature *C*-values assigned to mapped land use classes of the GlobCover V2.3[18] map from European Space Agency (ESA), and 2) in this study manually digitized land cover classes at a scale of 1:2,000 using satellite images (Google). The land cover map GlobCover V2.3 from European Space Agency (ESA) features 22 land cover types at 300 m resolution. The data were assigned *C*-values from the literature (Table 13) and reclassified to provide a *C*-factor map for the watershed (Figure 30). Literature *C*-values were used to reclassify the land cover map were compared to values in other studies from the South American continent, e.g. Carrasco-Letelier & Beretta-Blanco (2017) and da Cunha et al (2017).

Land use was also manually digitized in QGIS (version 2.18.24) to create a detailed *C*-factor map, based on Google Satellite data utilizing the *open layers plugin*, at a scale of c. 1:2,000. The digitized land cover features (Figure 31) were designated *C*-factor values from the literature, summarized in Table 14. From this manual classification of land cover data, it was observed that main land cover in the catchment composes tree-less grassland, making up 72.5% of the catchment, while c. 17.7% of the catchment is wooded. The digitized *C* factor map was rasterized and used as input for RUSLE calculation.

---

[17] https://land.copernicus.eu/pan-european/corine-land-cover
[18] http://due.esrin.esa.int/page_globcover.php
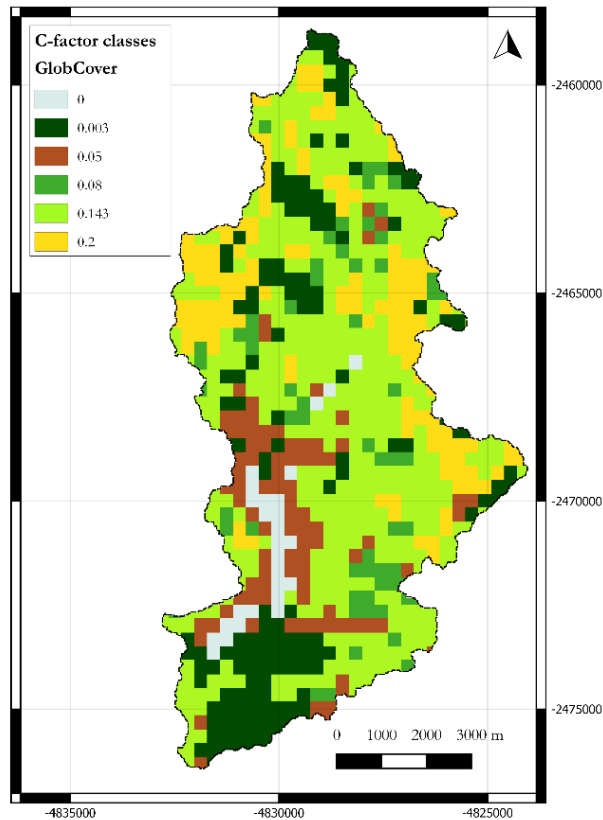
Figure 30 C factor map based on land cover classes from GlobCover V2.3 data.

The assigned literature C values are from Panagos et al, 2015. EPSG: 4326.

C *factor values conversion table for GlobCover data*

GlobCover raster value	GlobCover label	C-values from Panagos et al 2015	Detailed class
14	Rainfed croplands	0.2	Complex cultivation patterns
20	Mosaic cropland (50-70%) / vegetation (grassland/shrubland/forest) (20-50%)	0.15	Pasture
30	Mosaic vegetation (grassland/shrubland/forest) (50-70%) / cropland (20-50%)	0.08	Natural grassland
40	Closed to open (>15%) broadleaved evergreen or semi-deciduous forest (>5m)	0.003	Broad-leaved forest
50	Closed (>40%) broadleaved deciduous forest (>5m)	0.003	Broad-leaved forest
120	Mosaic grassland (50-70%) / forest or shrubland (20-50%)	0.05	Shrubland
130	Closed to open (>15%) (broadleaved or needle-leaved, evergreen or deciduous) shrubland (<5m)	0.05	Shrubland
210	Water bodies	0	Water

Table 13 C *factor values, description and source for conversion labels in*

GlobCover dataset.
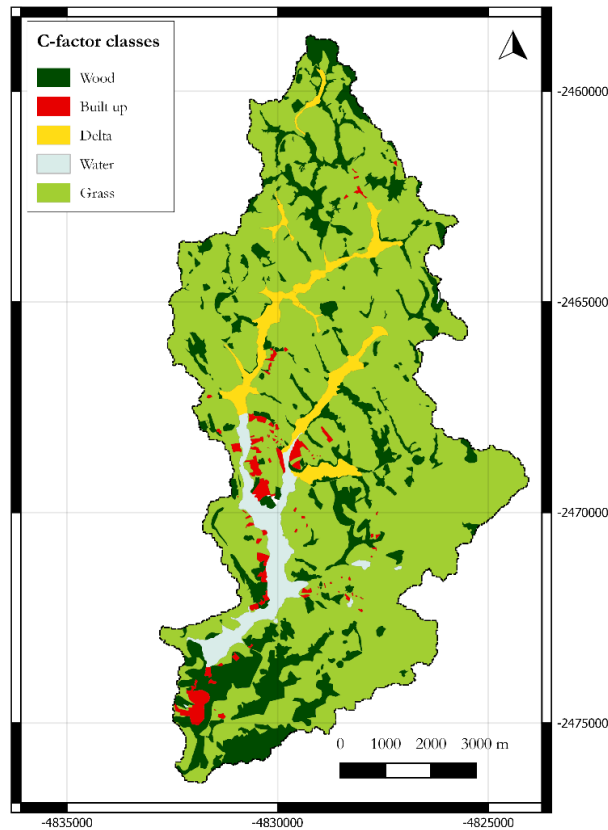
Figure 31 Detailed C-factor map of João Penido reservoir, digitized at scale 1:2000. EPSG: 4326.

C factor values conversion table for digitized map

Digitized land cover	Area (km^2)	Area% of catchment	C	Detailed class	Source
Wood	12.8	17.7	0.003	Broad-leaved forest	*Panagos et al, 2015*
Grassland	53.2	72.5	0.08	Natural grassland	*Panagos et al, 2015*
Delta	2.9	4.0	0.038	Swampy grassland	*da Cunha et al, 2017*
Built up	1.4	1.9	0	Built-up area	
Water	2.8	3.8	0	Water	

Table 14 C-factor values for digitized map of João Penido catchment.

Each land use class was designated its own *C*-value, derived from literature (Panagos et al, 2015) and correspondingly, *C*-factor values from the literature were used to simulate extreme scenarios for which *C*-factor maps were created for 3 alternative scenarios: 1) "forested", where the watershed is fully covered by broadleaved forest (*C*=0.003), 2) "deforested" where the vegetation cover is assumed to be constricted to low-growing grassland and shrubland species

(*C*=0.1), and 3) "bare", where land is assumed to be of such degraded state that very sparse vegetation is dominating the land cover (*C*=0.45). For these scenarios, it was assumed that areas covered by water and built-up areas (*C*=0) were still present in the catchment.

3.4.2.6 Support practices factor (P)

The support practices factor, *P*, represents the ratio of erosion associated with the conservation measures that control runoff erosion in tilled and managed soils (Renard et al, 1978). In the studied watershed, no known conservation practices are applied, and the *P* factor was therefore set to 1 for the whole catchment.

3.4.2.7 Calculation of RUSLE in GIS

RUSLE values could be calculated manually for the watershed by built-in *Raster calculator* in QGIS, resulting in a raster map of the catchment with RUSLE erosion rates. Raster maps of factors *C* and *LS* for the catchment were used as input together with constant values of factors R and K for the equation (see 3.4.2 RUSLE model). An NPE map was derived from factors *R*, *K*, *LS*, while the RUSLE map was derived from factors *R*, *K*, *LS*, and *C*, with *P* set to 1.

3.4.3 Post-flooding sediment volume in the reservoir

A reservoir outline shape-file was carefully delineated from generated slope data of the catchment and was checked against Google Satellite data in QGIS with the *open layers plugin*, at a scale of 1:2,000. The water surface area of the reservoir has been reported as 3.72 km^2, e.g. Bucci et al (2015). Vector calculations done in QGIS gave a reservoir water surface area of 2.66 km^2 for the dry season of 2016. The maximum area (m^2) of sediment accumulation in João Penido reservoir was for simplicity assumed to equal the areal extent of the watershed, and the thickness of post-flood sediment was derived from sediment core point observations (*N*=15) which were interpolated by creating a triangular irregular network (TIN). Water depth was measured in the field by sub-bottom survey and the point observations (*N*=85,882) of transects were combined with water depth data observed in the field during core sampling (*N*=21) (Figure 32).
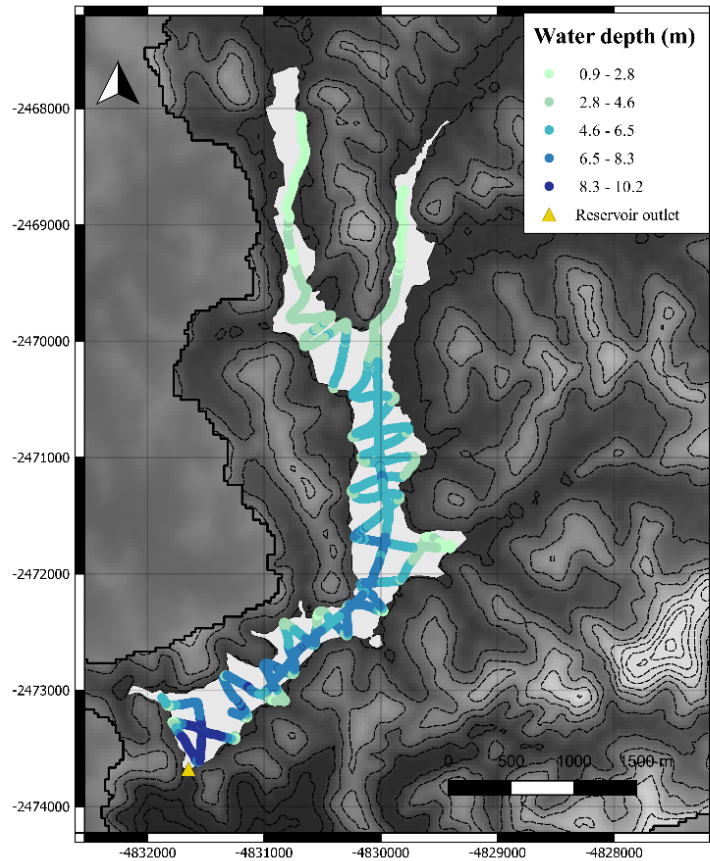
Figure 32 Sub-bottom tracks from survey of João Penido reservoir, 2016, and sediment core water depth observations from 2016 and 2017 campaigns. EPSG: 3857.

A shape-file created from the beachline was used to delineate the water surface extent. TIN interpolation was used to interpolate the water depth in the reservoir with QGIS software. The bathymetric map produced from sub-bottom data showed that the reservoir was deepest in the south-west part close to the reservoir outlet (Figure 33).
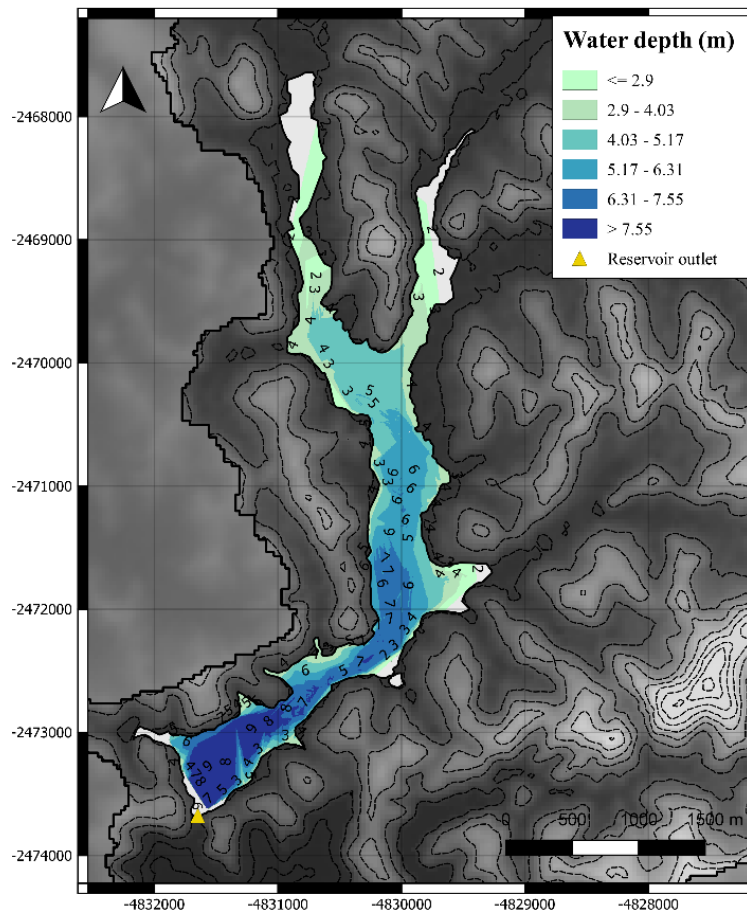
Figure 33 Bathymetric map of João Penido reservoir, from TIN interpolation of sub-bottom data. EPSG: 3857.

3.4.4 Sediment yield from reservoir sediments

Sediment yield (%) was calculated as the ratio of sedimentation in the reservoir over the gross erosion in the catchment. It was calculated from the average accumulation of sediment in the dam since 1934 (kg year^{-1}) divided by the mass of eroded sediment from the eroding catchment area (kg year^{-1}), according to:

$$Sediment\ yield = \frac{average\ accumulated\ sediment \times 1000}{erosion\ rate \times (catchment\ area - reservoir\ area)} \times 100$$

Where the average accumulated sediment was the calculated total mass of sediment (1,031,690.6 tonnes) by the reservoir age (82 years), erosion rate was the average erosion rate calculated by RUSLE (1.09 kg m^{-2} year^{-1}) and catchment area (68,420,000 m^2).

115

3.5 Summary of Chapter 3

This chapter summarized the field sites and methods of the study of POC transport and fate in a tropical catchment. This chapter explained and summarized: methods to determine input factors for the RUSLE model; GIS-analyses that were made to estimate total post-flooding sediment volume in the reservoir; analytical methods to determine bulk density, organic matter and carbon content, and C/N ratios; sieving procedures to separate fractions of soils and sediment. The results of this study are presented in Chapter 5.

Chapter 4. Methods Exmoor study, UK

This study focuses on the transformation dynamics of organic matter and carbon being transported from land to ocean. POC and DOC were measured in eight streams in northern Devon and north-western Somerset, which all drain waters of a typical coastal moorland landscape in the UK. Flocculation experiments were conducted to understand the effects of inorganic coagulants, which are present at various flocculation boundaries in the landscape, on formation of particulate organic matter and POC and the subsequent residual DOM quality. The change in DOM was measured to determine the influence of flocculation on water quality. The field, experimental and analytical methods of this study are presented in this chapter.

4.1 Field sites of Exmoor streams, Devon

Eight parallel running streams in catchments with headwater sources in Exmoor were chosen due to their similar geology, terrain, soils, vegetation and climate (Figure 34). Exmoor is an area of protected moor in the northern part of Devon and western part of Somerset in SW England. In Devon 90% of the land surface compose rural areas[19]. The north-running streams of the studied catchments drain moorland and soil of non-agricultural grade in Exmoor National Park, which gradually transition downstream along the river gradient into managed soils of higher agricultural grade (EPA maps, agricultural grade)[20], before entering the South-Central Bristol Channel of the outer Severn Estuary. Some of the gullies, through which the streams drain, are covered by forest classified as ancient woodlands[21], while others remain deforested for agricultural purposes. The land use in Exmoor national park (which partly overlaps the study catchments) comprise 55.8% farmland, 27.5% moorland, 12.2% woodland, 0.9% urban areas, and 0.2% ponds and reservoirs[22]. The site coordinates were noted in OSGB 1936 British National Grid (EPSG: 27700 with transformation: 1314) and in WGS 84 Pseudo-Mercator (EPSG: 3857).

---

[19] Waste Development Plan Documents, Strategic Flood Risk Assessment, Devon City Council, Minerals and Waste Development Framework, October 2011

[20] Dataset or shapefile reference

[21] Dataset © Natural England copyright. Contains Ordnance Survey data © Crown copyright and database right [2017].

[22] Exmoor national park authority, factsheet 2004.
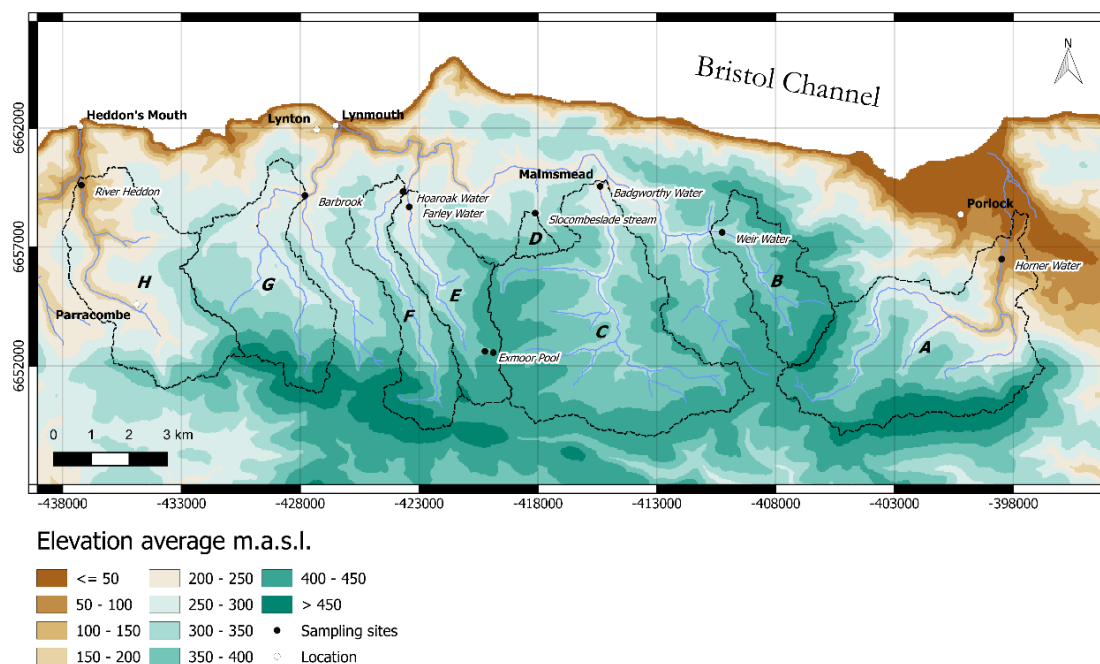
Figure 34 Sampling sites (A–I) in eight catchments (A–H) with Exmoor headwaters. The basemap, derived from SRTM arc-1-second, shows average elevation above sea level (m.a.s.l.). EPSG: 3857.

4.1.1 Climate

The Köppen climate classification system classifies Devon as *Cfb*, i.e. a warm temperate oceanic climate with warm summers. The average annual rainfall on Exmoor and northern coast amount to between c. 1000–2500 mm annually[23]. In SW England precipitation is in general highest during December–January and lowest in April–July (Devon City Council report[24]). Historical data from Horner Water gauge station at West Luccombe (LAT:459560, LON: 5672291) show that daily rainfall between 1961–2015 (20,088 observations) ranged between 0–110 mm day^{-1}, with a mean 4.25 mm day^{-1} (NRFA, 2018[25]). Daily flow rates from the same station, show an average daily river flow rate of 0.47 m^3 s^{-1} day^{-1}, with a min–max range of 0.018–10.4 m^3 s^{-1} day^{-1} on 14,169 measurement days over the years 1961–2017 (NRFA, 2018[26]). Similarly, Glendell et al (2014) reported

---

[23] www.metoffice.co.uk Publications and Factsheets:
https://www.metoffice.gov.uk/binaries/content/assets/mohippo/pdf/C:N/metlib_13_013_factsheet_7_final.pdf
[24] Waste Development Plan Documents, Strategic Flood Risk Assessment, Devon City Council, Minerals and Waste Development Framework, October 2011
[25] National River Flow Archive, data downloaded 2018-09-24.
[26] National River Flow Archive, data downloaded 2018-09-24.

total rainfall min–max range of 13.4–53.60 mm from 2010-08-21 to 2012-01-03. Average yearly temperatures at climate station Chivenor near Barnstaple range between 7.9–14.5 degrees C over years 1951–2017 (EPA, UK).

4.1.2 Terrain

The maximum elevation above sea level in the study area is c. 516 m.a.s.l. The area is characterized by rounded convex hills, where steep valley sides with up to 20–30% slope angles cut the bulging landscape (Miller & Miles, 1984). The headwaters drain the acidic moorland landscape of Exmoor (Figure 35).

Figure 35 Overview of landscape from moor to sea, facing north-east on Exmoor.

4.1.3 Geology and soils

The geology of the northern uplands of Devon comprises Middle and Upper Devonian rocks, which are minor aquifers with low permeability and therefore have low holding capacity for groundwater. The soil type overlying these rocks typically compose podzol or surface water gley soil (NRA, 1995). The study area is dominated by sandstones of the Hangman Sandstone Formation, slaty mudstone, siltstone and sandstone of the Lynton Formation near Lynmouth and

Lynton, and slaty metamudstones in the south-west of the study area belonging to the Ilfracombe Mudstone Formation (Whittaker & Leveridge, 2011) occurring in the area of study catchments *F, G*, and *H*. In the gorges, alluvial deposits of Quaternary sediments are present. Simplified lithology of the catchments is summarized in Table 15, Figure 36 and Figure 39a. The soil texture in the study area is dominated by silty loam to sandy loam (Figure 37).
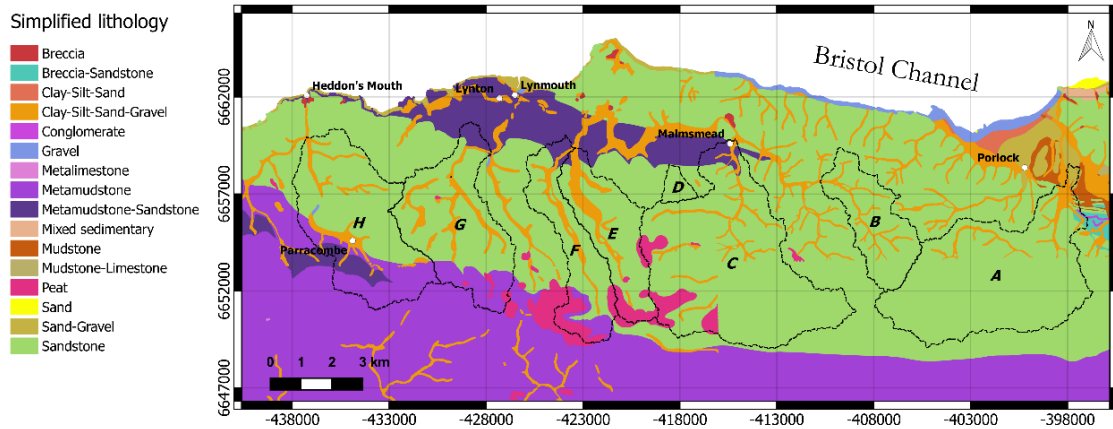
Figure 36 Simplified lithology of soil parent material of Exmoor catchments.
Data source: DiGMapGB-50 LEX-RCS system, 1:50,000 scale Geological Map
of Great Britain (British Geological Survey, 2011). EPSG: 3857.

Simplified lithology (%) of Exmoor catchments

	A	B	C	D	E	F	G	H	All
Breccia-Sandstone	0.5	-	-	-	-	-	-	-	0.11
Clay-Silt-Sand-Gravel	4.04	5.75	4.03	1.02	15.65	9.19	9.35	7.64	6.75
Conglomerate	0.04	-	-	-	-	-	-	-	0.01
Gravel	-	-	-	-	-	-	-	0.13	0.02
Metamudstone	-	-	-	-	-	10.54	16.05	24.17	6.71
Metamudstone-sandstone	-	-	2.68	-	2.24	5.53	3.9	7.44	2.98
Mudstone	0.5	-	-	-	-	-	-	-	0.11
Sand-Gravel	0.79	-	-	-	-	-	-	-	0.17
Peat	-	-	6.04	-	10.62	14.05	1.35	-	3.73
Sandstone	94.13	94.25	87.25	98.98	71.49	60.7	69.34	60.63	79.41

Table 15 Mapped land area (%) of parent material lithology in Exmoor
catchments, derived from DiGMapGB-50 LEX-RCS system, 1:50,000 scale
Geological Map of Great Britain (British Geological Survey, 2011).
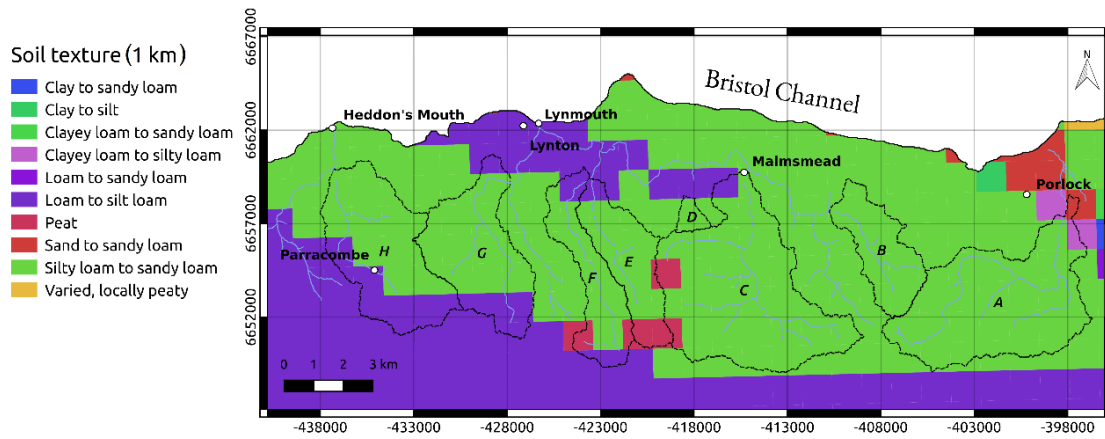
Figure 37 Soil texture map, 1 km resolution. Data source: UK Soil Observatory.
Contains British Geological Survey materials © NERC [2018]. EPSG: 3857.

4.1.4 Land cover classes

Land cover classes were derived from Land Cover Map 2015 by Rowland et al (2017) (Figure 38). The land cover classes (area %) for each study catchment are summarized in Table 16 and Figure 39b. The four main land cover components in the eight study catchments comprise acid grassland (51.1%), improved grassland (27.4%), heather (10.5%) and broadleaf woodland (9.4%). According to this dataset 0.2% compose suburban areas in the total area of studied catchments.
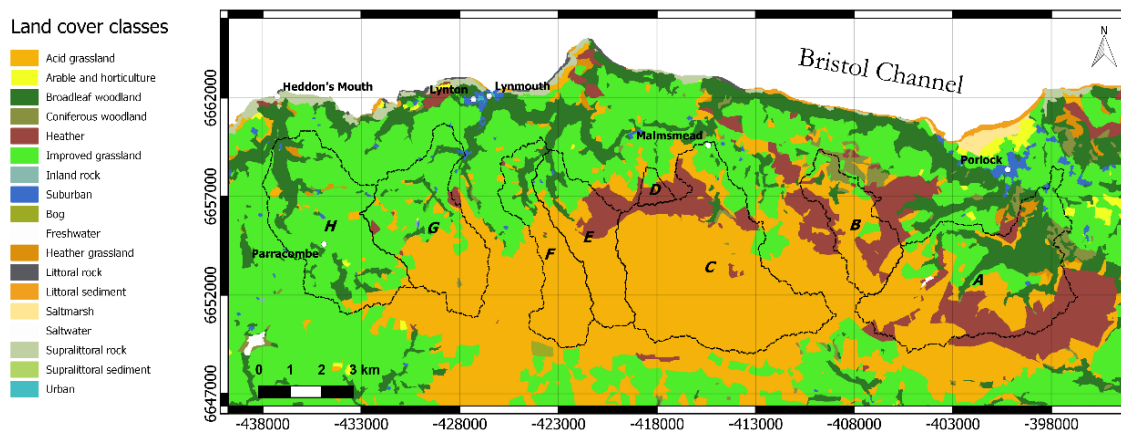
Figure 38 Land cover classes of the Exmoor stream catchments (highlighted).
Data source: Rowland et al (2017). EPSG: 3857.

Land cover classes (%) of Exmoor catchments

	A	B	C	D	E	F	G	H	All
Acid grassland	38.7	56.1	83.2	10.1	59.8	70.2	44	6.9	51.1
Arable and horticulture	0.1	-	-	-	-	-	0.1	0.2	0.1
Broadleaf woodland	20.3	3.1	1	-	6.9	7.5	5.1	17.3	9.4
Coniferous woodland	1.3	5.5	0.5	-	-	-	0.3	0.1	0.8
Freshwater	0.2	-	-	-	-	-	-	-	-
Heather	19.9	26.2	9.2	65.1	14.8	0.2	1.8	-	10.5
Heather grassland	1.2	0.1	-	-	-	-	-	1.1	0.4
Improved grassland	18.1	9	6	24.8	18.2	22.1	48.3	73.9	27.4
Inland rock	-	-	-	-	-	-	0.1	-	-
Suburban	0.2	-	0.1	-	0.3	-	0.4	0.4	0.2

Table 16 Land cover classes of the Exmoor catchments, derived from Land Cover Map 2015 (Rowland et al, 2017).

a)

b)
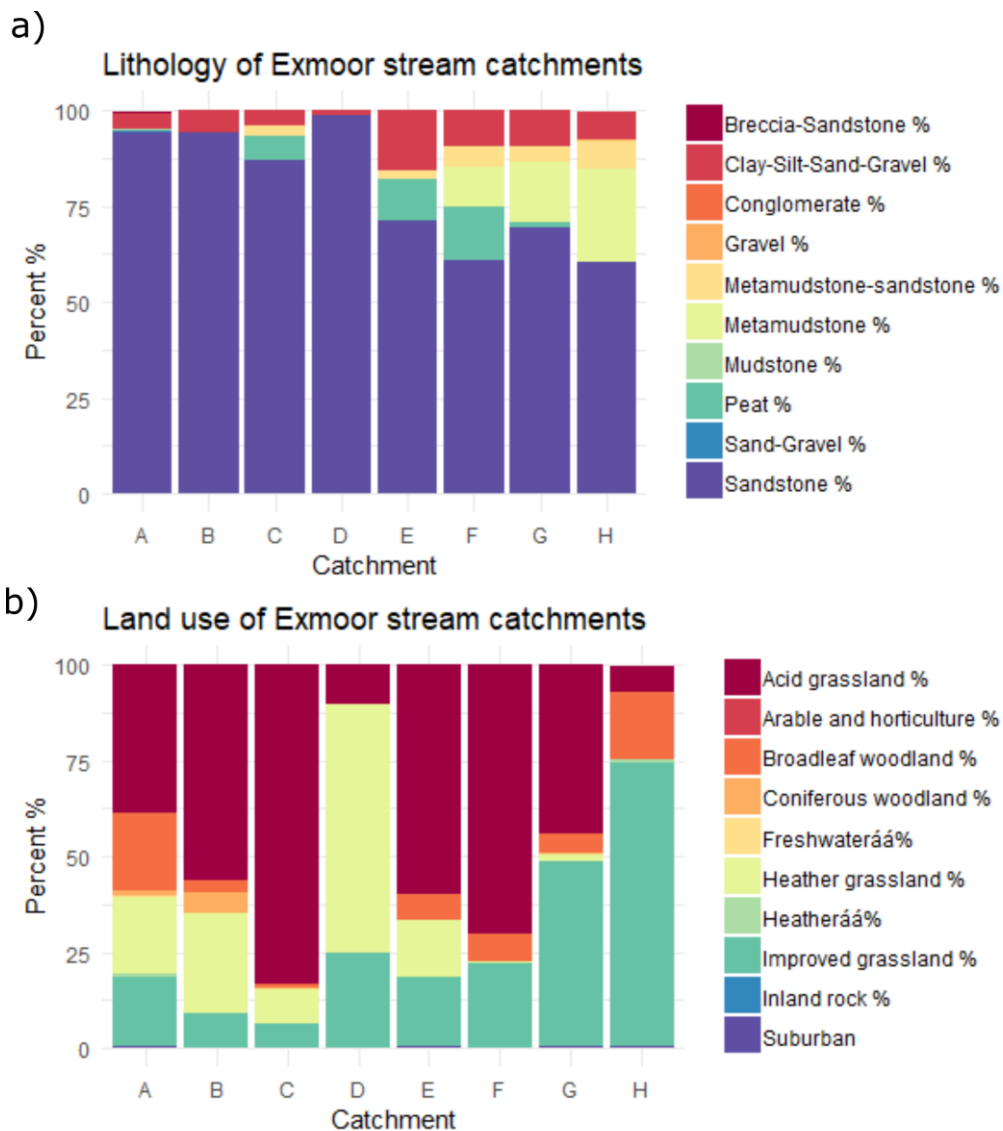
Figure 39 Distribution of a) lithology and b) land use of study catchments.

4.1.5 Water quality in streams of Exmoor

The waters of the study sites enter the Bristol South-Central Channel in the outer parts of the Severn Estuary, into which Owens (1984) reported an annual input of POC of 1.6% and DOC of 6.5% from freshwater streams. In Horner Water Glendell et al (2014) reported peak total suspended sediment amounting to 16.09–1642.54 mg L^{-1}, peak DOC concentrations of 4.67–7.59 mg L^{-1}, and POC concentrations between 2.60–199.49 mg L^{-1} between years 2010–2012.

4.1.6 Stream sites

A) Horner Water (–3.579655022, 51.19853524)

Horner Water drains a mixture of land cover classes and eventually enters the sea by Bossington Beach in Porlock Bay (Figure 40). The catchment area is 21.4 km^2 and upstream of the sampling site, which is located at c. 70 m.a.sl., the land cover mainly comprises acid grassland (38.7%), broadleaf forest (20.3%), and heather (20.0%). Most of the watershed is located on a sandstone formation (Hangman's Sandstone).

Glendell & Brazier (2014) reported a range of 2.60–20.86 mg L^{-1} of total particulate C (TPC) in Horner Water. They also showed that the concentrations of TPC was higher during base flow in an agricultural catchment neighbouring Horner catchment, which in contrast is a mixed land use catchment.

Figure 40 Sampling site A, Horner Water.

B) Weir Water (−3.685306968, 51.20484971)

Weir Water is a tributary to East Lyn River and has a catchment area of 7.0 km^2 which drains mainly acid grassland (56.1%), heather (26.2%) and improved grassland (9.0%). The sampling point is located underneath a small bridge at c. 300 m.a.s.l.

C) Badgworthy Water (−3.731420769, 51.21574435)

Badgworthy Water is a tributary to East Lyn River and the catchment area amounts to 25.2 km^2, making up the largest of the catchments in this study (Figure 41). The sampling point is located upstream of a weir at c. 240 m.a.s.l. and the main land cover classes constitute acid grassland (83.2%), heather (9.2%) and improved grassland (6.0%).

D) Slocombeslade stream (−3.755958119, 51.20941233)

This stream by Slocombeslade Wood is a small tributary to East Lyn River. The upslope catchment area of the sampling site amounts to roughly (0.9 km^2), making up the smallest catchment in the study. This small catchment is dominated by land cover classes heather (65.1%), improved grassland (24.8%) and acid grassland (10.1%). The sampling point is located at c. 300 m.a.s.l.

Figure 41 Sampling site C, Badgworthy Water, upstream of weir.

E) Farley Water (−3.803025297, 51.20786778)

Farley is a tributary to East Lyn River, and joins Hoaroak water coming from the west at Watersmeet before entering East Lyn River. The sampling site at Farley water is a direct runoff site from site I, which represents a headwater moor site for all catchments in this study. Main land cover classes compose acid grassland (59.8%), improved grassland (18.2%) and heather (14.8%). The catchment area amounts to 8.0 km^2. The sampling site is located at c. 230 m.a.s.l.

F) Hoaroak Water (−3.816252557, 51.2082984)

Hoaroak is a tributary to East Lyn River, and joins Farley water at Watersmeet before entering East Lyn River. The catchment area is 8.1 km^2 and drains land cover classes acid grassland (70.2%), improved grassland (22.1%) and broadleaf woodland (7.5%). The sampling site is located at c. 210 m.a.s.l.

G) Barbrook (−3.843015296, 51.21360397)

Barbrook runs into West Lyn River that enters Bristol Channel by the estuary at Lynmouth. The catchment area amounts to 12.9 km^2 upstream of the sampling point and the main land cover classes comprise improved grassland (48.3%), acid grassland 44.0%) and broadleaf woodland (5.1%). The sampling site is located at c. 200 m.a.s.l.

H) River Heddon (−3.927516072, 51.21602592)

River Heddon is a semi-wooded catchment with an area of 15.3 km^2 that flows into the estuary at Heddon's Mouth. The area upslope of the sampling point at c. 70 m.a.s.l. largely consists of land cover classes improved grassland (73.9%), broadleaf woodland (17.3%) and acid grassland (6.9%). Different to the other catchments, a large area of bedrock of catchment H compose metamudstones (24.17%).

I) Exmoor Pool (−3.77475500, 51.17675100)

Sampling site I, Exmoor Pool, is a semi-permanent water puddle at an elevation of c. 385 m.a.s.l. located in the same catchment as site E and composes a

headwater source to Farley Water (Figure 42). In this study, it is assumed that most groundwater water on Exmoor is similar in quality and chemical composition and site I therefore represents "headwater" and is compared to all sites in this study. This peaty site is classified as acid grassland cover underlain by sandstone.

Figure 42 Sampling site I, Exmoor Pool, the most elevated semi-permanent pool of running water at the mire headwater source.

4.2 Hydrological analysis

A DEM constructed from *SRTM arc-1-second* with 30 m resolution (*Earthexplorer*, downloaded 2018-09-11) of the study area was used as input for hydrological analysis. The DEM was transformed by the *Fill sinks (Wang & Liu)* tool and then Strahler stream order was calculated by *SAGA* tool *Strahler order* using b-spline interpolation as the resampling method (Table 17). The minimum slope in degrees was set to 0.01. A channel network as created by *SAGA channel network and drainage basins* module, using the SRTM-image as elevation input, with a threshold of 5, using b-spline interpolation. Catchment area was created

with multiple flow direction and b-spline interpolation. Watershed basins were then created with the tool *SAGA Watershed.*

Field sites Exmoor

Site	Stream	LAT	LONG	Watershed area (km^2)	Strahler order*
A	Horner Water	-3.57965502	51.19853524	21.4	3
B	Weir Water	-3.68530697	51.20484971	7	2
C	Badgworthy Water	-3.73142077	51.21574435	25.2	4
D	Slocombeslade stream	-3.75595812	51.20941233	0.9	2
E	Farley Water	-3.8030253	51.20786778	8	3
F	Hoaroak Water	-3.81625256	51.2082984	8.1	3
G	Barbrook	-3.8430153	51.21360397	12.9	3
H	River Heddon	-3.92751607	51.21602592	15.3	2
I	Exmoor pool	-3.77115836	51.16730385	8	1**

* Calculated from DEM
** Field observation only

Table 17 List of Exmoor water sampling sites.

4.3 Field sampling Exmoor

Surface water samples were collected bimonthly–monthly during 2017–2018 from the 9 sampling sites (Table 17) described above, comprising eight sites in eight catchments, named by letters A–H, complemented by a moorland site situated in catchment *E* on Exmoor, site I, which represented a headwater site for all other catchments. Temperature, pH and conductivity were measured directly in the flowing water by a portable pH & EC reader which automatically compensated for temperature (*Combo by Hanna, HI 98130*). The samples were transported to University of Exeter laboratories on the sampling day and stored dark and refrigerated (c. 4–6 ° C) before further treatment, experiment and analysis.

4.4 Experimental and analytical methods

4.4.1 Sample preparation

The raw stream samples were filtered with a vacuum pump to collect initial total suspended particulates (TSP) onto pre-combusted (100 ° C) >0.7 μm biologically inert 100% borosilicate microglass fibre filters (Fisherbrand™). The filters were

dried at 40°C for 24 hours before being weighed for TSP. The filtrates were stored dark and cold (4–6°C) before division into experimental replicates.

4.4.2 Experimental design of flocculation study

The experiment was set up at the laboratory facilities at the Department of Geography, University of Exeter. Each of the filtered stream site water samples were divided into four treatment groups: *T1*) control (no additives), *T2*) clay mixing (0.5 g added ITP32 plastic clay standard), *T3*) saline mixing (10 mL added saline mixture of deionized water and *Tropic Marin®* PRO-REEF salt standard), *T4*) combined saline and clay mixing, according to description above. The certified reference material used as a clay standard composed of IPT32 (CRM 1763-103, Brazil) which served as an anionic polyelectrolyte coagulant to remove colloids in treatments T2 and T4. The artificial saltwater standard comprised *Tropic Marin®* PRO-REEF with a salinity of 32.64 ppt[27]. Within the four treatment groups there were four replicates, each experiment was further complemented by four replicates of control blanks comprising deionized water treated according to the same procedure.

The treated samples were allowed to flocculate in acid-washed beakers with lids on magnetic stirrer boards for 22 hours before secondary filtration. Each flocculation experiment was conducted at room temperature (20–25°C) and inside a reflective container to avoid influence from insolation (Figure 43). The beaker magnets were set to moderate mixing at the bottom of the beakers, to induce moderate turbulence.

---

[27] compared to real average seawater with a salinity of 35 ppt (Atkinson & Bingman, 1998)

Figure 43 Flocculation experiment, experimental light-reflective igloo and closed sample jars.

In total 144 samples were analysed from the experimental study, accompanied by 16 blanks. The samples were filtered and stored in acid washed glass vials with silicone PTFE septa lids (Fisherbrand™ EPA) before further analysis.

4.4.3 Treatment groups

Treatment T1 compose the control group, where no additives have been reacted with the subgroup replicates, and the results from this group represent the colloid heterogeneity of the replicates.

Treatment T2 clay mixing, composed a 0.5 g additive of IPT 32 kaolinite standard to each of the subsample replicates. T2 aimed to mimic the input of minerogenic particles due to soil erosion. The clay standard was added as a dry powder, unlike the additives of treatments T3 and T4.

Treatment T3 saline mixing, composed an additive of 10 mL artificial seawater solution. The resulting salinity of treated samples was 32 ppt, compared to actual seawater salinity, commonly 35 ppt. T3 mimics the mixing of riverine water with marine seawater in estuaries. For T3 an additional study on the effect of salt water concentration was conducted on headwater samples from site I, to investigate the relationship of coagulation and flocculation with salinity.

Treatment T4 combined saline and clay mixing, composed of a mixture of 0.5 g plastic clay standard (IPT32) and 10 mL artificial seawater (same mixture

as in T3, mimicking the mixing of riverine water containing high total suspended particles (TSP) loads with marine seawater in estuaries.

4.4.4 Post-experimental analysis

Post-experimental analyses were undertaken partly at University of Exeter (dissolved organic carbon by liquid total carbon analyzer (TOC), particulate matter by loss on ignition) and partly with collaborators at Uppsala University, Sweden (mass spectrometry, absorbance, and fluorescence).

4.4.4.1 TOC analysis

Filtrates of raw stream samples and post-experimental samples were analysed for DOC by Shimadzu TOC-liquid analyzer for resulting organic carbon concentration at University of Exeter. The calculated standard error of the mean for standards and blanks were 4% (standard 50 mg L-1), 2% (5 mg L-1 standard) and 1% (analytical blanks). For comparison, selected replicate samples were also analysed for DOC at Uppsala University, Sweden, with a Shimadzu TOC-liquid analyzer.

4.4.4.2 Organic matter in stream TSP

Loss on ignition (LOI) was done at University of Exeter to determine the OM% of TSP in 110 sample filters that were oven-dried at 100°C in pre-weighed crucibles, before combustion at 500°C for 4 hours. The loss in weight corresponds to the weight of organic matter in the TSP noted on a 4-decimal balance.

4.4.4.3 Mass spectrometry

Mass spectrometry was used to determine the composition of DOM by direct infusion electrospray ionisation (ESI) Orbitrap mass spectrometry (Fleury et al, 2017) at Uppsala University, Sweden. The method utilizes solid phase extraction, using 100 mg Bond Elut PPL cartridges (Agilent Technologies) that were cleaned in a methanol bath overnight followed by rinsing with formic acid (0.1%). Due to the low concentrations of DOC in the stream water samples, replicates were combined into a single 160 mL sample per site and treatment.

Sample results were corrected against treatment blanks; peaks in samples that were present at three times or above the corresponding peak in the treatment blank were considered and corrected by subtracting the peak intensity of the blank from the peak intensity of the sample, before normalisation against total sample intensity. Compounds of raw and experimental treatment filtrate samples were grouped by black carbon, polyphenols, highly unsaturated hydrocarbons, aliphatics, peptides, and sugars, by formulae for weighted average H/C and O/C ratios, after Seidel et al (2014). While *van Krevelen* diagrams can be readily used to plot and relate specific clusters of similar compound structures derived from high-resolution mass spectra (Kim et al, 2003), it needs to be emphasized that this assignment of organic species into compound groups provides a very simplified overview of which molecular structures may be present in a DOM sample, and that the identified molecular formulae rather represent mixtures of isomers than any individual structural entity (Seidel et al, 2014). However, *van Krevelen* diagrams have been used extensively and successfully to visualize and assign these compound groups in studies on DOM characteristics, and provides a useful tool in tracking for instance diagenetic and decay effects in natural organic matter (Kim et al, 2003). In this study, the identified molecular formulae in residual DOM filtrates were inspected by principal coordinate analysis (PCoA) to identify effects of experimental treatments T2, T3 and T4 by pair-wise comparison to the control samples of T1.

4.4.4.4 Absorbance and fluorescence

Pre-filtered water samples were measured for UV-Vis absorbance in wavelengths 250–600 nm by Lambda35 UV-Vis Spectrometer (PerkinElmer Lambda 25, Perkin Elmer, Waltham, USA) at Uppsala University, Sweden.

Fluorescence excitation-emission matrix (EEM) spectroscopy is a common technique that performs detailed mapping of fluorophores and can be used to determine qualitative properties of residual dissolved organic matter in natural waters (Bauer & Bianchi, 2012; Bieroza et al, 2012). Synchronous fluorescence was measured on selected raw and experimental filtrate samples by a FluoroMax-4 Spectrofluorometer (FluoroMax-4, Jobin Yvon, Horiba, Kyoto, Japan) at Uppsala University, Sweden. Measurements were done with excitation-emission matrices (EEMs) at wavelength 250–445 nm by 5 nm increments and

131

300–600 nm by 4 nm increments, using daily Milli-Q water as blanks to correct for instrumental drift. Fluorophore components were identified by Parallel Factor (PARAFAC) analysis, discussed below.

4.4.4.5 PARAFAC analysis

A well-suited chemometric multi-way technique to identify DOM characteristics from fluorescence EEM spectra is PARAllel FACtor (PARAFAC, also known as canonical decomposition; CANDECOMP) analysis (Bro, 1997), which is a decomposition method in chemical sciences used to identify primary components of trilinear multi-way data (Stedmon & Bro, 2008, Murphy et al, 2014). One advantage of PARAFAC is that it utilizes threeway analysis and therefore does not suffer from rotational ambiguity, compared to other twoway analysis techniques where for instance spectral overlap complicate interpretation of results (Murphy et al, 2014). PARAFAC is a commonly used method for spectral decomposition and quantification of fluorescence EEMs into primary components (Murphy et al, 2013), for instance to characterise chromophoric components of organic matter to identify its various sources in the aquatic continuum (Stedmon et al, 2003). PARAFAC analysis was used to identify the components of cDOM in raw and experimental stream filtrate samples.

4.4.4.6 Freshness index (FRESH), fluorescence index (FI), and humification index (HIX)

The fluorescence index (FI) is a ratio between emission wavelengths 470–520 nm at excitation wavelength 37 and serves as an indicator of terrestrial and microbial sources where a higher FI (c. 1.8) indicates microbial origin, while a lower (c. 1.2) FI represent a terrestrial DOM (Fellman et al, 2010). Similarly, the freshness index (FRESH) is the ratio between the emission intensity at 380 nm and maximum intensity found between 420–435 nm at excitation wavelength 310 nm. FRESH is an indicator of how recently produced the DOM is. The humification index (HIX) is calculated from the area under 435–480 nm divided by the sum of peak areas from 300–345 and 435–480 nm at excitation wavelength 254 nm. Higher values of HIX indicate an increased degree of

humification (Hansen et al, 2016). FI, FRESH and HIX ratios were determined for cDOM in raw and experimental stream filtrate samples.

4.5 Summary of Chapter 4

In this chapter, the Exmoor field sites and methods were presented for the flocculation study. The sites were chosen for their similar drainage settings, land use and geology and represent a group that is well-suited for field replication. The results from this study are presented in Chapter 6.

Chapter 5. Results Brazilian reservoir catchment study

This study focused on the transport of POC in a semi-closed tropical headwater catchment which has been impacted by human perturbation through land use change and damming. Quantification of soil and organic carbon export from catchment slopes to the reservoir through zones of autochthonous organic matter production was undertaken to understand the fate of terrestrial (allochthonous) and aquatic (autochthonous) organic matter in this catchment. The results presented in this chapter summarize 1) the POC distribution and quality in the soils and sediments, 2) the erosion and sedimentation rates in the catchment and reservoir estimated by the RUSLE model and measured by field observations through fallout radionuclides, and 3) an estimate of the POC redistribution rates which reveals the fate of POC in the catchment.

5.1 POC inventories and quality in João Penido watershed

5.1.1 Soil and sediment properties

In this section basic properties (bulk density, particle size) for the samples collected in the field are presented.

5.1.1.1 Bulk density of soil and sediment samples

Mean bulk density for João Penido soils and sediments are summarized in Table 18. The mean bulk density of top soils was 1.03 g cm^{-3}. For top soils down to 20 cm depth, the mean bulk density amounted to 1.00 and 1.05 g cm^{-3} for shrubland soils and pasture soils respectively. This low soil bulk density is likely connected to high porosity and relatively coarse texture, as it is poor in organic matter. For reservoir sediments the average bulk density amounted to 1.37 g cm^{-3}, which is indicative of high porosity, but compared to catchment soils the sediments in general composed finer textures and contained relatively higher organic matter content. Pre-flooding material had an average bulk density of 1.61 g cm^{-3}. The standard deviation is high for these soils and sediment samples in the João Penido catchment, suggesting there is a high variability in factors influencing density in these soils and sediments, such as porosity, grain size, organic matter content and moisture (%). Maximum bulk density occurrerd in colluvium samples, which also showed the highest standard deviation (0.62-0.68).

Bulk density (g cm⁻³) of soil and sediment samples from João Penido

Sample type	Selection	N	Mean	Min	Max	StDev
Sediment <20 cm depth	All	242	1.43	0.48	2.85	0.41
Deltaic		15	1.47	0.97	2.07	0.26
Reservoir sediments		175	1.37	0.48	2.85	0.40
Pre-flood sediment		53	1.61	0.94	2.41	0.44
Soils <20 cm depth	All	323	1.03	0.31	4.09	0.40
Soil shrubland		116	1.00	0.53	1.69	0.23
Soil pasture (incl. colluvium site)		207	1.05	0.31	4.09	0.47
Colluvium <20 cm depth		27	1.33	0.67	4.09	0.68
Colluvium		43	1.11	0.44	4.09	0.62

Table 18 Bulk density of soil and sediment samples in João Penido watershed.

5.1.1.2 Particle size analysis (PSA)

90 samples from three soil profiles (eroding–stable–colluvium) and three reservoir sediment cores were analysed for grain sizes 2000>250 µm, 250>63 µm, and <63 µm separated by dry sieving (Figure 44, Figure 45). The texture of the soil and sediment samples was calculated to range from sandy-clay-loam to sand, with mean sand texture being 95.96% for soil and 93.79% for reservoir sediment. While the soil sites JP02 (shrubland) and JP17 (pasture) showed moderate variation in grain size with profile depth, sediment cores SED2, SED3 and SED5 displayed layers with coarser grain size which would be indicative of historical erosion events in the catchment or resuspension within the reservoir. The colluvium site JP28 showed some differences compared to the soil sites, with low content of the <63 µm faction in the surface of the profile and with increasingly finer fraction present at subsoil levels (>20 cm). Mean particle size of samples (N=26) in the upper 20 cm top soil sections of soil profiles were used to calculate K factor for RUSLE analysis using field observations (see section 3.4.2.2). The results of grain size analysis are summarized in Table 19. Soil (sd=1.56) showed lower variability in grain size than sediments (sd=4.16), which contained a higher amount of finer textures.

Average particle size % distribution

	N		Mean	Min	Max	StDev
Sediment	56	Sand	93.79	74.42	100	4.16
		Silt-clay	6.21	0	25.58	4.16
Soil	34	Sand	95.96	91.82	99.54	1.56
		Silt-clay	4.044	0.46	8.18	1.56

Table 19 Particle size analysis summary results.
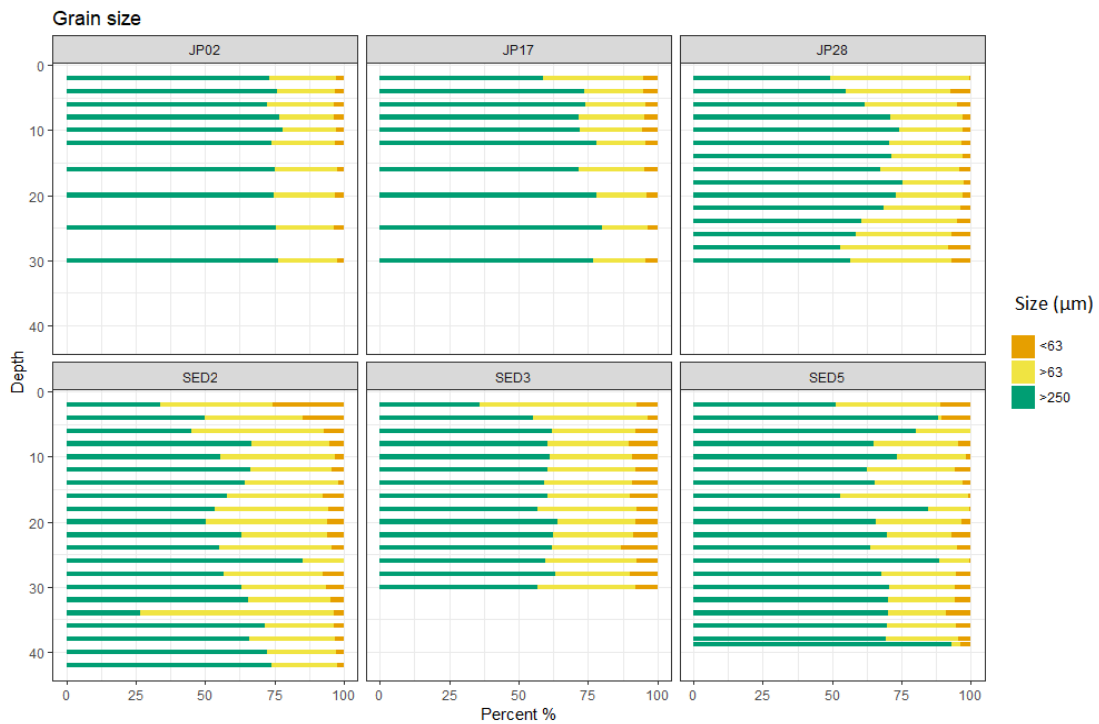
Figure 44 Grain size fraction (mass %) of classes: 2000>250 µm, 250>63 µm, <63 µm for soil cores JP02 (eroding site), JP17 (reference site) and JP28 (aggradation site), and sediment cores SED2, SED3, and SED5 from João Penido catchment.
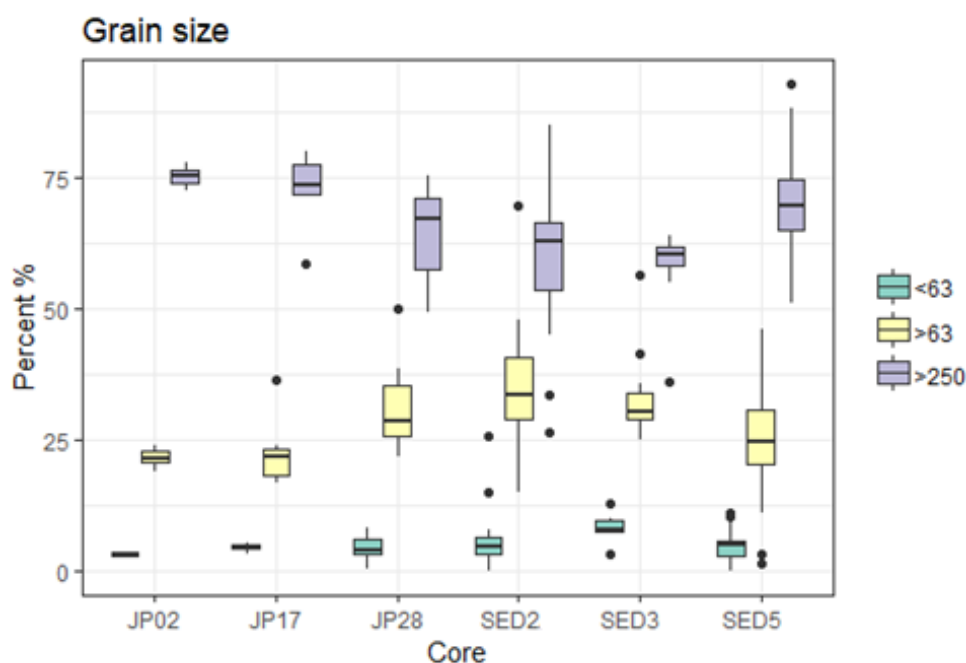
Figure 45 Boxplot showing grain size distribution of six soil and sediment cores.

5.1.2 Carbon, nitrogen and C/N ratio

100 sediment samples and 50 soil samples were analysed for total carbon (C_{tot}), totalt organic carbon (TOC), total nitrogen (N_{tot}) by a *ThermoScientific Flash 2000 Organic Elemental Analyzer*. An additional 401 soil and sediment samples were analysed for organic matter (OM%), organic carbon (OC%) and particulate inorganic carbon (PIC%) by loss on ignition (LOI), with results described in section 5.1.3. This section only presents results from samples analysed by the C/N-method (3.3.3). While OM% is readily determined by the LOI method, results of OC% from the C/N method were used to determine a conversion value which was used to calculate reasonable OC% for soil and sediment samples analysed by the LOI method (described in 3.3.5 Loss on ignition (LOI)).

TOC samples required pre-treatment by acid fumigation to remove carbonates, while C_{tot} duplicates were left untreated prior to analysis. Carbonate content was estimated from the difference C_{tot} and TOC. Additionally, 9 delta sediment samples, 16 sediment samples, and 25 soil samples were analysed for TOC and N_{tot}, by wet-sieved and density separated fractions (see section 3.3.4 for details). Particulate inorganic carbon (PIC) was calculated as the difference between non-fumigated samples (containing total carbon) and acid fumigated (containing organic carbon only) duplicate samples. The results revealed that

137

very little PIC% is present in João Penido samples, between 0–0.39% for soils and sediment (Figure 46).
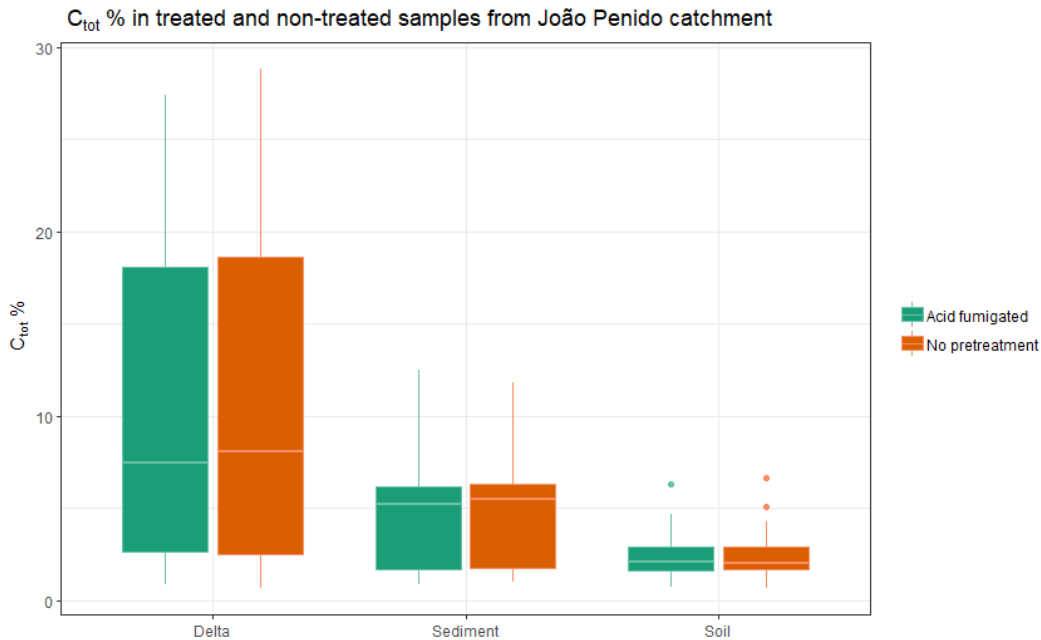
Figure 46 Comparison of C$_{tot}$% in acid fumigated (PIC removed) and non-treated (PIC present) samples from João Penido reservoir.

5.1.2.1 Organic carbon distribution

Acid fumigated samples showed varying OC% distribution in delta sediments, reservoir sediments and soils (Figures 47a, 47b, 47c, Table 20). The highest concentrations with a range of 0.83–27.41% and a mean of 11% occurred in delta sediments, for which a bimodal distribution was observed, which represents a mixture of allochthonous and autochthonous sources. For reservoir sediments the concentrations ranged between 0.83–12.51%, with a mean of 4.53%, also displaying two OC groups. Soil OC% ranged between 0.73–6.30% with a mean of 2.37%. OC content typically decreased with depth in soil profiles, while sediment sites showed varying content depending on sediment depth. Where the observed boundary between post-flooding sediment and pre-flood material occurs, OC concentrations typically decreased to levels of terrestrial soils. This suggests that pre-flood material compose inundated catchment soils. The highest OC concentrations (15–20%) were present in top sediment layers (<20 cm).

5.1.2.2 Total nitrogen distribution

The distribution of N_{tot} in the catchment showed highest concentrations in delta sediments, followed by reservoir sediments and relatively low concentrations in soils (Figure 48, Table 20). The bimodal distribution of N_{tot} in delta sediments is indicative of two organic matter sources, one with lower concentrations similar to terrestrial soils and one with higher concentrations assumed to originate from aquatic organic matter (Figure 48a). The concentrations of N_{tot} ranged between 0–1.71% and showed more variation with depth sediment cores compared to soil profiles (Figure 48b, 48c). The varying pattern with sediment layers is indicative of mixed organic matter input, which can be connected to historical growth patterns of macrophytes and input of soil organic matter.
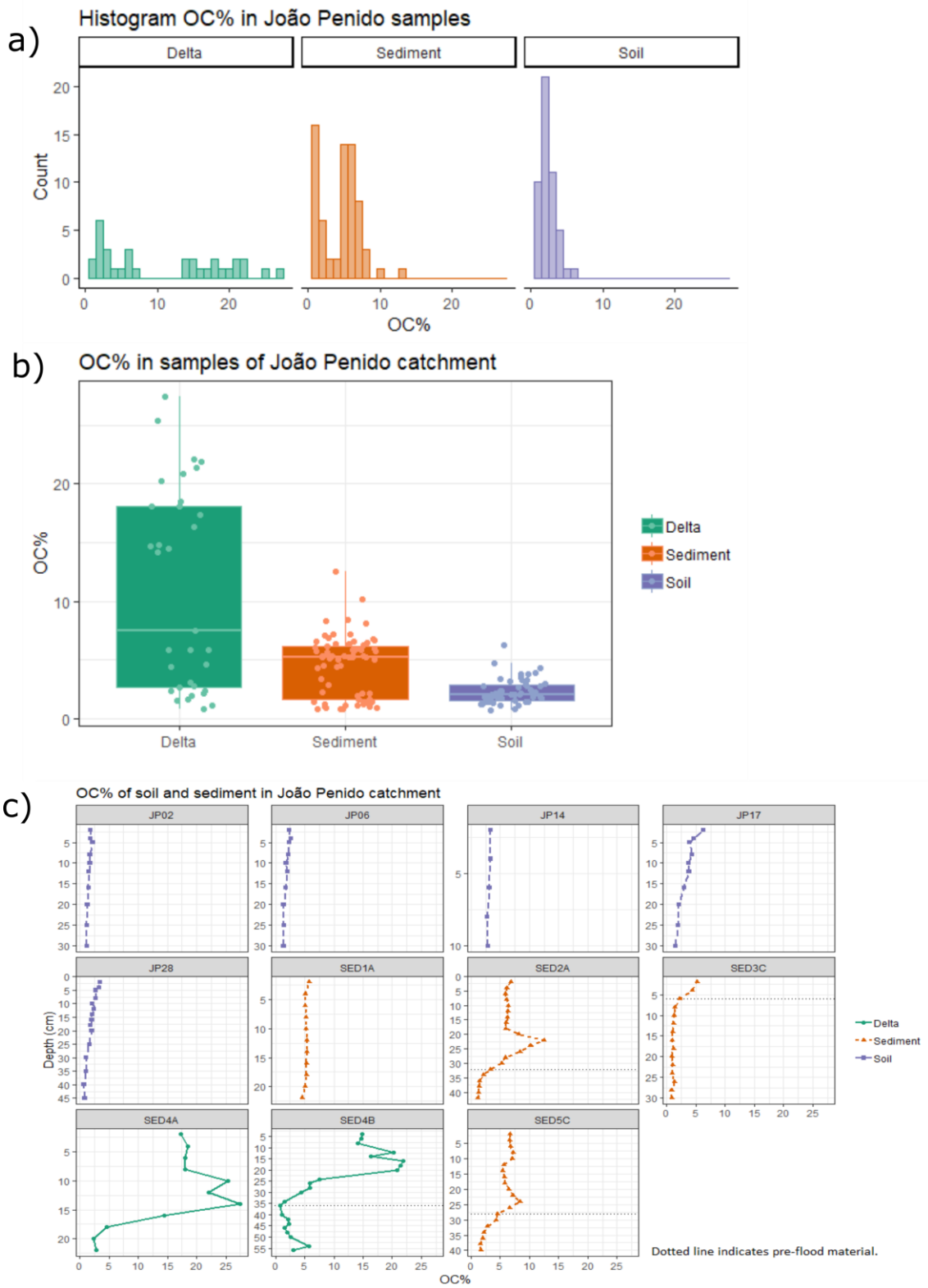
Figure 47 Distribution of OC% in delta, reservoir sediment and soil, displayed by a) histograms, b) boxplot, and c) depth profiles.
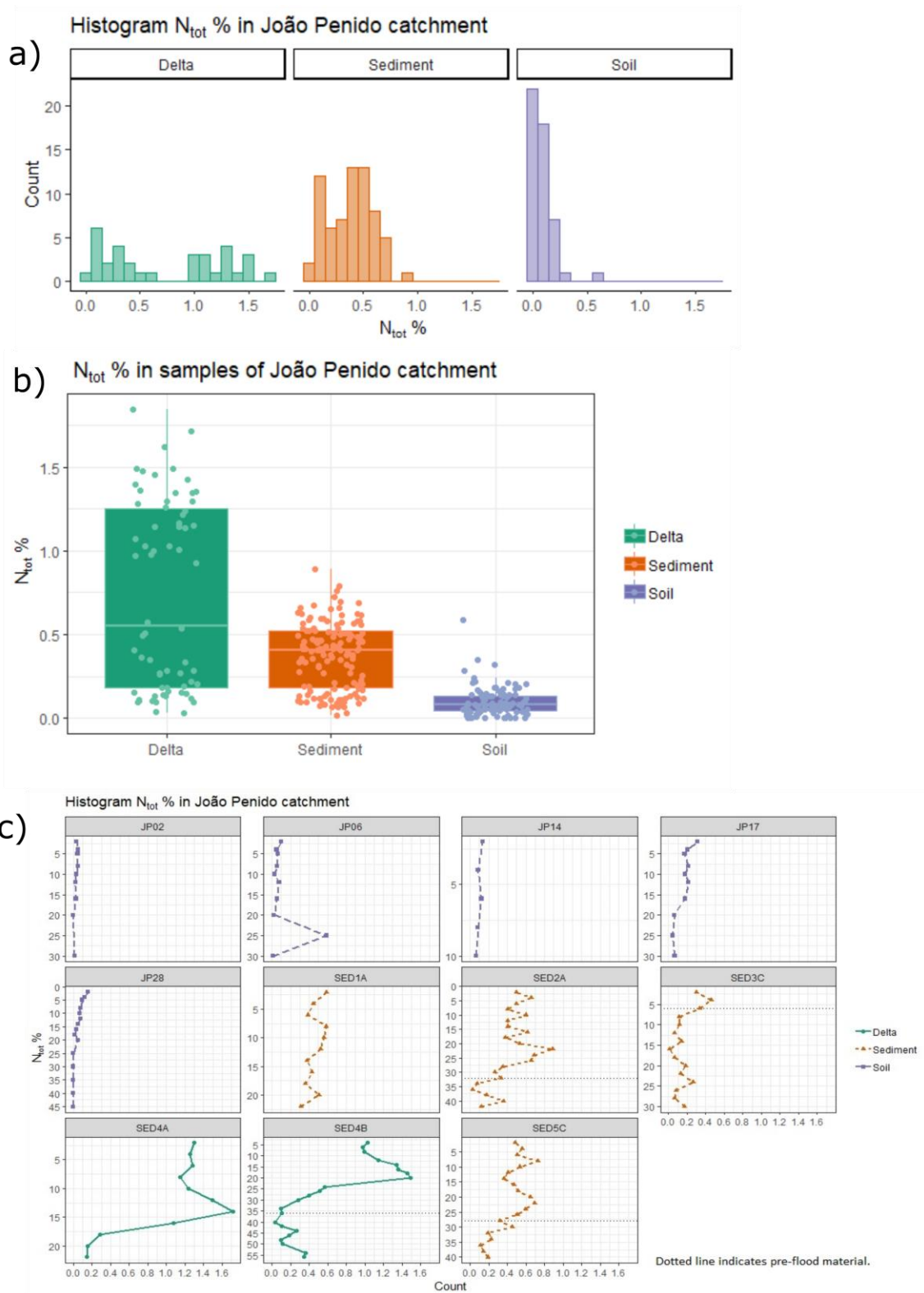
Figure 48 Distribution of N$_{tot}$% in delta, reservoir sediment and soil, displayed by a) histograms, b) boxplot, and c) depth profiles.

5.1.2.3 C/N distribution

The delta sediment cores showed C/N values of 8.04–29.90, with a mean of 15.34 (Table 20), indicating that the delta sediments (profiles 4A and 4B) contained organic matter of more autochthonous aquatic origin rather than allochthonous. Histograms (Figure 49a) and boxplots (Figure 49b) showed that C/N ratios were lowest for delta sediments and reservoir sediments, while highest for soils. Lake sediments in the deeper parts of the reservoir showed C/N ratios ranging 3.41–66.70, with a mean of 13.58, while soil samples displayed the highest C/N ratios of the catchment samples, ranging 2.52–116.43 with a mean of 40.28. Very high soil C/N ratios (>50) occurred in 10 samples, but these could not be explained by observations in the field. The mean C/N ratio of post-flooding sediments (excluding pre-flood material) from 5 cores was 13.49 ($N=5$, $sd=1.65$).

Descriptive statistics of C/N data of João Penido watershed

		N	Minimum	Maximum	Mean	StDev
Delta sediment	N%	33	0.04	1.71	0.73	0.5
	OC%	33	0.83	27.41	11	7.4
	C/N	33	8.04	29.9	15.3	4.7
Reservoir sediment	N%	68	0.01	0.89	0.38	0.3
	OC%	68	0.83	12.51	4.53	4.8
	C/N	68	3.41	66.7	13.58	14.6
Soil	N%	50	0.13	0.59	0.08	0.4
	OC%	50	0.73	6.3	2.37	4.9
	C/N	43	2.52	116.43	40.28	21.4

Table 20 Descriptive statistics of C/N data.

Samples of soil profiles (JP02, JP06, JP14, JP17, and JP28) typically showed C/N ratios above 20 (Figure 50). The top sediments of delta samples from profiles SED4A and SED4B showed mixed towards slightly more terrestrial C/N ratios, while the deeper sediments of SED4B indicated mixed source to a more aquatic origin with lower C/N values. Reservoir sediment showed the largest variability in C/N ratios ($sd=14.6$), which was expected due to its mixed sources of allochthonous and autochthonous POC.
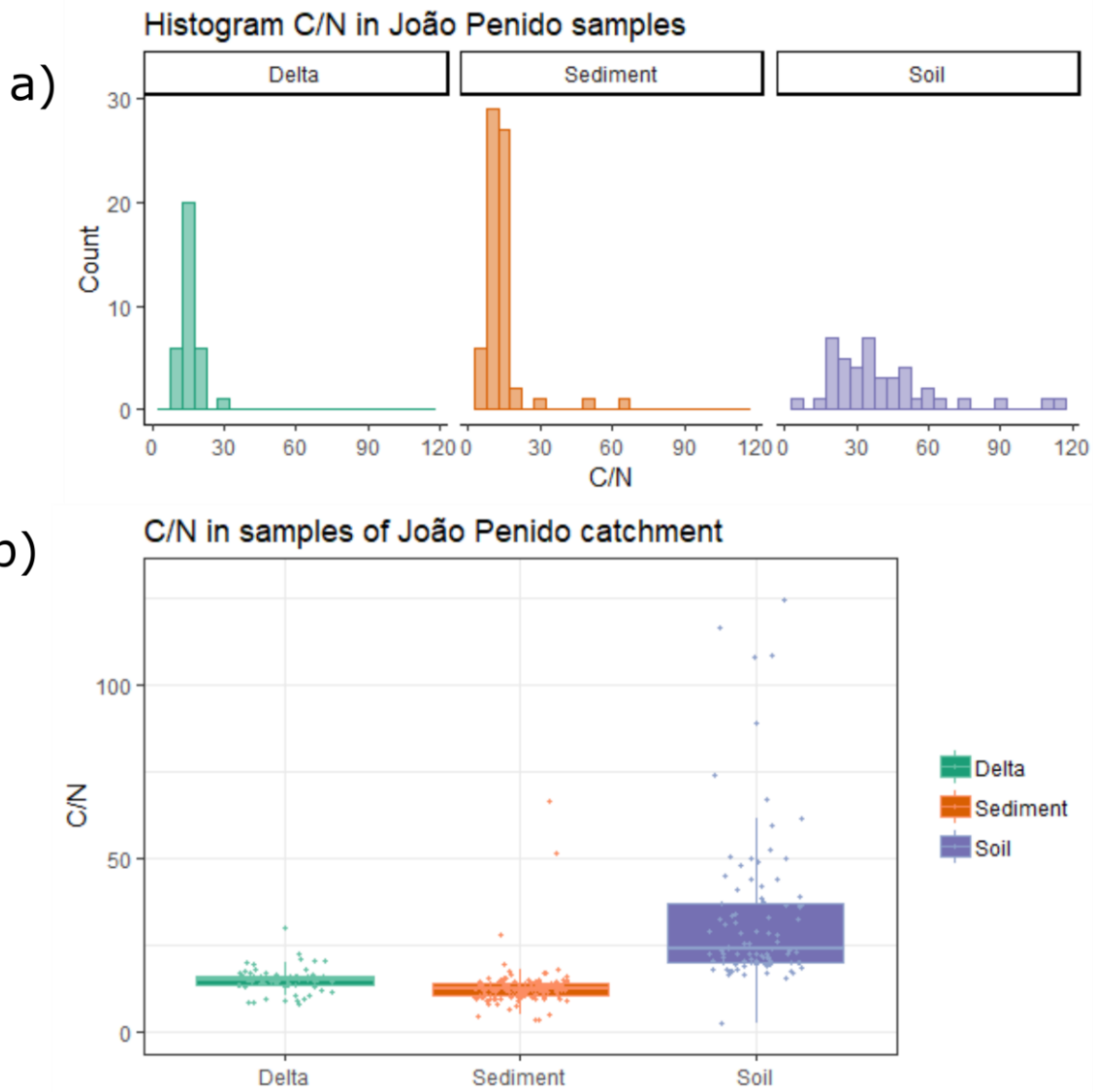
Figure 49 Distribution of C/N in delta, reservoir sediment and soil, displayed by a) histograms and b) boxplot.
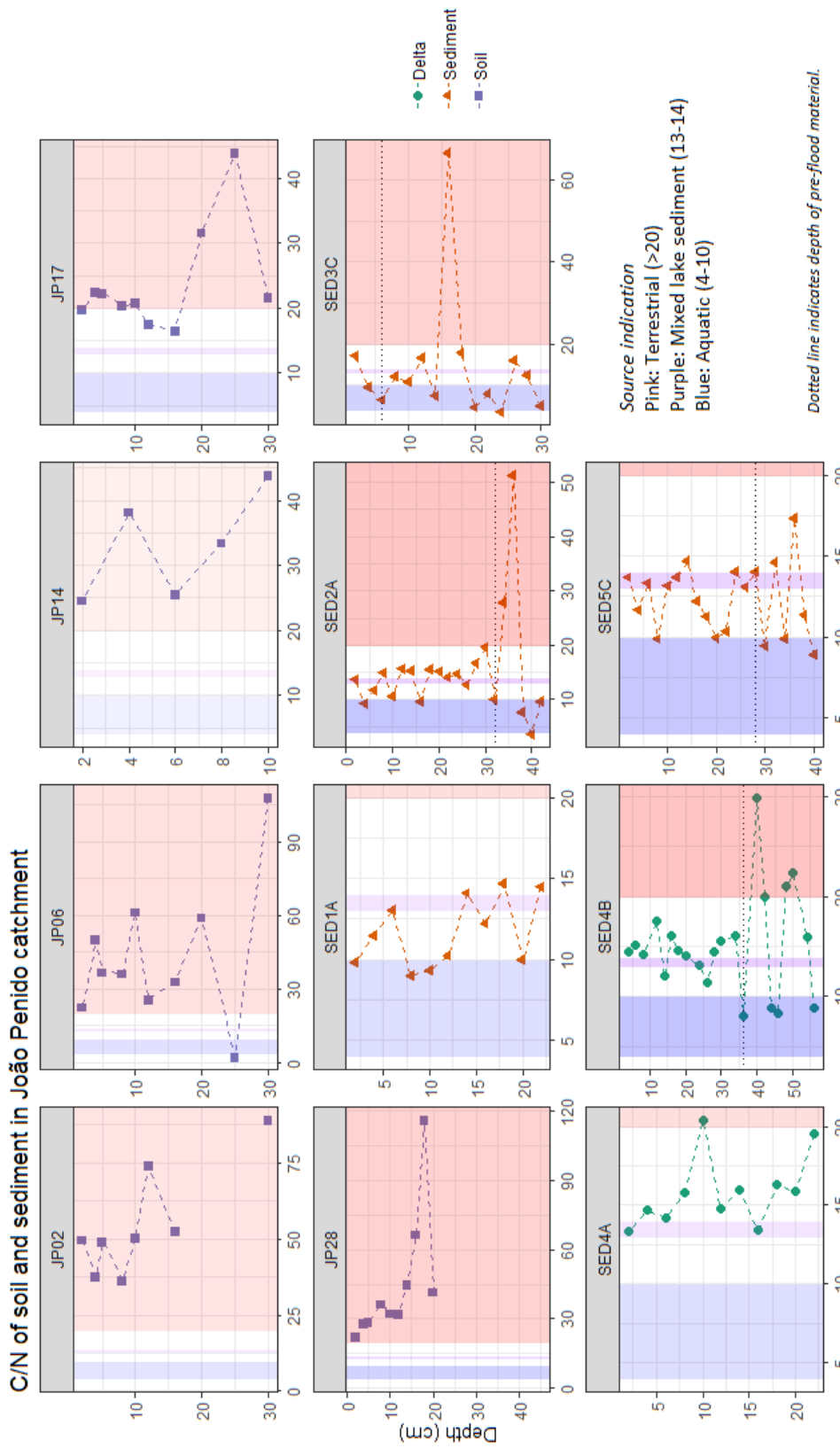
Figure 50 C/N ratios for acid fumigated samples from delta (SED4A, SED4B), sediment (SED5A, SED2A, SED3C, SED5C) and soil (JP02, JP06, JP14, JP17, JP28). Higher ratios (>20) indicate terrestrial organic matter, while low ratios (4–10) indicate aquatic organic matter, e.g. algae and macrophytes.

The sediment sites showed mainly low C/N values typical of lake sediments with aquatic origin, although a few outliers of SED2A and SED3C appear to have sediment layers indicative of terrestrial input. The differences in C/N signatures were distinct for the terrestrial and aquatic samples, and delta sediment showed similar trends to soil suggesting that some of the delta POC is of terrestrial origin.

5.2.3.4 C/N of samples from density fractionation

Wet-sieved samples separated into fractions 2000>250 μm, 250>53 μm and <53 μm showed maximum C/N values (17.22–126.15) in fine fraction soil samples from pasture sites (Figure 51). All fractions from samples of pasture soils showed more enriched OC% and N% content compared to shrubland, while the highest concentrations occurred in reservoir sediments (Figure 52).
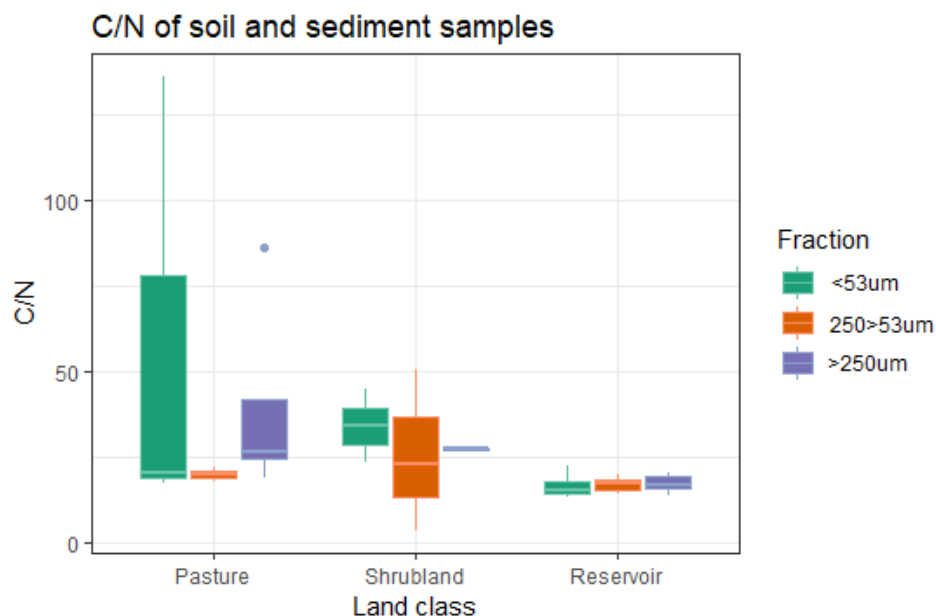
Figure 51 C/N ratios in density wet-sieved fractions of soil (pasture, shrubland) and sediment (reservoir) samples. The finer soil fractions show the maximum C/N ratios.
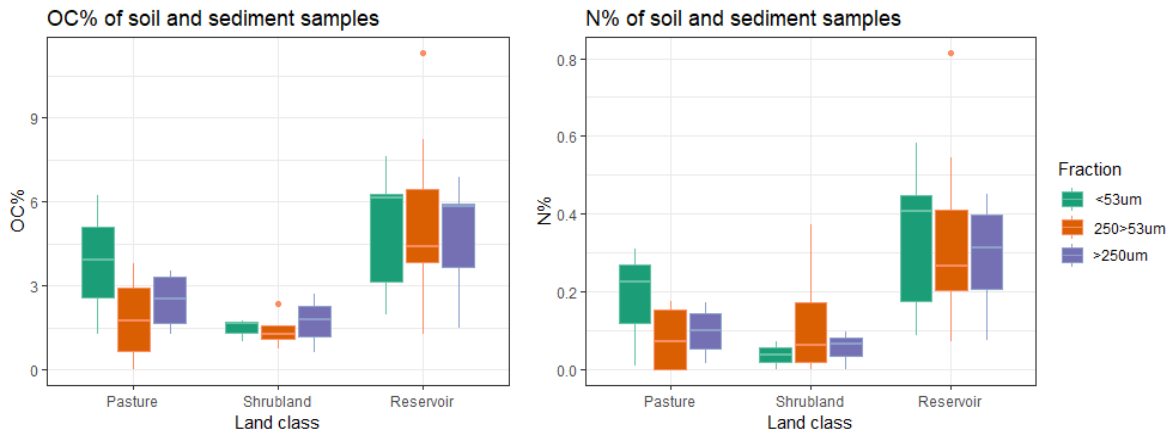
Figure 52 Density-separated samples showing C% and N% of the heavy fraction (>1.65 g cm^{-3}).

Only 6 samples provided enough light inter-aggregate organic material from density fractionation for analysis. These light samples appear to follow a separate mixing line compared to the heavy fractions (Figure 53).
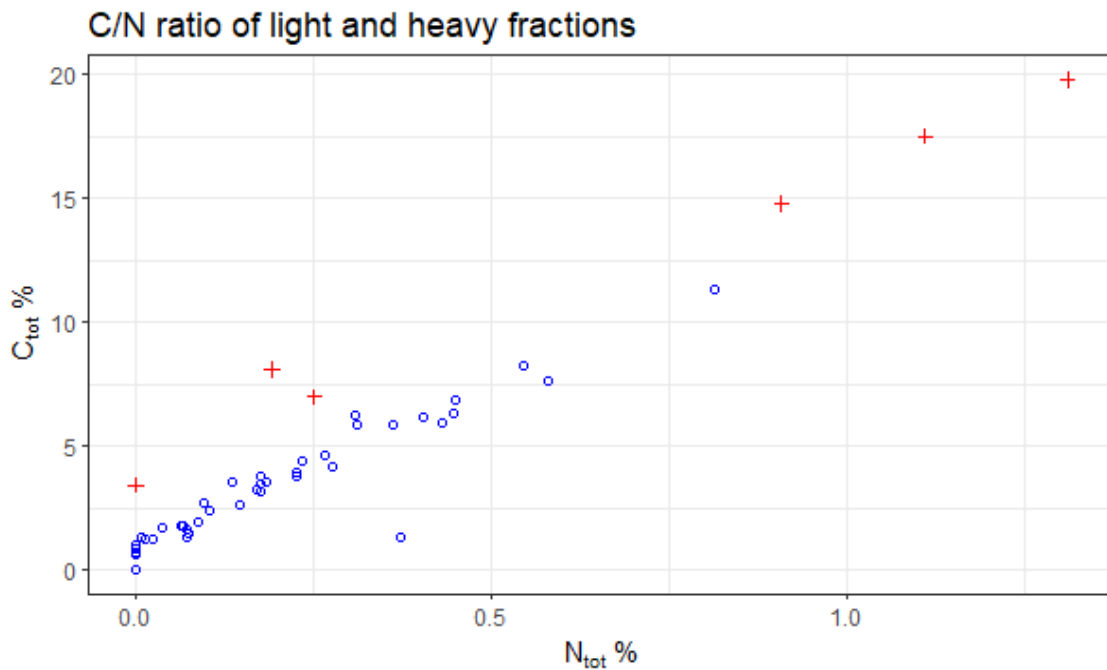
Figure 53 Relationship of carbon and nitrogen in light (red crosses) and heavy (blue circles) density-separated fractions (light<1.65 g cm^{-3}<heavy).

5.1.3 Loss on ignition analysis of organic matter (OM), organic carbon (OC%) and carbonates (PIC%)

Basic statistics of particulate OM, OC and PIC content of soils (upper 20 cm), delta sediments, reservoir sediments, pre-flood material and terrestrial colluvium are summarized in Table 21. The highest concentrations of organic matter were present in delta (30.76%) and reservoir sediments (22.51%), while soils (13.99%), colluvium (9.29%) and pre-flood soils (11.46%) showed similar low mean concentrations.

Descriptive statistics loss on ignition (LOI) data

		N	Mean	SE mean	StdDev	Min	Max	Range	Variance
OM%	Soil (top 20 cm)	169	13.99	0.35	4.5	7.21	63.83	56.62	20.24
	Colluvium	49	9.29	0.49	3.43	4.12	16.13	12.02	11.78
	Delta sediment	17	30.76	4.59	18.92	1.66	62.79	61.13	357.89
	Reservoir sediment	133	22.52	0.9	10.32	8	72.09	64.09	106.56
	Pre-flood	32	11.46	0.88	5	4.38	28.1	23.72	25.04
OC%	Soil (top 50 cm)	169	2.8	0.07	0.9	1.44	12.77	11.32	0.81
	Colluvium	49	1.86	0.1	0.69	0.82	3.23	2.4	0.47
	Delta sediment	17	7.69	1.15	4.73	0.41	15.7	15.28	22.37
	Reservoir sediment	133	5.63	0.22	2.58	2	18.02	16.02	6.66
	Pre-flood	32	2.86	0.22	1.25	1.09	7.02	5.93	1.57
PIC%	Soil (top 50 cm)	129	0.92	0.13	1.52	0	16.7	16.7	2.3
	Colluvium	32	0.5	0.03	0.17	0.3	0.9	0.6	0.03
	Delta sediment	16	1.19	0.19	0.75	0.1	2.5	2.4	0.56
	Reservoir sediment	110	1.5	0.09	0.9	0.4	7.7	7.3	0.81
	Pre-flood	18	0.52	0.07	0.3	0.2	1.1	0.9	0.09

Table 21 Descriptive statistics of OM%, OC% and PIC% in upper 20 cm soil and sediment layers João Penido catchment.

5.1.3.1 Organic matter (OM) %

The distribution of OM% showed highest concentrations in delta sediments (1.66–62.79%) and reservoir sediments (8.0–72.09%) compared to top soils (7.21–63.83%), colluvium (4.12–16.13%) and pre-flood material (4.38–28.1%) which showed similar trends in OM content (Figure 54). In general, top soils and sediments displayed higher contents of organic matter, compared to subsoils and deeper sediments (Figure 55b). Some shallow pre-flood material samples

147

occurred in top sediments (upper 20 cm) where the post-flooding sediment layer was thin, but did not display markedly higher concentrations that sublayers.
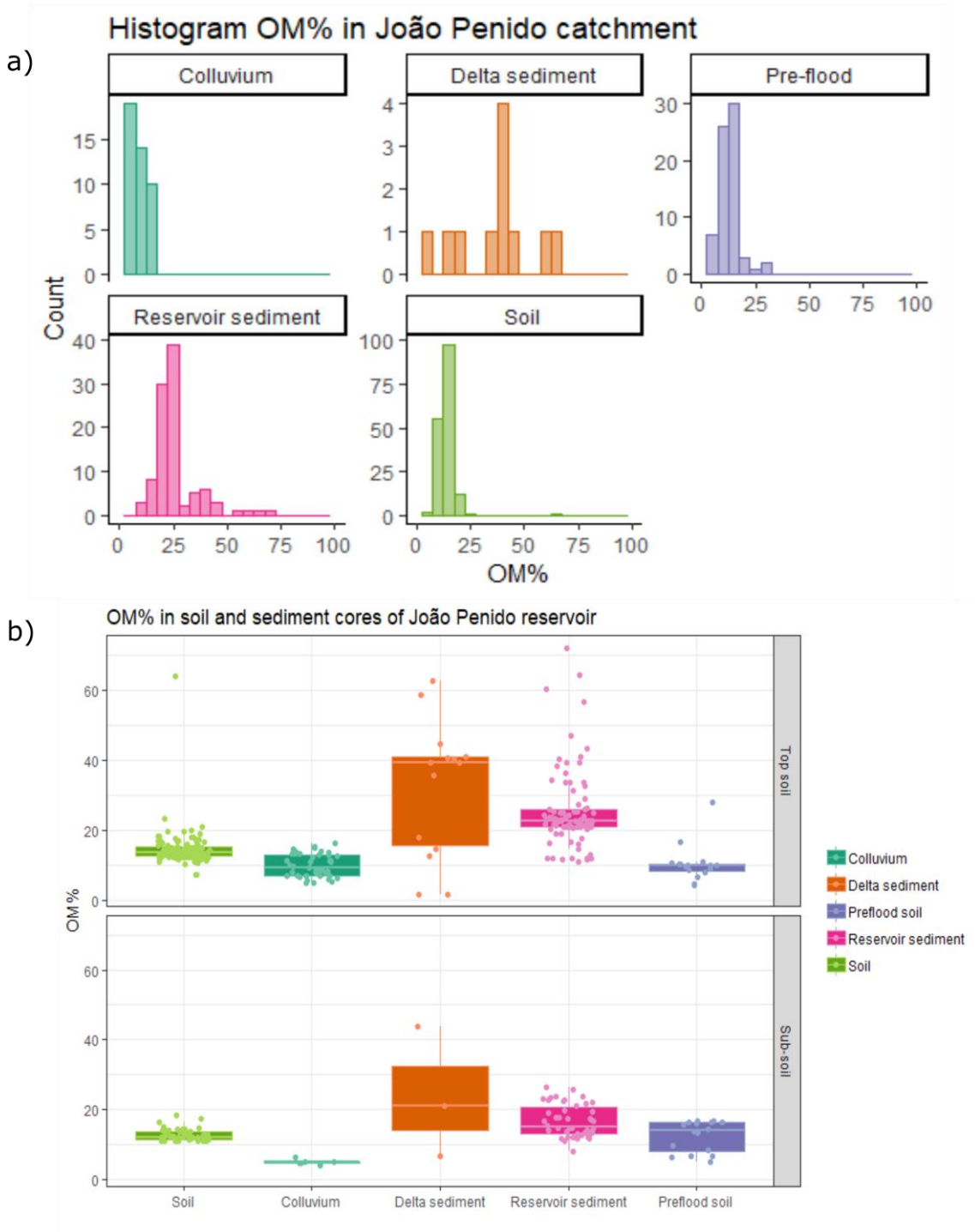
Figure 54 Distribution of OM% in João Penido catchment soils and sediments from LOI analysis, displayed as a) histograms, and b) boxplots. Top soil (upper 20 cm) and sub-soil (below 20 cm) show similar distribution for the chosen classes.

The carbonate vs. OM% showed different trends for sediments and soils with slightly elevated PIC% in deltaic and reservoir sediments. Reservoir sediments, especially waterlogged delta sediments, showed up to ca 4 times higher OM content compared to colluvium. The inundated soils below the post-flooding sediment showed a mean value of 2.86% for OC and 11.46% OM, which is more similar to values of catchment soils.

5.1.3.2 Organic carbon (OC) %

Organic carbon (OC) was calculated from by a conversion factor of 20% for soils and 25% for sediments, derived from C/N analysis (3.3.5). The results showed OC% ranging between 0.82–12.77% for soils, where non-managed shrubland had a mean of 2.93% and pasture soil had a mean of 3.32%. Sediments showed OC% between 0.41–18.02%, where deltaic sediments had a mean of 7.69% and reservoir sediments a mean of 5.09%. The pre-flood material showed OC content between 3.02–5.67%, with a mean of 4.14%. The delta samples contained the widest range of OC% values, whilst eroding soils rarely exceeded values above 10%. Plotting organic matter against organic carbon showed that different media varied in organic carbon content relative to organic matter content (Figure 55).
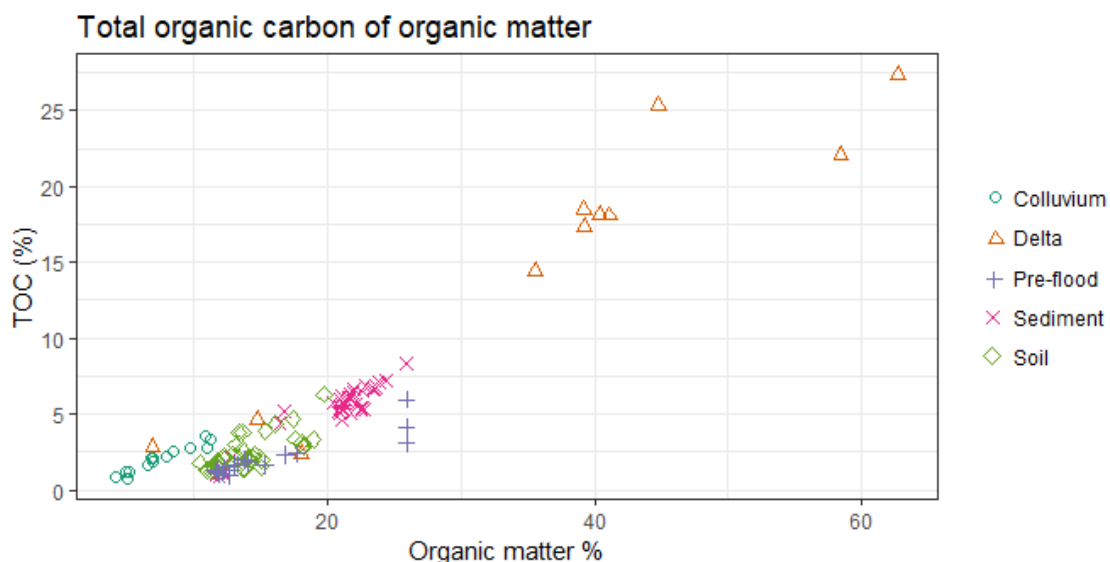
Figure 55 Relationship of TOC% and OM% in soil, delta sediment, post-flooding reservoir sediment and pre-flood material.

149

5.1.3.3 Carbonates %

Carbonates were abundant in low concentrations in the study area, with a mean of 0.8% for soils and 1.3% for sediments. In general, the lowest mean concentrations were present in colluvium, while higher mean values were found in delta sediments and reservoir sediments (Figure 56). These results differ from the results of TC analysis, where PIC was determined as the difference between the non-fumigated (TC) and fumigated (TOC) samples. The differences arise partly from the uncertainties of the loss on ignition method, and partly from the differences in sample size, where LOI samples (0.8-11.0 g) were larger than for TC analysis (14.8–19.7 mg).
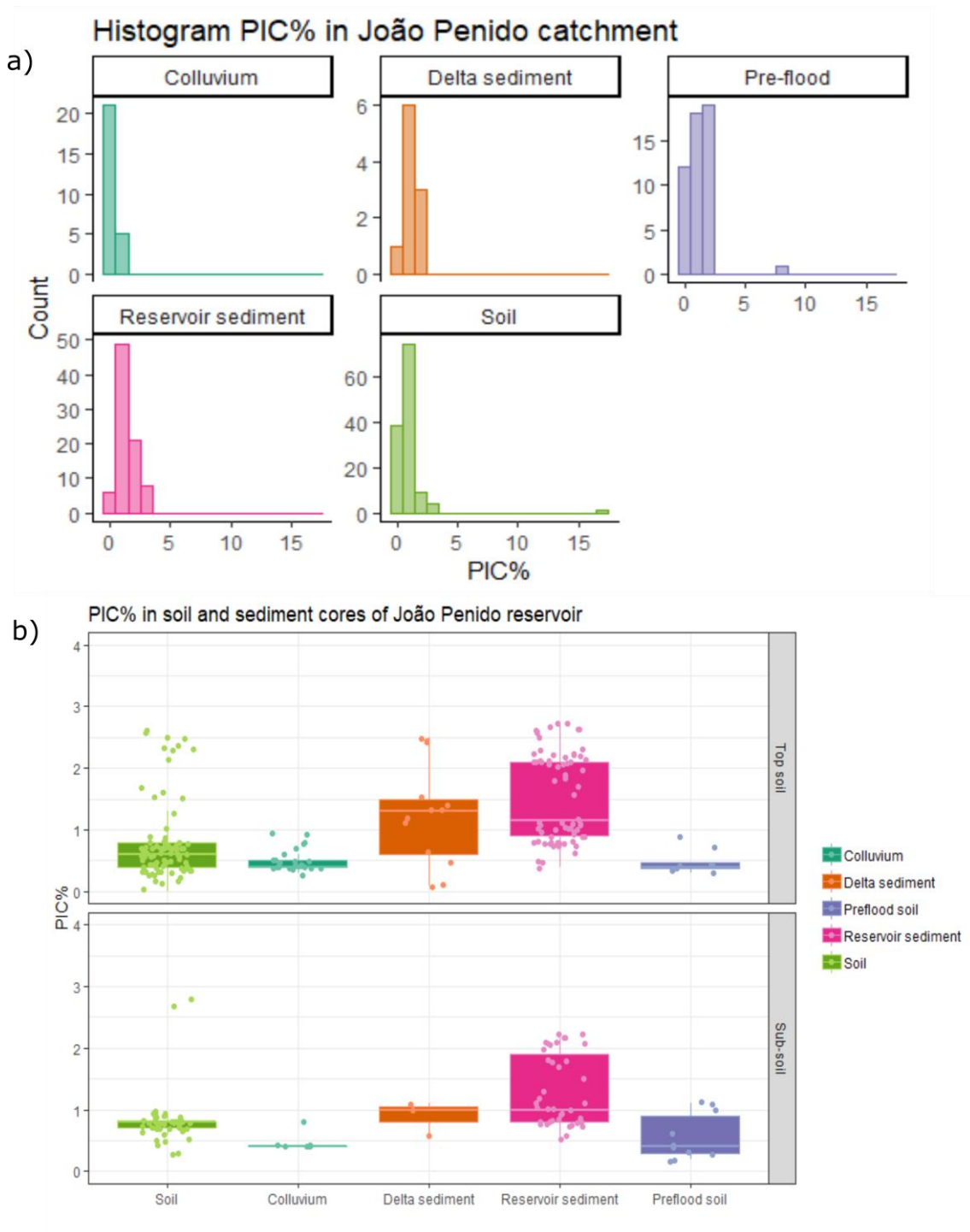
Figure 56 Distribution of PIC% in João Penido catchment soils and sediments from LOI analysis, displayed as a) histograms, and b) boxplots.

5.2 Erosion in João Penido watershed

This section summarizes the output of fallout radionuclides and RUSLE model to assess the soil erosion rates and sedimentation in João Penido watershed, using database and field observations.

5.2.1 Fallout radionuclide results

The concentrations and inventories of ^{137}Cs and ^{210}Pb$_{ex}$ in soils and sediments are presented in this section.

5.2.1.1 Radionuclide concentrations and inventories

336 samples were analysed for ^{137}Cs concentrations, out of which 174 samples provided a positive ^{137}Cs-signal. For ^{210}Pb, 254 soil samples were measured. From sediment sites, 76 sediment samples were analysed for ^{137}Cs and ^{210}Pb$_{ex}$. Radionuclide inventories used for soil erosion modelling are summarized in Table 22 (complete cores) and in Table 23 (samples of soil profiles). *Shapiro-Wilks* normality test showed that radionuclide sample concentrations (mBq g^{-1}) were not normally distributed: ^{137}Cs (W=0.46, p<0.005) and ^{210}Pb$_{ex}$ (W=0.45, p<0.05). *Spearman correlation* between ^{137}Cs and ^{210}Pb$_{ex}$ concentrations (mBq kg^{-1}) was weakly positive (r_S = 0.198, p = 0.045), while the correlation between ^{137}Cs and ^{210}Pb$_{ex}$ site inventories (Bq m^{-2}) was higher (r_S = 0.50, p = 0.015).

Summary table fallout radionuclides

Core depth (cm)	Core	^{137}Cs N positive samples /total	^{137}Cs activity (mBq g^{-1})	Inventory ^{137}Cs (Bq m^{-2})	E/A	$^{210}Pb_{ex}$ N positive samples /total	$^{210}Pb_{ex}$ activity (mBq g^{-1})	Inventory $^{210}Pb_{ex}$ (Bq m^{-2})	E/A
30	JP02	7/10	8.2	129.3	E	10/10	247.5	12611.3	A
30	JP03	6/10	1.6	282.1	A	10/10	201.8	16701.1	E
30	JP06	6/10	10.0	183.5	E	10/10	313.9	6769.6	E
30	JP11	6/11	5.5	479.1	A	10/10	260.2	22551.2	E
30	JP12***	2/11	79.7	/	A	11/11	204.7	18678.3	E
30	JP14	7/12	25.8	554.7	A	12/12	169.8	17348.8	E
30	JP15	10/14	5.7	124.9	E	14/14	128.4	17560.6	A
30	JP17*	6/10	6.3	219.8	Ref	10/10	316.1	8924.5	E
30	JP18	7/10	6.2	108.5	E	10/10	581.1	47881.1	A
30	JP19**	8/10	8.8	192.3	E	10/10	253.2	11892.3	E
50	JP21	13/16	19.1	410.5	A	16/16	831.6	48014.3	A
20	JP23	6/10	11.1	177.0	E	10/10	370.9	21980.4	E
25	JP24	4/11	8.5	921.1	A	11/11	503.4	45485.7	E
30	JP25	11/12	7.9	119.1	E	12/12	157.2	7268.6	E
30	JP26	6/12	12.6	189.9	E	12/12	361.5	26722.3	E
45	JP28	7/15	8.5	136.3	E	15/15	481.3	43000.2	E
25	JP29**	7/10	19.3	313.8	A	10/10	318.7	29297.6	A
30	JP30	6/11	2.1	30.9	E	11/11	228.4	14393.7	A
18	SED1	7/9	9.8	24.8		9/9	2847.8#	46815.2#	
42	SED2	11/21	46.9	132.4		20/21	1479.4#	46533.7#	
30	SED3	10/15	17.3	1756.5		15/15	761.0#	92681.0#	
22	SED4	5/10	6.2	240.1		11/11	956.0#	22571.4#	
40	SED5	15/20	96.6	21855.3		20/20	2236.5#	77954.5#	
	Total	*173/281*				*279/280*			

*Reference site **Only $^{210}Pb_{ex}$ ***Sample missing #Extreme values

Table 22 Analysed sample activities and inventories for complete FRN profiles in João Penido catchment and reservoir, where ^{137}Cs erosion/deposition is E = erosion and A = aggradation, respectively.

	N	Mean ^{137}Cs inventory (Bq m^{-2})	Median ^{137}Cs inventory (Bq m^{-2})	N	Mean ^{210}Pb$_{ex}$ inventory (Bq m^{-2})	Median ^{210}Pb$_{ex}$ inventory (Bq m^{-2})
Reservoir sediment	5	4801.8	240.1	5	57311.2*	46815.2*
Pasture	11	256.3	189.6	11	27669.1	26722.3
Shrubland	6	292.3	232.8	6	16031.6	17348.8

*Table 23 Summary of ^{137}Cs and ^{210}Pb data for soil and sediment profiles in João Penido catchment. * denotes the extreme ^{210}Pb$_{ex}$ values.*

^{137}Cs activities showed irregular concentrations in shrubland and pasture soil profiles ranging between 1.6–79.7 mBq g^{-1} , with most of the activities concentrated in top soil (<20 cm) (Figure 57, Figure 58). The ^{137}Cs inventory for the reference core (site JP17) was 219.83 Bq m^{-2}, which was similar to both the median ^{137}Cs inventories of all shrubland sites of sampling location A (232.8 Bq m^{-2}) and the median of all pasture sites of sampling location B (189.9 Bq m^{-2}). The mean inventory of all soil sites amounted to 269.0 Bq m^{-2}, with a mean value for all shrubland sites of 292.3 Bq m^{-2} and pasture sites correspondingly was 256.3 Bq m^{-2}, which was substantially higher than the reference inventory and indicated that the mean inventories were less representative for these sites.
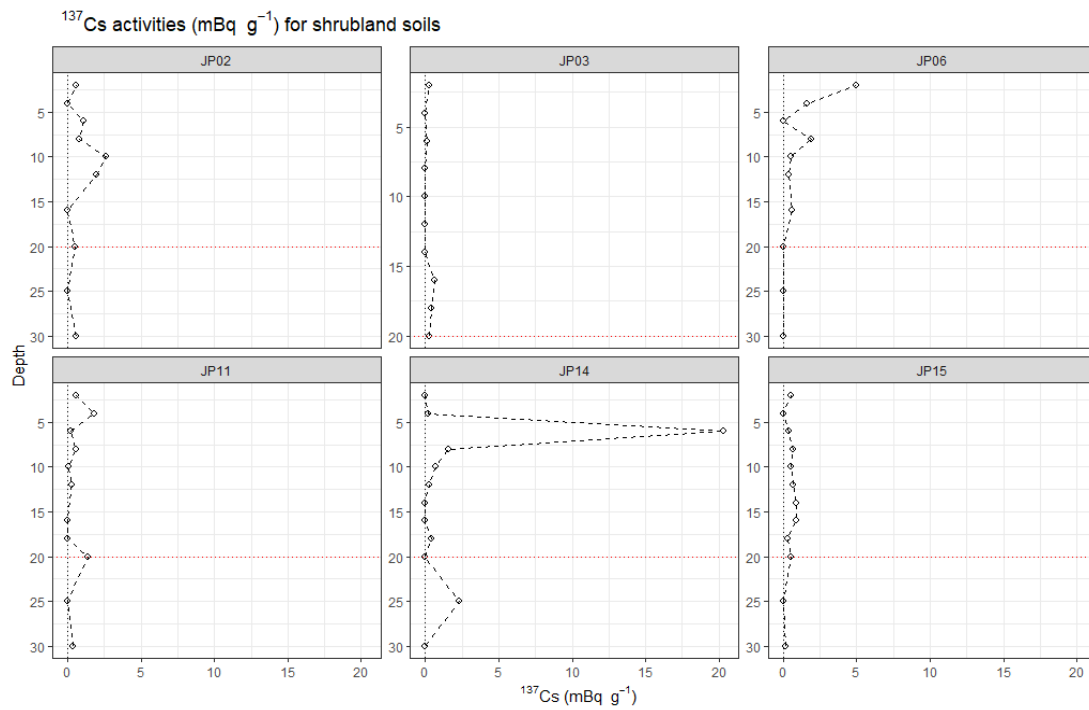
Figure 57 ¹³⁷Cs activities (mBq g⁻¹) in shrubland soil profiles. Red line delineates top and sub soil boundary (20 cm).
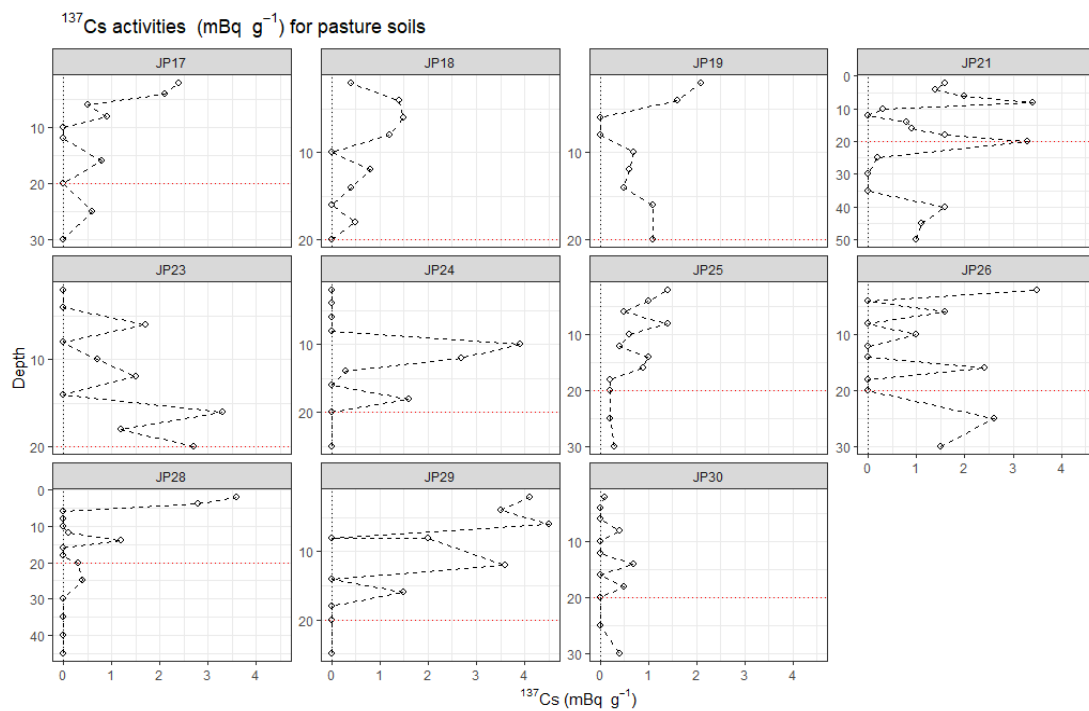
Figure 58 ¹³⁷Cs activities (mBq g⁻¹) in pasture soil profiles. Red line delineates top and sub soil boundary (20 cm).

The $^{210}Pb_{ex}$ concentrations in the soil cores of João Penido mainly showed the typical declining profiles that are characteristic for continuous fallout (Figure 59, Figure 60). The activities ranged between 128.4–831.6 mBq g^{-1}. $^{210}Pb_{ex}$ inventories in soil profiles ranged between 6769.6–48014.3 Bq m^{-2}, with the reference site (JP17) $^{210}Pb_{ex}$ inventory being 8924.5 Bq m^{-2} and the mean inventory of all soil sites was 23171.2 Bq m^{-2}.
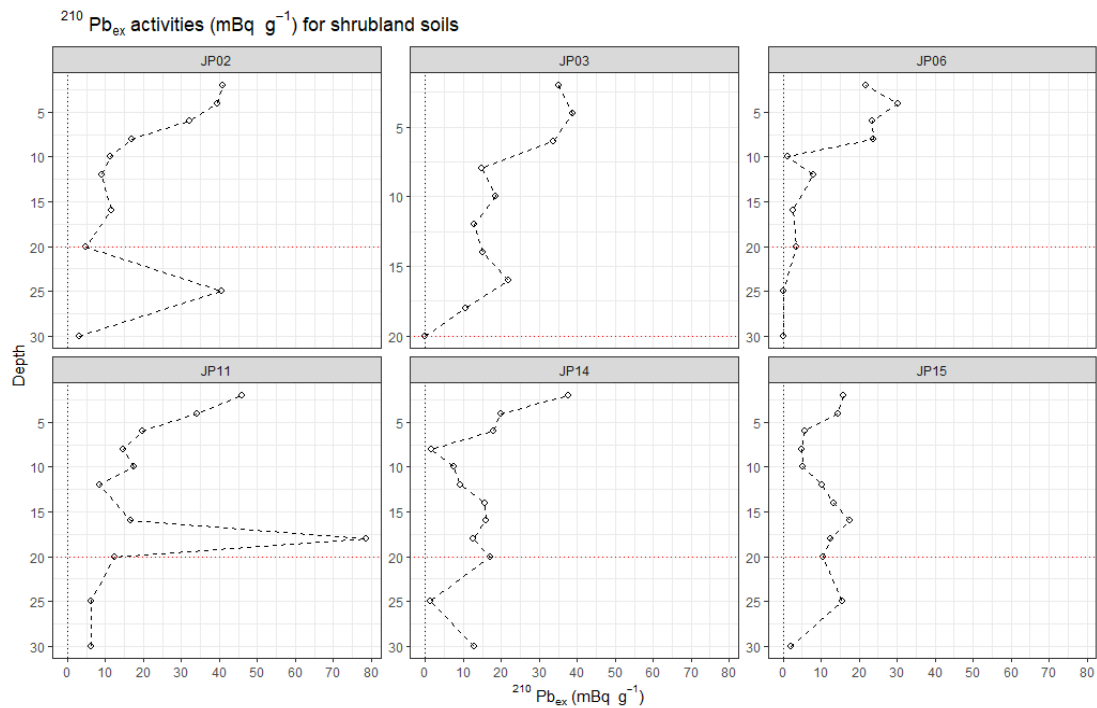
Figure 59 $^{210}Pb_{ex}$ activities (mBq g^{-1}) in shrubland soil profiles. Red line delineates top and sub soil boundary (20 cm).
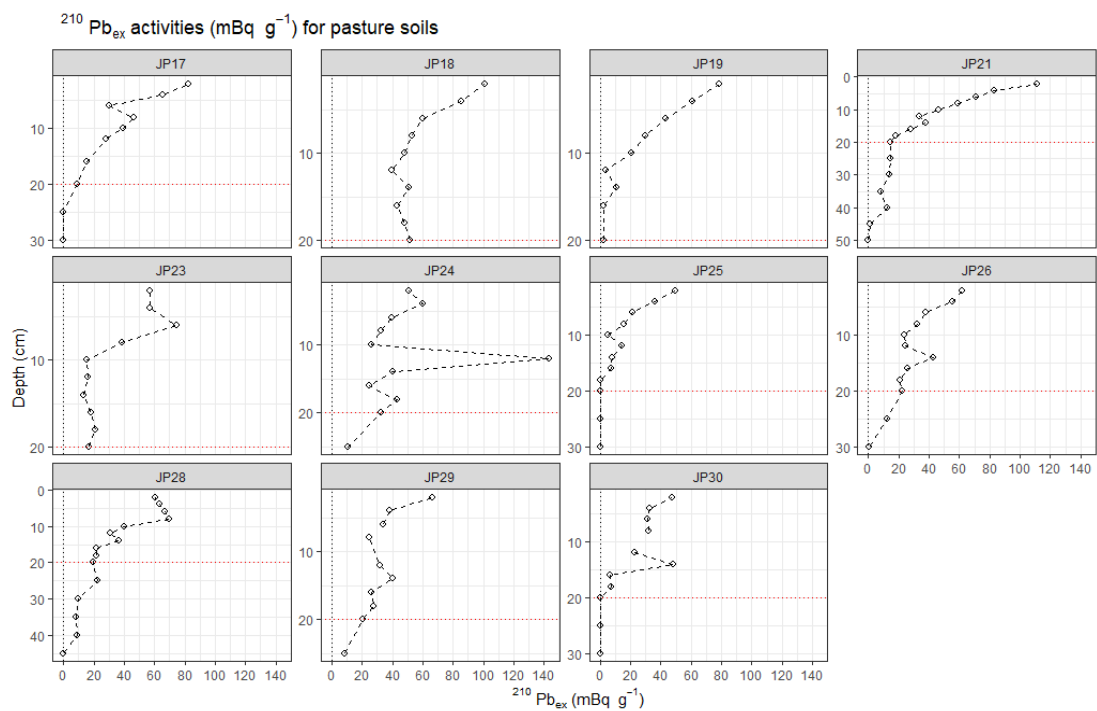
Figure 60 $^{210}Pb_{ex}$ activities (mBq g^{-1}) of pasture soil profiles. Red line delineates top and sub soil boundary (20 cm).

The mean pasture and shrubland inventories amounted to 27714.6 and 16031.6 Bq m^{-2}, respectively. Supported $^{210}Pb_{supp}$ occurred with continuous concentrations along the depth-profile throughout the measured cores, with a mean of 28.8 mBq g^{-1} for shrubland soils, and 45.2 mBq g^{-1} for pasture soils.

5.2.1.2 Radionuclide distributions in soil and colluvium profiles

Examples of a soil profile with typically declining ^{137}Cs and $^{210}Pb_{ex}$ activities of soil increments with depth from the pasture reference site JP17 are displayed below (Figure 61, Figure 62).

157
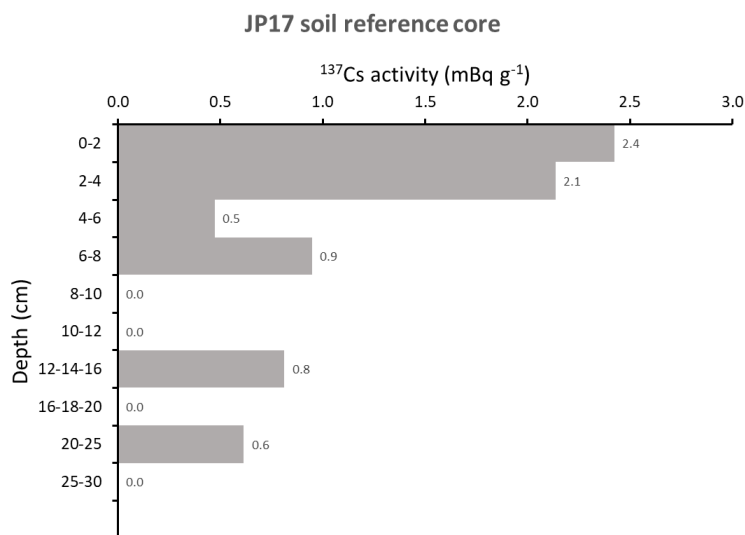
Figure 61 ^{137}Cs activities (mBq g^{-1}) of reference core (site JP17).
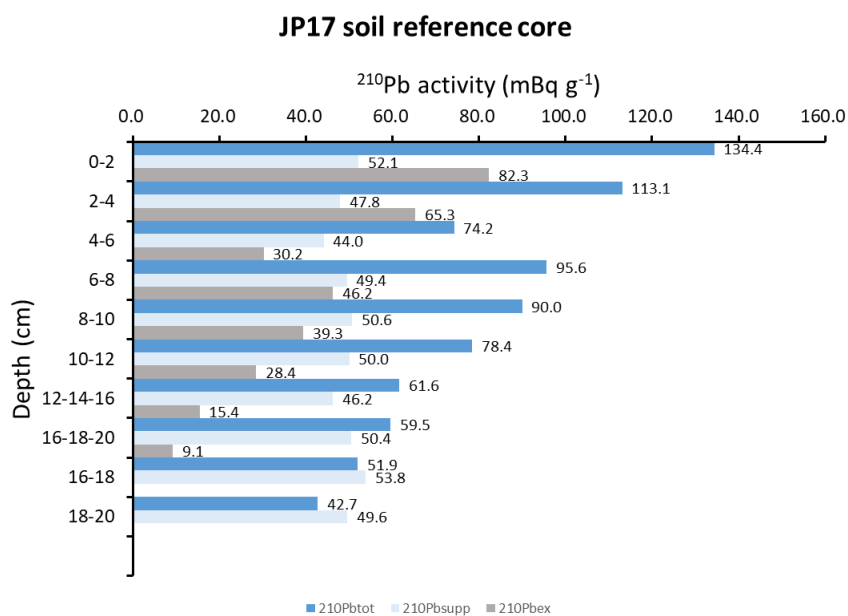
Figure 62 ^{210}Pb activities (mBq g^{-1}) of pasture reference core (site JP17). The total inventory of ^{210}Pb$_{ex}$ is 8924.5 Bq m^{21}, showing a typical ^{210}Pb$_{ex}$ profile with higher activities in the top soil decreasing with soil depth. The concentrations of supplemental ^{210}Pb (^{210}Pb$_{supp}$) in the soil profile samples average 49.4 Bq kg^{-1} throughout the profile, showing continues concentrations with depth.

Maps of ^{137}Cs and ^{210}Pb$_{ex}$ radionuclide inventories show the distribution of inventories for the sampling sites, presented in Figure 63, Figure 64, Figure 65, and Figure 66. Generally ^{210}Pb$_{ex}$ inventories showed somewhat higher inventories compared to corresponding ^{137}Cs inventories relative to the chosen

reference site (JP17) in the field. As expected, the inventories were typically lowest at eroding areas with steeper slope angle, whilst highest in depositional environments in troughs and depressions, as shown for inventories at site location A (Figure 64). Contradictory, at site location B lower inventories of ^{137}Cs were found at depositional sampling sites, e.g. colluvium profile JP28 and JP25, which could be connected to low abundance of ^{137}Cs-sorptive clay fractions (<63 μm) in these profiles, however this does not appear to fully explain these low inventories.
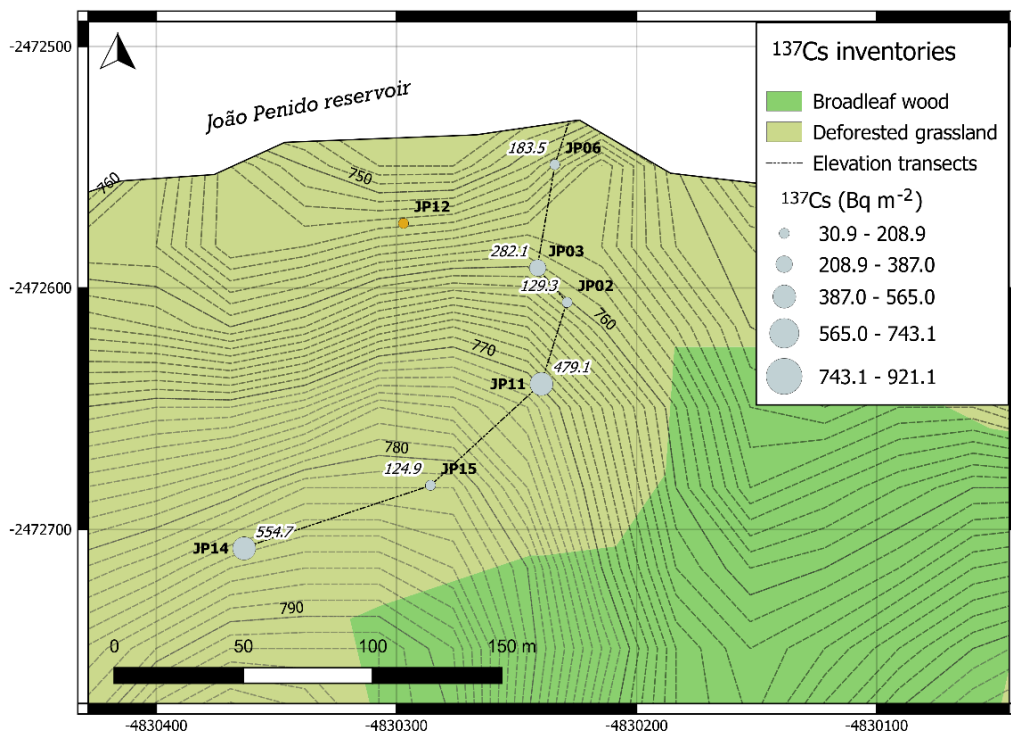
Figure 63 ^{137}Cs-inventories at shrubland sampling location A, in João Penido reservoir catchment. Scale is set for both sampling locations A and B. EPSG: 3857.
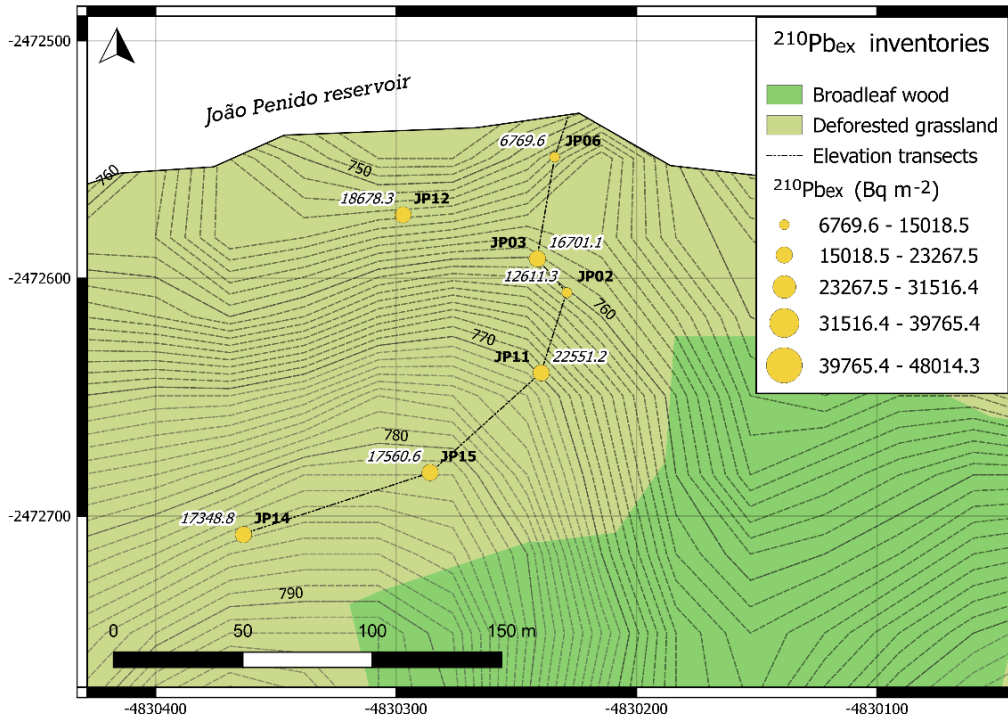
Figure 64 $^{210}Pb_{ex}$-inventories at pasture site A, in João Penido catchment. The reference site JP17 is located at sampling location B. Scale is set for both sampling locations A and B. EPSG: 3857.
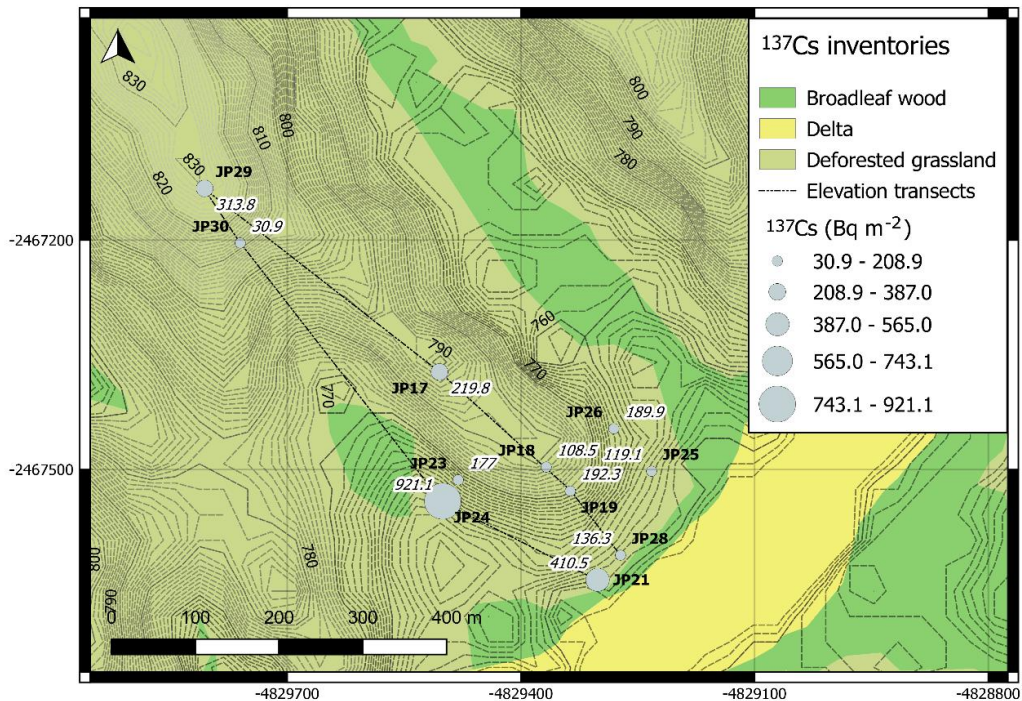
Figure 65 ^{137}Cs-inventories at pasture site B, in João Penido catchment. EPSG: 3857.

160
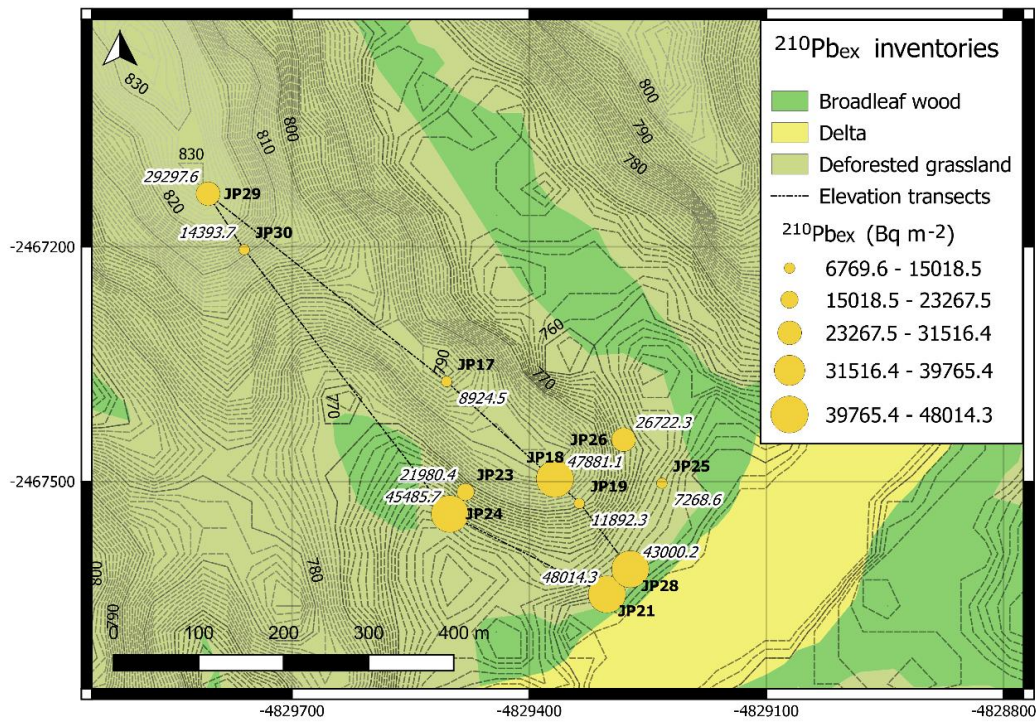
Figure 66 $^{210}Pb_{ex}$-inventories at pasture site B, in João Penido catchment. EPSG: 3857.

5.2.1.3 Radionuclide inventories of sediment profiles

In sediment cores ^{137}Cs concentrations ranged between 6.2–96.6 mBq g^{-1} (Figure 67). In comparison, others have reported ^{137}Cs activities of 0.47–5.31 mBq g^{-1} in Brazilian estuarine sediments of Bahia state (Angeli et al, 2016). ^{137}Cs inventories in sediment cores ranged between 24.8–21855.3 Bq m^{-2}, with a mean ^{137}Cs inventory of the measured lake sediment sites of 4801.8 Bq m^{-2}, while the median inventory amounted to 240.1 Bq m^{-2} (Figure 68). A ^{137}Cs peak was found in core SED5 at depth 30–32 cm, which is below the boundary of post-flooding sediment and observed pre-flood material. In this case, either resuspension of sediment has occurred to deposit coarser material on top of the sediment layer representing year 1963 (with the ^{137}Cs peak) or the determined depth of the pre-flood boundary from core observations was subject to error. By the simple assumption that 1963 represents the year of maximum fallout of ^{137}Cs, the peak of activity (29.9 mBq g^{-1}) in reservoir sediment core SED5, which was sampled in the deepest part of the reservoir, was used to determine the average sedimentation rate for that core by dividing the sediment depth (cm) with the

161

difference in years between sampling and year 1963. From ^{137}Cs data, the average sedimentation rate for the site of reservoir sediment core SED5 was calculated to 0.6 cm year^{-1}.
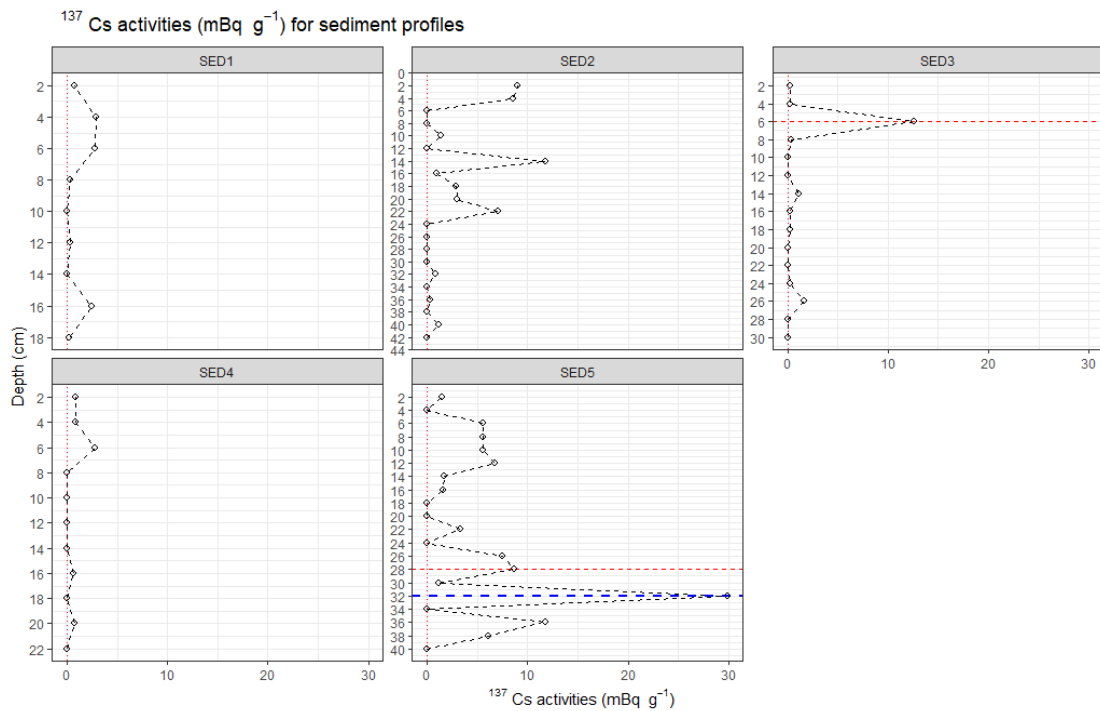
Figure 67 ^{137}Cs activities in sediment samples of João Penido reservoir. Vertical red dotted line denotes zero concentrations and inventory. Horizontal red dashed line denotes observed pre-flood boundary. The blue dashed line denotes a peak in [137]Cs.
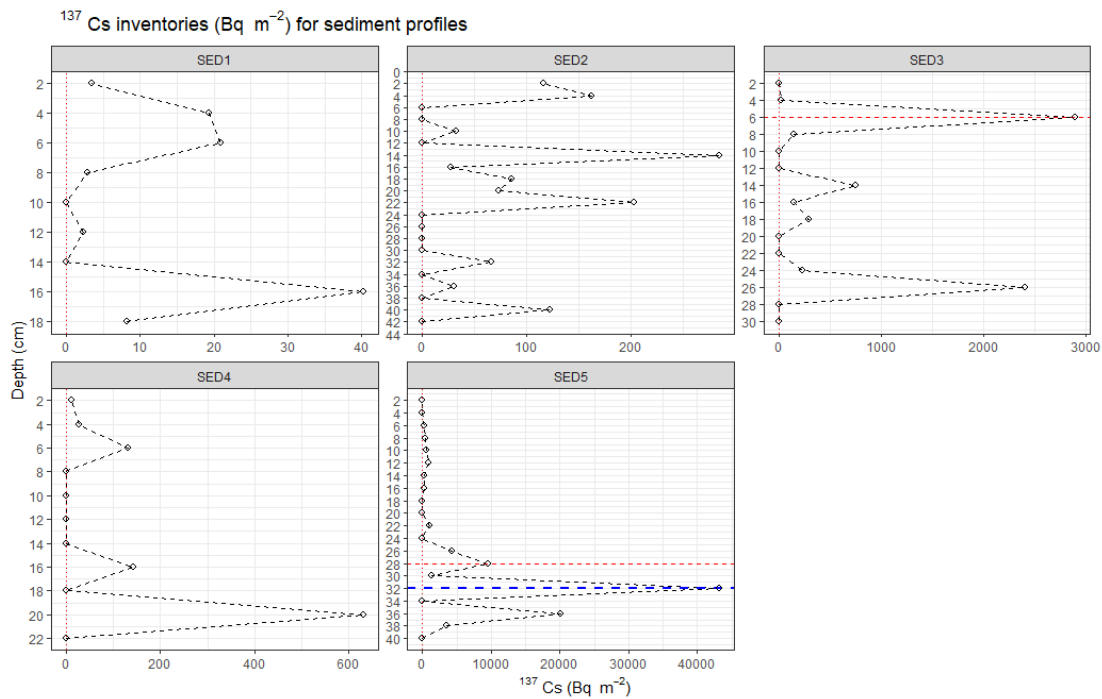
Figure 68 ^{137}Cs profiles of reservoir sediments. Vertical red dotted line denotes zero ^{137}Cs inventory. Horizontal red dotted line denotes pre-flood material, while the blue dashed line represents ^{137}Cs peak, representing year 1963. Scales are set to free.

For sediment profiles, ^{210}Pb$_{ex}$ concentrations ranged between 761.0–2847.8 mBq g^{-1}. Other studies have reported ^{210}Pb$_{ex}$ values for lake sediments of 23.28-95.91 mBq g^{-1} (Angeli et al, 2016) and estuarine sediments of 1586.04–1845.11 mBq g^{-1} (Lubis et al, 2006). The inventories ranged between 22571.4–92681 Bq m^{-2}, with a mean ^{210}Pb$_{ex}$ inventory of 57311.2 Bq m^{-2} and a median inventory of 46815.2 Bq m^{-2}. These inventories are very high, compared to other studies. Both ^{137}Cs and ^{210}Pb$_{ex}$ concentrations of the reservoir sediments are presented in Figure 69.

Concentrations of ^{137}Cs and ^{210}Pb$_{ex}$ (mBq g^{-1}) with depth in sediment cores
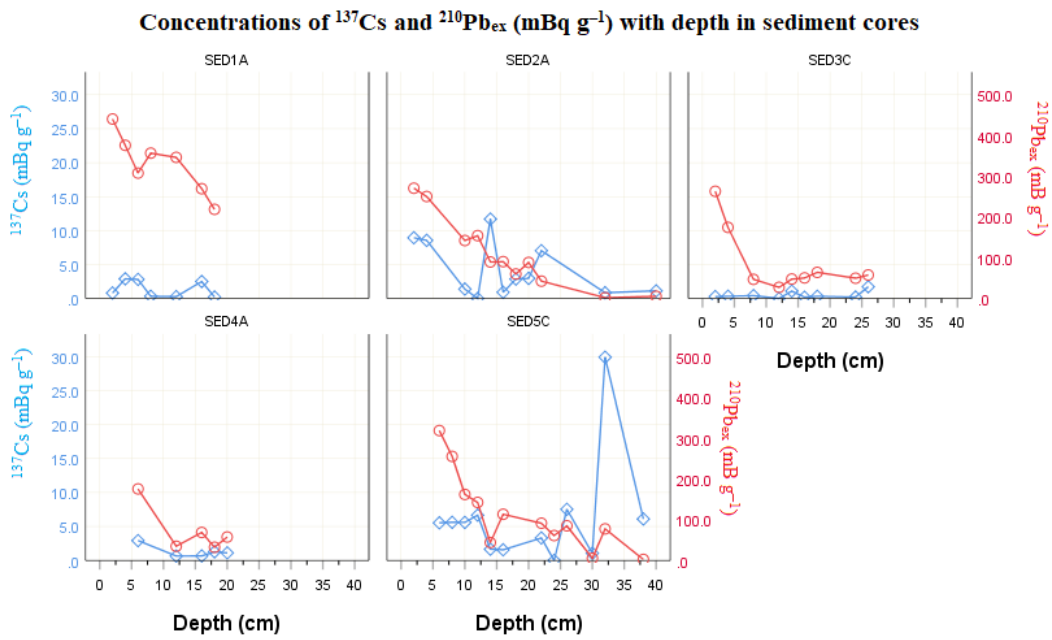
Figure 69 Radionuclide concentrations (mBq g^{-1}) in João Penido reservoir sediments.

5.2.2 Conversion model results

The results from conversion model calculations of erosion rates in João Penido catchment are presented here.

5.2.2.1 Profile distribution model (PDM) erosion output

The mean erosion rate for all eroding sites calculated by the profile distribution model corresponds to 0.45 kg m^{-2} year^{-1}, or correspondingly 4.5 tonnes ha^{-1} year^{-1}. The mean erosion rate for the shrubland site was 0.41 kg m^{-2} year^{-1} and the mean erosion rate for the pasture site was 0.47 kg m^{-2} year^{-1}. PDM-output is summarized in Table 24.

PDM-^{137}Cs soil erosion rate (kg m^{-2} year^{-1})				
Land cover	*N*	*Mean*	*Min*	*Max*
Shrubland	6	0.42	0.04	1.03
Pasture	10	0.47	0.06	1.74
All	8	0.45		

Table 24 Erosion rates calculated by the Profile distribution model (PDM) for ^{137}Cs.

5.2.2.2 Diffusion and migration model (DMM) erosion output

The diffusion and migration coefficients for ^{137}Cs and ^{210}Pb$_{ex}$ were calculated for the reference site JP17, using D=22.56, V=1.08 for ^{137}Cs, and D=0.88, V=0 for ^{210}Pb$_{ex}$. The model requires a value for relaxation mass depth that represents penetration of fresh fallout (not to be confused with h_0 which relates to the profile distribution, used for PDM-^{137}Cs calculation of erosion rates) and a value of 4 kg m^{-2} was chosen for all samples. Diffusion and migration model (DMM) output is summarized in Table 25. Results suggests that erosion rates based on DMM-^{137}Cs range between 4.95–6.01 kg m^{-2} year^{-1} for shrubland sites and 3.95–6.94 kg m^{-2} year^{-1} for pasture sites, with a mean of 5.71 kg m^{-2} year^{-1} for all sites, corresponding to 57.1 tonnes ha^{-1} year^{-1}. For ^{210}Pb$_{ex}$ data, erosion rates obtained by DMM range between 1.61–2.03 kg m^{-2} year^{-1} for shrubland sites, and between 1.00–1.98 kg m^{-2} year^{-1} for pasture sites, with an overall mean of 1.63 kg m^{-2} year^{-1} which corresponds to 16.3 tonnes ha^{-1} year^{-1}. These erosion rates are closer to PDM output for ^{137}Cs. The erosion output from DMM showed similar trends for both ^{137}Cs and ^{210}Pb$_{ex}$ with some exceptions (Figure 70, Figure 71, Figure 72, Figure 73).

DMM soil erosion rates (kg m^{-2} year^{-1})

		^{137}Cs			^{210}Pb$_{ex}$		
Land cover	N	Mean	Min	Max	Mean	Min	Max
Shrubland	7	5.56	4.95	6.01	1.79	1.61	2.03
Pasture	10	5.80	3.95	6.94	1.53	1.00	1.98
All	17	5.71			1.63		

Table 25 Diffusion and Migration Model (DMM) erosion results by ^{137}Cs and ^{210}Pb$_{ex}$ for João Penido catchment.
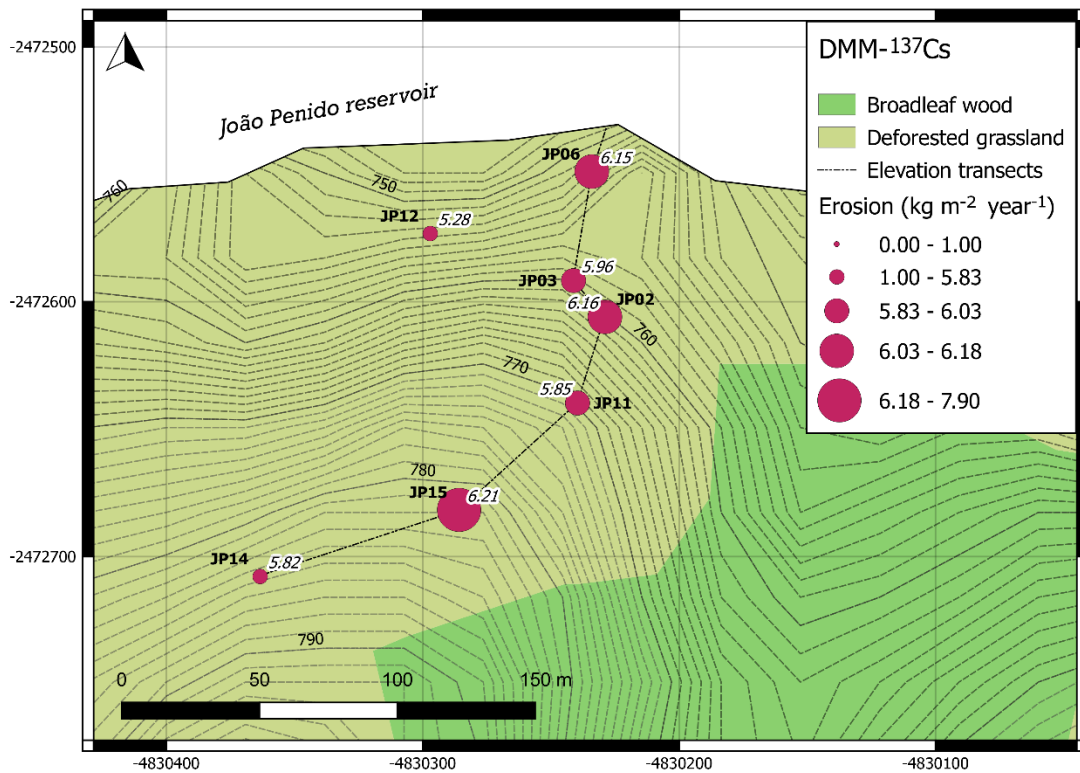
Figure 70 DMM erosion by ^{137}Cs at site A.
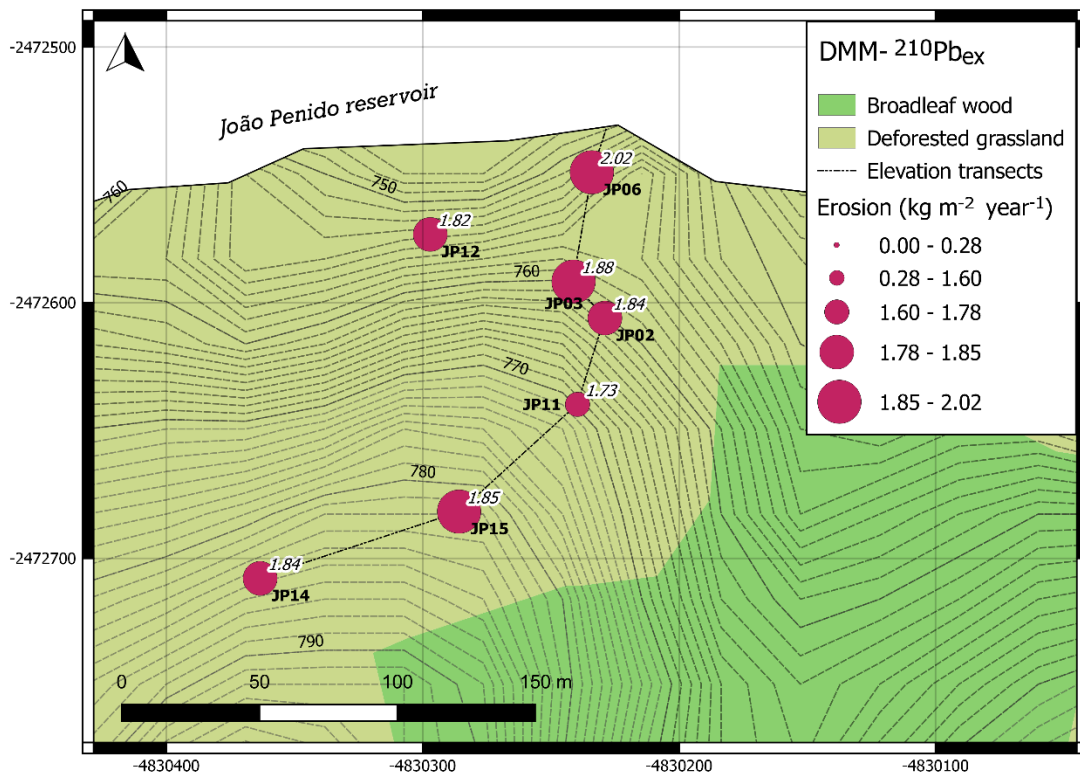
Figure 71 DMM by ^{210}Pb$_{ex}$ at site A.
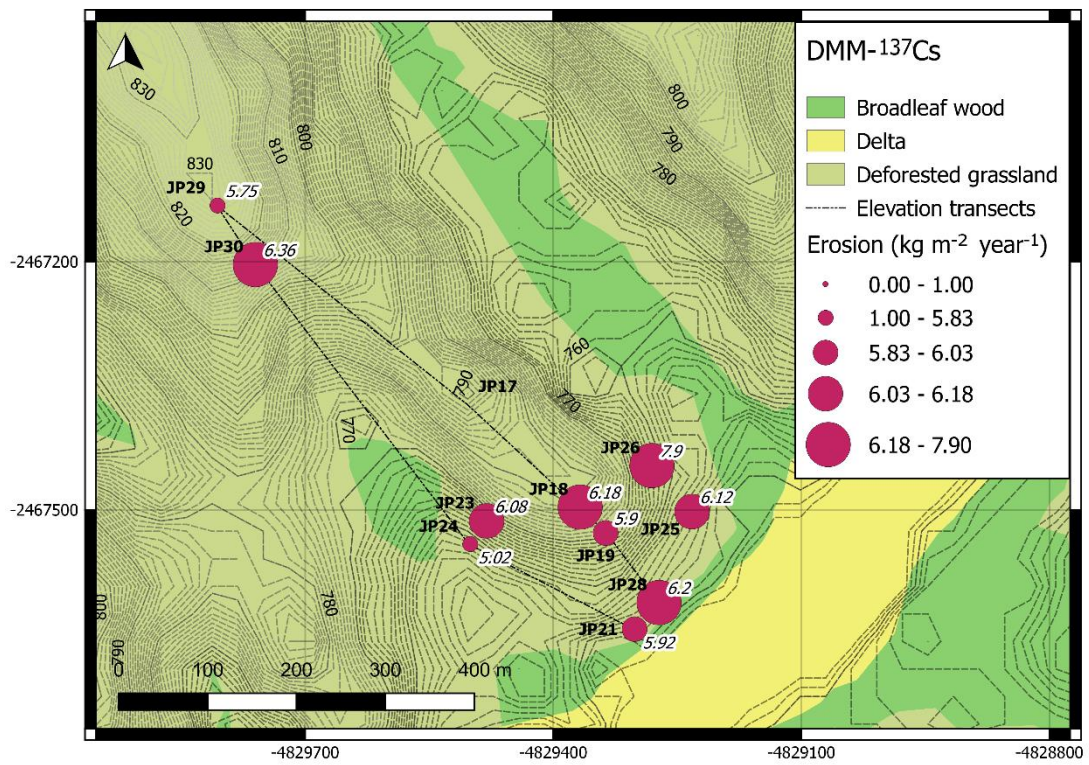
Figure 72 DMM erosion rates by ^{137}Cs at site B.
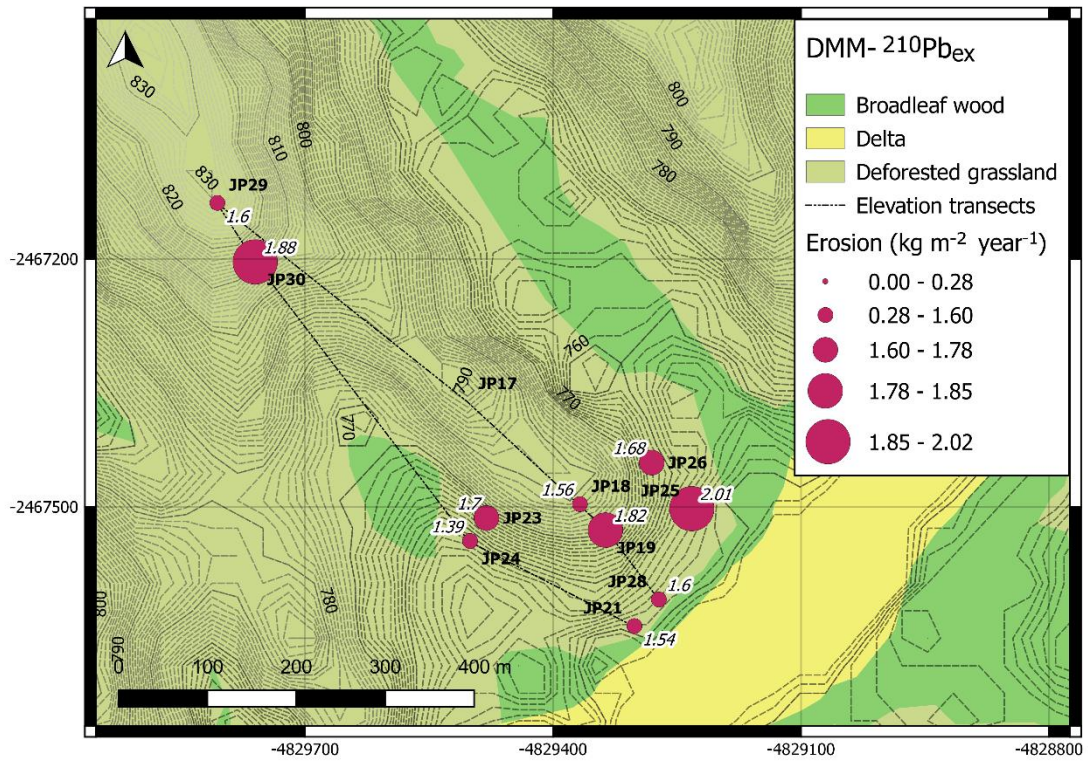
Figure 73 DMM erosion rates by ^{210}Pb$_{ex}$ at site B.

167

5.2.2.3 SAR from radionuclide data

SAR from sedimentation rates derived from $^{210}Pb_{ex}$ models CIC and CRS are summarized in Table 26. Initially SAR from $^{210}Pb_{ex}$ models are reported in the unit kg m^{-2} year^{-1}, which gives a sediment mass input rate per area unit rather than an annual linear thickness increase (cm year^{-1}) which is achieved from observations of post-flooding sediment thickness (see section 3.3.5.1). Linear SAR were calculated from CRS-age for each depth increment (2 cm) and an annual average accumulation in mass could be directly translated into a yearly sediment flux so that variation in SAR could be analysed. The results are presented in Figure 74.

Average sedimentation rates (cm year^{-1})

Core	CIC model	CRS model	based on ^{137}Cs peak
SED1	8.01	0.03	
SED2	4.83	0.07	
SED3	4.34	0.00004	0.07
SED4	3.71	0.03	
SED5	2.22	0.53	0.5

Table 26 Summary of ^{210}Pb SAR based on CIC and CRS models.

The ^{210}Pb ages obtained from CRS model results for five sediment cores showed consistent age chronology, whereof two of the cores, sites SED3 and SED5 contained material older (pre-flood material) than the year the reservoir was established (1934). In general, sedimentation rates appeared to have increased for sites SED1 and SED2, while it showed variable rates for SED4 and SED5, and the sedimentation rates for SED3 showed negligible variation with depth. The CRS model showed results which agreed with the maximum ^{137}Cs concentrations found in sediment cores, out of which only sites SED3 and SED5 were found to contain the specific bomb peak (assumed year 1963). The calculated CRS ages showed that sediment profiles SED1, SED2 and SED4 contained younger sediments. Results from the CIC model gave SAR values that were higher than both SAR derived from core thickness of post-flooding sediment and from ^{137}Cs observations.
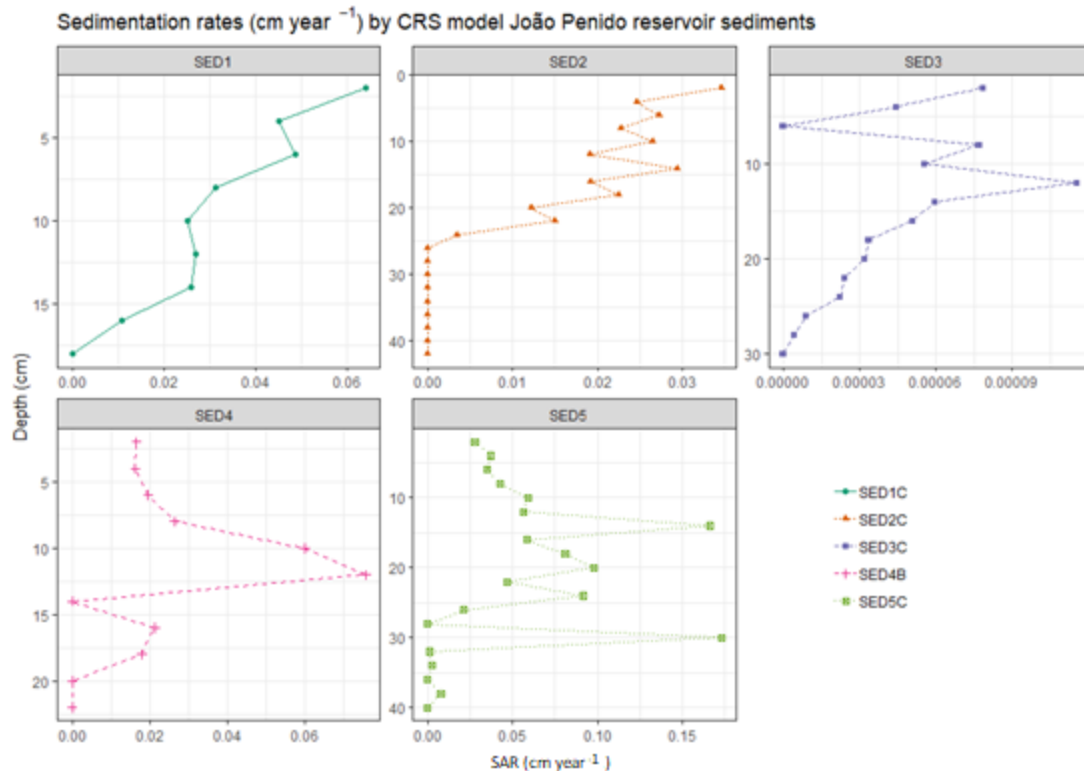
Figure 74 Sedimentation rates (cm year⁻¹) for João Penido sediment sites. Pre-flood material appears at 32 cm depth for SED2, and at 28 cm depth for SED5, where SAR is either zero or lower than in the rest of the core profiles. Pre-flood material was observed at a depth of 6 cm for SED3, and affirming CRS-calculated SAR showed negligible variation in this profile.

5.2.2.4 Post-flooding sediment volume and mass

Sediment volume was interpolated from post-flooding thickness observations (*N*=15) by IDW. The resulting interpolated map (Figure 75) showed sediment thickness ranging between 0.06–0.52 m across the reservoir reach. The interpolated average sediment thickness equalled 0.27 m. Total post-flooding sediment volume was then calculated with the SAGA tool *Raster volume*, resulting in 753058.8 m³. This equalled roughly an average sediment accumulation of 9183 m³ year⁻¹ in the reservoir since it was built in 1934, with an average linear sediment accumulation rate of 0.3 cm year⁻¹. The average sediment density was assumed to be 1.37 g cm⁻³, and the mass of sediment in the reservoir was then calculated to 1031690.56 tonnes.
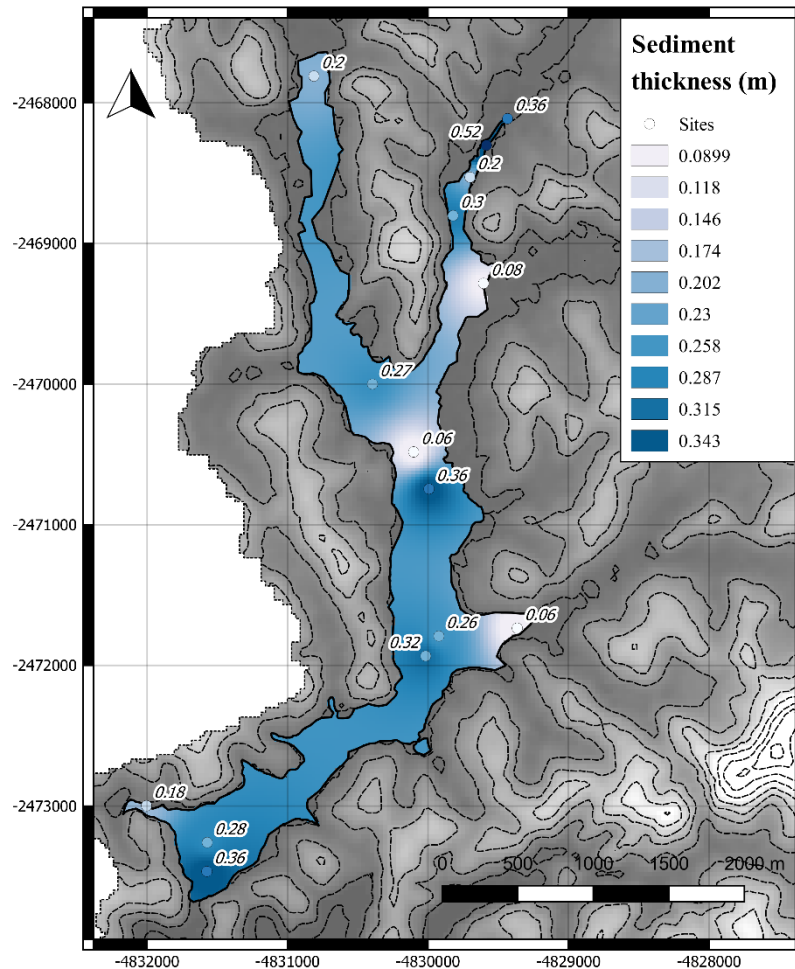
Figure 75 Post-flooding sediment thickness (m) map of João Penido reservoir.
EPSG: 3857.

5.2.3 RUSLE output

The RUSLE model was used estimate soil erosion in the João Penido catchment, from five factors representing: rainfall erosivity, R; soil erodibility, K; length–slope factor LS; land use and cover factor, C; and management practices, P (described in section 3.3.2). The results present natural potential of erosion (NPE), current state of erosion (S_fieldCK), and simulated forested and deforested states with C factor inputs from database and digitized values. The various simulations are summarized in Figure 76.

171
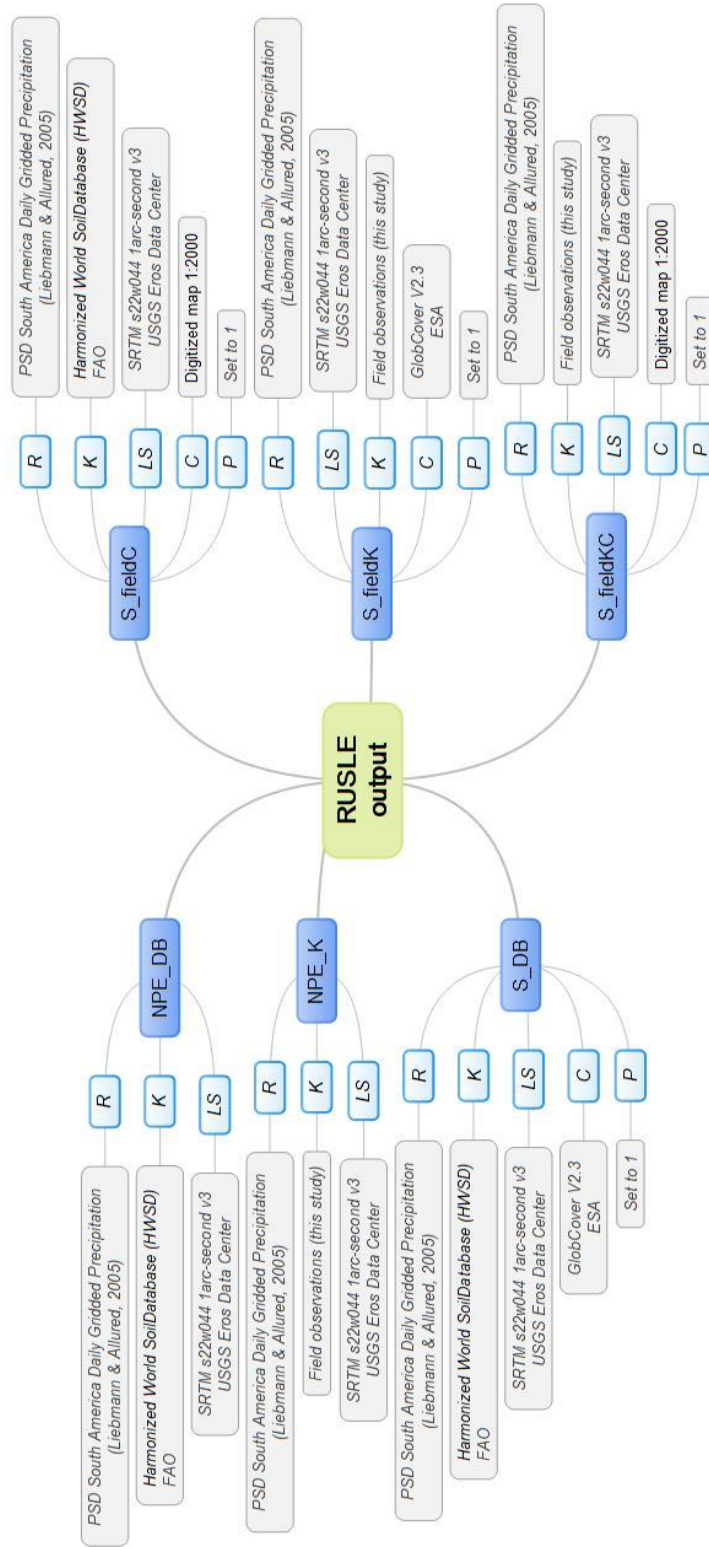
Figure 76 Input for primary RUSLE simulations of this study.

5.2.3.1 Natural potential of erosion (NPE)

For João Penido reservoir the natural potential of erosion (NPE) was calculated for catchment raster cells from factors derived from databases (NPE_DB) and with K from field observations (NPE_K). NPE_DB ranged between 1.52–6812.60 tonnes ha^{-1} year^{-1} (Figure 77, Table 27), with a mean erosion rate of 324.86 tonnes ha^{-2} year^{-1} and a standard deviation of 356.67 tonnes ha^{-1} year^{-1}. When K was derived from field observations (this study) the simulated NPE_K output ranged between 0.79–3541.29 tonnes ha^{-1} year^{-1}, with a mean of 168.87 tonnes ha^{-1} year^{-1} and a standard deviation of 185.41 tonnes ha^{-1} year^{-1}. NPE from S_fieldK was ca 52% lower than for NPE_DB output. This difference indicates the importance of accurate assessment of the value for the soil erodibility factor K.

5.2.3.2 Model outputs for current state of erosion in João Penido catchment

RUSLE output using database input only (S_DB) showed that current erosion ranged between 0–1259.16 tonnes ha^{-1} year^{-1}, with a mean erosion rate of 37.78 and a standard deviation of 53.96 tonnes ha^{-1} year^{-1} (Figure 78, Table 27). This gave a mean database derived erosion rate of 14.78 g m^{-2} day^{-1} or 3.78 kg m^{-2} year^{-1} from terrestrial soils in the catchment. The highest erosion rates were found on hillslopes as a result of steepness, while low slope crests and depressions showed lower erosion rates. Low C factor values clearly decreased the simulated erosion rates from land cover classified as wooded and built-up areas. For S_DB, low C factor values from the land cover map decreased soil erosion even in elevated areas with high LS factor values.
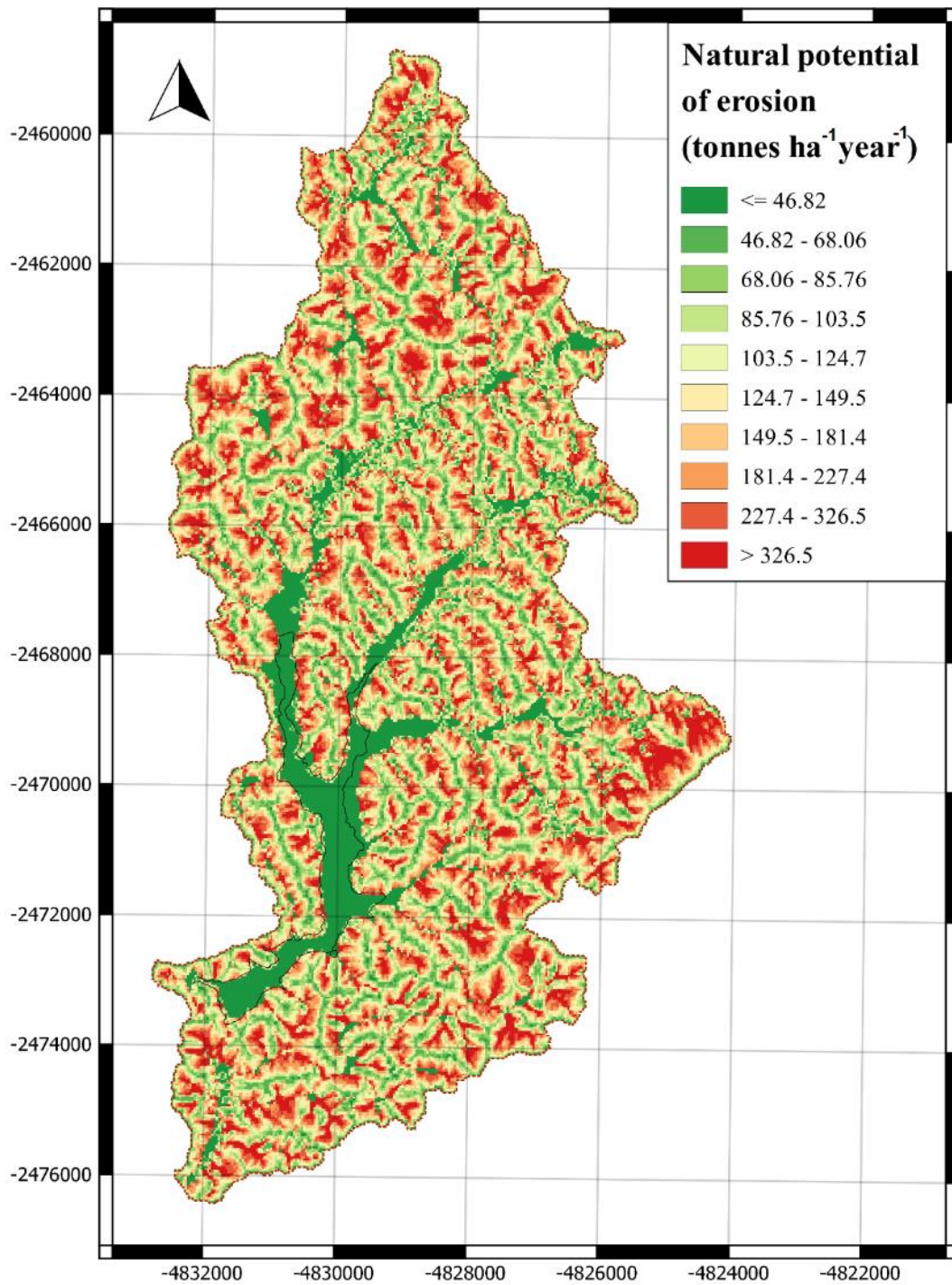
Figure 77 Natural potential of erosion (NPE) of the João Penido catchment, based on database values (R, LS) and field observations (K). The reservoir area is delineated. EPSG: 3857.
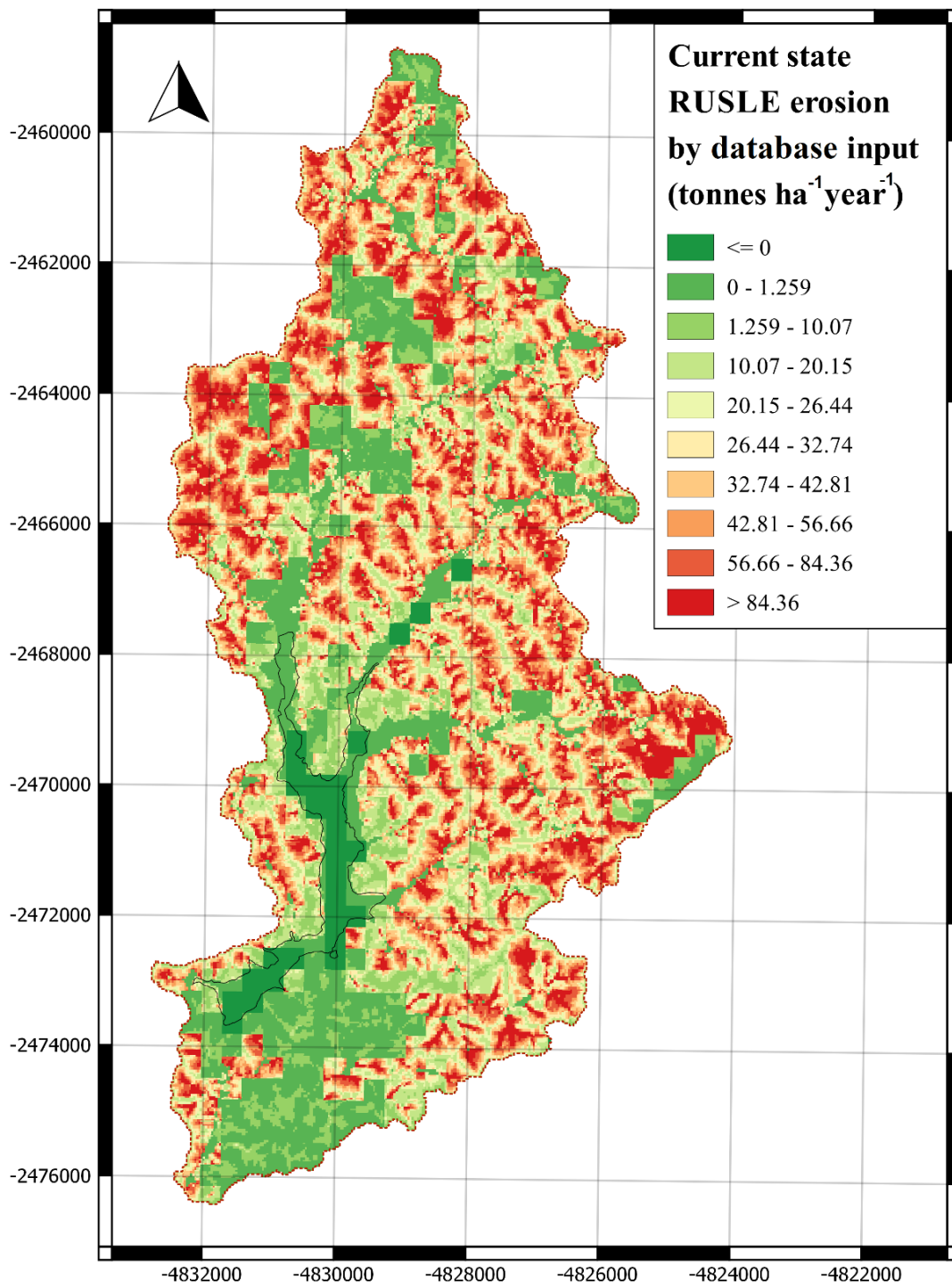
Figure 78 RUSLE output S_DB, based on database input only for current state of erosion in the João Penido catchment. The reservoir area is delineated. EPSG: 3857.

Database derived factors K and C could be replaced by observations from the field to improve the RUSLE output. Soil observations were used to calculate the K factor and digitizing of satellite data was done to produce a more detailed land cover map, which was assigned literature C values. With observed input data for the K factor (S_fieldK), the resulting average erosion rate from the catchment was 19.64 tonnes ha^{-1} year^{-1}, corresponding to 1.96 kg m^{-2} year^{-1}, 5.38 g m^{-2} day^{-1} (Table 27). RUSLE output with a digitized C factor (S_fieldC) gave a mean erosion value of 20.88 tonnes ha^{-1} year^{-1} (sd=28.00). When both field observations of K and C were used as input data, the simulation (S_fieldKC) resulted in a mean erosion rate was 10.85 tonnes ha^{-1} year^{-1} (corresponding to 1.09 kg m^{-2} year^{-1}, or 2.99 g m^{-2} day^{-1}) with a standard deviation of 14.55 tonnes ha^{-1} year^{-1} (Figure 79). For S_fieldCK the improved land cover map reduced erosion in wooded and built-up areas of the catchment and the highest erosion rates were confined to the steeper slopes of hills.

The resulting RUSLE output from analysis with various input data, derived from databases and observations, are summarized in Table 27; S_fieldCK was expected to be the result closest to the actual contemporary erosion state of the catchment.

RUSLE output (tonnes ha^{-1} year^{-1})

	S_DB (database input)	NPE_DB (database input)	S_fieldC (digitized C)	S_fieldK (observed K)	NPE_fieldK (observed K)	S_fieldCK (observed K and digitized C factor)
Mean	37.8	324.9	20.88	19.64	168.9	10.85
Min	0	1.5	0	0	0.8	0
Max	1259.2	6812.6	545.01	654.53	3541.3	283.3
SD	54	356.7	28	28.04	185.4	14.5 5

Table 27 Comparison of RUSLE output using factors derived from database information, field observations, and digitized land cover.
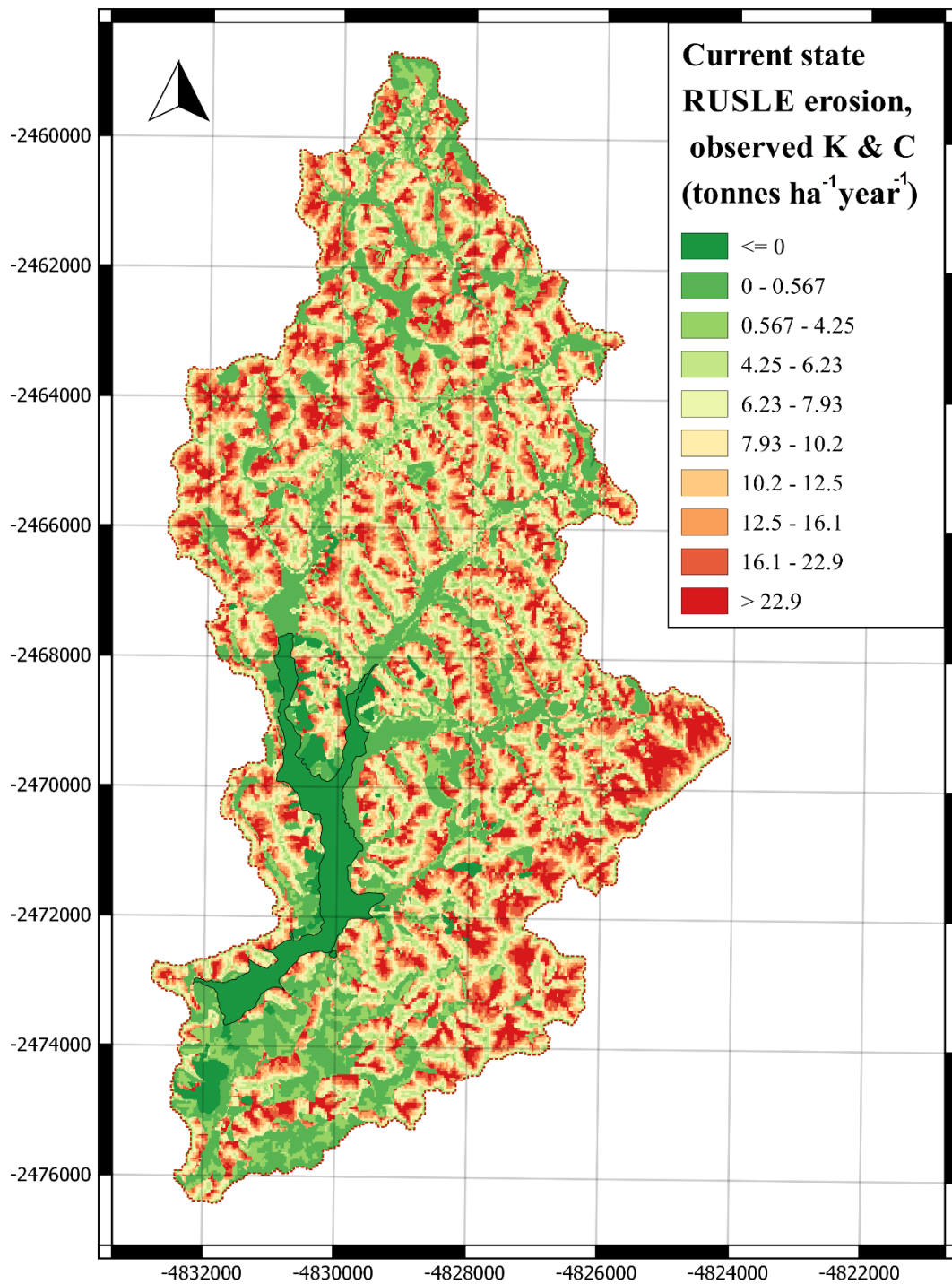
Figure 79 RUSLE output S_fieldCK, from database input, observed K factor and digitized C factor map. This is the closest approximation to actual erosion in João Penido catchment. The reservoir area is delineated. EPSG: 3857.

5.2.3.3 Simulated scenarios: forested state and deforested states

The RUSLE model was used to determine the current state of erosion in the João Penido watershed, and to simulate three erosion scenarios of the watershed being completely forested and similarly deforested at two levels by using literature *C* values as input for the *C* factor; a completely forested state was attained by setting the *C* factor to 0.003, which is representative of broad-leaved forest; the two deforested states were given *C* factors of 0.1 and 0.45, representing the lower and upper range of sparsely vegetated areas (Panagos et al, 2015). In the simulations built-up areas as well as standing water (the main reservoir and other larger ponds in the catchment) were unchanged (set to a *C* factor value of 0).

When using database input (S_DB) the scenarios showed higher erosion rates than when using S_fieldKC utilizing observations from the field. Reclassified land cover values from the *GlobCover* dataset were used as input for the *C*-factor, together with the *HSWD* database derived value of *K*. The completely forested state showed erosion rates ranging between 0–20.51 tonnes ha^{-1} year^{-1} (*sd*=1.19). The deforested state with assumed grassland showed erosion rates between 0–683.72 tonnes ha^{-1} year^{-1} (*sd*=39.17). The extremely bare state showed erosion rates between 0–2076.73 tonnes ha^{-1} year^{-1} (*sd*=176.3). The results are summarized in Table 28.

RUSLE simulations (tonnes ha^{-1} year^{-1}) from database input (S_DB)

	Forested state (C=0.003)	S_DB (C=0–0.2)	Deforested state (C=0.1)	Deforested state (C=0.45)	NPE_DB
Mean	1.03	37.8	34.1	153.39	324.86
Min	0	0	0	0	1.52
Max	20.51	1259.2	683.72	2076.73	6812.6
SD	1.19	53.96	39.17	176.26	356.69

Table 28 Results of simulated RUSLE erosion rates in João Penido watershed for current state, simulated completely forested state, deforested state and extremely deforested state by using S_DB (database input).

Simulated scenarios based on factor input from S_fieldCK yielded lower erosion values for the João Penido catchment. The forested state (*C*=0.003) based on S_fieldCK showed erosion rates ranging between 0–10.66 tonnes ha^{-1} year^{-1},

with a standard deviation of 0.63 tonnes ha^{-1} year^{-1}. The S_fieldCK deforested state (C=0.1) with assumed grassland showed erosion rates between 0–355.4 tonnes ha^{-1} year^{-1} (sd=20.9). The second, more extreme, deforested S_fieldCK scenario (C=0.45) showed erosion rates between 0–3541.3 tonnes ha^{-1} year^{-1} (sd=185.4). The results are summarized in Table 29.

RUSLE simulations (tonnes ha^{-1} year^{-1}) from database and field observations (S_fieldCK)

	Forested state (C=0.003)	*S_fieldCK (C=0–0.2)*	*Deforested state (C=0.1)*	*Deforested state (C=0.45)*	*NPE_fieldCK (observed C and K)*
Mean	0.52	10.85	17.47	78.62	168.87
Min	0	0	0	0	0.79
Max	10.66	283.3	355.4	1599.34	3541.29
SD	0.63	14.55	20.94	94.22	185.41

Table 29 Results of simulated RUSLE erosion rates in João Penido watershed for current state, simulated completely forested state, deforested state and extremely deforested state by using S_fieldCK (combined field and database input).

5.2.3.4 RUSLE erosion of deforested grasslands

Maps were generated for the field sampling locations A and B from RUSLE outputs showing current state of erosion (S_fieldCK*)*. For visual interpretation, discrete interpolation divided by quantiles (10 classes) was used (Figure 80, Figure 81). In addition to the colour scale of S_fieldCK, point values of field sampling sites were extracted to be compared with radionuclide data. The unit is tonnes ha^{-1} year^{-1}. When only the deforested grasslands in the catchment were considered for RUSLE analysis, the resulting erosion rates ranged between 0–283.30 tonnes ha^{-1} year^{-1}, with a mean of 10.64 tonnes ha^{-1} year^{-1}. These values were very similar to the S_fieldCK, which indicated that erosion was important mainly in the deforested grasslands of the catchment.
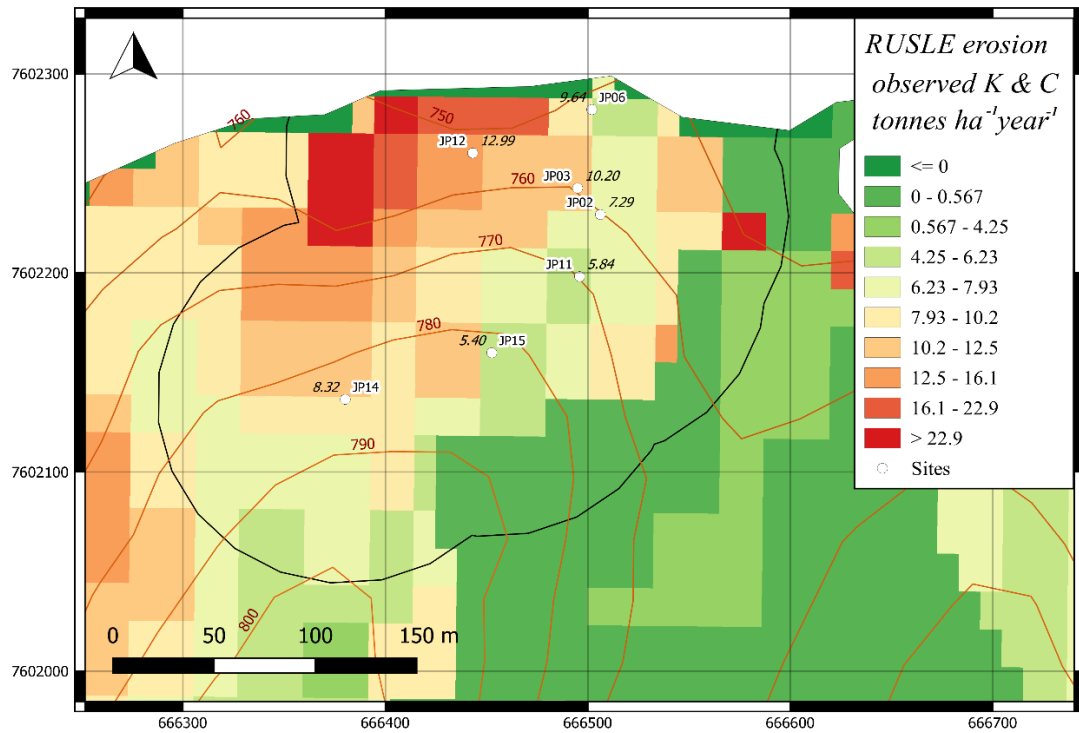
Figure 80 RUSLE output S_fieldCK and field observations (points) for site A, João Penido catchment. Black delineation shows 100 m buffer area from field sampling sites. Notice that in the map the delineated beachline does not take into account the pixel size of each raster point of S_fieldCK, which is why some areas of <=0 erosion appear on land by the edge of the reservoir. EPSG: 3857.

179
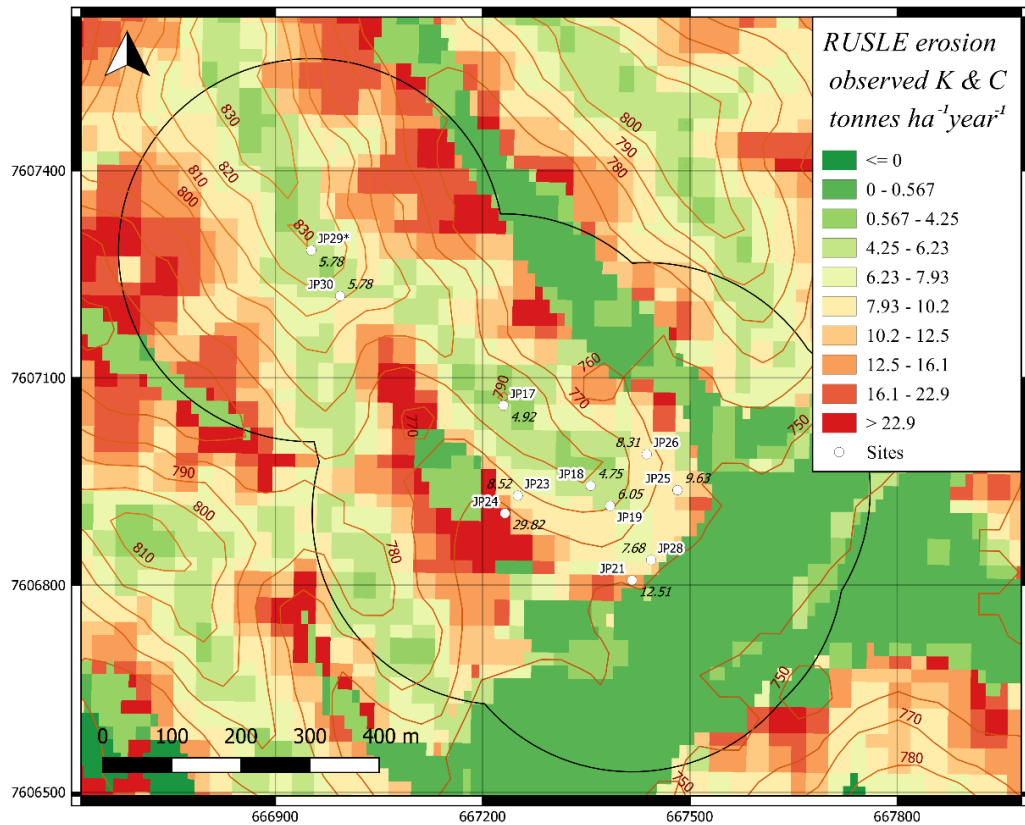
Figure 81 RUSLE output S_fieldCK and field observations (points) for site B, João Penido catchment. Note that <=0 indicates negative erosion, or deposition. Black delineation shows 300 m buffer area from field sampling sites. EPSG: 3857.

Soil erosion rates simulated by the RUSLE model showed improvement with increased detail in input factors, going from database to field observations. Simulations of the presence of vegetation cover in the catchment established that the current state of erosion (S_fieldCK) composed a state between a completely forested and a completely deforested catchment, where grasslands composed the land cover class most susceptible to erosion and allochthonous POC export.

5.3 POC transport and fate in João Penido watershed

5.3.1 POC concentrations in soils and sediment

POC inventories POC_{inv} (g m^{-3}) for soil are summarized in Table 30. Point data of average POC concentrations of the top 10 cm soil were compared to TWI and showed *Pearson correlation* of –0.69. The POC% soil profiles showed that many

of the shrubland sites had low variability in POC content with depth, compared to pasture sites which were more enriched in top soils (Figure 82). POC of terrestrial sites showed typically declining concentrations with depth in colluvium profiles, whilst more or less uniform concentrations with depth in soil profiles. The average SOC stock for catchment soils was calculated to c. 58 t ha^{-1}.

POC inventories of uppermost top soil (10 cm)

Site	JP02	JP03	JP06	JP11	JP14	JP15	JP17**	JP19	JP25	JP28	JP29*
POC (kg m^{-3})	50.4	53.8	56.1	62.1	81.8	95.1	38.5	76.2	62.2	119.6	57.3

*Reference
**Top 8 cm

Table 30 POC inventories of surface soil (10 cm).
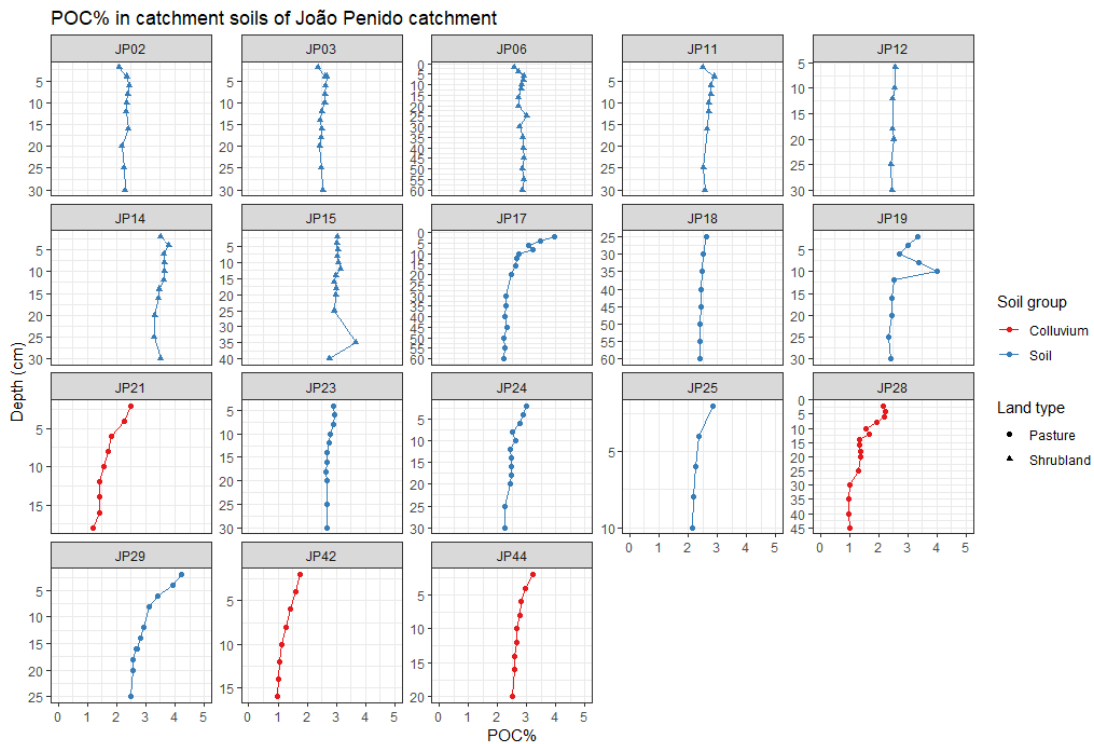
Figure 82 POC% in soil profiles of João Penido catchment. JP42 and JP44 are complementary sites at sampling location C, located further up one of the deltaic arms of the reservoir.

The sediment profiles presented in Figure 83 showed that POC concentrations tend to be lower in pre-flood material beneath the post-flooding sediment. As expected, POC% also tends to be higher in sediment profiles of reservoir arms

181

and at the deltaic site (SED4, SEDJP01, SEDJP05, SEDJP07, SEDJP08, SEDJP09, SEDJP10, SEDJP13, SEDJP16), due to the shallower waters being abundant in growing macrophytes and algae in these parts of the reservoir. Most of the deeper open water sites of the main reservoir body (SED1, SED2, SED3) lack the declining POC% profile typical of the shallow reservoir arm sites, although the accumulation sites at SED5C and SEDJP17 showed a distinct difference in POC% of post-flooding sediment and sub-bottom pre-flooding material. The IDW interpolated POC distribution in the reservoir is presented in Figure 84.

Figure 83 POC% profiles of sediment cores in João Penido reservoir. Dotted line indicates observed pre-flood material.
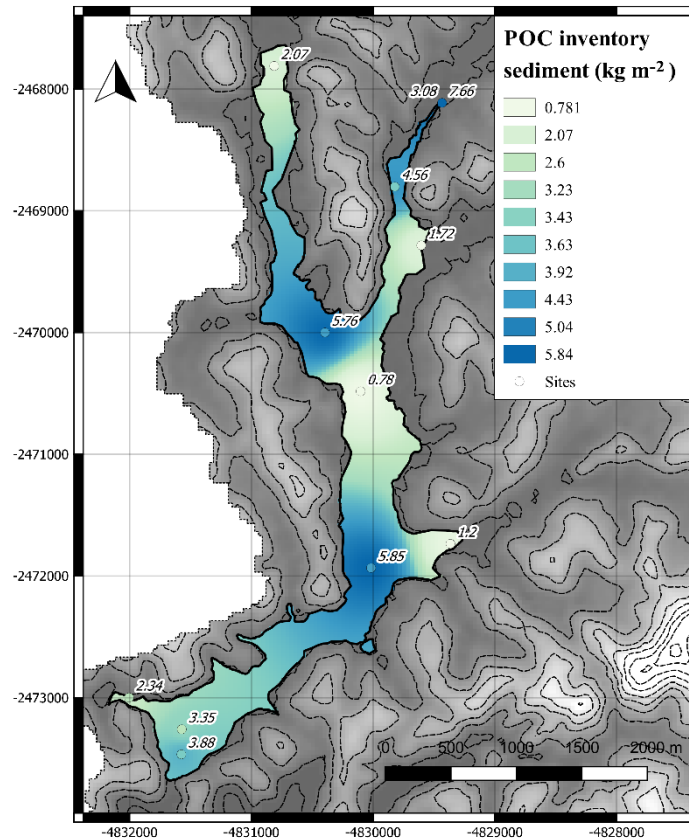
Figure 84 Reservoir sediment POC inventory (kg m^{-2}). The interpolation is presented by quantiles in 10 classes. EPSG: 3857.

5.3.2 POC erosion of catchment soils

Soil POC erosion in the catchment was calculated as the product of POC inventory and soil erosion rates, according to:

$$POC_{erosion} = A_{yearly} \times \%POC$$

Where A_{yearly} is the annual erosion rate (kg m^{-2} year^{-1}) obtained from RUSLE, PDM-^{137}Cs and DMM-[210]Pb$_{ex}$ data presented in this study and *%POC* was the average POC concentration (2.8%) of top soils (upper 20 cm). The results are summarized in Table 31 and show that the RUSLE output based on database input only is 72% higher than for erosion methods based partly or wholly on field observations.

Average POC erosion from various methods

POC erosion (tonnes ha^{-1} year^{-1})	Mean value
Calculated from RUSLE (database)	1.1
Calculated from RUSLE (database and observed *C* & *K*)	0.3
Calculated from RUSLE (database and observed *C* & *K*, of soil sites)	0.3
Calculated from PDM-^{137}Cs	0.1
Calculated from DMM-^{210}Pb$_{ex}$	0.5

Table 31 Average soil POC erosion of top soils (upper 20 cm) in João Penido catchment.

The results from all model outputs indicated that average POC erosion from top soils ranged between 0.1–1.1 tonnes ha^{-1} year^{-1}. From top soils located on deforested grassland (52,297,820.9 m^2) this would amount to a potential of 522.9–5,752.8 tonnes year^{-1} of remobilised soil POC in the catchment. POC erosion based on the RUSLE output utilizing database input and observations of K with digitized C factor gave a mean rate of 0.3 tonnes ha^{-1} year^{-1}, ranging between 0–8 tonnes ha^{-1} year^{-1} (Figure 85).
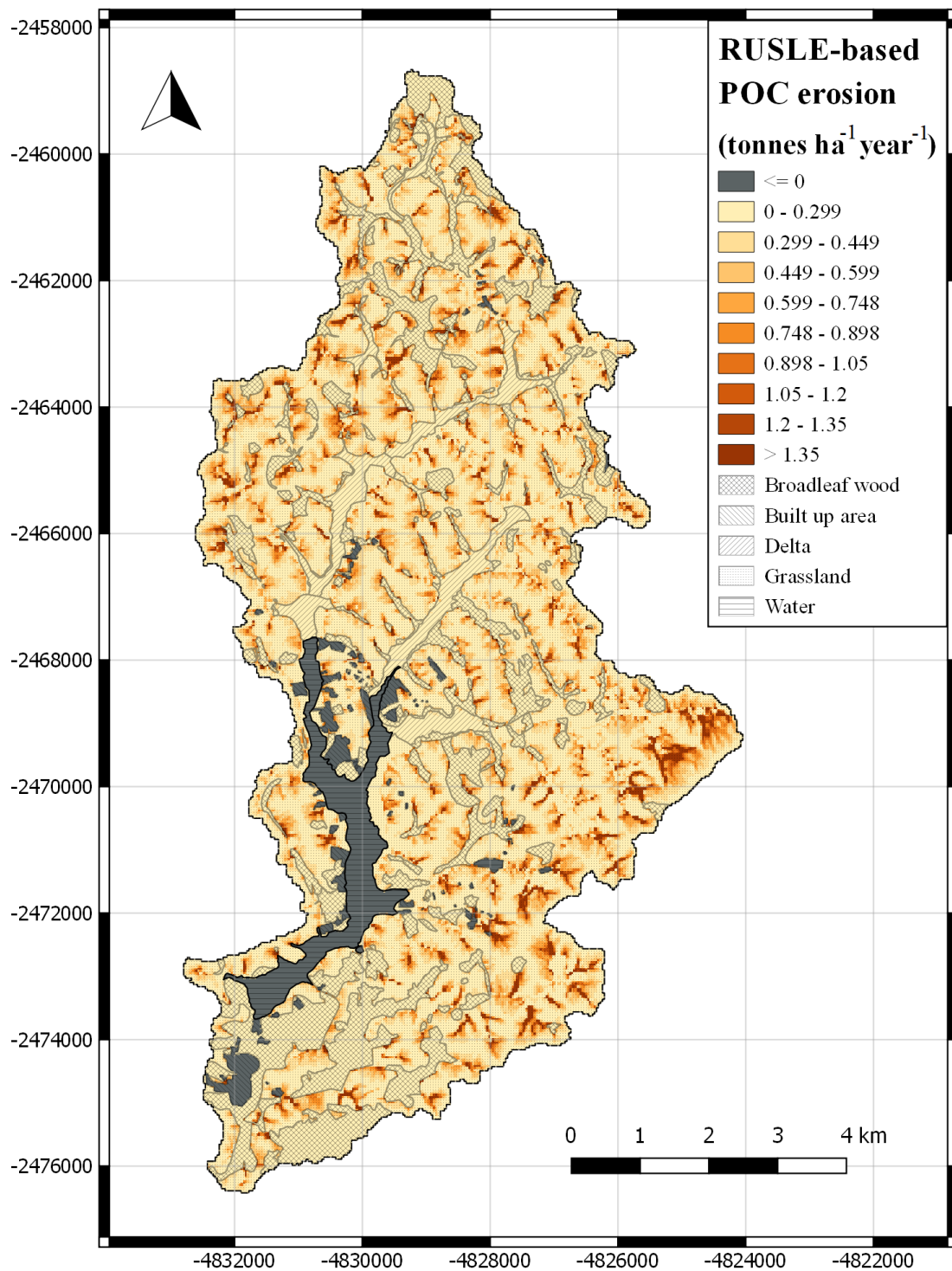
Figure 85 RUSLE-based POC erosion (tonnes ha⁻¹ year⁻¹) of surface soils (upper 20 cm) in João Penido catchment. The RUSLE output based on database and digitized C & observed K was used, resulting in POC erosion ranging 0–7.96 tonnes ha⁻¹ year⁻¹. EPSG: 3857.

5.3.3 SAR and POC accumulation

The average sediment depth (N=15) in João Penido reservoir was 0.254 m. Calculated SAR (cm year^{-1}) and accumulation of POC (g m^{-2} year^{-1}) from OC data for sediment core samples in João Penido reservoir are summarized in Table 32. From field observations the sedimentation rate was calculated by dividing the thickness (cm) of the accumulated post-flooding sediment layer by the age of the reservoir (82–83 years depending on the year of sampling: 2016 or 2017), which gave SAR values between 0.07–0.44 cm year^{-1} in the reservoir. The POC accumulation rates were calculated by quantifying the inventory of POC (g) in the post-flooding sediment divided by the area of the sample corer (0.0028 m^2) and the age of the reservoir (years). Figure 86 shows calculated SAR in the reservoir by inverse distance weighting interpolation.

Summary table SAR in reservoir João Penido

Site	Sampling date	Total C (g)	Yearly C input (g year^{-1})	Sedimentation rate (cm year^{-1})	OC accumulation (g m^{-2} year^{-1})	Depth pre-flood material (cm)
SED3C	20160609	2.19	0.03	0.07	9.57	6
RM13	20170714	3.35	0.04	0.07	14.6	6
RM10*	**20170714**	**4.83**	**0.06**	**0.1**	**21.03**	**8**
RM01	20170714	5.81	0.07	0.22	24.99	20
RM16	20170714	6.55	0.08	0.22	28.55	18
SED4A***	20160609	8.61	0.11	0.26	37.5	-
SED5C	20160609	9.39	0.11	0.32	40.89	28
RM17*	**20170714**	**10.86**	**0.13**	**0.44**	**47.31**	**36**
RM09*	**20170714**	**12.76**	**0.15**	**0.4**	**54.9**	**30**
RM06	20170714	16.11	0.19	0.29	69.34	27
SED2A	20160609	16.38	0.2	0.39	71.35	32
SED4B*	**20160609**	21.46	0.26	0.41	93.46	**36**
RM07**	20170714	-	-	0.07	-	52
RM08**	20170714	-	-	0.24	-	20
RM12**	20170714	-	-	0.31	-	26
RM11**	20170714	-	-	0.43	-	36
Min		2.19	0.03	0.07	9.57	6
Max		21.46	0.26	0.44	93.46	52
Mean		9.86	0.12	0.27	42.79	25.4
Median		9	0.11	0.27	39.19	27
Standard Deviation		5.89	0.07	0.13	25.54	12.78

*gap-filling has been implemented **only SAR available ***no pre-flood material detected in core

Table 32 SAR and POC accumulation rates from OC data.

While SAR vary across the reservoir gradient, the OC data showed OC accumulation with a minimum and maximum OC accumulation rate of 5.99 and 93.46 g POC m^{-2} year^{-1}, respectively.

Average POC mass per volume (kg m^{-3}) was calculated by:

$$POC_{density} = \frac{POC_{tot}}{V}$$

Where POC_{tot} is the mean total mass of POC in the sediment cores (0.00986 kg) and V is the post-flooding volume of the core, derived from the core area (0.0028 m^2) and mean post-flooding sediment thickness (0.254 m). The average $POC_{density}$ was 13.86 kg m^{-3}.

An estimate of the total POC (kg) in the reservoir was then calculated as a product between the average POC mass per volume (13.86 kg m^{-3}) and calculated total reservoir sediment volume (753058.8 m^3). Based on these input factors the result gave a total POC inventory of 10440 tonnes in the reservoir post-flooding sediment. This would on average require a yearly net POC input of c. 127 tonnes year^{-1} into the reservoir storage since the year the dam was built (1934).

Figure 86 Maps showing sediment accumulation rate (cm year^{-1}) in João Penido reservoir. EPSG: 3857.

5.3.4 POC pathways and budget

A summary of POC pathways and budgets are presented in Table 33. If it is assumed that soil derived POC is relatively recalcitrant and that the average value of 2.8% is universal for the catchment soils, the eroded input of terrestrial POC into the reservoir sediments since 1934 would amount to c. 2934 tonnes, or c. 28% of the total POC mass of the sediments, which indicates that 72% of the sediment POC is of autochthonous origin. If 2.8% of the total terrigenous sediment input representing POC would amount to 28,887 tonnes, out of which 2934 tonnes was present in the reservoir, this suggests that an overall 90.2% has been exported from the reservoir as mineralisation products or by outlet

discharge. A schematic diagram with inventories and rates of POC erosion and sedimentation, visualizes the transport of POC in João Penido catchment (Figure 87).

POC pathways and budgets

Erosion rates	Mean value	Unit
RUSLE (database)	37.8	tonnes ha^{-1} year^{-1}
RUSLE (observations of *C* and *K*, complete watershed)	10.9	tonnes ha^{-1} year^{-1}
RUSLE (observations of *C* and *K*, point samples of pasture and shrubland sites A and B only)	9.1	tonnes ha^{-1} year^{-1}
PDM-^{137}Cs	4.5	tonnes ha^{-1} year^{-1}
DMM-^{210}Pb$_{ex}$	16.1	tonnes ha^{-1} year^{-1}

POC erosion	Mean value	Unit
Calculated from RUSLE (database)	1.1	tonnes ha^{-1} year^{-1}
Calculated from RUSLE (database and observed *C* and *K*)	0.3	tonnes ha^{-1} year^{-1}
Calculated from RUSLE (database and observed *C* and *K*, of soil sites)	0.3	tonnes ha^{-1} year^{-1}
Calculated from PDM-Cs	0.1	tonnes ha^{-1} year^{-1}
Calculated from DMM-Pb	0.5	tonnes ha^{-1} year^{-1}

Catchment properties	Value	Unit
Catchment area	72140000	m^2
Area deforested grassland	52297821	m^2
% area deforested grassland in catchment	72	%
Reservoir area	3720000	m^2
Reservoir perimeter	22584	m

Total soil sediment remobilised in catchment deforested grasslands	Mean value	Unit
Calculated from RUSLE (database)	197686	tonnes year^{-1}
Calculated from RUSLE (database and observed C & K)	56743	tonnes year^{-1}
Calculated from RUSLE (database and observed C & K, of soil sites)	47486	tonnes year^{-1}
Calculated from PDM-^{137}Cs	42884	tonnes year^{-1}
Calculated from DMM-^{210}Pb$_{ex}$	84200	tonnes year^{-1}

Total soil POC remobilised in catchment deforested grasslands	Mean value	Unit
Calculated from RUSLE (database)	5535	tonnes year^{-1}
Calculated from RUSLE (database and observed C & K)	1589	tonnes year^{-1}
Calculated from RUSLE (database and observed C & K, of soil sites)	1330	tonnes year^{-1}
Calculated from PDM-^{137}Cs	1201	tonnes year^{-1}
Calculated from DMM-^{210}Pb$_{ex}$	2358	tonnes year^{-1}

Reservoir sediment	Value	Unit
Calculated total volume of sediment	753059	m3
Calculated total mass of sediment	1031691	tonnes
Average sediment density	1370	kg m^{-3}
Age reservoir postflooding sediment	82	years
Average accumulation of sediment in dam since 1934	12582	tonnes year^{-1}
Accumulation of sediment in dam since 1934 for each m^2	3.4	kg m^{-2} year^{-1}

Reservoir POC	Value	Unit
Average total mass of POC in all sediment cores (post-flooding)	9.86	g
Average core volume	0.0007112	m^3
Average total POC in sediment cores	13.86	kg m^{-3}
POC mass calculated from mean POC inventory	10440	tonnes
Calculated POC mass of sediment	1.4	%

Sedimentation rates	Mean value	Unit
Core observations	0.27	cm year^{-1}
CRS-^{210}Pb$_{ex}$ for SED5	0.5	cm year^{-1}
SAR based on ^{137}Cs peak in sediment core SED5 at 32 cm depth	0.6	cm year^{-1}
Calculated average SAR (QGIS) for the reservoir	0.3	cm year^{-1}
Accumulation of POC in dam since 1934	127	tonnes year^{-1}
Accumulation of POC in dam since 1934 for each m^2	105	kg m^{-2} year^{-1}
Calculated sediment yield	20.3	%

Table 33 Summary of erosion rates, sedimentation rates and inventories of POC.
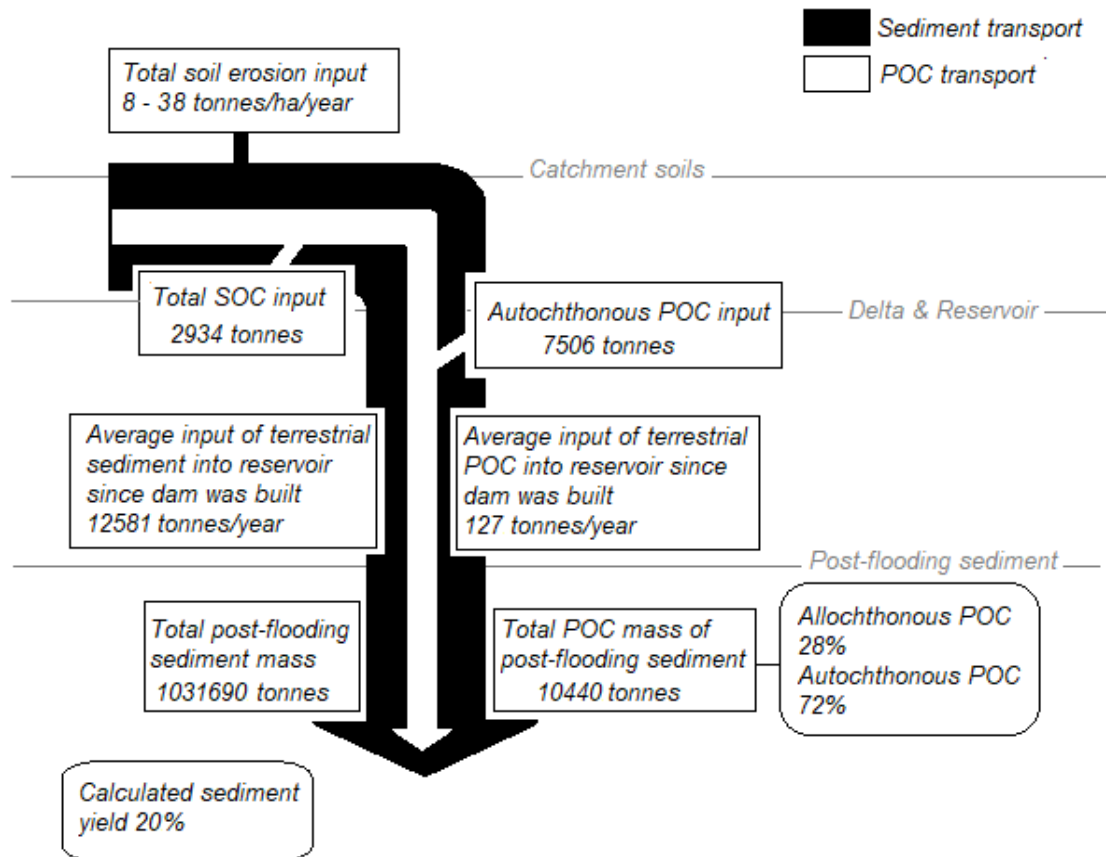
Figure 87 Schematic diagram showing the net sediment and POC input into João Penido reservoir since the dam was built in 1934.

5.4 Summary of Chapter 5

This chapter summarized the results of: particle size analysis of selected samples; organic matter, organic carbon and inorganic carbon concentrations and inventories of soils and sediment by loss on ignition; C/N ratios of selected soil and sediment samples; fallout radionuclide activities and inventories; conversion model results of Profile Distribution Model and Diffusion and Migration Model; RUSLE model output; and POC export in the catchment. These results are further discussed in Chapter 9.1 Brazilian catchment study.

Chapter 6. Results Exmoor riverine POC study

This study aimed to investigate the transformation effects of flocculation on natural organic matter in streams draining Exmoor. The results increase understanding on the effects of coagulants typical of flocculation boundaries in the landscape, such as clay particles inputted into streams by soil erosion, and saline mixing of freshwater at the estuarine boundary. The results presented in this chapter summarize 1) monitored characteristics of eight parallel draining stream and headwater moorland site, 2) initial results from the conducted flocculation experiment, and 3) residual DOM quality of post-experimental samples.

6.1 Seasonal monitoring of riverine organic matter

Seasonal trends in monthly–bi-monthly data of pH, EC, temperature, TSP and POM are summarized in this section.

6.1.1 Characteristics of Exmoor stream water

Figure 88 shows the seasonal change in stream pH, electrical conductivity and water temperature. pH ranged between 6.16–8.15, with a mean of 7.12 for stream sites while the moor headwater site I had an average pH of 4.94. The highest observed pH (8.15) was observed for site A. In the winter months the pH range appeared more similar (6–6.5) for all downstream sites, and could be connected to the winter precipitation discharge. Electrical conductivity ranged between 0.00–0.11 mS cm^{-1}, with a mean of 0.05 for all sites. Over the sampling period with the exception of 2017-12-01, site H showed higher electrical conductivity than the other sites, with an average of 0.09 mS cm^{-1}, indicating a noticeable difference in background water quality which can be an influence from land use and lithology in this drainage basin. The average measured water temperature over the monitoring season ranged between 4.20–14.40 degrees C.
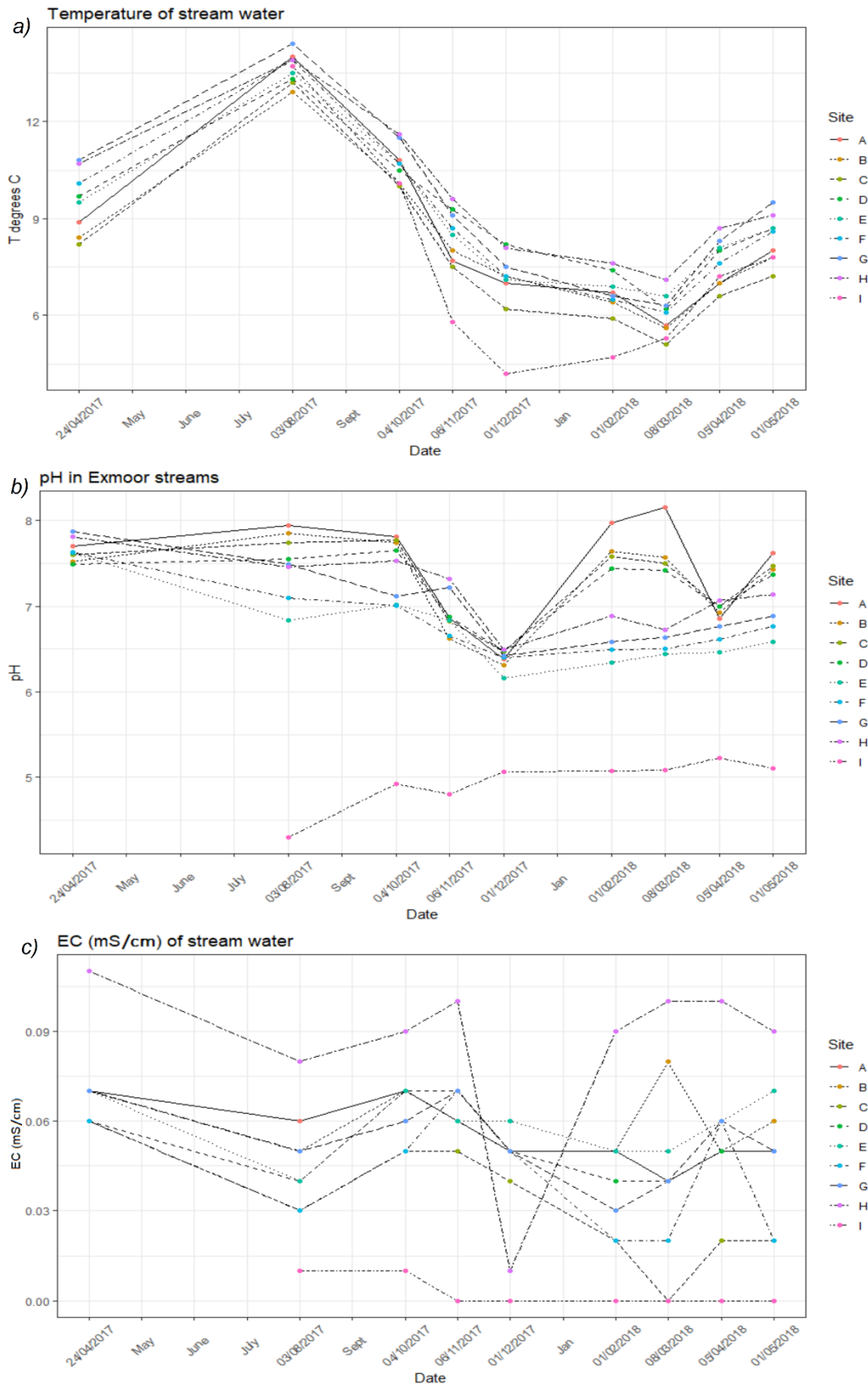
Figure 88 Seasonal change in stream water temperature, pH and electric conductivity of the studied Exmoor streams.

An estimate of total dissolved solids (TDS) in stream water can be made from measurements of electrical conductivity (EC) by the following expression (Taylor et al, 2018):

TDS (mg L^{-1}) = k_e×EC (µS cm^{-1})

Where k_e is a constant, commonly between 0.55–0.85 (Walton, 1989) – the typically used average of 0.70 was used in this study (Figure 89). Although the TDS could only be crudely calculated, it gave an indication of the water quality at the various sites. The headwater site I showed low to absent TDS concentrations, while site H showed the highest concentrations, with one exception in December 2017 possibly explained by dilution from high water discharge.
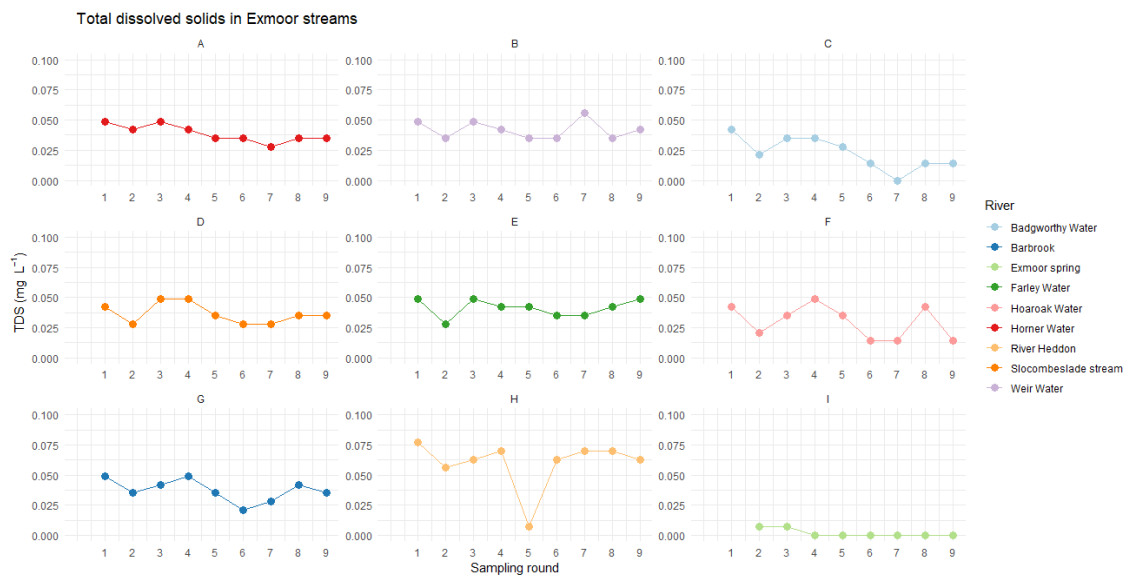
Figure 89 Total dissolved solids (TDS) calculated from electrical conductivity measurements.

6.1.2 Dissolved organic carbon (DOC)

Stream samples from sampling rounds 1–4 analysed at University of Exeter showed total dissolved organic carbon (DOC) ranging between 0.09–22.6 mg L^{-1}, with a mean of 4.3 and a median of 2.1 mg L^{-1} (N=35). The highest DOC concentrations were found in samples from the headwater site I on Exmoor ranging 11.85–22.59 mg L^{-1}, with a mean of 15.48 mg L^{-1} (N=3), while the stream

194

sites showed similar average DOC concentrations with a mean of 3.1 mg L^{-1} (Figure 90). Samples from sampling round 1 (2017-04-24) analysed at Uppsala University showed DOC concentrations ranging between 0.31–8.91 mg L^{-1}. The measured DOC concentrations are comparable to other studies in the South West of UK, e.g. Ritson et al (2019) found seasonal mean DOC of 2.14(±0.09)–2.70(±0.08) mg L^{-1} at their monitoring sites in the Exe basin (Devon), and in a study of two other catchments in Exmoor National Park that had mean DOC concentrations of 9 and 13 mg L^{-1} (range of 4–21 mg L^{-1}) (Grand-Clement et al, 2014). DOC values of site A (Horner Water) ranged 1.36–4.81 mg L^{-1} (N=4) for sampling rounds 1–4. These values represent DOC concentrations at relatively low water levels. For comparison Glendell et al (2014) reported observed DOC concentrations of 4.67–7.59 mg L^{-1} (N=11) in Horner Water during high discharge events.
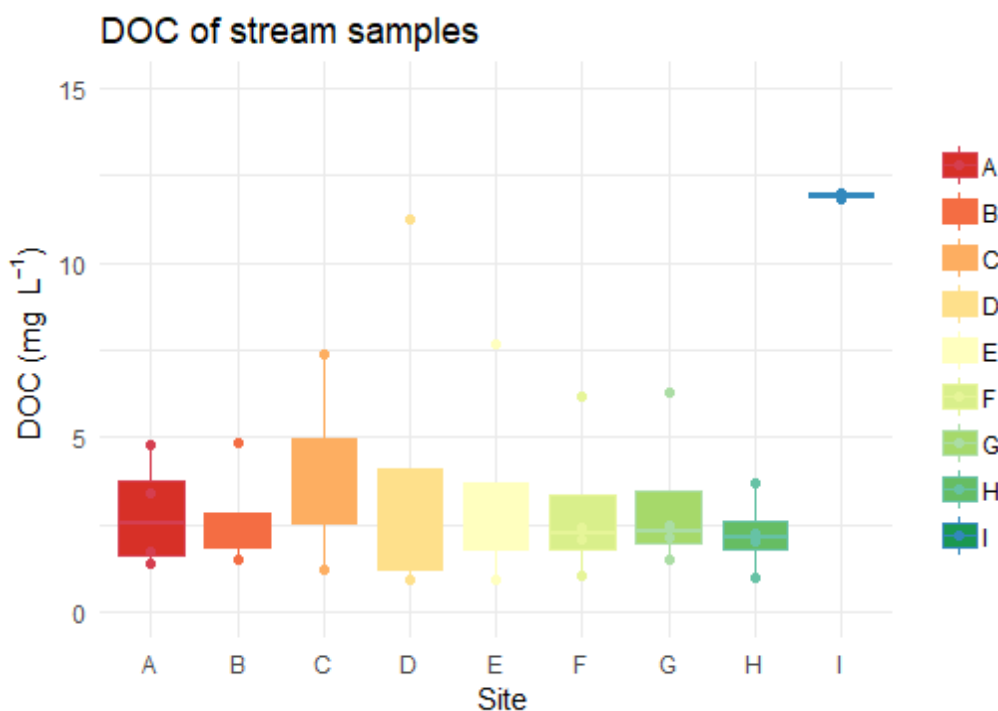
Figure 90 Stream DOC concentrations of sites A-I for sampling rounds 1-4.

6.1.3 Total suspended particulates (TSP)

Total suspended particulates (TSP) of stream samples from 9 sampling campaigns (*N*=69) are summarized in Table 34 and Figure 91. The maximum observed TSP content in stream water was 9.0 mg L^{-1} for site G, while the highest average TSP was found for site H (1.95 mg L^{-1}). OM content of TSP ranged between 1.95–7.61%, with a mean of 3.3%, and most of the particulate suspended matter was minerogenic. *Spearman correlation* was 0.95 (*p*<0.001) for OM and TSP (Figure 92, 94).
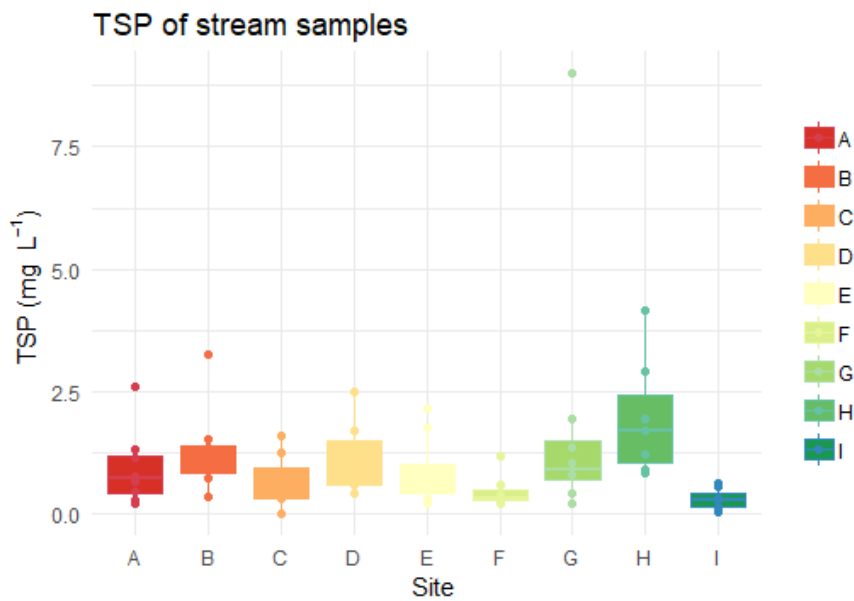
Figure 91 TSP (mg L^{-1}) in Exmoor streams.
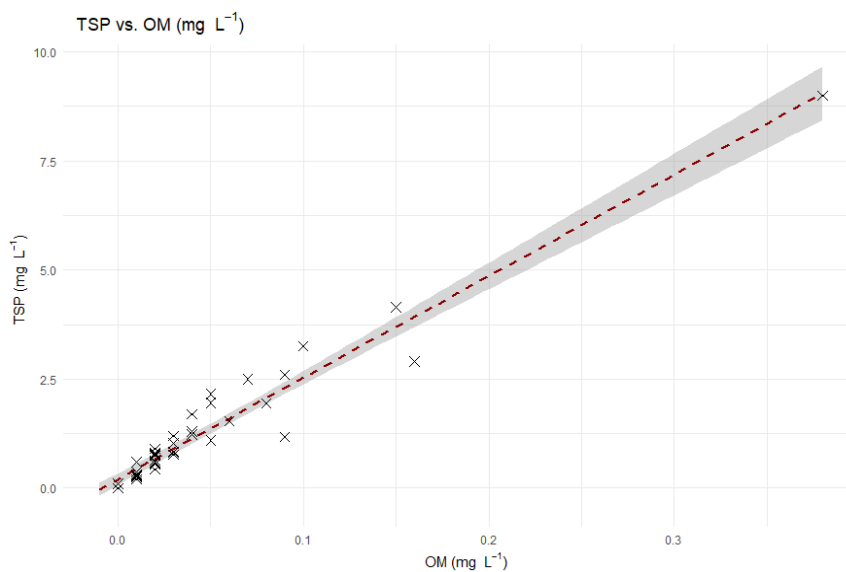
Figure 92 TSP and OM (mg L^{-1}) in stream samples.

6.1.4 Particulate organic carbon (POC)

POC was calculated from the OM content of the TSP by a conversion factor of 0.58, according to Pribyl et al (2010). Calculated stream water POC ranged between 0–0.38 mg L^{-1} (N=43) (Figure 93, Table 34), with the highest average POC content found in samples from site H. The average observed stream POC concentrations range between 0.01–0.1 mg L^{-1}.
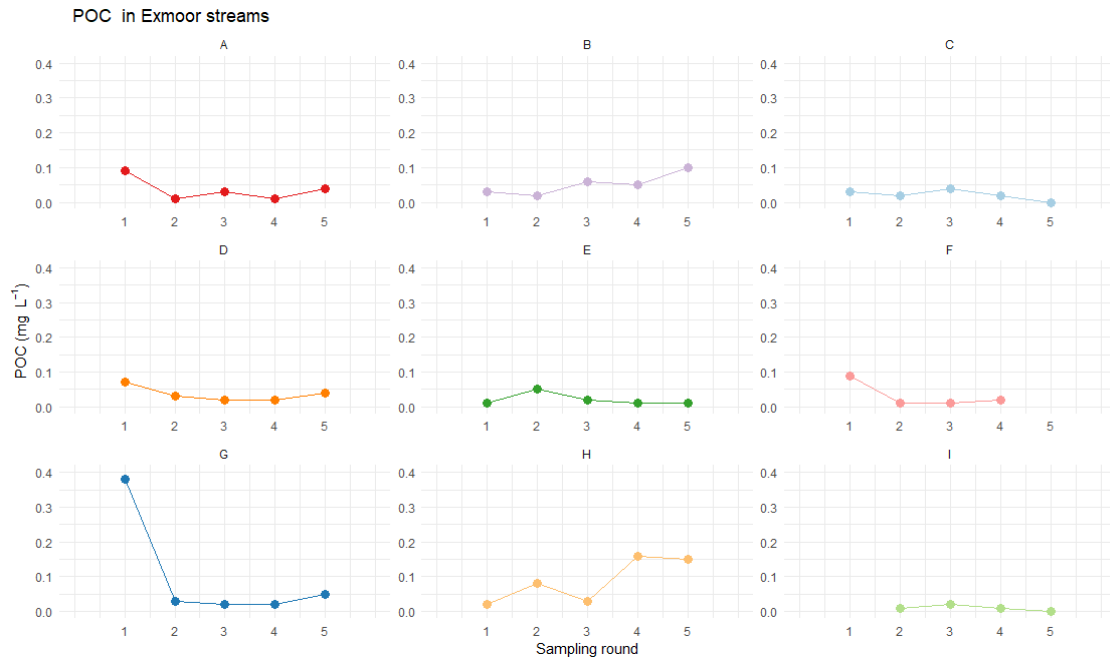
Figure 93 POC in Exmoor streams for sampling round 1-5.

Summary table of seasonal stream sampling between 2017-2018

Site	Sampling Rounds	mean DOC (mg L^{-1})	Sampling Rounds	mean TSP (mg L^{-1})	Sampling Rounds	mean calculated POC (mg L^{-1})
A	1-3	2.63	1-9 (excl.8)	0.92	2-5	0.03
B	1-3	2.85	1-9 (excl.8)	1.3	1-5	0.06
C	1-3	3.86	1-9 (excl.8)	0.7	1-5	0.02
D	1-3	4.51	1-9 (excl.8)	1.15	1-5	0.04
E	1-3	3.65	1-9 (excl.8)	0.85	1-5	0.02
F	1-3	3.09	1-9 (excl.8)	0.35	1-4	0.03
G	1-3	3.3	1-9 (excl.8)	1.94	1-5	0.1
H	1-3	2.23	1-9 (excl.8)	1.67	1-5	0.09
I	1-2	17.31	1-9 (excl.1&8)	0.29	1-5	0.01

Table 34 Summary of mean DOC, TSP and POC mg L-1 for stream sites during the sampling year 2017-2018.

197

6.1.5 Stream water properties summary

Spearman correlation (Figure 94) showed that DOC (mg L^{-1}) samples was negatively correlated with EC (–0.56, $p<0.001$) and while positively correlated with water temperature (0.45, $p<0.01$). TSP correlated positively with EC (0.26, $p<0.05$). As electrical conductivity is influenced by dissolved ionic solutes, water quality plays a role in the resulting conductivity of a stream. Some studies of boreal systems have found negative relationship between DOC and conductivity (e.g. Oni et al, 2013), while other studies in tropical regions have found a strong positive correlation between EC and DOC (e.g. Monteiro et al, 2014). For stream site H which consistently had higher EC (except 2017-12-01) it is plausible that active ions were influential in the high background EC, e.g. ions from the bedrock The inverse relationship indicates that colloidal interactions between DOC and inorganic ions might reduce conductivity in the streams.
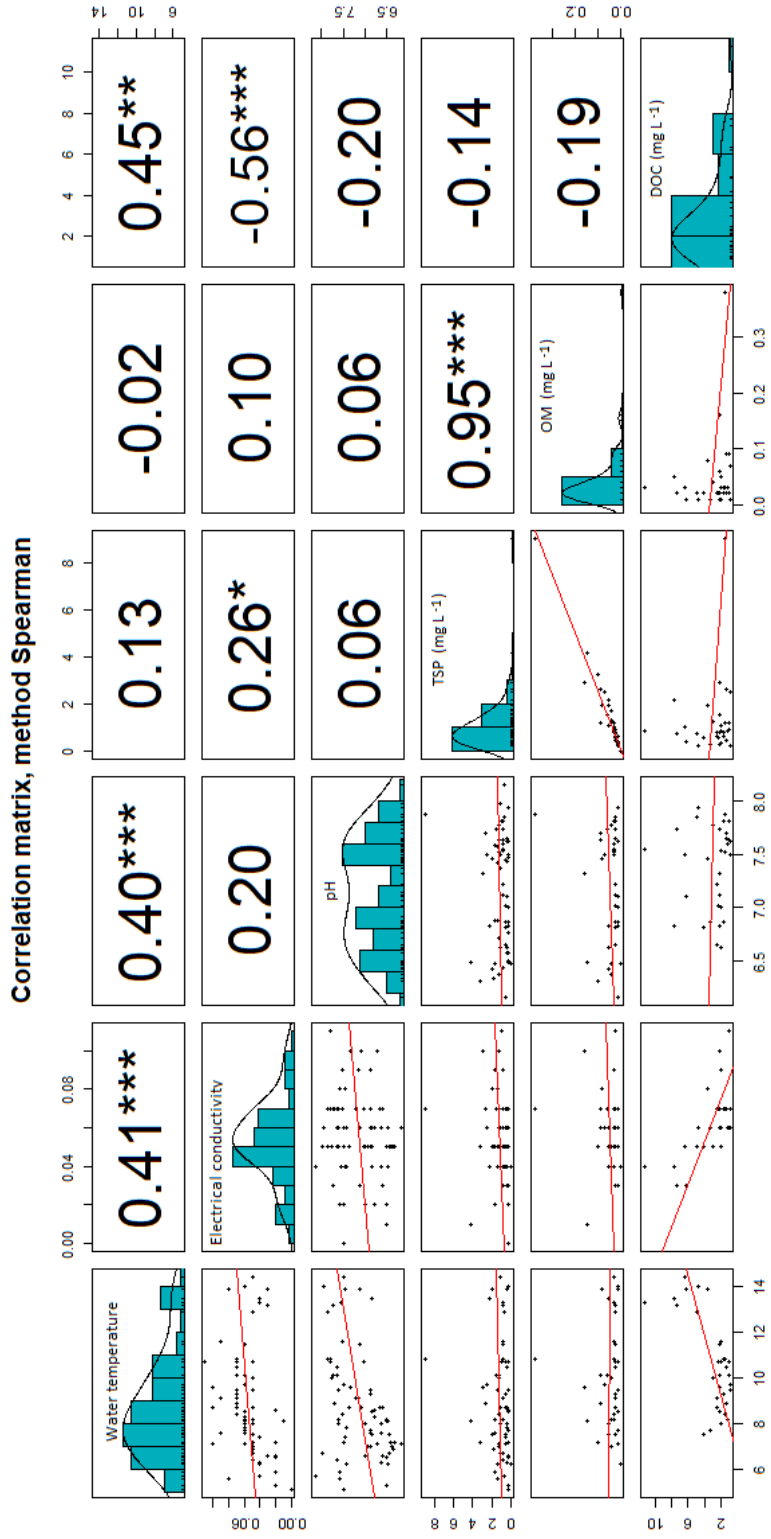
Figure 94 Correlation of stream water properties (* p<0.05, ** p<0.01, ***p<0.001).

199

6.2 Flocculation experiment

Flocculation experiments were undertaken to investigate the effect of flocculation on organic matter chemistry in stream water. Initial experiments were conducted on stream samples collected during sampling rounds 1, 2, 3, 4, 5. The treatments composed T1: control, T2: clay, T3: salt, and T4: mixture of clay and salt, where clay and salt standards were used as coagulants. Four replicates from each site were run in each experiment, together with four additional blanks. During this phase residual DOM filtrates were collected and stored for analysis of DOC, and absorbance and fluorescence spectra, and chemical analysis by mass spectrometry at Uppsala University, Sweden. However, the analytical results were erroneous due to suspected contamination from the storage sample tubes. As these results were considered non-representative they are not presented here. DOC was also measured in residual DOM samples from the flocculation experiment of sampling round 3 at University of Exeter. These samples were stored for a shorter time period between experiment and analysis and were considered less influenced by long-term contamination. Results showed that most of the residual filtrates of T1, T2, and T4 underwent small changes in DOC, compared to the raw stream DOM sample (Figure 95).
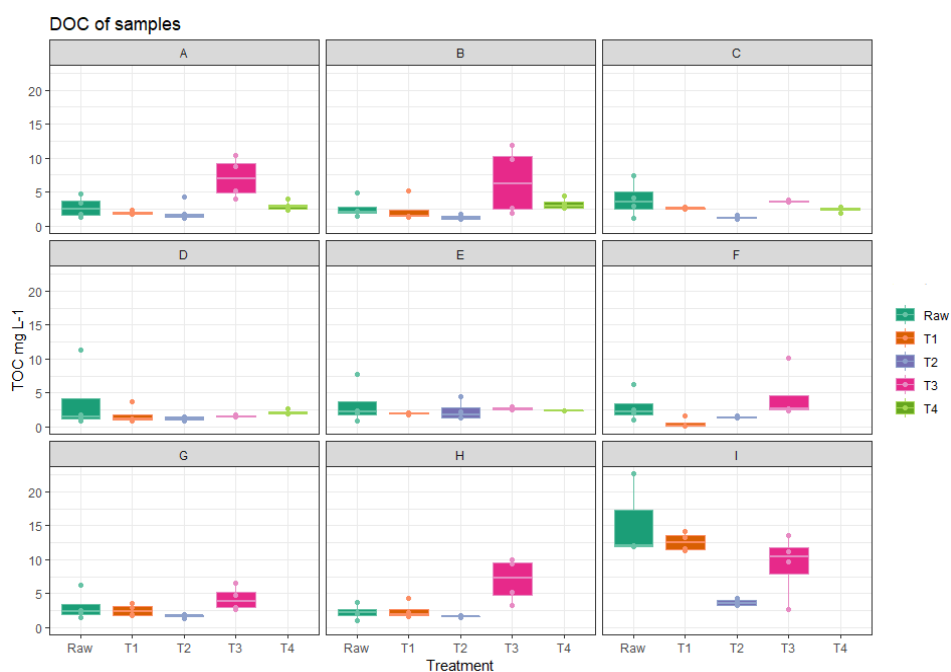
Figure 95 DOC change in flocculation samples. DOC was not measured in treatment samples T4 of sites F-I.

For the replicate samples of sites A, B, F, G, and H, DOC analysis appeared to give results with relatively large error, showing higher DOC concentrations for treatment samples than the raw stream sample, while site I showed most decrease in DOC change for treatments T2 and T3. DOC was not measured in T4 samples for sites F–I, due to the indicated error. Sample tubes were changed from plastic centrifuge tubes to acid washed glass vials with silicone PTFE septa lids (Fisherbrand™ EPA) for post-experimental filtrates of sampling round 9, and these samples were then used for the actual interpretation of flocculation effects on residual DOM chemistry, further discussed in *6.3 Case study on organic matter quality*.

An interesting observation during the flocculation experiments was the change in pH. Limited pH observations were made before and after flocculation experiments, and in general residual filtrates showed an increase in pH for T1, while decreasing pH was observed in samples with added coagulants of T2, T3, and T4 treatments (Figure 96).
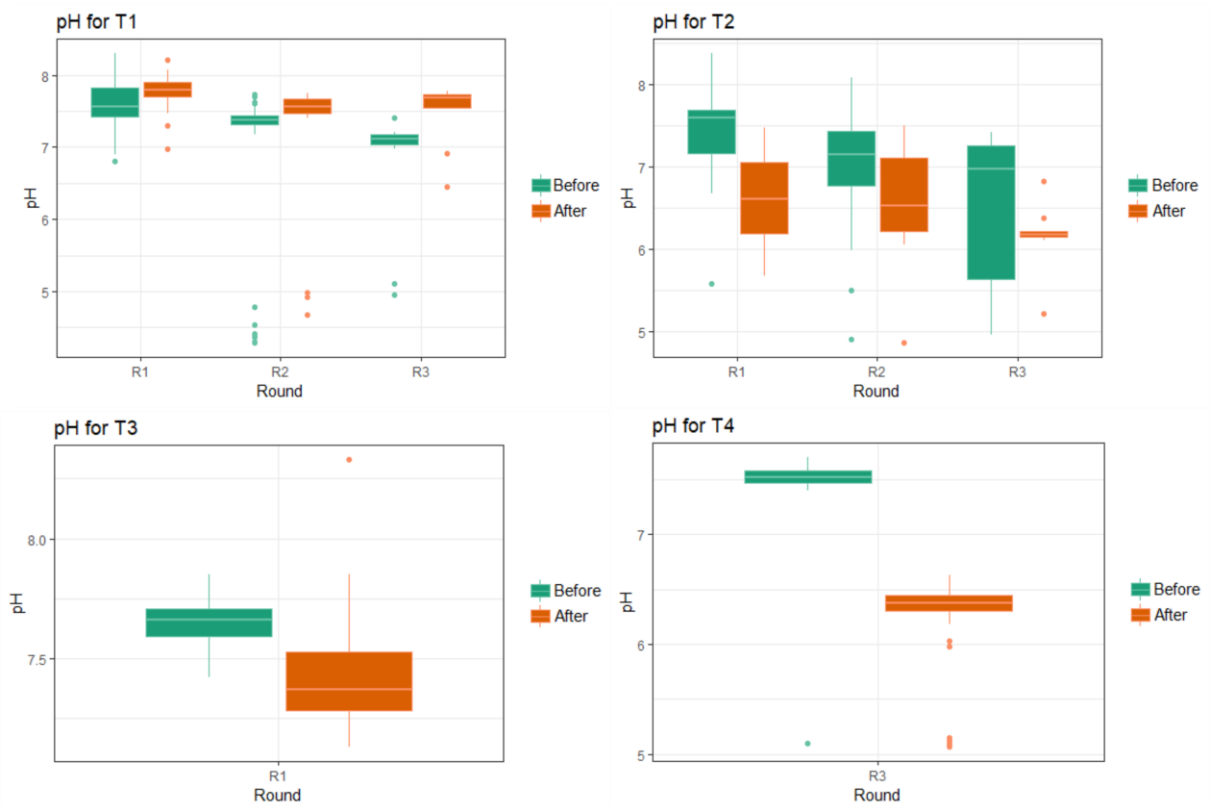
Figure 96 Average pH changes in flocculation experiment treatments (pH was not measured in all treatment samples).

6.3 Case study on organic matter quality

For the flocculation experiment conducted in May 2018 (sampling round 9) organic matter quality was analysed by mass spectrometry, absorbance and fluorescence at the laboratory of the Department of Ecology and Genetics at Uppsala University, Sweden. The results showed that different coagulants had various effect on stream water DOC and preferentially removed organic compounds from residual DOC into produced flocs. Mass spectrometry and optical characterisation showed that compared to control samples (T1) treatments with coagulants (T2, T3, T4) influenced the composition and fluorescence spectra of the treated samples.

6.3.1 Components from excitation-emission matrices (EEMs)

Parallel Factor analysis (PARAFAC) was used to identify 4 main components (C1–C4) using the *drEEM toolbox* (Mathworks, Inc., Natick, MA) for Matlab (Table 35). The components were ordered by intensity of samples and represented humic material (C1 and C2), protein like material (C4), and a non-classified component (C3).

Components of PARAFAC model

Component	*Representation*
C1	humic
C2	humic
C3	unidentified
C4	protein-like

Table 35 Four components of the PARAFAC model.

For stream samples, a relative comparison to the control samples of treatment T1 showed that for treatments T2 and T4 (treatment with clay standard) C2 appeared to have been lost during the experiment, indicating that DOM sorbed to the coagulating agent. C1 showed a similar pattern for treatment T2, but remained unchanged for treatment T4. For the mixed-coagulant treatment T4, an increase in components C3 and C4 was observed, which showed that these components were affected by desorption of OM from the clay standard when the salt standard was added to the solution. This suggests that there is counter-action between the salt and clay standards in this mixed treatment, resulting in overall

less net absorption of DOM compared with the T2 treatment which utilized the clay coagulant only. Additional tests of blanks showed the same pattern, that there was OM desorption from the clay in the saline solution of treatment T4. In general the effect of treatments on DOM sorption into flocs followed from high to low: T2>T4>T3. This showed that 1) clay was the most efficient coagulant in this experiment, 2) the efficiency of clay as a coagulant decreased by counter-acting salt ions in treatment T4, which lead to desorption of internal DOM from the clay standard, and 3) the salt treatment had a coagulation effect but was less efficient than any of the clay treatment and the combined clay and salt treatment.

For the moorland site I components C1 and C2 decreased by up to 80% for clay treatments T2 and T4. One possible explanation is that the relatively higher DOM concentrations in samples from this site, compared to the low concentration stream samples, diluted the desorption effect in the mixed-coagulant treatment.

6.3.2 Freshness index (FRESH), fluorescence index (FI), and humification index (HIX)

Clay treatments T2 and T4 showed strongest effect on the peak spectra and site I was clearly distinct from the other samples, reflecting higher concentrations of dissolved organic matter and carbon. Peak A, C and M reflect terrestrial sources of organic matter, where peak A and C typically reflect humic acids (Cory et al, 2010). These were in general low for the T2 treatment for all stream sites except for site D. In treatment samples, protein-like components of peak T increased compared to the raw stream samples for all stream sites, but not for the headwater moor site I. Patterns for peak B were less clear and showed no obvious trends.

The freshness index (FRESH) ranged between 0.6–0.7 for raw samples of stream sites and 0.43 for the headwater site I. FRESH increased in treatment samples compared to raw stream samples for clay treatments (T2 and T4) in samples from all sites, typically with highest values in T2 (Figure 97). The salt treatment (T3) did in some cases not lead to any relevant change in FRESH compared to the raw stream samples. For comparison, blank samples (which initially had a high FRESH index) displayed a decrease in FRESH with added salt.
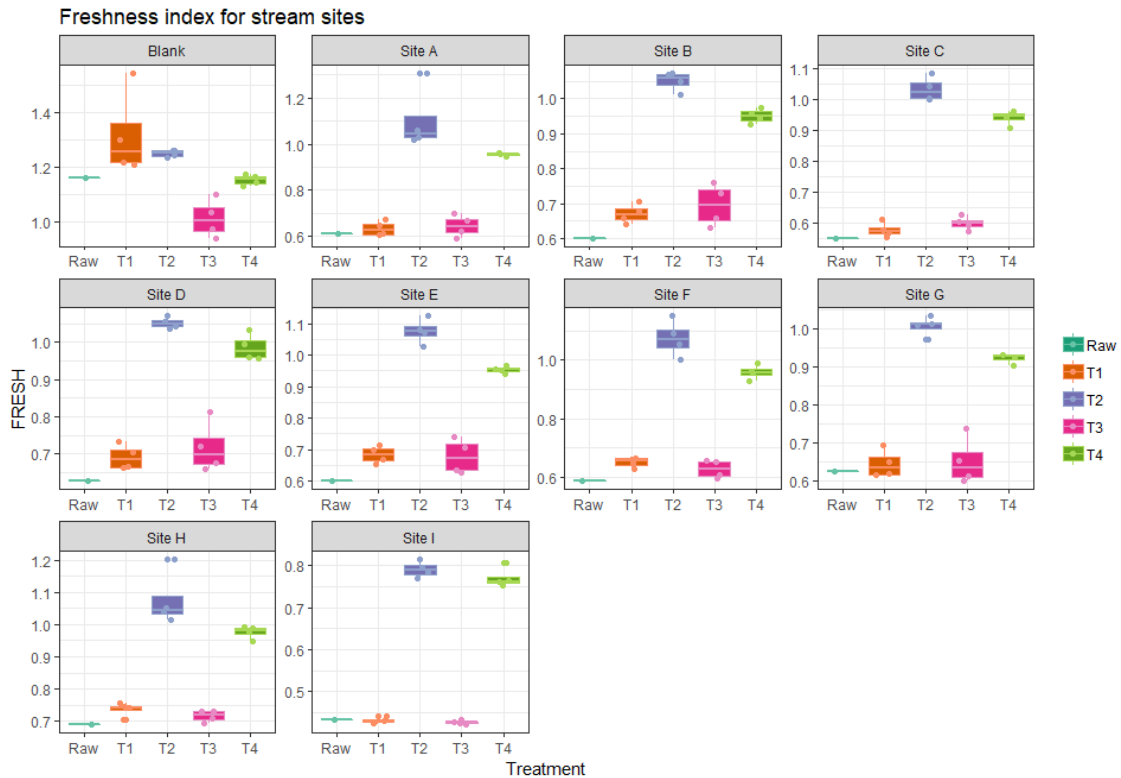
Figure 97 Freshness index for raw and treatment samples of blanks and site samples.

The fluorescence index (FI) ranged between for raw samples of stream sites 1.4–1.6 and 1.3 for the headwater site. FI increased in most treatment samples with added coagulants (T2, T3, and T4) compared to the raw stream samples and T1 (Figure 98). The highest increase was seen in clay treatments T2 and T4, typically with highest values for T4, while moderate change was observed for T3.
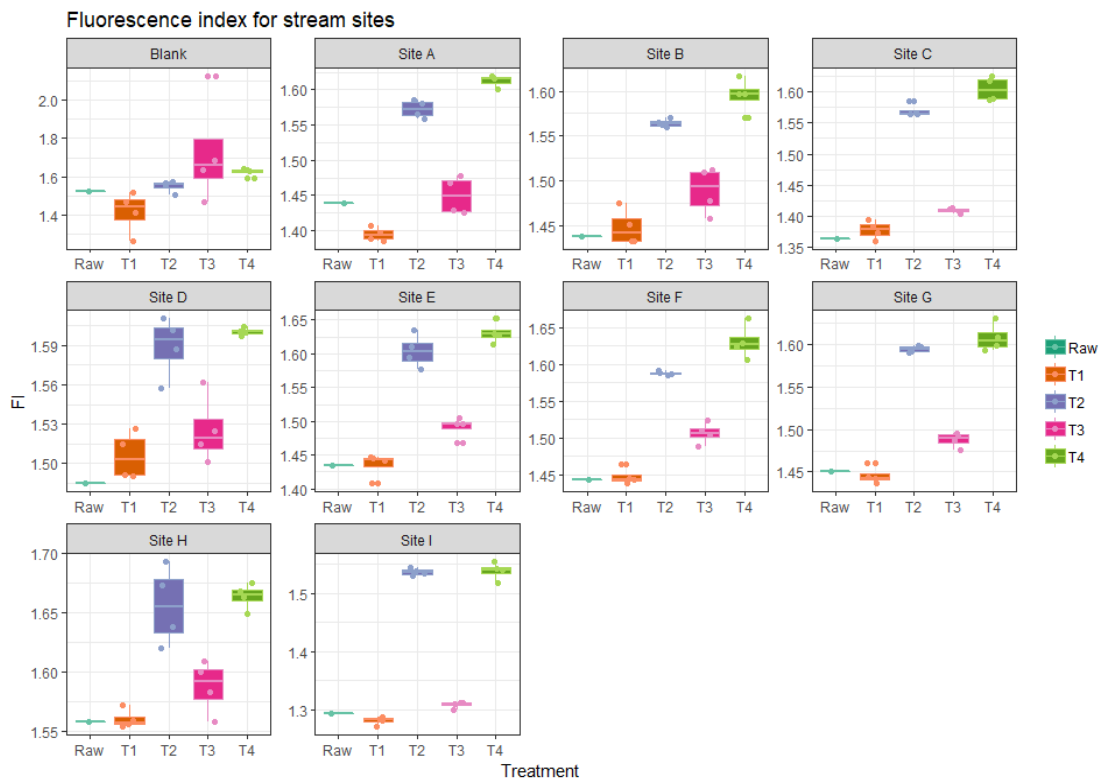
Figure 98 Fluorescence index for the blanks and treatment samples.

For stream sites the humification index (HIX) ranged 3.8–8.5 and amounted to 17.3 for the headwater site. In most cases the humification index decreased in treatment samples compared to the raw sample, suggesting that humic organic matter had been preferentially removed from the dissolved phase during flocculation experiment (Figure 99). The decrease was most extreme for clay treatments (T2 and T4), while the salt treatment only showed strong decrease for sites C and D. For sites E, F and H the humification index was higher for T3 than T1, suggesting that humified material had been reduced in the residual DOC.

205

Figure 99 Humification index for blanks and treatment samples.

Analytical blanks (Milli-Q® water) were used to determine the effect of each treatment on the peak spectra. The coagulant that left a major signal in the blank spectra was clay (T2 and T4); the humification index was highest for the clay treatments, the freshness index was lowest for the salt treatment (T3) and most treatments with added coagulants showed higher fluorescence index compared to the control sample (T1) (Figure 100).
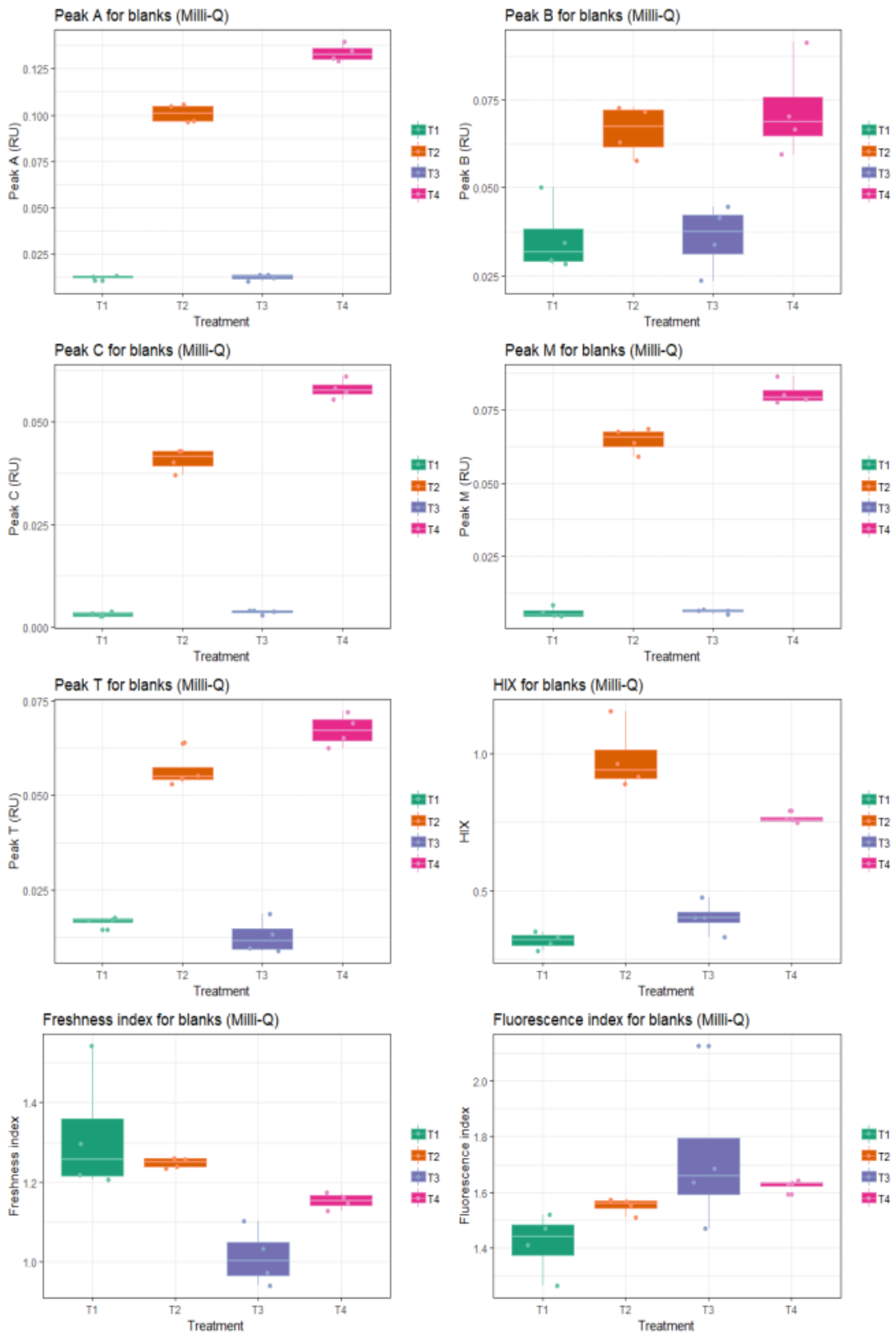
Figure 100 Analytical blanks (Milli-Q®) showed the effects of coagulants on optical spectra. Clay (T2 and T4) left major signatures. Negative values for Control samples are omitted.

6.3.3 Mass spectrometry

Analysis by mass spectrometry revealed that treatments with coagulants showed change in relative peak intensity and percentage distribution of classified organic compound groups in post-experimental residual DOM (Figure 101). The mass spectra represents signal intensities of ions as a function of mass-to-charge ratio and the calculated percentage composes the abundance of each designated compound group (described in the Chapter 4) relative to all other compound groups in the sample (Figure 102). For most of the sites, clay treatments T2 and T4 decreased the abundance of residual black carbon and polyphenols by absorption of compounds structures within these groups, which were highest in site I samples (T1 and T3). An exception was site A, which to a degree showed the opposite patterns of absorbed compound groups compared to the other sites. An explanation for this exception could be the presence of structural isomers (with the same molecular formulae but other chemical structures), which were classified into the same compound group but possibly exhibit recalcitrant chemical behaviour. Peptides and sugars showed low to no presence in the stream samples with c. 1% for a few sites in treatments T2, T3, and T4.
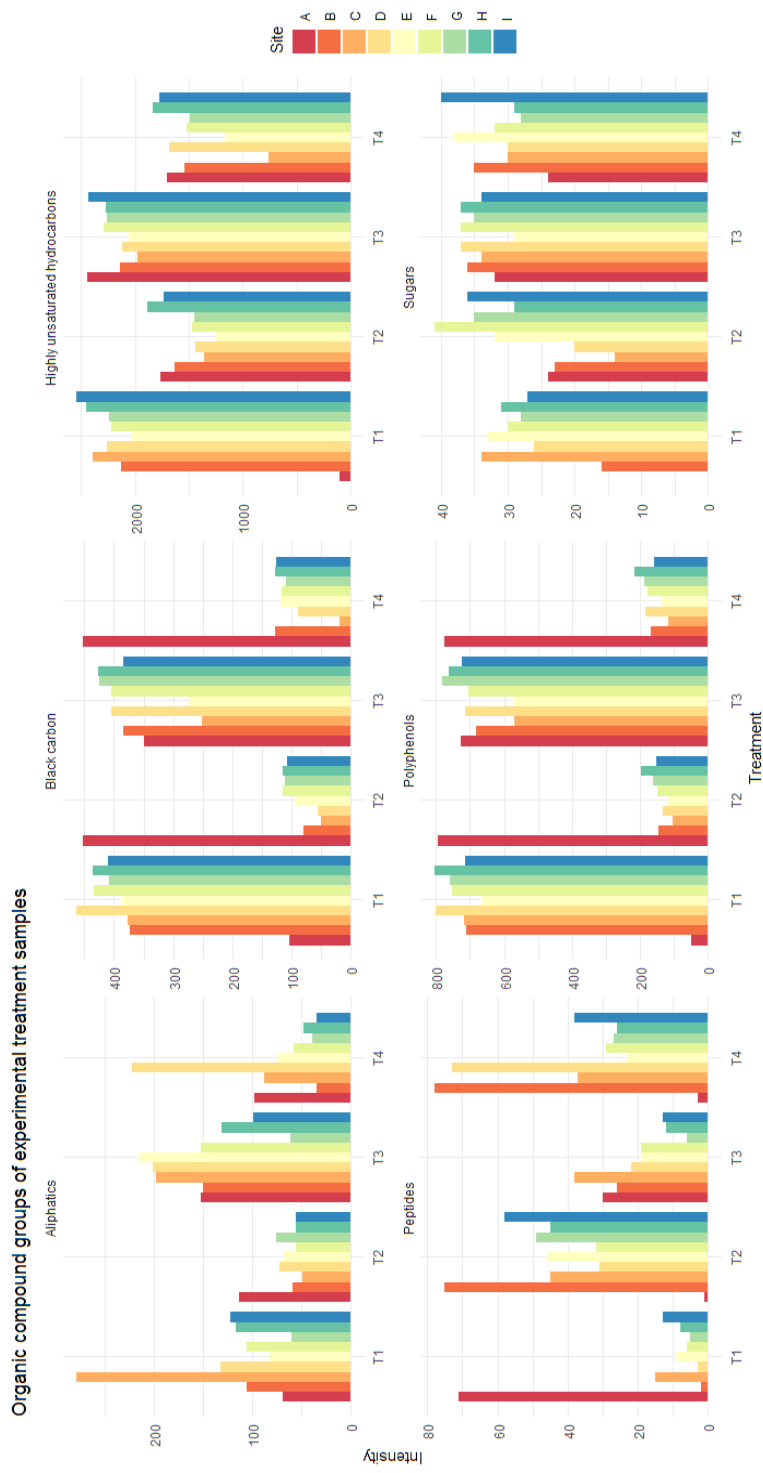
Figure 101 Mass spectrometry results presented as intensity by treatment for each identified compound group. Scales are set to free.
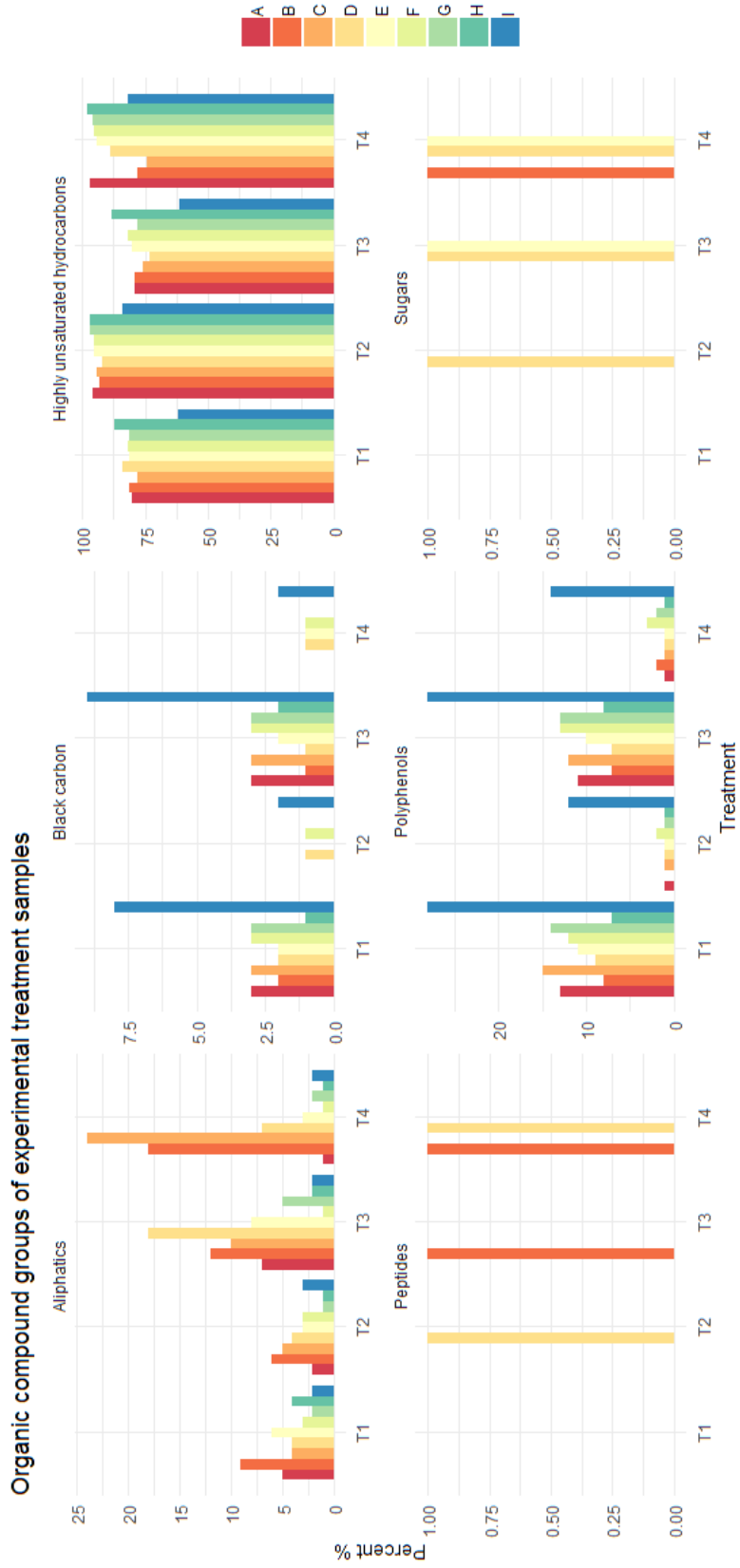
Figure 102 Percent distribution of carbon compounds by mass spectrometry revealed the effect of treatments on post-experiment residual DOM. Scales are set to free.

Principal component analysis (PCA) visualized the association of organic compound groups per treatment. The PCA scree plot of eigenvalues (Figure 103a) showed that the first two principal components (PCs) explained 98.7% of the total variance and a graph of variables (Figure 103b) displayed the correlation trend of the assigned compound groups for PC1 and PC2, where aliphatic compounds in general showed no association with the other compound groups. The contribution of the variables are summarized in Table 36 for the four main PCs. The treatment-grouped PCA biplot of PC1 (67.8%) and PC2 (30.9%) (Figure 104a) showed that organic compound concentration trends were similar for T1 and T3 while T2 distinctly deviated, and T4 showed a mixed T2-T3 trend. When displaying PC1 (67.8%) against PC3 (1.2%), concentration ellipses showed similar treatment effects for T2 and T4 with clear decline in polyphenols and black carbon, likely caused by the effect of clay in both of these treatments (Figure 104b).

PC variable contributions to total variance

	Dimension 1	Dimension 2	Dimension 3	Dimension 4
Black carbon	33.83	4.30	58.45	3.42
Polyphenols	34.90	2.75	37.75	24.60
Highly Unsaturated	31.20	12.23	2.31	54.26
Aliphatics	0.07	80.72	1.50	17.71

Table 36 PCA variable contribution to total variance for compound groups.
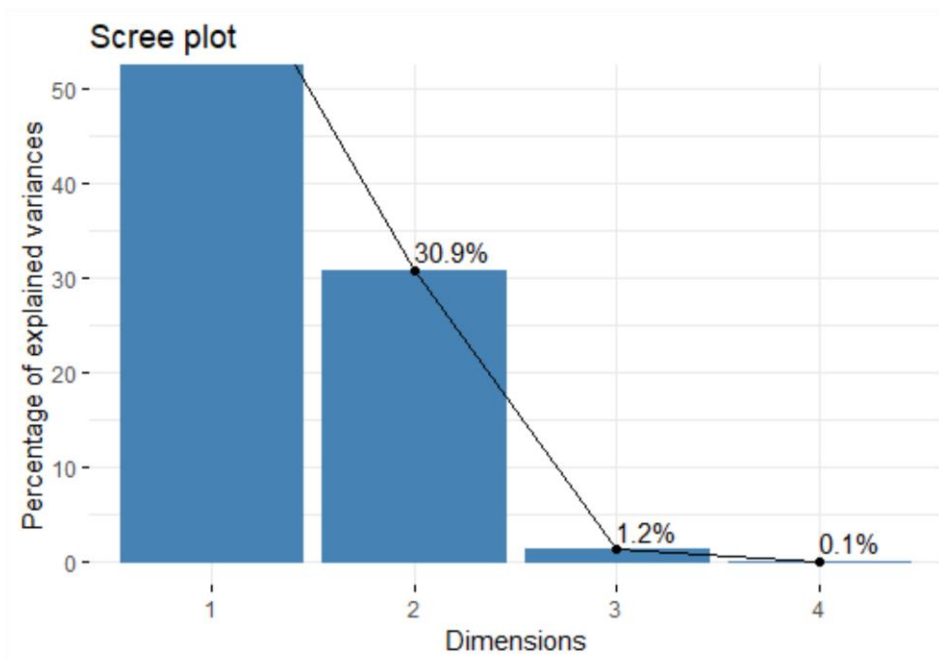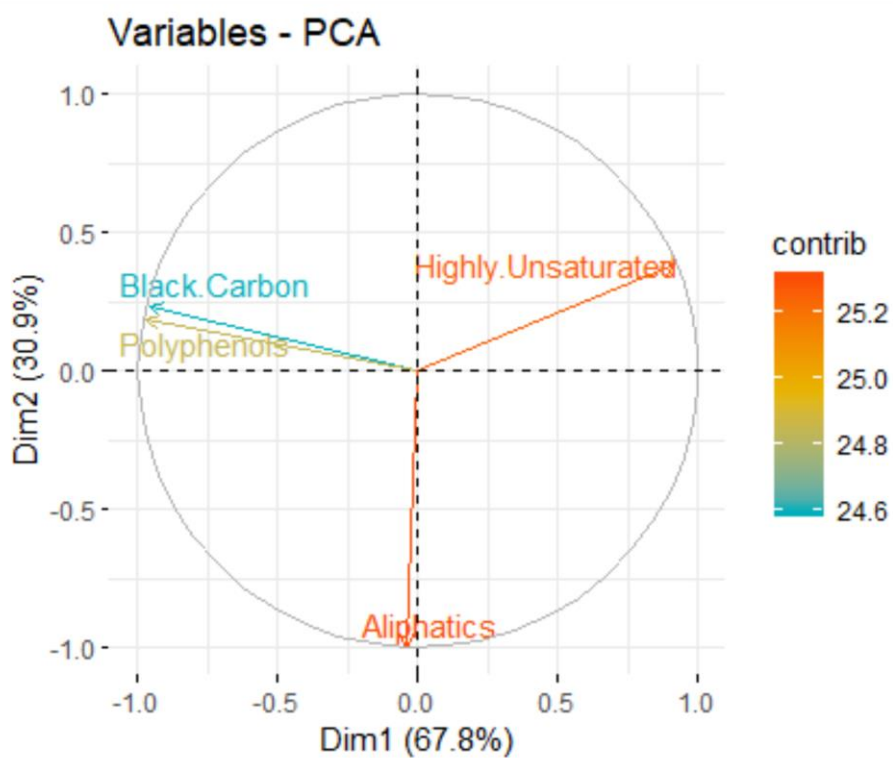
Figure 103 PCA visualization of organic compounds per treatments T1-T4, showing a) scree plot of PCA eigenvalues, and b) graph of variables.
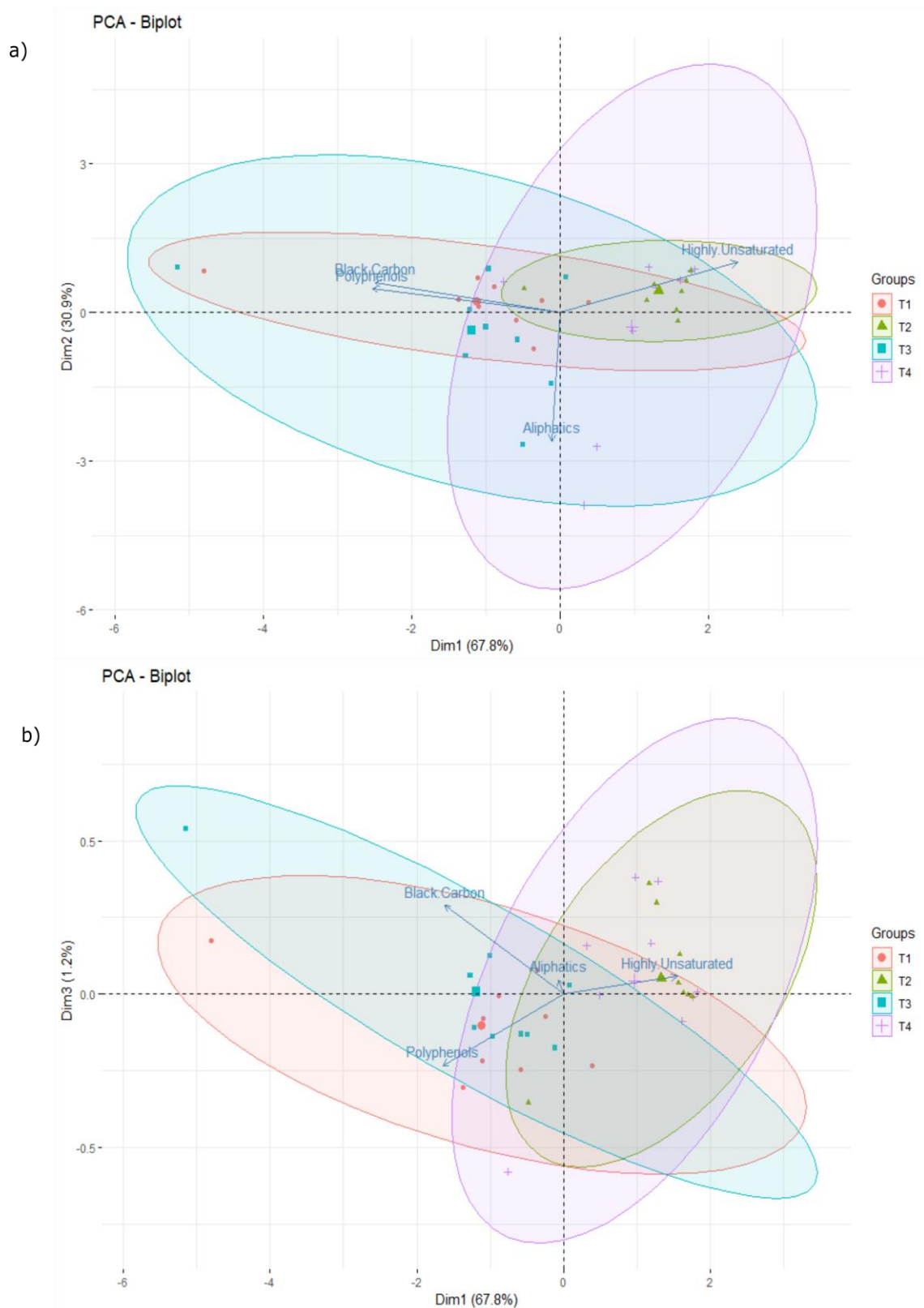
Figure 104 PCA visualization of organic compounds per treatments T1-T4, showing a) biplot of PC1 and PC2, and b) biplot of PC1 and PC3.

Patterns of weighted average ratios of H/C and O/C (H/C$_{WA}$ and O/C$_{WA}$, respectively) were useful to confirm patterns of treatments in residual DOM (Figure 105a, 105b). Both clay treatments T2 and T4 showed signals of increased H/C$_{WA}$ due to absorption of aromatic compounds (which exhibit low H/C ratios), while O/C$_{WA}$ ratios decreased compared to T1. For some sites, T4 increases less than T2, which could be caused by desorption of OM from the clay standard. T3 also increased H/C$_{WA}$ except for sites F, H and I, whilst O/C$_{WA}$ patterns of T3 were similar to T1. O/C$_{WA}$ decreased for treatments compared to the control samples, due to adsorption of compounds containing oxygen. These results partly confirm that the DOM composition was similar for all stream sites, and that treatments appear to have consistent flocculation effects on stream DOM. *Van Krevelen* diagrams of principal component 1 (PCoA1) showed that for all stream samples (excluding the headwater site I) PCoA1 was associated with the treatment and HIX and FRESH fluorescence indices, explaining 75%, 28% and 57% for T2, T3, and T4 respectively, while PCoA2 was primarily associated with PCoA2 for T1–T3 (Figure 106). Similar to trends shown by H/C$_{WA}$ and O/C$_{WA}$, pairwise comparison with the plot of control samples of T1 revealed preferential removal of structures, where *van Krevelen* visualizations of differences between T1–T2 (116b), T1–T3 (116c), and T1–T4 (116d) showed that in general high H/C (more aliphatic) and low O/C structures remained in residual DOM samples, while low H/C (more aromatic) and high O/C structures were sorbed to flocs. The effect appeared to be strongest for the clay treatment, weaker for the mixed treatment where salt had desorbed native organic compounds from the clay standard, and weakest for the salt treatment.
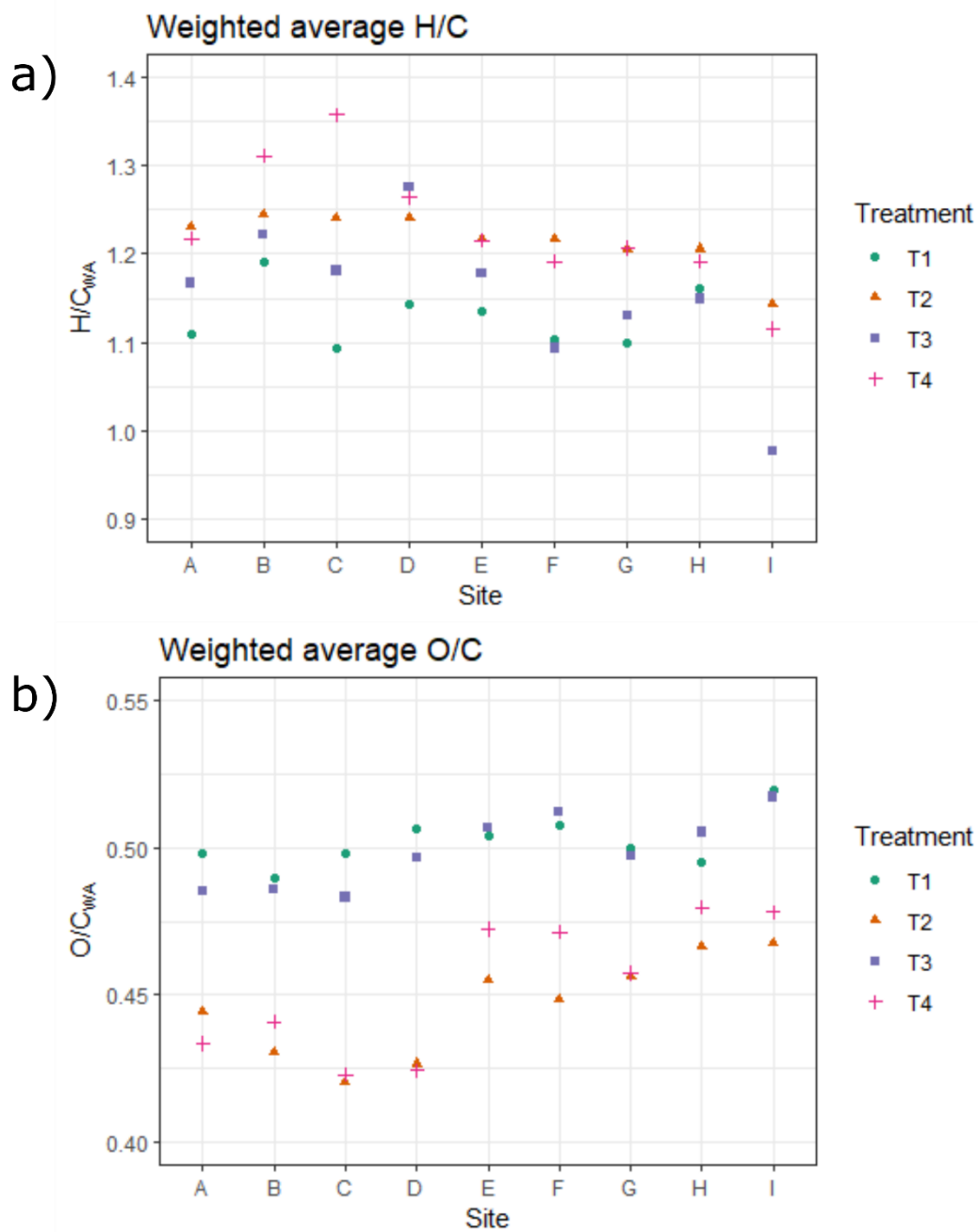
Figure 105 Weighted averages of H/C and O/C per stream site, showing the effect of treatments on residual DOM.
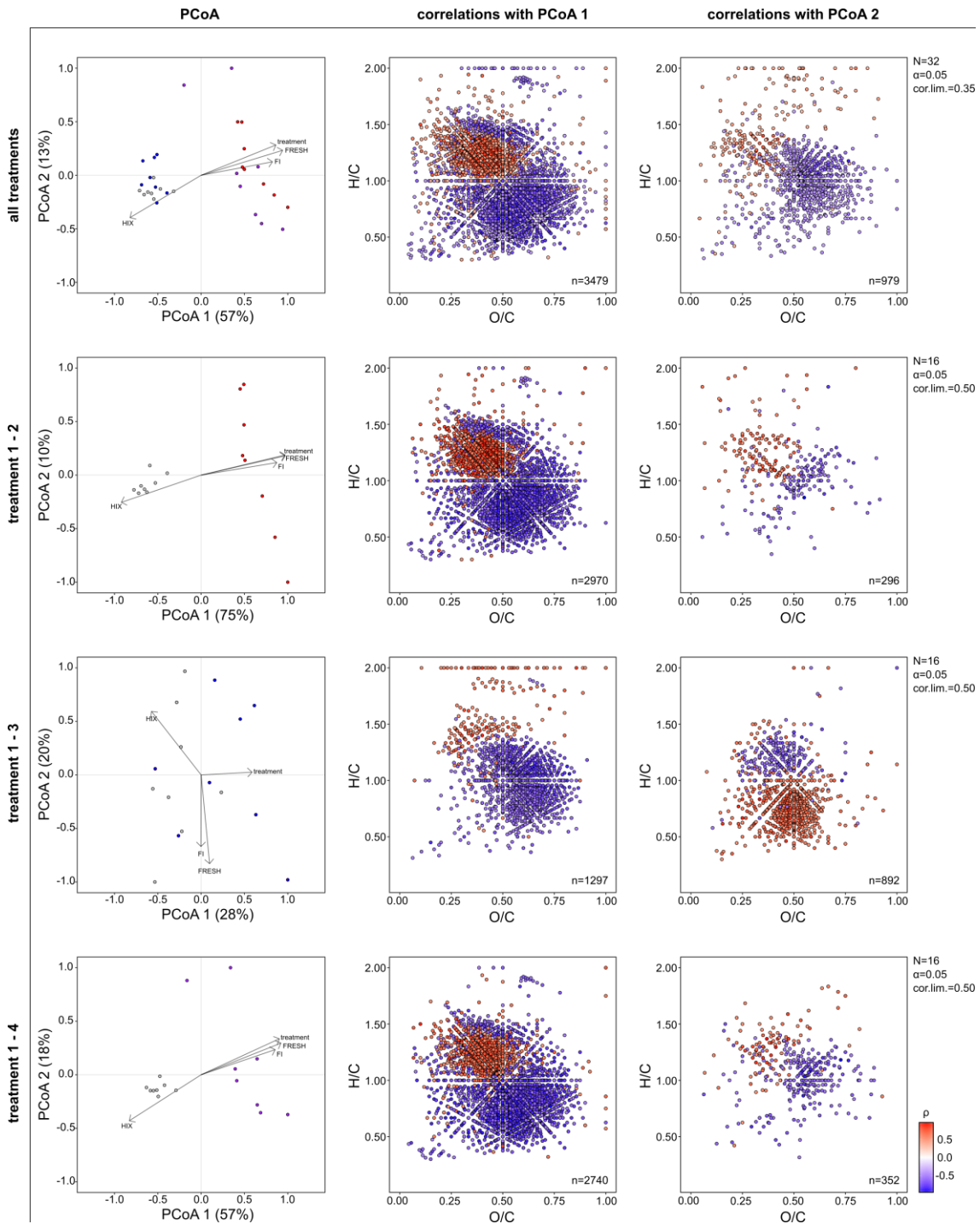
Figure 106 DOM composition compared between treatments. Left column: principal coordinate analysis (PCoA) loadings of treatments: control T1 (grey), clay T2 (red), T3 salt (blue) and clay-salt mixed T4 (purple) with sample characteristics as ordination drivers (arrows); middle column: Spearman rank correlation coefficients of individual molecules with PCoA1; right column: Spearman rank correlation coefficients of individual molecules with PCoA2. Figure courtesy M. Groeneveld, 2019.

6.4 Summary of Chapter 6

This chapter summarized the results of a flocculation study investigating the seasonal variation in organic matter and carbon loads of stream water and the flocculation potential by clay and salt coagulants with respect to water quality in eight streams that drain parallel gradients of a coastal moorland. The results in this study showed that:

- The studied streams exhibited low concentrations of riverine organic matter in dissolved and particulate phase during low discharge flow over monthly–bimonthly sampling,

- that the efficiency of flocculation treatments to remove DOM from the dissolved phase followed T2>T4>T3,

- although the most effective coagulant was clay, the overall effect was counteracted by desorption of OM native to the clay standard by mixing with salt,

- flocculation processes preferentially removed humic substances with high aromaticity and terrestrial signature from samples during the experiment, indicating that coagulant characteristics control OM transformation in the LOAC despite small variations in natural water quality amongst the sampled streams.

These results are further discussed in 9.2 Exmoor study.

Chapter 7. Discussion on particulate organic carbon dynamics along the land–ocean aquatic continuum (LOAC)

This section discusses 1) the results of the two case studies of POC transport and dynamics in this work, and 2) incorporates the interpretation into the wider discussion of POC transport and dynamics along the LOAC.

7.1 Brazilian catchment study

This study focused on the transport of POC in a semi-closed tropical headwater catchment impacted by land use change and damming. Soil erosion was calculated from field observations of fallout radionuclides (FRN) ^{137}Cs and ^{210}Pb$_{ex}$ and the results were used to validate a soil erosion model, RUSLE, with which overall soil erosion in the catchment was simulated. The results showed that the sole use of database-derived input factors in the model overall yielded a 52% higher average soil erosion rate in the catchment than the closer to real-world model results which utilized input factors partially derived from field observations and digitized land cover. The results from soil properties, TOC/TN and loss on ignition analysis further confirmed that the relative composition of allochthonous and autochthonous POC in reservoir post-flooding sediments changed with depth, where the autochthonous component decreased from surface sediments with depth. This indicates that there is a higher turnover rate for autochthonous sediments compared to allochthonous sediment in the reservoir.

7.1.1 Soil erosion

7.1.1.1 Fallout radionuclide inventories

As expected, the radionuclide inventories of ^{137}Cs showed low concentrations in the Brazilian soil profiles of the João Penido catchment, as ^{137}Cs fallout on the South American continent has been less prominent than in e.g. Europe, North America and Oceania. For João Penido soils, the ^{137}Cs inventories ranged between a minimum and maximum of 30.9–858 Bq m^{-2} and these values appear sensible when compared to other studies conducted in similar deforested lands and pasture in sub-tropical soils and climate (*Cwa*) of South-Central regions in Brazil, e.g. Correchel et al (2006) reported ^{137}Cs inventories ranging between 0–1038 Bq m^{-2}, with an average reference inventory value of 422±14 Bq m^{-2};

Andrello et al (2004) reported sample inventories ranging between 90–403 Bq m^{-2}. Other studies in Brazil have reported similar ^{137}Cs soil reference core values of 314 Bq m^{-2} (Correchel et al, 2005), 422 Bq m^{-2} (Bacchi et al, 2005), 272±20 Bq m^{-2} (Correchel et al, 2006), 292 Bq m^{-2} (Andrello et al, 2014) for the corresponding years of their studies. In comparison, other studies on the South American continent have found reference inventories of 367 Bq m^{-2} in Uruguay (Alonso et al, 2012) and an average inventory of 1108 Bq m^{-2} for a site in Argentina (Bujan et al, 2003).

While ^{137}Cs concentrations in general are low or absent in soil samples from the João Penido catchment, the ^{210}Pb$_{ex}$ concentrations showed distinct inventories and potential as a soil erosion tracer. Little information on ^{210}Pb$_{ex}$ from soil data is available worldwide (Zheng et al, 2007), however some reported inventories of reference sites range from 3305 Bq m^{-2} in Morocco (Benmansour et al, 2013), 7598 Bq m^{-2} in Italy (Porto et al, 2012), and 18902.2 Bq m^{-2} in China (Zheng et al, 2007). For João Penido catchment, the ^{210}Pb$_{ex}$ inventory for reference site JP17 amounted to 8924.5 Bq m^{-2}, which is within the expected range compared to other worldwide reference inventories. The soil ^{210}Pb$_{ex}$ inventories in this study (soil and sediment) ranged between 4887.3–48014.3 Bq m^{-2}, and compared to other ^{210}Pb$_{ex}$ studies worldwide these values appear sensible, e.g. Porto et al (2104) reported ranges of 52–43801 Bq m^{-2} from a site in Italy, and Zheng et al (2007) found a range of 6184.87–20386.88 Bq m^{-2} in China. For João Penido catchment ^{210}Pb$_{ex}$ of soil profiles at sites of erosion and deposition showed correspondingly lower and higher inventories than the chosen reference site, which is in line with the method. Being a geogenic radionuclide that is constantly replenished in soils, for Brazilian soils ^{210}Pb$_{ex}$ showed better potential as a soil erosion tracer than the otherwise commonly used ^{137}Cs. Additionally, ^{210}Pb$_{ex}$ could become one of the main medium-term tracers of soil redistribution worldwide in the future, as the usefulness of anthropogenic ^{137}Cs inventories is being reduced with its decay in the environment.

7.1.1.2 Erosion and deposition rates from radionuclide conversion models

DMM results for ^{137}Cs in João Penido catchment soils averaged 5.71 kg m^{-2} year^{-1}, several times higher than corresponding PDM-^{137}Cs and DMM-^{210}Pb$_{ex}$ output which averaged 0.82 and 1.63 kg m^{-2} year^{-1} respectively. Another study using

the PDM-^{137}Cs in other parts of Brazil with climate class *Cwa* have found average erosion rates of 23 tonnes ha^{-1} year^{-1} in South-Central Brazil (Bacchi et al, 2000). The DMM-^{210}Pb$_{ex}$ and PDM-^{137}Cs results of this study were of the same order of magnitude as the studies mentioned above, while the DMM-^{137}Cs appears to have overestimated erosion in the study catchment.

The results suggest that the DMM method was less a robust method for ^{137}Cs inventories in this particular catchment, where fallout of ^{137}Cs has been sparse. The discrepancy could possibly be explained partly by the low fallout and residual concentrations of ^{137}Cs in the soils, but another potential explanation is the affinity of this radionuclide to organic matter. In general the ^{137}Cs concentrations were lowest in terrestrial colluvium, which normally should show enrichment of ^{137}Cs, indicating deposition of sediment. The low organic matter content of the colluvium profiles (which were lower than in the soil profiles of the hillslopes), suggested that ^{137}Cs sorbed to organic matter had been depleted in the colluvium with the removal of the organic matter and redeposited elsewhere. PDM appears to be a model less sensitive to gaps in ^{137}Cs increment concentrations within the soil profile, as the irregular presence of ^{137}Cs in the profiles give less credible diffusion and migration coefficients used for soil erosion calculations by DMM.

Compared to the ^{137}Cs inventories, ^{210}Pb$_{ex}$ inventories in the colluvium samples showed typical profiles with the highest concentrations in the top soils and declining concentrations with depth, and higher inventories at accumulating soil and colluvium sites than in eroding hillslope soil profiles. Even with the affinity to organic matter, unlike for ^{137}Cs, ^{210}Pb$_{ex}$ inventories showed consistent declining profile patterns despite the lower content of organic matter in colluvium.

In areas with high fallout the diffusion and migration model (DMM) offer more robust results than the profile distribution model (PDM) (Porto et al, 2003), but for the João Penido soils the DMM-^{137}Cs results did not agree well with results of PDM-^{137}Cs and DMM-^{210}Pb$_{ex}$. For this catchment ^{210}Pb$_{ex}$ appears to be a more reliable soil erosion tracer than ^{137}Cs, when using the diffusion and migration model.

7.1.1.3 RUSLE results

RUSLE model output showed that the current state of erosion (S_fieldCK) in João Penido catchment averaged 10.85 tonnes ha^{-1} year^{-1}. This figure was derived partially from field observation of *K* and detailed land use digitization in the catchment for factor *C*. When solely database-derived input factors were used for the model, the output (S_DB) resulted in an average of 37.8 tonnes ha^{-1} year^{-1}, or c. 52% higher erosion rates for the catchment. Both S_fieldCK and S_DB outputs were within the same order of magnitude as other RUSLE studies in Brazil have found, e.g. Medeiros et al (2016) who found erosion rates of 30 tonnes ha^{-1} year^{-1}, da Cunha (2017) who reported 48 tonnes ha^{-1} year^{-1}, and similarly USLE results of 55.45 tonnes ha^{-1} year^{-1} in a study by Beskow et al (2009). In particular the database derived output showed close similarity to the other RUSLE studies mentioned.

Although the S_DB output overestimated soil erosion compared to the S_fieldCK output, the current state of erosion can be considered related to current land use practices in this perturbed catchment and therefore higher than in a naturally forested environment. Results from simple simulations (which assumed a single *C* value for the whole catchment with the exception of water bodies and built up areas) showed that the modelled current state of erosion lies in-between those of a completely forested (*C*=0.003) and completely deforested states (*C*=0.1; *C*=0.45). As expected, all of the simulations indicated that developed vegetation cover decreases soil erosion in the catchment when these outputs are compared to the perturbed catchment scenarios. A forested state of the catchment would yield a mean erosion rate of 0.52 tonnes ha^{-1} year^{-1}, which is c. 95% lower than that of the actual current state of erosion in the catchment (S_fieldCK: 10.85 tonnes ha^{-1} year^{-1}), whilst the simulated mean erosion rate of a completely deforested state (17.47 tonnes ha^{-1} year^{-1}) would yield a 61% higher average erosion rate than the current state of erosion in the João Penido watershed. Similar trends have been found by Juinor et al (2019) who studied perturbation of mainly sugar cane plantations in a catchment with similar soils, vegetation and climate in São Paolo state of Brazil, where net erosion amounted to 0.03 tonnes ha^{-1} year^{-1} for natural vegetation cover (savannah), 3.5 tonnes ha^{-1} year^{-1} for current perturbed land use and cover, and 12.6 tonnes ha^{-1} year^{-1} for simulated expansion of sugar cane plantations in their studied catchment.

The *LS* factor of this catchment ranged between 0–29.54, which is lower than the values obtained for the João Penido catchment.

The difference between RUSLE results S_DB and S_fieldCK showed that the database derived model output mainly underestimated and overestimated erosion rates in land use classified as deforested grasslands in the catchment (Figure 107). This is sensible as wooded and built up areas were assumed to experience negligible erosion and thus were assigned low *C* values, and therefore grasslands in particular were more sensitive to other influential factors inputted into the model, such as the terrain-controlled *LS* factor.
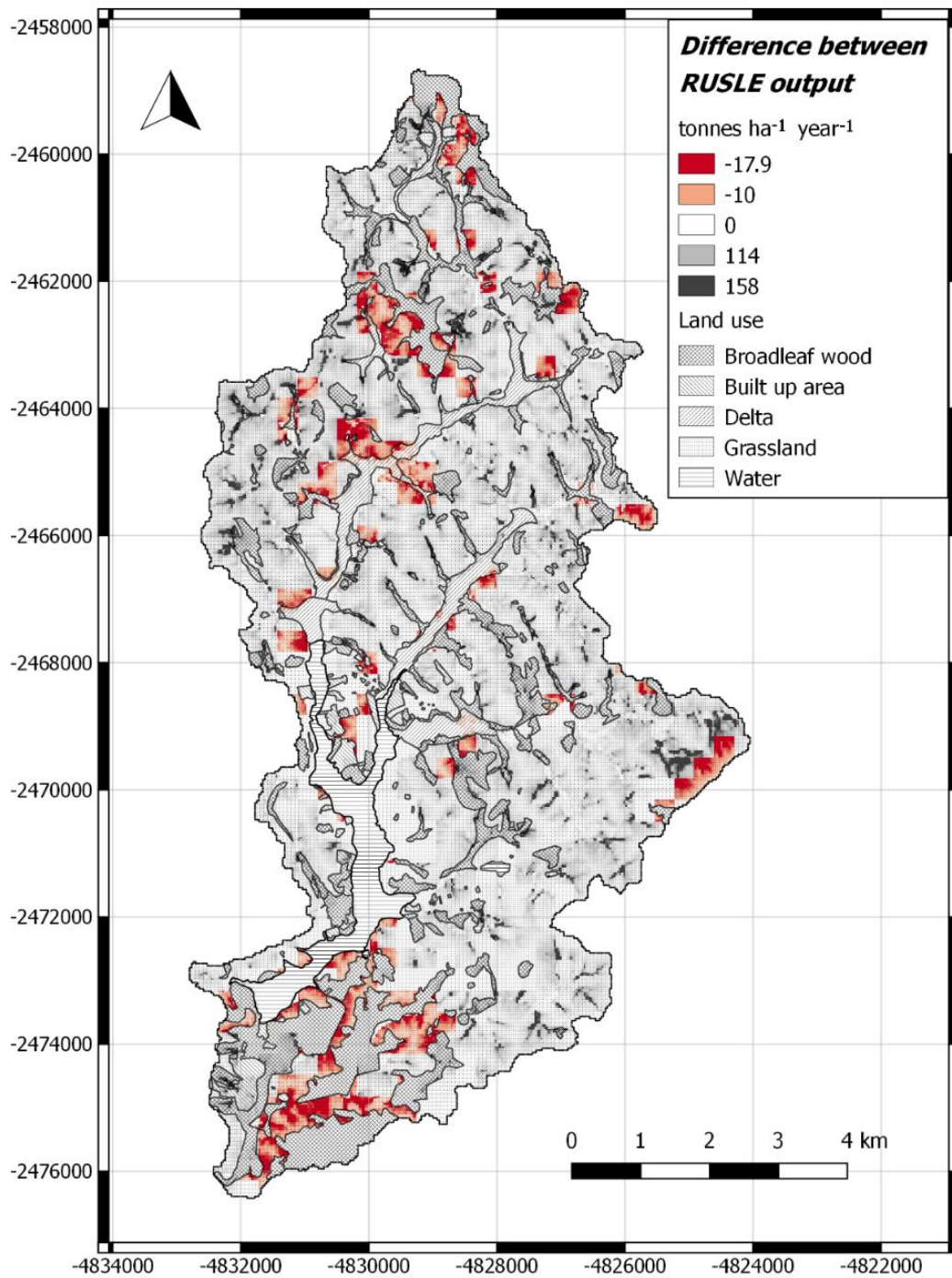
Figure 107 Difference between RUSLE output based on database input only (S_DB) and RUSLE output S_fieldCK partly field based (observed C and K factors). EPSG: 3857.

The RUSLE results showed that areas classified as grassland contributed to most soil loss in the catchment. In the field it was observed that large areas of these grasslands were used as pasture for cattle, and were likely to experience moderate soil erosion from reworking of the ground surface layer. Visible erosion scars and soil remobilisation were observed in the field both in grasslands with pasture and shrubland.

The erosion rates obtained by the RUSLE model in the study catchment appeared sensible, both when compared to other RUSLE studies in the region and when compared to observed soil erosion from radionuclide data in the field, calculated sedimentation rates and the estimated sediment volume in the reservoir.

7.1.1.4 Comparison of soil erosion by RUSLE modelled output and field observations from radionuclides

The average erosion rate of top soils (upper 20 cm) obtained by the RUSLE output partially based on field observations (S_fieldCK) was within the same order of magnitude as the calculated erosion rates from fallout radionuclide field observations (Chapter 5, Table 33). The ^{137}Cs and ^{210}Pb$_{ex}$ results appear to vary similarly for most of the FRN sites, despite the DMM-^{137}Cs results being consistently higher than DMM-^{210}Pb$_{ex}$ and PDM-^{137}Cs results. It appears that for this site in Brazil, the PDM method is less sensitive to irregular radionuclide concentrations in the soil profiles and therefore provides a more robust result than the DMM method when using ^{137}Cs as a soil erosion tracer. Other studies that have compared output from RUSLE with fallout radionuclide theoretical models have found a varying agreement between the methods, e.g. in a study by Martinez et al (2009) it was found that RUSLE produced soil erosion rates c. 10 times higher than the theoretical ^{137}Cs models PDM and DMM for a catchment in temperate Australia, while Meusburger et al (2013) found that both methods (^{137}Cs-PDM and RUSLE) gave results on the same order of magnitude for a catchment in temperate South Korea. The varying agreement is likely influenced partly by the accuracy of input factors for the RUSLE model, partly by the results obtained from radionuclide activities from the field sites. In this study, the results showed acceptable agreement between the RUSLE model and ^{137}Cs-PDM and

$^{210}Pb_{ex}$-DMM for the compared grassland sites (Figure 108) and RUSLE thus appears suitable for the deforested Atlantic rainforest biome.
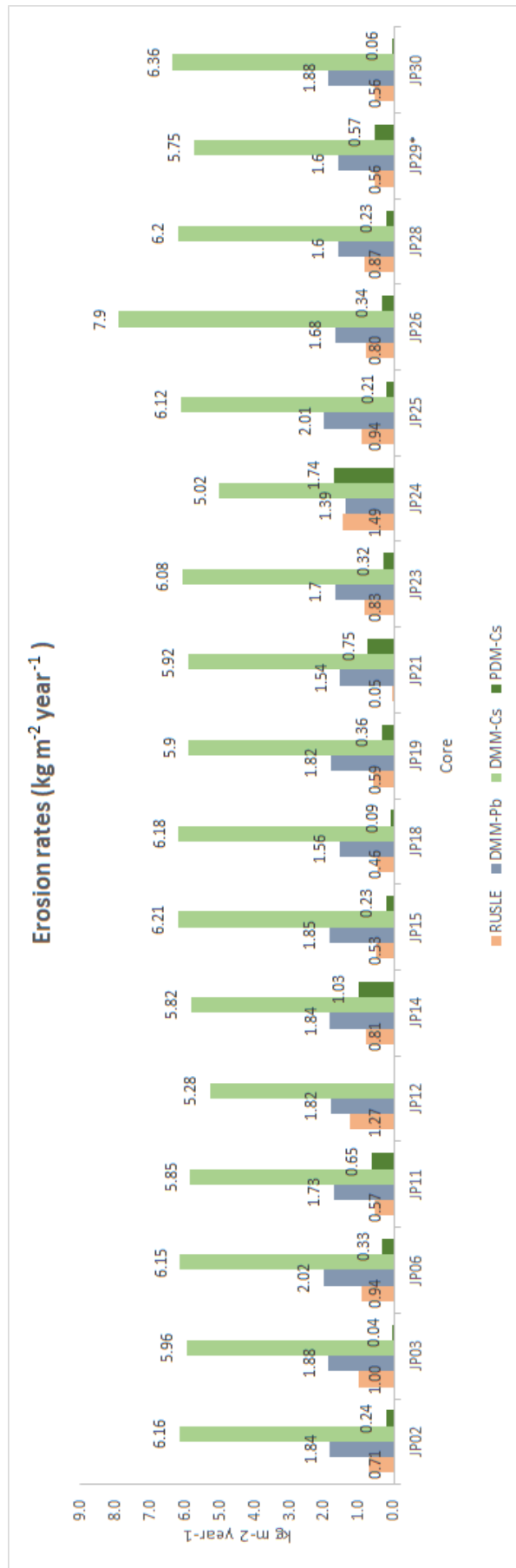
Figure 108 Compared erosion rates from fallout radionuclide models and RUSLE model.

Note that for JP12 the PDM-^{137}Cs value was not calculated.

7.1.2 Fate of POC

7.1.2.1 POC redistribution in the catchment soils and sediments

The soil samples in this study were retrieved from pasture and shrubland, which represents ca 70% of the catchment (digitized *C* factor map). Although these soils can be considered relatively poor in organic matter and carbon, the redistribution of existing SOC may be mineralised and released as inorganic C species when exposed to the atmosphere or enter the aquatic system to contribute to buried organic matter in the reservoir. Compared to SOC stocks from national surveys such as Batjes et al (2005) who summarized SOC distribution in different soil groups of Brazil and reported mean concentrations of 5.2 kg C m^{-2} for the upper 30 cm and 9.6 kg C m^{-2} for the upper 100 cm of ferralsols of Brazil, the soil carbon inventories (with its low content of inorganic carbon) found in this study are within the same comparable range with an average of 5.6 kg C m^{-2} in the upper 20 cm of catchment top soil.

The resulting POC erosion map derived from RUSLE model output and average POC inventory in catchment grassland soils, indicate that a mean of 0.3 tonnes ha^{-1} $year^{-1}$ is mobilized annually in the surface soil layer. This assumes negligible erosion in land use classes such as built up areas and broadleaf woods of the catchment.

The reservoir sediment characteristics showed that the average organic matter concentration in top sediments (2 cm) was 28.3%, while the remaining mass composed inorganic material (Figure 109) and that at 30 cm depth the average concentration was 10.7% lower. This low concentration (c. 17%) was maintained with depth. As pre-flood material have OM concentrations similar to terrestrial soils, it is likely that overlying layers of post-flooding sediment with low concentrations compose mainly terrestrial aggregate-bound SOC, and that surface sediments compose partly terrestrial allochthonous matter (equivalent of average soil OM%, c. 13.99%) and additional autochthonous OM. Simplified, the autochthonous part would compose the difference between total OM% and assumed allochthonous OM%, which when using the average concentrations amount to an average of 8.53% (22.55–13.99%). If these assumptions were valid the dominant source of OM in the reservoir sediments would be terrestrial. These estimations only consider matter-dry weight and therefore do not represent dissolved OM in e.g. pore space solution of these fluffy post-flooding sediments.

227

Post-flooding sediment bulk density was calculated to 1370 kg m^{-3} and this relatively low bulk density suggests that the porosity and water content are high in the post-flooding surface sediment, in which the concentrations of DOM become important, however this parameter was not specifically measured in this work.

a) Soil (ex. colluvium)

$y = 14.179e^{-0.003x}$
$R^2 = 0.1626$

b) Reservoir (Post-flood)

$y = 24.313e^{-0.015x}$
$R^2 = 0.1543$
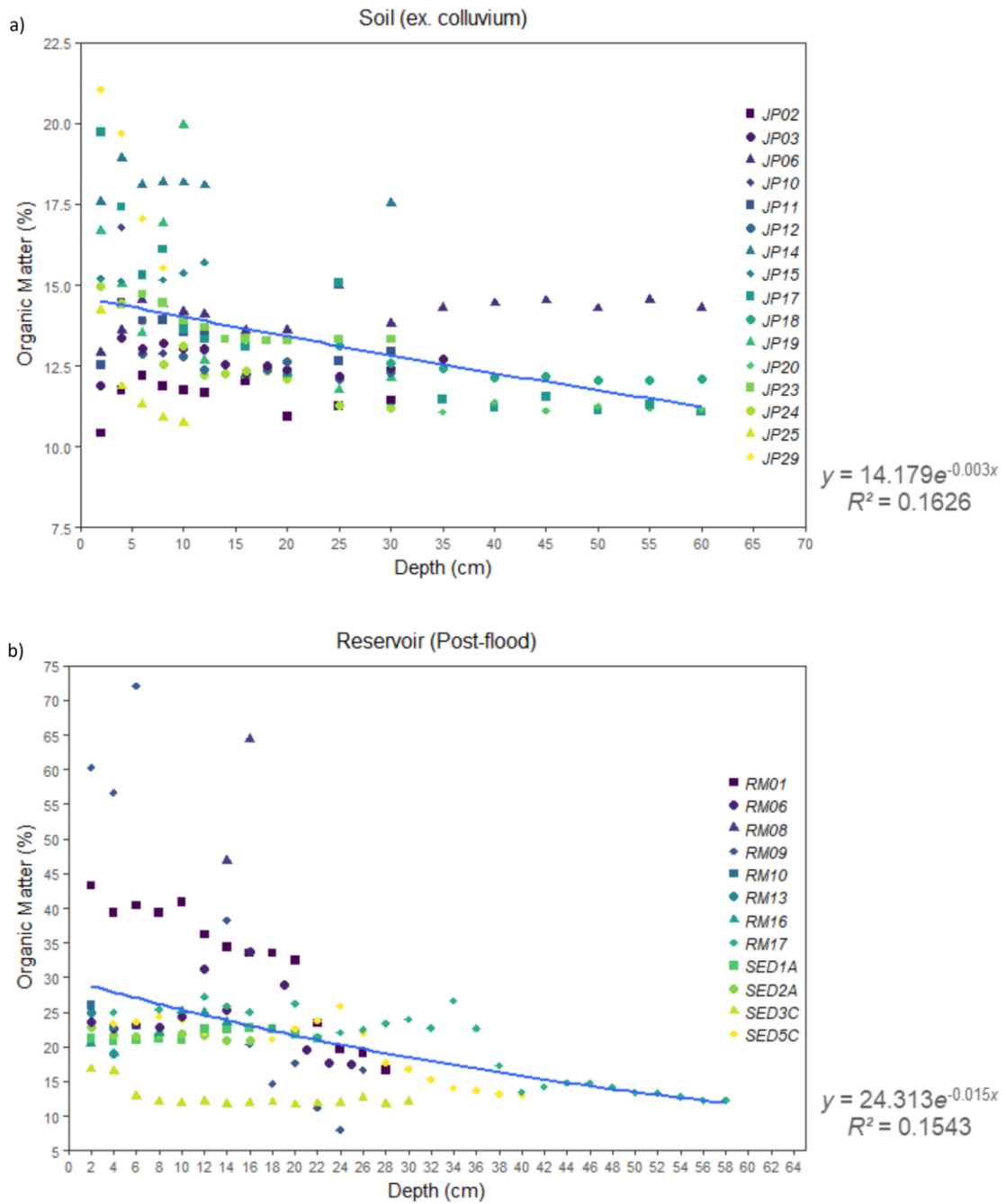
Figure 109 All observations of organic matter content (%) in a) soil (excluding colluvium) and b) sediment (Reservoir (Post-flood)) of João Penido catchment, generally showing higher contents in the upper 20 cm of profiles. The fit is exponential. Equations and R^2 for the exponential fit are shown on the right of 109a and 109b, respectively.

In João Penido reservoir, POC contributions from allochthonous and autochthonous sources might be dependent on seasonal variation due to the local climate. In a study of reservoir Kentucky Lake, USA, by Yurista et al (2001), it was found that autochthonous POC was mainly inputted into the reservoir during the summer months while allochthonous POC dominated during winter. In contrast, a study on POC sedimentation in oligotrophic Loch Ness in Scotland, Jones et al (1997) showed that allochthonous sources composed the dominant form of POC, with peak inputs in late winter to spring explained by higher input from riverine discharge. Upstream allochthonous POC mainly consist of litter and soil organic carbon, and primarily rainfall erosion events control these terrestrial inputs. In summer autochthonous POC sources such as growing macrophytes, algae and biofilms are likely more important for POC production and sedimentation. For the eutrophic João Penido reservoir, POC mass of post-flooding sediments were crudely estimated and any seasonal variability could not be determined from the samples collected and analysed, but it is probable that both growing biota and mobilized SOC from rainfed soil erosion processes contribute with POC into this reservoir.

C/N ratio of sediment POC showed the typical mixed-source limnic signature of organic matter composition in João Penido reservoir, while pre-flood material had more terrestrial like signatures, which appears to confirm the boundary of post- and pre-flood material. Although the C/N data showed mixed terrestrial and aquatic signatures in post-flooding sediments, peaks in C/N indicate high input of terrestrial organic matter. These peak sediment layers are likely related to events of high erosion input. Particle size appears more varied with depth in sediment cores compared to soil cores, which likely is connected to varying particle size input from soil erosion into the reservoir due to high-energy runoff during rainfall events in the catchment, where higher energy has mobilized coarser grain fractions.

7.1.2.2 Concentrations of organic matter and OC quality

Comparison between the OC data obtained from C/N analysis and calculated from OM data obtained by LOI analysis, revealed that the commonly used conversion factor of 0.58 (Pribyl et al, 2010) is too high for soils of João Penido watershed, when converting OM concentrations obtained from LOI analysis to

OC concentrations. Soils showed varying OM% content with respect to land use, and soil samples from pasture in general displayed a wider range of OM% than samples from non-managed shrubland. For terrestrial soils the lowest C% values appeared in colluvium, mainly in subsoils at depths >15 cm. In general, POC% decreased with depth in most pasture and colluvium profiles, while shrubland soils often showed lower content in the surface layer with mostly consistent POC content with depth. An explanation for this is that pasture is being continuously fertilized which promotes plant growth and organic matter input, while shrubland soils remain nutrient poor and often compose sandy texture in the top layer. Soil organic matter inventories appeared to be of consistent concentrations for all the eroding soil sites, but lower for seasonally dry colluvium. Soil to sediment transects revealed that colluvium was depleted in organic matter compared to eroding soils. This OM has likely been washed out and accumulated in reservoir sediments together with autochthonous OM. In sediments the density separated samples showed that the C/N signature of post-flooding sediment showed increasingly more terrestrial like signatures with depth, suggesting that this SOC is preferentially preserved with depth.

For the aquatic sediment sites, sites in the delta and shallow reservoir arms (depth c. 1 m) showed the highest POC content, while they were depleted further out in deeper (c. 8–10 m) reservoir sediments. C/N ratios were typically lower in reservoir sediments compared to deltaic sediment and soils and the C/N data also showed that deeper sediments were characterized by lower concentrations of carbon and nitrogen compared to the surface sediments. A higher C/N ratio is associated with terrestrial soil organic matter, which agreed with the distribution in the João Penido sediments.

7.1.2.3 OC accumulation in sediments

The calculated OC accumulation rates appear to be sensible for João Penido catchment. The average POC content of terrestrial soils from LOI data (2.8%) in the João Penido catchment and pre-flood material (2.9%) beneath post-flooding sediment in the reservoir suggest that the mineral associated POC content is general for soil particles in the catchment. If it is assumed that the mean soil POC value of 2.8% in this study is recalcitrant both in terrestrial soils and in eroded soils that have entered and been redeposited in the reservoir, while the average

reservoir sediment POC value is 4.5%, this would suggest that the excess POC in the sediment is of aquatic origin. Most of the sediment cores in the shallower water profiles showed POC profiles with declining concentrations with depth, indicating that there had been vertical loss of organic carbon from the surface sediment to the pre-flood material. The similar POC content of terrestrial soil and pre-flood matter suggest that mineral aggregate bound POC is physically protected from processes which transform organic carbon (e.g. microbial mineralisation), and that the organic matter loss primarily is associated with autochthonous organic matter. If it was assumed that the average difference (2.1%) of the total POC in the reservoir was of aquatic origin, this would be an equivalent of autochthonous POC amounting to c. 4883 tonnes of the total POC mass (10440 tonnes) in the reservoir post-flooding sediment, or almost 47% of the total POC in post-flooding sediment being autochthonous.

The other way of estimating the relative contributions of allochthonous and autochthonous POC was from SOC data. Assuming that the mean top soil value of 2.8% was universal for eroding catchment soils and the deposited allochthonous post-flooding sediment, the net allochthonous POC mass of total POC mass would amount to 2934 tonnes, or 28%, indicating that c. 72% of total POC mass was of autochthonous origin. This simplified estimate assumed that the allochthonous sediments were completely recalcitrant, which is unlikely.

7.1.2.4 Correlation between soil and sediment parameters

There have been numerous studies which have established that fallout radionuclides ^{137}Cs and ^{210}Pb$_{ex}$ typically display the same redistribution pattern as SOC in the landscape (Martinez et al, 2010; Teramage et al, 2013). In this study, soil ^{210}Pb$_{ex}$ concentrations showed positive correlation with OC% (*Spearman*, r_S =0.73, $p<0.05$) while soil ^{137}Cs concentrations showed a weak positive relationship (*Spearman*, r_S =0.31, $p<0.05$). For sediments the ^{210}Pb$_{ex}$ concentrations showed a weaker positive correlation (*Spearman*, r_S =0.47, $p<0.05$) and ^{137}Cs concentrations remained similar to soil values (*Spearman*, r_S =0.31, $p<0.05$). Correlation of soil and sediment parameters are summarized in Figure 110 and Figure 111, respectively.
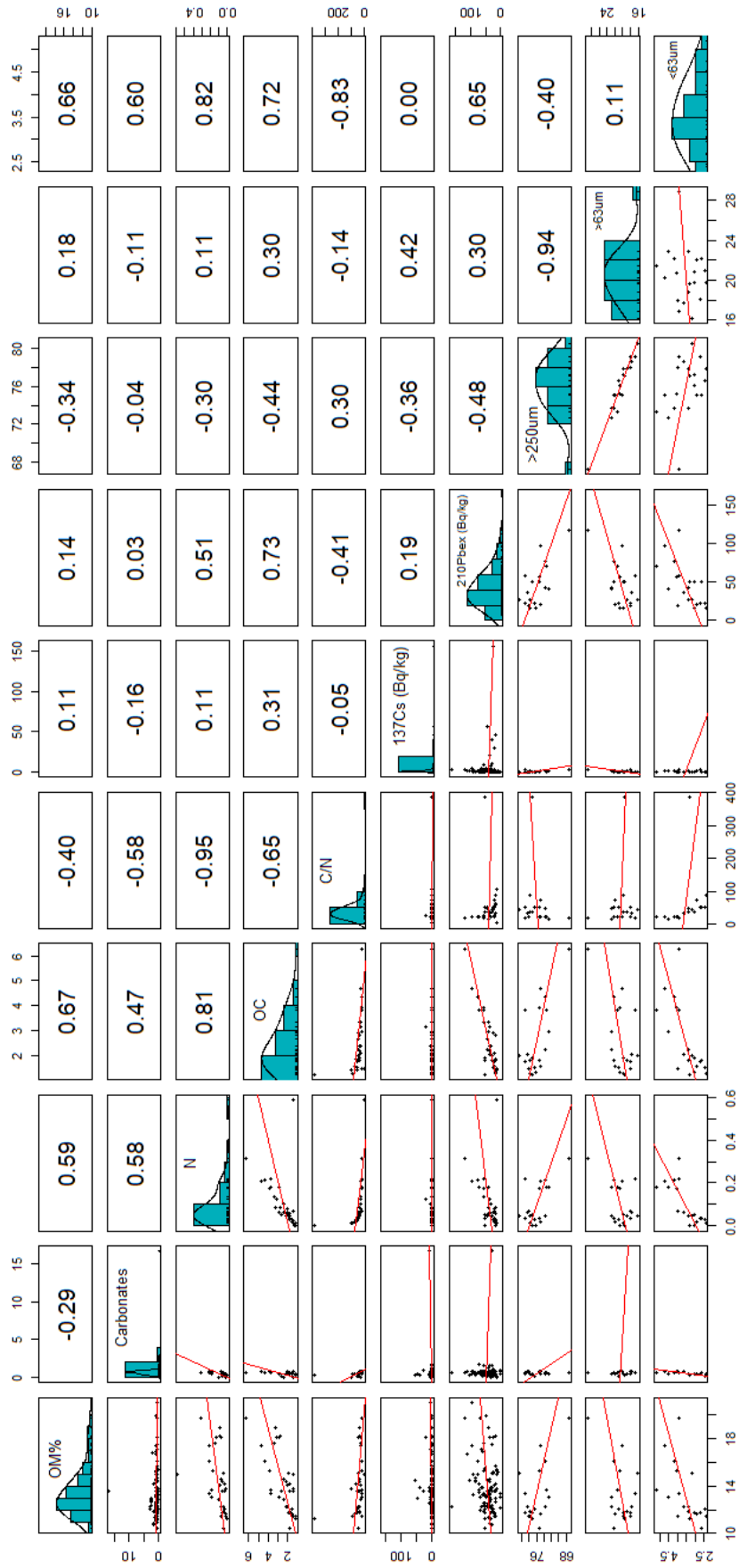
Figure 110 Correlation matrix of soil parameters.

233

234
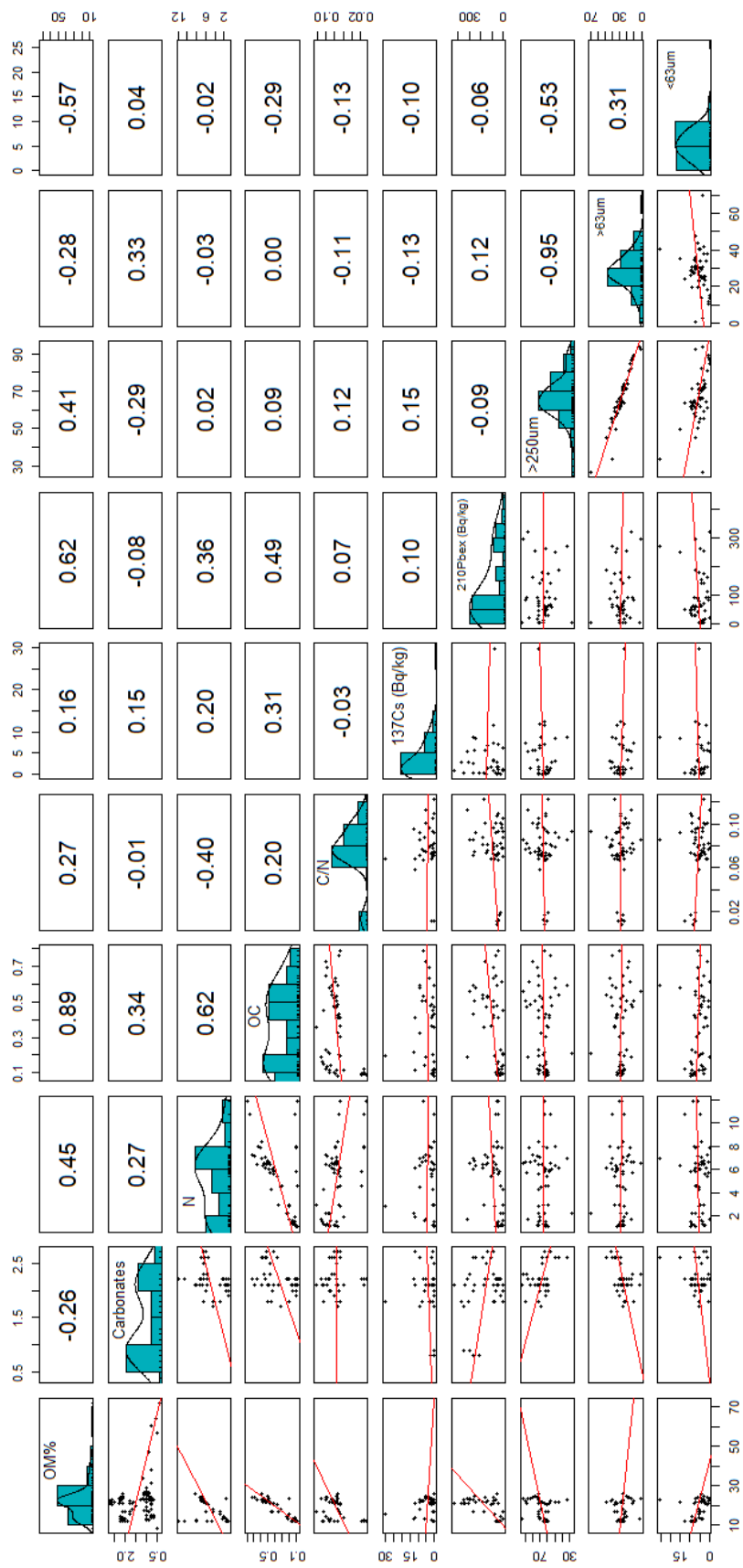
Figure 111 Correlation matrix of sediment parameters.

^{137}Cs concentrations showed low correlation with POM – the highest correlation was found for colluvium as visualized in Figures 112. Generally, POM showed weak negative correlation with ^{210}Pb$_{ex}$ (r_S =–0.35, $p<0.05$). In colluvium and soil the pattern indicates that ^{210}Pb$_{ex}$ is associated with POM in the samples (Figure 113).
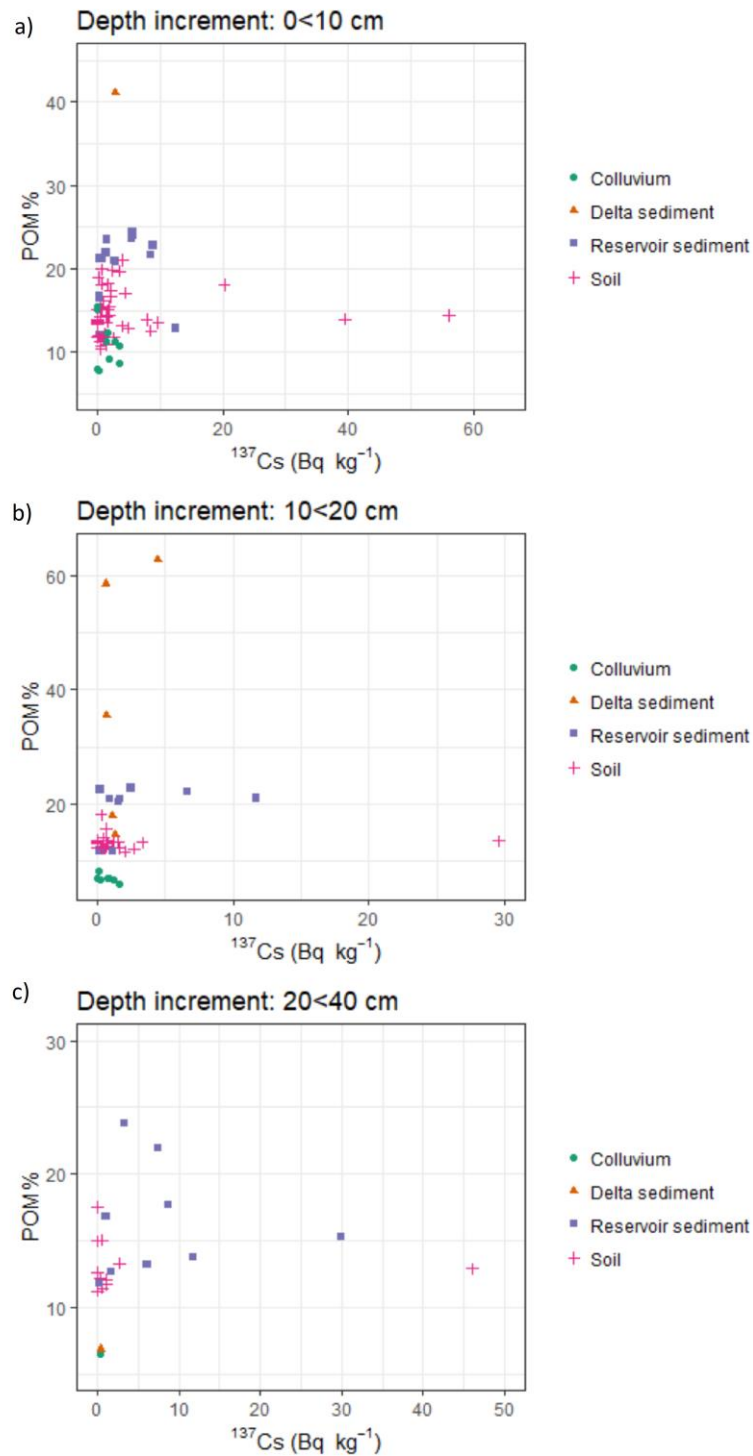
Figure 112 POM (%) and and ^{137}Cs concentrations (Bq kg^{-1}) in João Penido catchment soil and sediment at depths a) 0<10 cm, b) 10<20 cm, and c) 20<40 cm.
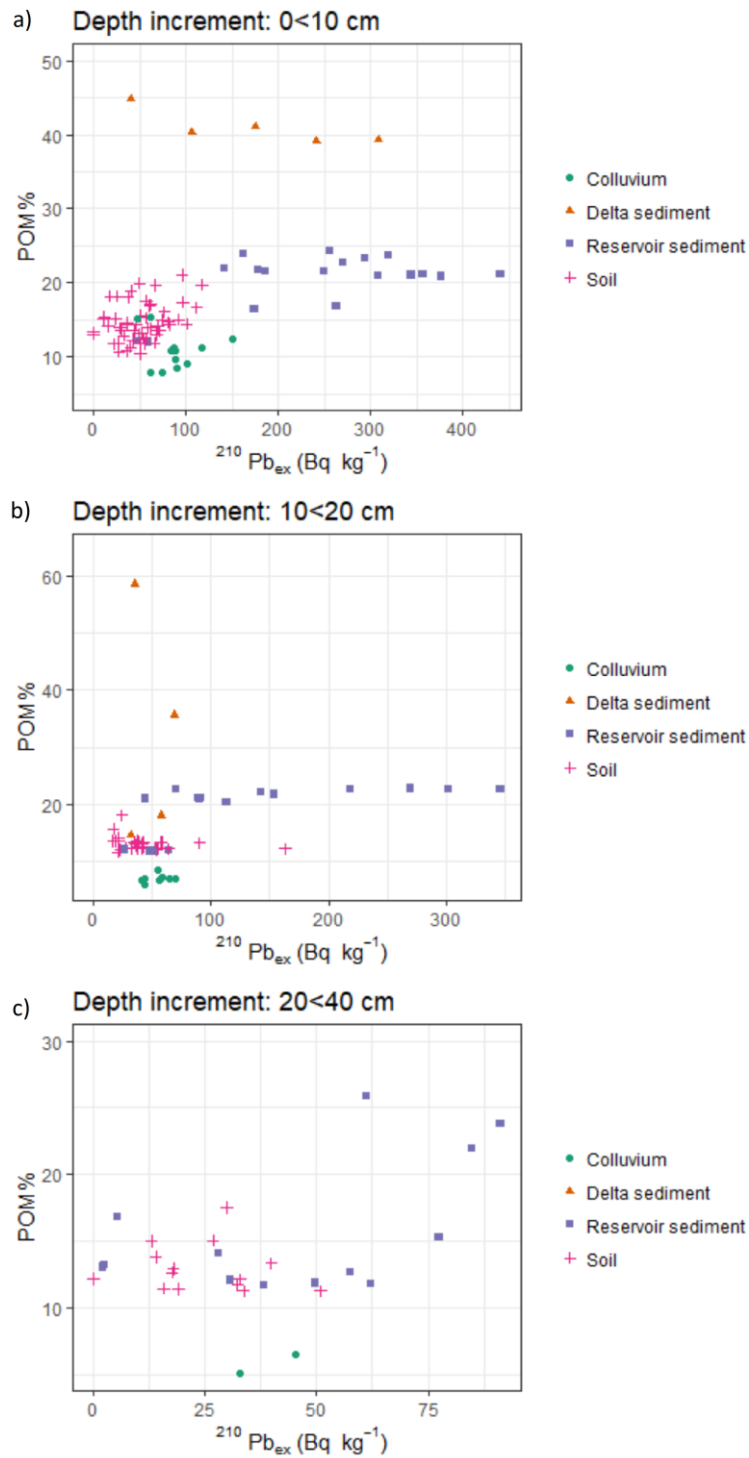
Figure 113 POM (%) and $^{210}Pb_{ex}$ concentrations (Bq kg^{-1}) in João Penido catchment soil and sediment at depths a) 0<10 cm, b) 10<20 cm, and c) 20<40 cm.

For soil the <63 µm fraction showed strong negative correlation with C/N (*Spearman*: r_S=–0.83, p<0.05) and positive correlation with $^{210}Pb_{ex}$ concentrations (*Spearman*, r_S =0.65, p<0.05). $^{210}Pb_{ex}$ showed strong affinity to the fine fraction in the terrestrial environment compared to the aquatic sites, where correlation was weakly negative where organic matter appears to be more related to $^{210}Pb_{ex}$ concentrations.

In this study no significant correlation between radionuclide concentrations and the grain size fractions was found. While ^{137}Cs concentrations did not correlate significantly with any grain size fraction in this study, $^{210}Pb_{ex}$ concentrations showed weak negative correlation with >250 µm (–0.340), and weak positive correlation with >63 µm (0.278), and <63 µm (0.182). The lack of correlation of ^{137}Cs in the samples appears to be connected to the largely low concentrations of this radionuclide in this landscape, which showed irregular or absent activities in profile samples in general, which reduces the motivation of using ^{137}Cs as a soil tracer at this location.

OC% and N% (determined from C/N analysis) showed strong positive correlation with the <63 µm fraction (r_S =0.719 and r_S =0.82 respectively, p<0.01) in the catchment soils, while these parameters showed weakly negative correlation with the coarser (>250 µm) fraction.

7.1.3 Limitations of the Brazilian catchment study

When comparing modelled RUSLE output in the João Penido catchment with other studies in Brazil and on the South American continent, it is important to clarify that there are differences in chosen input factors. It is expected that variance is evident depending on which databases or field observations that are being used for the modelling procedure, because sources, quality and resolution of input factor values differ amongst accessible information. A reasonable range of output for catchments with similar properties and climate, for instance achieving values of the same order of magnitude, should be considered acceptable yet all modelled output should be used with caution. Compared to other comparable studies which also mainly utilized database input, the results of this study was of the same order of magnitude. The more detailed RUSLE

output, which partly used field observations, resulted in erosion rates closer to radionuclide derived soil erosion, however the sites of comparison were restricted to the land cover type deforested grassland. In this study it was assumed that soil erosion from wooded and built-up areas would be negligible compared to the deforested areas, however this was not confirmed in the field.

RUSLE output based on database data was of the same order of magnitude as output based partially on field observations, however database derived RUSLE output showed less agreement when comparing the modelled result with erosion rates based on radionuclide data. If field observations cannot be made for a specific catchment, database output would be the first available result for a researcher, but the non-validated results might over- or underestimate soil erosion in the studied catchment and need to be considered.

The radionuclide data were limited partly by the irregular fallout (e.g. of ^{137}Cs) in the study area, but also partly by the conversion models used. The different conversion models showed differences in results for ^{137}Cs, where the simpler PDM model provided erosion rates closer to erosion rates obtained by DMM-^{210}Pb$_{ex}$, than the DMM-^{137}Cs output which showed consistently higher erosion rates for the sites compared. One explanation could be that the PDM is less sensitive to the irregular fallout and provides a more robust conversion. All the conversion results were based on the assumption that the chosen reference site was accurately assigned, which in itself could be one of the reasons to why only erosion rates and no deposition rates were reflected in the results. The chosen reference site fulfilled the required criteria, however whilst showing a good ^{210}Pb$_{ex}$ profile it did suffer from some gaps in increment inventories with depth for ^{137}Cs. In this study, the distribution of FRN profiles in the field was pre-determined by random points in GIS, and selected transects were used to interpret the downslope trend of radionuclide inventories for sites in the João Penido catchment, as well as to compare point values of FRN derived erosion with the modelled RUSLE output. Other studies have utilized grid based approaches when sampling FRN profiles which provides neat interpretation of FRN inventories. A grid based approach requires an extensive number of sampling locations but provides efficient maps of inventories. In this study the aim was mainly to determine the downslope trend and to compare RUSLE output with validation points.

239

While the method to acquire $^{210}Pb_{ex}$ data from soil sites was well established and showed that this radionuclide has good potential as an erosion tracer, the analytical method for samples from the aquatic sites in the reservoir was restricted. The samples showed unrealistically high concentrations of $^{210}Pb_{ex}$, which likely was an effect from either sample preparation with insufficient sealing of the sample capsules or the use of an unsatisfactory standard to calibrate for ^{210}Pb spectra in the well-detector used. Insufficient sealing of the sample capsules used for analysis in this well-detector could have led to radon escape from the sample tubes and thus equilibrium was not reached between ^{226}Ra and the gaseous daughter ^{222}Rn before gamma analysis, which could have led to erroneous spectral photopeak at 352 keV. Alternatively, it is possible that the ^{210}Pb standard used for calibration of the well-detector instrument was insufficient, as the calculated average detector efficiency from standards was partly based on old standard measurements for the instrument. These standards were of the right geometry and mass, similar to samples analysed in this instrument, but the results used were possibly outdated for the analytical batch of the João Penido samples. The standard that was used during the actual batch run was of other geometry and served mainly as a control for instrumental drift. The resulting Pb concentrations gave too high inventories of $^{210}Pb_{ex}$ in the post-flooding sediments, but when used in the CRS model would still indicate the relative relationship between shallow and deeper sediments and the sediment accumulation rates therefore appeared reasonable. However, the source of this error requires further attention and shows that appropriate quality control with adequate standards is important for validating results in order to discard possible erroneous output.

Both methods of estimating the reservoir sediment volume gave similar results, which shows that the GIS method can be effective as an automated tool for this estimation. Even though the field point observations were not placed in a regular grid, they still gave a rough estimate of the amount of post-flooding sediment that have accumulated in the reservoir since it was built. The export of sediment at the reservoir outlet was not taken into account and the amount of sediment that has been exported downstream remains unknown. The estimate however gave net value of accumulated sediment in the reservoir. It needs to be noted that in this work the most south western part of the catchment was included

in the watershed analysis due to the method of initial basin delineation, however later elevation analysis showed that stream segments in this part of the catchment were unlikely to connect directly to the João Penido reservoir itself. The crude delineation composes a source of error in the sediment yield estimates in this work, where sedimentation to a degree was underestimated as a consequence of the erroneous total catchment area (by initial delineation) being used in the calculations.

The estimated quantity of the allochthonous component of terrestrial POC in post-flooding sediments is based on many assumptions about the average SOC content in the catchment soils, the quantity of inputted soil mass into the reservoir over the years since the dam was built, and recalcitrance of the mineral-associated organic carbon fraction. Because of all these assumptions, this output can only provide a simplified picture of the actual carbon transport and fate in this catchment, however the results appear to be within a plausible order of magnitude for such a system.

The results indicated that soil-derived aggregate-bound POC was an important source of organic carbon in the reservoir sediments of João Penido, but sample numbers from density fractionated C/N samples were insufficient to determine whether OC storage is controlled by allochthonous or autochthonous POC. Further analysis of a higher sample number, would statistically increase the confidence of the results. An overview of the OM and OC budget in the calculated mass of the reservoir sediments suggested that with depth heavy aggregate-bound and therefore physically protected OM increased in relation to free light organic matter.

Some extreme values of soil C/N were observed in the results. Average C/N ratios of world soils range between 9.9–25.8 (Batjes et al, 2014) and in this study the average SOC value amounted to 48.08, which was likely skewed by outliers in the dataset. Five samples had C/N ratio >100, mainly samples from the deeper layers of the soil profiles. Either the nitrogen content was depleted for these outlier samples, or something happened during the analytical processing. Other analyses of qualitative properties were not measured in this study, but would have contributed to the interpretation when discriminating between allochthonous and autochthonous POC in the post-flooding sediments.

7.1.4 Summary João Penido project

In summary, the study in João Penido catchment showed that

- POC erosion from surface soils calculated by RUSLE and SOC inventories amounted to an average rate of 0.02–0.11 kg m^{-2} year^{-1},

- A large component of the POC in post-flooding sediments was autochthonous, but that in deeper layers organic carbon bound to soil-aggregates from allochthonous sources composed a major component of POC,

- Soil erosion measured in the field by empirical methods utilizing fallout radionuclides revealed that ^{137}Cs was less useful, whilst ^{210}Pb$_{ex}$ showed more potential as a soil erosion tracer,

- The RUSLE model worked adequately in this deforested environment, however the results varied greatly depending on which input factors were used. It was demonstrated that the RUSLE model was a useful tool to calculate average erosion rates in the catchment (validated by field observations) and that the accuracy of the modelled results increased with improved detail in input factors.

7.2 Exmoor study

In this study, streams draining the Exmoor area were monitored for riverine POC content and flocculation experiments were conducted to determine the effects of treatments by two coagulants on the qualitative properties of DOM in stream water. These coagulants were selected to imitate natural flocculation boundaries in the landscape: clay representing the soil erosion boundary in the freshwater landscape; salt representing the saline mixing boundary in the estuarine environment. An additional clay and salt treatment was added to investigate the effects of mixing. The results showed that whilst the streams varied in POC content and water quality parameters such as electrical conductivity, pH, and DOM content, the experimental output showed that organic components groups in general were reduced in residual DOM depending on which flocculation agent that was used.

7.2.1 Stream water quality of the individual catchments

The calculated stream POC concentrations were only representative for the specific sampling occasions of this study, and therefore were likely to represent concentrations closer to the yearly minimum than maximum. Site H showed consistently higher electrical conductivity than the other streams over the measurement period, suggesting that the total dissolved ion load was in general higher for this stream. This might be derived from a combination of factors, e.g. it could be an effect of dissolved clay minerals in groundwater input from the metamudstone rocks in the drainage basin, or an effect of land use in the catchment which has been converted from natural to largely improved grassland. Another but less likely explanation is the location of the sampling site, with its low elevation and vicinity to the sea, making the surrounding area a possible recipient of airborne sea spray deposition near the coast. On sampling during round 5 at site H the EC was unusually low (0.01 $\mu S\ cm^{-1}$), but showed the highest TSP load (4.15 mg L^{-1}), which could be caused by a dilution effect due to high discharge.

7.2.2 Qualitative properties of filtrate DOM

The flocculation experiment initially showed that pH decreased in treatments with added coagulants, which implied that the residual filtrates had been acidified by chemical change. Results from mass spectrometry indicated that some assigned organic component groups were preferentially removed in post-experimental residual DOM as an effect of the experimental treatments. For clay treatments T2 and T4, black carbon and polyphenols decreased in samples from all streams. Especially the headwater site I showed high abundance in black carbon and polyphenols. In general, components that remained in residual DOM after clay treatments T2 and T4 were highly unsaturated hydrocarbons, while aliphatics appeared to be more randomly affected by flocculation. Principal component analysis revealed trends for the organic compounds by treatment. Polyphenols and black carbon were highly correlated and in general showed negative correlation with highly unsaturated hydrocarbons. Sugars, peptides and aliphatic compounds were in general associated, but showed less correlation for T3 where peptides appeared negatively correlated with phenols and black carbon. Sugars and peptides were not present detectable concentrations for T1.

243

Preferential removal of humic substances was found for samples treated with coagulants, where molecular structures with low H/C and high O/C were absorbed, showing that for these stream samples more aromatic humic substances contributed to the POC pool during the flocculation experiment. These results also agree with other studies which have measured the effect of coagulants on DOM, for instance Lavonen et al (2015), who studied DOM removal in water treatment plants, found that fluorescent DOM which correlated with properties such as low H/C ratios and oxygen-containing groups were preferentially removed from residual DOM. Similarly, Sanchez et al (2014) used the PARAFAC model to study effects of aluminium based coagulants on DOM and found that humic substances were preferentially removed regardless of coagulant type, as well as Banaitis et al (2006) who studied changes in residual DOM composition after sorption to the natural minerals gibbsite and goethite. As a parallel, in their study Pisani et al (2011) demonstrated that photodissolution released primarily humic-like components and to a lesser degree protein-like structures, from samples which had been subjected to photoirradiation, which further demonstrates the presence of humic-like structures in floc products. *Van Krevelen* diagrams showed overlap between positively and negatively correlated molecular formulae, which could possibly be explained by the number of isomers present in each sample, which exhibit the same formulae but compose different chemical structures (Sleighter & Hatcher, 2008).

The implications of the results is that erosion of aged soil organic matter with typically aromatic and humic-like properties would preferentially be sorbed to produce floc products in the LOAC. For instance leachates of DOM from soil solution which drain into streams, could therefore contribute to floc products in the presence of a coagulant. Depending on the chemical and physical protection in mineral aggregates in total suspended particulates in stream water, heavy mineral associated POC could also act to remove coagulants from the water column. Natural flocculation boundaries occur where flocculation agents mix with OM in the LOAC. In the estuarine environment competing coagulants may desorb OM from the flocs, and contribute to the marine food web.

Fluorescence peak spectra showed the trend of preferential organic compound sorption into flocs, which has been observed in other studies (Asmala et al, 2014). Clay treatments T2 and T4 showed strongest effect on the peak

spectra and site I was clearly distinct from the other samples, which could be an effect of the higher concentrations of dissolved organic matter and carbon at this site. Peak A, C and M reflect terrestrial sources of organic matter, where peak A and C typically reflect humic acids (Cory et al, 2010). These were in general low for the T2 treatment for all stream sites except for site D. In treatment samples, protein-like components of peak T increased compared to the raw stream samples for all stream sites, but not for the headwater moor site I. Patterns for peak B were less clear and showed no obvious trends.

Changes in fluorescence indices with treatments implied that preferential removal of humic-like terrestrial molecular structures were removed from residual samples. A higher freshness index (FRESH) suggests that material in the dissolved phase was relatively fresher than the organic matter that had been absorbed to the floc products during the experiment. FRESH was higher for downstream stream sites than for the headwater site, where a terrestrial signature of plant material of the mire vegetation would dominate. In treatment samples, FRESH increased especially for the clay treatments, further indicating that humified organic matter was preferentially absorbed to flocs.

A higher fluorescence index (FI) indicates a more microbial origin of the organic matter (e.g. leachates from bacteria and algae) while a lower FI is derived from terrestrial plant and soil organic matter (Fellman et al, 2010). For raw stream samples, a low FI was found for the mire site I of c. 1.3, while most of the stream sites showed a mixed signature between 1.4–1.6. The relatively high FI in the treatment samples indicated that terrestrial OM had been lost from the dissolved phase and taken up by floc products during the experiment, especially in clay treatments.

The humification index (HIX) indicates the degree of humification. For treatment samples HIX mostly decreased in the residual DOM, which further indicated that preferential flocculation of humified matter during the flocculation experiment occurred.

Both the mass spectrometry and the fluorescence data presented in this study showed that coagulants effectively reduced humic substances in residual DOM, which agrees with other studies (e.g. Lavonen et al, 2015) that have found that coagulants preferentially remove DOM with terrestrial characteristics from the dissolved phase. With the coagulant concentrations used in this study, the

clay coagulant contributed to more DOM loss, than salt treatments. A change in coagulant concentration and properties may play a role in how much DOM and which molecular structures that are susceptible to sorption. Similar molecular structures were preferentially removed from solution by both coagulants, suggesting that the type of coagulant was of less importance, and that instead the characteristics of the aromatic oxygen-rich compounds determine the susceptibility to sorption. This agrees with the studies mentioned above, where a range of different coagulants had the same effect on DOM removal (Banaitis et al, 2006; Sanchez et al, 2014; Lavonen et al, 2015).

7.2.3 Downstream effects on riverine organic matter

When comparing sites I (headwater) and the connected site E (downstream site) of catchment E, the fluorescence index increased, humification index decreased and the freshness index increased downstream. This result reflects that the organic matter properties in the stream water increased in relative freshness, attained more microbial origin and contained relatively less humified materials. In a "pipeline scenario" a possible explanation for these results could be dilution effects in the downstream water sample compared to the headwater sample, while in a "reactor scenario" additions of other terrestrial organic matter, in-stream organic matter production of microbial origin, physicochemical processes such as photolysis, and removal of organic matter from the dissolved phase into flocs through flocculation processes, could alter the signatures of the residual stream DOM.

In this study, results from the flocculation experiment showed that added coagulants changed the composition of the residual DOM. Representing mixing of stream DOM with minerogenic matter from soil erosion (clay treatment), saline mixing (salt treatment) and soil-saline mixing (clay and salt treatment), the results showed that while saline mixing (T3) alone had least flocculation effect, the addition of clay particles (T2) lead to sorption of organic matter, with a preference for humic substances. The overall DOM sorption in the mixed treatment (T4) was to a degree counteracted by salt ions, which desorbed clay-bound DOM from the clay standard. Variations in flocculation also depend on mineral composition, stream chemical composition and solution ionic strength, which affect the stability

factor (α) (Edzwald et al, 1974), however these are parameters that were not investigated in this work.

While saline mixing at the estuaries is a natural process, flocculation due to increased soil erosion caused by land use change might further change the composition of downstream riverine organic matter. Not only is soil erosion increasing the net input of minerogenic aggregate-bound organic matter and charged clay minerals into streams, but the hydrological response to precipitation in a catchment is additionally affected by land use. In natural to semi-natural catchments peak discharge might be lower and less intense due to longer residence time of precipitation in heterogeneous vegetation and stable soils, compared to rapid discharge peaks in agricultural catchments affected by plant monoculture and tillage practices. Low discharge not only affect water retention time for suspended particulates and dissolved aquatic species in the streams, but also allows time for other transformation processes such as photodegradation and flocculation of organic matter to take place.

7.2.4 The effect of salt mixing on minerogenic-bound organic matter

When conducting the standard control run using only deionized (DI) water standards that were treated by T1–T4, results showed that the mixture of salt and clay standard (T4) lead to desorption of organic matter from the clay standard.

In nature, this process could be important at the freshwater–ocean boundary, where freshwater transporting total suspended particulates (e.g. soil particles) interact with salt ions in estuaries and as a result desorption of aggregate bound SOC might provide substrates for biological consumption or contribute to other flocculation. The aggregate bound SOC is often more humidified than relatively fresh organic litter products and in the case of the clay and clay-salt treatments T2 and T4 of stream samples, the fluorescence data showed that humified matter was commonly more prone to sorb to coagulants, leaving relatively fresher DOM residue in suspension. The fluorescence index (FI) increased in residual DOM in the treated stream samples, which similarly indicate that terrestrial organic matter from litterfall and soil were preferentially sorbed. Implications of this sequestration is that formed flocs that are prone to sink and accumulate at sites of deposition could to a large degree consist of mainly terrestrial matter. Other studies have for instance found that downstream the

247

coastal mixing boundary, terrestrial POC becomes less abundant in the water column and instead composes a major contributor in sediments with increasing salinity (Wanatabe & Kuawe, 2015). Further, flocculation experiments that test the effect of a range of salinities simulating estuarine mixing have confirmed that flocculation of terrestrial DOM takes place even at low salinities, concluding that the residual DOM which reaches the sea after flocculation processes have taken place, substantially differ in compound properties compared to pre-flocculation DOM (Asmala et al, 2014). These alterations in DOM composition contribute to the discriminative processes that control which organic compounds reach the open sea (Asmala et al, 2014). Further, Kothawala et al (2012) showed that dark incubation of DOM reduced primarily the humic substances as a result of biological recycling and flocculation. As mineral aggregate bound soil organic matter typically compose these humified organic compounds, it is possible that desorption of soil organic matter from total suspended particulates could contribute to either the microbial food chain or successive flocculation at the estuarine boundary. Produced flocs remove organic matter from the dissolved phase and settle at sites of accumulation, which compose possible storage and burial sites of organic carbon. In the studied streams, most of the estuarine boundaries compose outlets directly connected to Bristol Channel, where aquatic species, dissolved and particulate, are redistributed by wave action instantly without much accumulation in a bay. Organic matter entering the sea at these outlets might therefore be transported far from the shore before sedimentation, or may be available as biological substrates already at the estuarine boundary.

7.2.5 Limitations of the Exmoor stream study

The monthly–bimonthly monitoring scheme compose a narrow window of observations from these streams. The concentration range of water quality parameters, pH, and EC presented in this study do therefore not necessarily represent average water quality of these streams, yet the information gathered suggest that in general these streams are poor in both dissolved and particulate organic matter over most of the year. Other studies have shown higher maximum concentrations of particulate carbon (e.g. Glendell et al, 2014).

In this study, the residual DOM composition was only measured for samples from one single sampling occasion in May 2018. Initially used sample

polypropylene sample tubes showed out to be inappropriate in storing post-experimental filtrates, as contamination occurred. Therefore results from organic compound and component analysis were reduced to one sampling occasion, when glass vials were used for storage, however the composition of organic matter in these streams is likely connected to occasional–seasonal variation, influenced by e.g. soil erosion events, seasonal input of litterfall, and biological activity of microbial films. The results of this study implicates that depending on the coagulant there is preferential removal of specific carbon groups during flocculation, and therefore the quantity of DOM that flocculate in stream water might be limited due to the initial compound composition. This complicates quantification and modelling of flocculation in streams, perhaps more in those that are both of heterogeneous composition and are subject to seasonal variation at higher latitudes.

The post-experiment floc particulates that were captured on glass fibre filters and were analysed by loss on ignition were of such small quantities that high uncertainties lie in the gravimetric method, even with a 4-decimal balance. Small differences in absorbed moisture in the filters which were oven dried and weighed before and after filtration could have caused error in the measurement.

Another limitation compose the possible reactions between organic matter which desorbed from the clay standard in the mixed treatment (T4) that may have influenced the composition of the organic substances measured in the residual DOM. Although the influence might be of minor importance for the measured flocculation, it could still affect the results to some degree.

This experiment only tested the effects of two coagulants (salt and clay). In nature, the dissolved phase of organic matter is complex and the different types of coagulants that may be continuously, seasonally or occasionally present in stream waters are numerous (e.g. dissolved metal ions, clay minerals, organic coagulants). Water chemistry was not analysed in this study and therefore the effects of flocculation on stream samples shown by the results could have been influenced by sample heterogeneity of e.g. metal concentrations that were not taken into account. However the analytical blanks that were analysed composed homogenous samples and it could be assumed that the residual organic compound composition in these samples were representative of flocculation effects. It is still important to remember that the experimentally measured effects

might not be representative when mixed conditions exist, as those in natural stream waters.

7.2.6 Summary Exmoor project

In summary, the flocculation experiment showed 1) preferential removal of aromatic and oxygen-rich humic-like structures for treatments with coagulants, and 2) added salt standard had a desorption effect on the native OM of the clay standard, which diluted and reduced the overall flocculation effect.

In addition, this study developed a methodology which successfully investigate the effects of flocculation by coagulants on samples from DOM poor streams. While results from TOC-L analysis were less reliable due to the low initial OC content, mass spectrometry, absorbance and fluorescence analysis were of sufficient resolution to determine the molecular formulae for classified compound groups of the DOM. These methods have been shown to be a helpful tool for determining the chemical characteristics and of natural stream water and improves current understanding of DOM composition in various systems of the LOAC. More in-depth analysis could investigate the behaviour of DOM components at other concentrations of added coagulants.

7.3 POC transport and dynamics along the LOAC

In this study, the transport and nature of POC was investigated in soils and reservoir sediments of a tropical catchment. This semi-closed system allowed for quantification of reservoir net input of sediment from eroding catchment soils. With the results found it was possible to estimate total POC input and net inventories in post-flooding reservoir sediments, however further investigation and additional methods are required to improve these estimates, especially in order to determine the various sources of POC.

The main objective of the modelling study in João Penido catchment was to calculate POC erosion from catchment soils and deposition into the reservoir. The range of average soil erosion output for wholly database based input to partially field based input of RUSLE for grassland sites that were compared to radionuclide inventories fell within the range of radionuclide results, although the partially field based RUSLE output agreed best with PDM-^{137}Cs and DMM-^{210}Pb$_{ex}$

results, which were the FRN conversion models that showed best potential in the field. It was expected that the RUSLE model would work sufficiently well in the João Penido catchment, as it in other studies has been successfully implemented for catchments with various terrain, climate and land uses. In particular, the results from the database based RUSLE output agrees well with other studies in the region, which supports the motivation to use this model in this type of landscape.

The main objective of the POC study in João Penido catchment was to determine the net inventories and sources of POC in post-flooding sediments. While the total POC inventory could be estimated from sediment core observations and calculated sediment volume, the relative net contributions from allochthonous and autochthonous sources could only be approximated. This estimation is based on a number of assumptions that may be more or less realistic for the João Penido reservoir, such as the assumption that the average organic carbon content will be retained in soil particles entering the post-flooding sediment due to physical protection of organic matter in mineral-aggregates and that mineralisation of autochthonous and bioavailable organic matter has been continuous over time, which would result in a depth gradient with relatively more allochthonous POC with depth. The C/N results indicated that top sediments displayed mixed terrestrial–lacustrine signatures, while deeper sediments showed more separated signatures for sediment increments, however the number of samples were too few to determine any obvious patterns. Of the density fractionated sediment samples only one sample (SED4B, at 2–4 cm) had sufficient light fraction to be compared to the heavy fraction for the three separated particle sizes. Although the light fraction showed higher C/N ratios for the medium (250–53 µm) and fine fraction (<53 µm), the difference was too small to indicate a source other than "mixed" with certainty. Unanswered questions of this work compose the full comprehension of organic carbon sources in the reservoir post-flooding sediments, and the fate of the carbon currently in limnic storage. To answer those questions, studies on for instance recalcitrance of various forms of POC would continue to enhance the understanding of POC fate in reservoirs like João Penido, by studying the other parameters of source, state of decomposition and physical protection.

251

For the POC transformation study in Exmoor, UK, the results indicated that the fraction of organic carbon in stream water is typically low for the studied streams. While other studies have detected higher concentrations during rainfall events, e.g. for Horner Water, the monitoring scheme in this study was not of enough resolution to catch the extremes of the seasonal variation. Any continued studies could possibly implement high discharge events to determine the OM quality and the flocculation rates of riverine organic matter of such events. Results from the flocculation experiment indicated that humic like substances were preferentially removed from the dissolved phase, which corroborates other studies that have linked carbon transformation dynamics in mainly the estuarine part of the LOAC to the properties of bioavailable substrates delivered by stream water discharge that become utilized by the marine food web. A change in POC properties in the upstream LOAC, e.g. as an effect of land use change, could therefore have implications for transformation processes further downstream. The resulting effects is outside the scope of this study, but has a part in future modelling of carbon transport and fate. This study focused on a narrow compartment of the wide range of transformation processes that occur in catchment streams, it investigated the change in organic properties of residual DOM as an effect of flocculation, which showed that aromatic oxygen-rich compounds were preferentially removed by both types of coagulants.

Questions that remain to be answered are for instance what the effect of seasonal variation are on flocculation processes, what the connection between other transformation processes are and how these influence each other, e.g. photooxidation and biomineralisation, and to what degree flocculation products are recalcitrant or bioavailable.

Chapter 8 Conclusions

This study investigated POC transport and fate in a tropical reservoir catchment and effects of flocculation on riverine dissolved organic matter. For the Brazilian reservoir study, it was found that:

- RUSLE model output that utilized field observations from the study site showed closer relationship with fallout radionuclide field data, than did the RUSLE output which was entirely based on database input.

- Simulations of land use change showed that the current state of erosion was in-between the two simulated extreme scenarios of a completely forested and a completely deforested state, which emphasized the importance of the factor of vegetation cover in this type of landscape.

- Despite the ^{137}Cs signal being sparse in Brazilian soils, the inventories showed some erosion and deposition patterns for the soil sites, however it seemed that ^{210}Pb$_{ex}$ is a more powerful erosion tracer present in this area. The continuous fallout of the natural radionuclide ^{210}Pb$_{ex}$ makes it an interesting tracer to use in the future, especially in the Southern hemisphere, as artificial ^{137}Cs signals are diminishing in the environment.

The results of this work are supported and support other studies in the field. Comparable studies using the RUSLE model in similar environments in South America have reported results of the same order of magnitude as those in this work (Medeiros et al, 2016; da Cunha et al, 2017; Beskow et al, 2009), and the ^{137}Cs inventories reported in this study are similar to inventories in other nearby regions of Brazil (Correchel et al, 2006; Bacchi et al, 2005; Andrello et al, 2004). In Brazil, few studies have focused on using ^{210}Pb$_{ex}$ as a soil erosion tracer and most have used it for aquatic sedimentation settings, however ^{210}Pb$_{ex}$ soil inventories in this work were comparable to other studies from worldwide sites.

Although uncertainties lie in the calculations of the net post-flooding sediment volume of João Penido reservoir, it was also found that:

- For João Penido, the calculated sediment yield amounted to 20.3%,
- the ratio of allochthonous and autochthonous POC of the post-flooding sediments was estimated to 2:5, indicating that the dominating source of POC in this eutrophic reservoir was of autochthonous origin.

The experimental study on flocculation dynamics of dissolved organic matter in stream water samples from Exmoor revealed the following:

- The efficiency of flocculation agents in treatment order was clay, mixed clay and salt, and salt treatments, T2>T4>T3 respectively.
- Preferential removal of humic substances was found for samples treated with coagulants, where molecular structure with low H/C and high O/C were absorbed, showing that more aromatic humic substances contribute to the POC pool during flocculation processes for these streams.
- that the impact of treatments with coagulants primarily controlled residual DOM characteristics, despite small differences in water quality between the stream sites.

This work led to development of a useful method to determine the effects of flocculation on stream water DOM, which provides insights into POC dynamics in the LOAC when it appears in the form of organic flocs. This method could further be used to investigate dissolved and particulate organic matter fractions in other systems belonging to the LOAC, where it is of importance to understand the transformation processes of POC.

Appendix 1

Brazilian project

Manuscript 1: Measuring and modelling terrestrial soil erosion input into a tropical freshwater reservoir, Brazil, using fallout radionuclides ^{137}Cs and ^{210}Pb and RUSLE

J.T.C. Snöälv[1], R. Mendonça[2,3], R. Lauerwald[4], T.A. Quine[1] and S. Sobek[2]

[1]Department of Geography, University of Exeter, Exeter, UK
[2]Department of Limnology, Uppsala University, Uppsala, Sweden
[3]Department of Biology, Federal University of Juiz de Fora, Juiz de Fora, Brazil
[4]Department of Earth and Environmental Sciences, Université Libre de Bruxelles, Brussels, Belgium

Corresponding author: Jo Snöälv (j.snoalv@gmail.com)

Key words: soil erosion, RUSLE, fallout radionuclides, LUC, sub-bottom profiling, reservoir

Abstract

Land use change (LUC), such as deforestation and agriculture, contribute to increased erosion and subsequent redistribution of soil particles in the landscape, while the increased number of artificial dams and reservoirs result in sediment traps in the landscape which can store much of this relocated soil. In Brazil, the Atlantic forest biome has been reduced to 8% of its original extent over the past c. 500 years, to be converted into agricultural land of plantations and pasture, which raises concerns not only about intense ecosystem degradation but also about increased soil degradation in the landscape. In this study, modelled soil erosion by Revised Universal Soil Loss Equation (RUSLE) was used to estimate soil erosion in a highly perturbed and largely deforested tropical catchment in Brazil. The modelled results were validated by field observations of fallout radionuclides (FRN) used to quantify soil erosion and sedimentation in the catchment. Further, simulated RUSLE scenarios of extreme cases of total deforestation and total forestation were compared to the current state of erosion.

The results show that modelled RUSLE output of soil erosion in this tropical catchment agrees with field observations, indicating that RUSLE is an adequate tool when addressing soil erosion in this type of increasingly common deforested Brazilian landscape.

Plain Language Summary

Soil erosion and sedimentation was modelled and measured in deforested soils of a reservoir catchment in south-eastern Brazil. The results indicate that land use change (LUC) severely impact soil erosion rates in this landscape and that RUSLE is a reliable tool for soil erosion assessment in this type of landscape.

1 Introduction

Soils are important. Being a historically vast resource utilized by humans for growing crops since the agricultural revolution of the Neolithic (Lev-Yadun et al, 2000), with finite reserves soils have been degraded substantially worldwide. Land use change (LUC) and anthropogenic activities such as agricultural practices, deforestation, and overgrazing, accelerate natural soil erosion (Ritchie & McHenry, 1990; Porto et al, 2012). Globally, 25% of agricultural lands have been classified as highly degraded (FAO, 2011). Not only cultivated lands are under anthropogenic pressure, but deforestation and conversion of forested lands lead to increased losses and nutrient exhaustion of soils previously stabilized by roots and nourished with plant litter. Clear cutting has been attributed a major cause of soil erosion in many historical and present agricultural societies (Anselmetti et al, 2007).

About 25% of the land area in Brazil is used for agriculture and total soil erosion rates from these cultivated soils (including pasture) amount to c. 800 million tonnes year^{-1} (Merten and Minella, 2013). Clear cutting of forested land with subsequent conversion into cultivated fields or pasture not only increases land degradation, but also reduces natural ecosystem function and diversity. A highly impacted biome in South America is the Atlantic forest, which composes a biodiversity hotspot that mainly over the past c. 500 years has been reduced to less than 12% of its original extent of almost 1.5 million km^2 on the South American continent (Ribeiro et al, 2011). Similarly, in Brazil, deforestation

256

practices have reduced corresponding Brazilian Atlantic forest (Mata Atlântica) to c. 8% of its original extent (Colombo & Joly, 2010). Atlantic forest contains exceptional biodiversity from a wide range of altitudes over coastal to inland areas that stretch from tropical to subtropical regions over the continent, but is threatened by severe habitat loss and increased fragmentation due to land use change (Ribeiro et al, 2009) and the increased land degradation which typically follows deforestation.

Further, soil erosion not only compose a loss of an ecosystem or farming resource in which plants can grow, but increased mobilisation of soil particles can also lead to downstream problems when allochthonous sediment is deposited in fields, floodplains, and lakes and artificial dams (Zapata et al, 2003). Manmade dams and reservoirs are effective sediment traps in the landscape that contribute to the acreage of semi-permanent water bodies which may act as emission hotspots of greenhouse gases such as carbon dioxide (CO_2) and methane (CH_4) (Barros et al, 2011; Maeck et al, 2013). Reservoirs also act as containers holding limnic storage of eroded soil and organic matter. While human impact has increased global soil erosion input into the aquatic continuum with about 2.3±0.6 Giga-tonnes year^{-1}, there has been a reduction in sediment loads reaching the coastal oceans by 1.4±0.3 Giga-tonnes year^{-1} due to entrapment within reservoirs and dams (Syvitski et al, 2005). When accounting for the effect of sediment trapping modelled global average input of sediments from the continents to coastal oceans amount to about 19 Pg year^{-1} (Beusen et al, 2005) and globally over 100 Giga-tonnes of sediment is estimated to be retained within reservoir storage, containing 1–3 Giga-tonnes of carbon (Syvitski et al, 2005). Moreover, about 75% of the organic carbon (OC) that is deposited in reservoir sediments is derived from allochthonous sources (Maavara et al, 2017). Eroded soil particles that end up in reservoir storage remove organic carbon from terrestrial soils and contribute with soil organic matter (SOM) to either fuel mineralisation or add input of OC to semi-permanent reservoir storage. Human perturbation on the natural landscape that leads to this increased flux of soil particles into the aquatic continuum and reservoir storage results not only in geomorphic disturbance but also degradation of terrestrial soil carbon deposits which previously were stabilized by the original forested ecosystem.

In many regions of the world, reliable data on soil erosion is sparse despite the general acceptance that net soil loss from the landscape composes a major problem (Zapata, 2003). Since soil degradation impact both the sustainability of agriculture in cultivated landscapes, and the environmental conservation of protected areas, a primary step towards effective environmental management and soil conservation is quantification of soil erosion and deposition (Porto et al, 2012; Gaspar et al, 2013). Several techniques have been developed to estimate soil erosion, e.g. field observations such as terrestrial laser scanning and radionuclide methods, and modelling approaches comprising three types of erosion models: 1) quantitative, 2) empirical, and 3) physically based models (Terranova et al, 2009). Revised Universal Soil Loss Equation (RUSLE) is an upgraded empirical soil loss model based on the original Universal Soil Loss equation (USLE) model developed originally by United States Department of Agriculture (USDA). The spatial scale of RUSLE composes field–hillslope range (Terranova et al, 2009), although numerous studies have applied this model on global scale (Yang et al, 2003; Naipal et al, 2015) and the model has been successfully applied in various regions, terrains and climate.

Effective methods to measure soil erosion in the field include the use of fallout radionuclides (FRN) (Gaspar et al, 2013). FRNs are radioactive isotopes that readily fix onto mineral surfaces and primarily follow the physical processes which relocate soil particles (Quine & Van Oost, 2007). Assuming that the distribution of FRN follow soil mobilization, these therefore serve as good indicators of erosion and deposition by water, wind and tillage (Mabit et al, 2008). Two common radionuclide tracers compose 137-caesium (^{137}Cs) and excess-210-lead (^{210}Pb$_{ex}$). The isotope ^{137}Cs is a fission product from ^{137}I decay, an anthropogenic fallout radionuclide which does not appear naturally. It was released into the atmosphere during bomb tests in the period 1950–1970 (Nouira et al, 2003), and, in particular, in the Northern Hemisphere from the Chernobyl accident in 1986 (Tang et al, 2006). Despite the Chernobyl incident, main fallout of ^{137}Cs occurred in years 1962–1964 (>50%), and 80% of deposition had occurred by 1964 (Quine & Van Oost, 2007). The radioactive fallout is considered uniform, and despite some deliverance being through local dryfall in the vicinity of key sources, the main deposition is via rainfall precipitation (Ritchie & McHenry, 1990; Mabit et al, 2008; Dercon et al, 2012). The ^{137}Cs radionuclide

has successfully been used to study medium-term (up to c. 50 years) soil erosion rates in managed and non-cultivated soils in the past (Ritchie & McHenry, 2007) and composes a straightforward method to identify the relocation of soil particles by physical processes. As one of the most common radionuclides used within FRN research, ^{137}Cs has been used in over 4000 studies worldwide (Mabit et al, 2014).

Fallout of ^{137}Cs has been more prominent in the Northern Hemisphere than in the Southern Hemisphere and show higher concentrations in the environment around for instance centres of nuclear tests and the Chernobyl power plant (Tang et al, 2006; Dercon et al, 2012). Earlier studies have shown that the ^{137}Cs activities obtained in Brazilian soils of the Southern Hemisphere generally occur at levels c. 10 times lower compared to data from the Northern Hemisphere (Bacchi et al, 2000). Despite the relatively low activities of ^{137}Cs in soils of the Southern Hemisphere, in a long-term runoff monitoring study to evaluate the use of ^{137}Cs in Brazilian soils, Correchel et al (2006) found that where this radioisotope is detectable it provides confident results. The generally low activities of ^{137}Cs in the Southern Hemisphere cannot be overcome, however, activity measurements of excess (unsupported) ^{210}Pb$_{ex}$ with a half-life of 22.26 years can be complementary to ^{137}Cs studies (Mabit et al, 2008). The redistribution of ^{210}Pb$_{ex}$ in the landscape is, similar to the ^{137}Cs distribution, mainly connected to physical relocation of soil particles, as it too readily adsorbs to mineral surfaces as well as organic matter. The continuous fallout additionally retain soil profiles with the highest ^{210}Pb$_{ex}$ activities at the surface and declining activities with depth (Walling et al, 1995). Because the ^{210}Pb$_{ex}$ inventory is continuously replaced, historic records of erosion rates up to ca 100 years are obtainable, compared with ^{137}Cs which fallout is associated with bomb tests in 1950–1960 (Gaspar et al, 2013).

The objectives of this study were 1) to determine soil erosion rates and the amount of allochthonous sediment that goes into limnic storage of a small drinking water reservoir within a largely perturbed tropical watershed in Brazil, to assess the impact of LUC on soil and sediment redistribution in an Atlantic forest biome affected by deforestation and damming, and 2) to evaluate the performance of the RUSLE model to predict soil erosion in this type of landscape. The results of this study would reveal typical characteristics of soil redistribution

259

rates and fate in an increasingly common perturbed landscape of south-eastern Brazil.

2 Materials and Methods

2.1 Study area

João Penido reservoir (LAT: −21.675459, LONG: −43.394960) supplies drinking water to the city Juiz de Fora in state Minas Gerais, Brazil (Figure 1). The watershed area amount to ca 772 km^2 and is situated in terrain at ca 684–1061 m.a.s.l. (DEM analysis) with the main water body being located at ca 746 m.a.s.l. DEM analysis displayed catchment slope values ranging between 0–36.7 degrees. The watershed composes a minor contributing sub basin to the large Paraíba do Sul River watershed. João Penido composes a mesotrophic system having a medium level of water quality which has likely degraded in quality due to land use change in the watershed (Bucci et al, 2015). The land surrounding the reservoir in the catchment is mainly used for residential purposes and as pasture for cattle. Main parts of the land in direct connection with the reservoir beachline compose deforested shrubland.

Figure1 Field site

The region is classified by the *Köppen* classification system as *Cwa*, with a sub-tropical climate having dry winters and rainy summers, with the hottest months having mean temperatures >22°C. Annual regional rainfall for south-eastern Brazil range between 1200–1600 mm year^{-1} (da Silva, 2004). Metamorphic rocks, such as Neoproterozoic schist and Rhyacian orthogneiss (CPRM 1:1M, 2018)[28] dominate the catchment lithology. The main soil type composes orthic ferralsol or ultisol (CPRM, 2016), characterized by highly weathered soil units. Mass movement of soil on the hillslopes, which cause scarring in vegetation and provide unprotected patches of ground with higher erosion potential than protected soil covered by vegetation was observed in the field. Deforested

---

[28] URL: http://portal.onegeology.org/OnegeologyGlobal/

grasslands dominate in the catchment, which is mapped as semi-deciduous forest belonging to the Atlantic forest biome[29].

2.2 Soil and sediment sampling

Field work was conducted in the dry season of 2016. Soil samples from hand dug pits were collected with soil profile samplers (Figure 3). The top 20 cm in the soil profile was subsampled by 2 cm increments (100 cm^3), while the 20–60 cm section of the soil profile was subsampled by 5 cm (2500 cm^3) intervals. Sites with terrestrial sediments were sampled in the flat (<1 degree slope) seasonally inundated soils. Larger particulates (pebbles, stones, roots) were removed and samples were packaged into plastic zip-bags. The samples were weighed, air dried, and shipped to University of Exeter laboratories.

Figure 3

Sediment core were retrieved with a gravity corer from a boat from the delta and various sites of the reservoir (Figure4). The cores were sub sectioned into 2 cm increments, air dried, and transported to the laboratory at University of Exeter. Additional sediment cores were sampled in 2017.

Figure4

2.3 Bathymetric measurements by sub-bottom profiler

The bathymetric survey in João Penido reservoir was performed in June 2016, with a parametric sub-bottom profiler (Innomar SES-2000) which detects the sediment-water interface at 100 kHz frequency. Shore-to-shore zigzag transects were made at 10 km h^{-1} along the entire length of the reservoir, and the output data were geo-referenced using an on-board GPS receiver. The echograms were interpreted using the Innomar ISE software (version 2.95).

---

[29] Mapa de Vegetacão do Brasil (1992)
http://mapas.mma.gov.br/mostratema.php?temas=vegetacao

2.4 Analytical methods

Samples were oven-dried at 40 °C for 24–48 hours, weighed, ground, and passed through a <2mm sieve, and stored in enclosed containers for a minimum of 20 days to reach equilibrium between ^{210}Pb fallout from [222]Rn decay, before γ detection of fallout radionuclides in high purity germanium (HPGe) coaxial detectors (ORTEC). Photopeaks of [137]Cs (662 keV), [210]Pb (46 keV) and [226]Ra (352 keV) were recorded with GammaSpec® software for soil samples (c. 50) and sediment samples (c. 4–6 g) with a set detection time of 86400 s.

2.5.1 Bulk density, porosity and grain size analysis

Dry bulk density was determined by:

$$\rho_b = W_d/V_t$$

Where ρ_b is the bulk density, W_d is the dry weight, and V_t is the total volume. Grain size was analysed on the <2000 μm fractions of 90 samples from 3 sediment cores and 3 soil cores. The fractions that were separated were >2000 μm, 2000–250 μm, 250–63 μm, and <63 μm.

2.5.2 Fallout radionuclide inventories

Soil samples were analysed for [137]Cs (*N*=350) and [210]Pb$_{ex}$ (*N*=296). From sediment sites, 76 samples were analysed for ^{137}Cs and [210]Pb$_{ex}$. Activity of a sample was calculated by (Mabit et al, 2014):

$$A = \frac{Ne^{\lambda t_0}}{\varepsilon I_y M t_c}$$

where *A* is the concentration of activity (activity per mass) of the radionuclide (Bq kg^{-1}), *N* is the net peak area, λ is the decay constant (ln2/$t_{1/2}$)*, t_c is the counting time, t_0 is the difference in time between sampling and measurement, *M* is the mass of the sample (kg), ε is the absolute efficiency, and I_y is the gamma intensity

or probability of emission. The calculated activities were corrected by the number of days between sampling and analysis.

The areal activity (Bq m^{-2}) was calculated by:

$$A_S = \Sigma C_i \rho_i H_i$$

Where C_i is the activity of the ith sample depth section (Bq kg^{-1}), ρ_i is the bulk density of the ith sample increment (kg m^{-3}), and H_i is the depth of the ith sample increment (m). The basis of soil redistribution by fallout radionuclides assumes that the inventory of an eroding site is lower than the reference site inventory, whilst an accumulation site has a higher inventory. The inventory, ^{137}Cs$_{inv}$, was calculated by:

$$^{137}Cs_{inv} = A \times \rho \times d$$

Where A is the concentration of activity (Bq kg^{-1}) in a sample, ρ is the soil bulk density (kg m^{-3}), and d is the depth (m) of the sample. The inventory is reported in units of Bq m^{-2}.

Soil site JP17 was the chosen reference inventory for all soil cores in the study area. This site was assumed to undergo neither net erosion nor net deposition, showed continuously decreasing ^{137}Cs activities with profile depth, and 80% of the total ^{137}Cs inventory was found in the top 20 cm.

2.5.3 Conversion models

The conversion models that were used for soil sites in this study are the Profile distribution model (PDM) for ^{137}Cs, and the Diffusion and migration model (DMM) for ^{137}Cs and ^{210}Pb$_{ex}$. The constant rate of supply (CRS) model was used for delta and reservoir sediments. It was assumed that the main atmospheric fallout of ^{137}Cs occurred in 1963 due to bomb testing, and composes the only source accounted for in the interpretation of ^{137}Cs-data for these Brazilian soils. It was also presumed that ^{210}Pb fallout is continuous over time, which would yield reference inventories in steady state balance.

The profile distribution model uses an exponential relationship for the vertical inventory of ^{137}Cs at an undisturbed site, and was calculated by (Zhang, 1990):

$$A'(x) = A_{ref}(1 - e^{-\frac{x}{h_0}})$$

Where *A'(x)* is the concentration ^{137}Cs above depth *x* (Bq m[-2]), A_{ref} is the reference inventory of [137]Cs (Bq m[-2]), *x* is the depth from the soil surface (kg m^{-2}), and h_0 is the profile shape coefficient (kg m^{-2}) or relaxation depth of the profile. h_0 is calculated by least squares regression between the variables ln *A(x)* and the cumulative mass depth (kg m^{-2}), according to e.g. Porto et al (2001).

For an eroding site, soil loss was calculated by (Rodway-Dyer et al, 2010):

$$Y = \frac{1}{(t-1963)} h_0 \left(1 - \frac{X}{100}\right)$$

Where *Y* is the yearly soil loss (t ha^{-1} year^{-1}), *t* is the sampling year, h_0 is the relaxation depth (kg m^{-2}), and *X* represents the percentage of reduction of total ^{137}Cs inventory (%) described by:

$$X = (A_{ref} \times A)/(A_{ref} \times 100)$$

Where A_{ref} is the reference inventory of [137]Cs (Bq m[-2]), and *A* is the total ^{137}Cs inventory (Bq m[-2]).

The diffusion and migration model was used to interpret [210]Pb_ex inventories in terrestrial soil samples, by an Excel *add-in* presented in Walling et al (2007). It requires input parameters such as the diffusion coefficient (*D*) with a unit of kg[2] m^{-4} year^{-1}, the downward migration rate (*V*) with a unit of kg m^{-2} year^{-1}, and the relaxation depth (h_0) with the unit kg m^{-2}. The calculations of the DMM method have been thoroughly described by others (Walling et al., 2002: Porto et al, 2014). The diffusion and migration coefficients for ^{137}Cs and [210]Pb_ex were calculated for reference site JP17, using *D*=22.56, *V*=1.08 for ^{137}Cs, and *D*=0.88, *V*=0 for [210]Pb_ex. The model requires a value for relaxation mass depth that represents

penetration of fresh fallout (not to be confused with h_0 which relates to the profile distribution, used for PDM-^{137}Cs calculation of erosion rates) and a value of 4 kg m^{-2} was chosen for all samples.

2.5 Modelling soil erosion rates with RUSLE

The upgraded empirical soil loss model Revised Universal Soil Loss Equation (RUSLE) is based on the original Universal Soil Loss equation (USLE) model, initially developed by United States Department of Agriculture (USDA). It composes a product of the following six factors:

$$A = RKLSCP$$

where *A* is the calculated yearly mean soil erosion (metric tonnes ha^{-1} year^{-1}), *R* composes the yearly rainfall erosivity factor, *K* is the soil erodibility factor, *S* and *L* compose the slope steepness and slope length factors respectively, *C* is the vegetation and crop management factor, and *P* represents specific erosion control practices. The combined product of *L* and *S* factors compose the topographic factor, *LS*, which can be derived from DEM data. The input data sources are summarized below.

A DEM was created from 30 m resolution Shuttle Radar Topography Mission data (*SRTM s22w044 1arc-second v3),* downloaded in 2016 from USGS Eros Data Center[30]. Slope values range between 0–36 degrees in the João Penido catchment (Figure).

The R factor was calculated by the expression by Renard & Freimund (1994) was used:

$$R = 0.0483 \times P^{1.610}$$

Where *P* is the annual average rainfall in mm year^{-1}, estimated from the database PSD South America Daily Gridded Precipitation (Liebmann & Allured, 2005), which temporal range is 1940–2012, obtained from *South American Precipitation data provided by the NOAA/OAR/ESRL PSD, Boulder, Colorado, USA, from their*

---

[30] https://earthexplorer.usgs.gov/, downloaded in 2016

Web site[31] *at* http://www.esrl.noaa.gov/psd/ (downloaded 2017-10-30). Data was extracted from raster point (LAT, LONG: −4832176.366, −2471825.954) to calculate the annual average precipitation for an area that includes the João Penido catchment.

The soil erodibility factor (K) can be derived from database soil properties data or be derived from field observations. The dominating soil type in João Penido catchment is orthic ferralsol (latosol) which has been identified with a typically low K value, e.g. 0.0162 Mg ha h ha^{-1} MJ^{-1} mm^{-1} (Medeiros et al, 2015). In this study, the K factor was calculated from soil properties of field samples by utilizing the equation from Stewart et al (1975):

$$K = [2.1 \times 10^{-4}(12 - OM)M^{1.14} + 3.25(s - 2) + 2.5(p - 3)]/100$$

Where p is the permeability class, and s is the structure code, and M is the product of particle structure, based on clay, silt, and sand content, defined as (Wischmeier & Smith, 1978):

$$M = silt\% \times (100 - clay\%)$$

Further, the K value is converted from U.S. customary units into S.I. units (Mg ha h ha^{-1} MJ^{-1} mm^{-1} or t ha h ha^{-1} MJ^{-1} mm^{-1}) by a conversion factor of 0.1317 (Wang et al, 2016). For João Penido reservoir, p was set to 3 (moderate) and s was set to 3 (medium-coarse and granular). Input data from observations showed an average soil OM value of 13.09% (N=125) and grain size data from 26 samples displayed a mean of 3.71% for silt and 96.28% for sand in the upper 20 cm of available soil profiles. Since clay was not separated from the <53 μm fraction in this study, it was set to zero.

The *LS*-factor is a dimensionless value which represents erosion effect of topography. An SRTM-derived DEM was implemented through the SAGA tool *LS-factor, field based*, to calculate the *LS* factor by equations from Desmet & Govers (1996).

The cover and management (C) factor describes the effect of vegetation cover on erosivity in the landscape and its unitless value ranges from 0−1 (Kouli

---

[31] https://www.esrl.noaa.gov/psd/data/gridded/data.south_america_precip.html

266

et al, 2008). For João Penido watershed, literature *C*-values from Panagos et al (2015) and da Cunha et al (2017) were assigned to a land cover map digitized in QGIS using Google Satellite data through the *open layers plugin*, at a scale of c. 1:2,000. Five land cover classes (built up areas, delta, grassland, water, wood) were identified in the studied catchment and the digitized features were assigned literature C factor values.

The support factor (*P*) composes a ratio of erosion related to conservation practices that control runoff erosion in cultivated soils (Renard et al, 1978). In João Penido catchment, the *P* factor was set to 1, as conservation practices are unknown.

3 Data

3.1 RUSLE modelling results

The resulting annual average precipitation (years 1940–2012) equalled 1540.69 mm year^{-1}, which gave an *R* factor value of 6535.34 MJ mm ha^{-1} year^{-1}. This fell within the range of the above-mentioned studies on rainfall erosivity.

The *K* factor for João Penido reservoir catchment corresponded to 0.0040 tonnes ha h ha^{-1} MJ^{-1} mm^{-1}. This value was similar to *K* values found in other South American studies using USLE and RUSLE, e.g. Carrasco-Letelier & Beretta-Blanco (2017) who obtained *K* factor values ranging 0.0073–0.0088 tonnes ha h ha^{-1} MJ^{-1} mm^{-1}, and Galdino et al (2016) who found a *K* factor range of 0.0047–0.0551 tonnes ha h ha^{-1} MJ^{-1}mm^{-1} in their study of cultivated pasturelands in central Brazil. For two classes of ferralsols specifically, Galdino et al (2016) reported specifically *K* factor values of 0.0145 and 0.0193 tonnes ha h ha^{-1} MJ^{-1}mm^{-1}.

The resulting LS-factor map display dimensionless values ranging between 0.03–104, with a mean of 6.85. Similar results have been found in other studies, e.g. Galdino et al (2016) obtained a min–max range of 0–104 and a mean of 1.80 in their regional study of cultivated catchments in central Brazil of similar topography.

The digitized land cover features (Figure 116) were designated *C*-factor values from the literature. The main land cover composed tree-less grassland, making up 72.5% of the catchment, while c. 17.7% of the catchment was wooded.

3.1.5 Natural potential of erosion (NPE)

For João Penido reservoir the natural potential of erosion (NPE) was calculated for catchment raster cells from factors derived from databases (NPE_DB) and with K from field observations (NPE_K). NPE_DB ranged between 1.52–6812.60 tonnes ha^{-1} year^{-1} (Figure 77, Table 27), with a mean erosion rate of 324.86 tonnes ha^{-2} year^{-1} and a standard deviation of 356.67 tonnes ha^{-1} year^{-1}. When K was derived from field observations (this study) the simulated NPE_K output ranged between 0.79–3541.29 tonnes ha^{-1} year^{-1}, with a mean of 168.87 tonnes ha^{-1} year^{-1} and a standard deviation of 185.41 tonnes ha^{-1} year^{-1}. NPE from S_fieldK was ca 52% lower than for NPE_DB output. This difference indicates the importance of accurate assessment of the value for the soil erodibility factor K.

3.1.6 RUSLE output

Soil observations were used to calculate the K factor and digitizing of satellite data was done to produce a more detailed land cover map, which was assigned literature C values. With observed input data for the K factor (S_fieldK), the resulting average erosion rate from the catchment was 19.64 tonnes ha^{-1} year^{-1}, corresponding to 1.96 kg m^{-2} year^{-1}, 5.38 g m^{-2} day^{-1} (Table 27). RUSLE output with a digitized C factor (S_fieldC) gave a mean erosion value of 20.88 tonnes ha^{-1} year^{-1} (sd=28.00). When both field observations of K and C were used as input data, the simulation (S_fieldKC) resulted in a mean erosion rate was 10.85 tonnes ha^{-1} year^{-1} (corresponding to 1.09 kg m^{-2} year^{-1}, or 2.99 g m^{-2} day^{-1}) with a standard deviation of 14.55 tonnes ha^{-1} year^{-1} (Figure 79). For S_fieldCK the improved land cover map reduced erosion in wooded and built-up areas of the catchment and the highest erosion rates were confined to the steeper slopes of hills.

The resulting RUSLE output from analysis with various input data, derived from databases and observations, are summarized in Table 27; S_fieldCK was expected to be the result closest to the actual contemporary erosion state of the catchment.

3.1.7 Simulations of a forested and deforested watershed

The RUSLE model was used to determine the current state of erosion in the João Penido watershed, and to simulate three erosion scenarios of the watershed being completely forested and similarly deforested at two levels by using literature *C* values as input for the *C* factor; a completely forested state was attained by setting the *C* factor to 0.003, which is representative of broad-leaved forest; the two deforested states were given *C* factors of 0.1 and 0.45, representing the lower and upper range of sparsely vegetated areas (Panagos et al, 2015). In the simulations built-up areas as well as standing water (the main reservoir and other larger ponds in the catchment) were unchanged (set to a *C* factor value of 0).

When using database input (S_DB) the scenarios showed higher erosion rates than when using S_fieldKC utilizing observations from the field. Reclassified land cover values from the *GlobCover* dataset were used as input for the *C*-factor, together with the *HSWD* database derived value of *K*. The completely forested state showed erosion rates ranging between 0–20.51 tonnes ha^{-1} year^{-1} (*sd*=1.19). The deforested state with assumed grassland showed erosion rates between 0–683.72 tonnes ha^{-1} year^{-1} (*sd*=39.17). The extremely bare state showed erosion rates between 0–2076.73 tonnes ha^{-1} year^{-1} (*sd*=176.3). Simulated scenarios based on factor input from S_fieldCK yielded lower erosion values for the João Penido catchment. The forested state (*C*=0.003) based on S_fieldCK showed erosion rates ranging between 0–10.66 tonnes ha^{-1} year^{-1}, with a standard deviation of 0.63 tonnes ha^{-1} year^{-1}. The S_fieldCK deforested state (*C*=0.1) with assumed grassland showed erosion rates between 0–355.4 tonnes ha^{-1} year^{-1} (*sd*=20.9). The second, more extreme, deforested S_fieldCK scenario (*C*=0.45) showed erosion rates between 0–3541.3 tonnes ha^{-1} year^{-1} (*sd*=185.4).

3.2 Post-flooding sediment volume and mass

Pre-flood observations (*N*=15) were used to interpolate sediment thickness by inverse distance weighting (IDW). Sediment thickness ranged between 0.06–0.52 m across the reservoir for the cores sampled in years 2016–2017 (Figure 118). Total post-flooding sediment volume was then calculated with the SAGA tool *Raster volume*. The resulting post-flooding sediment volume was calculated

to 753,058.8 m^3. The mass was estimated from the calculated sediment volume and average density of post-flooding sediment (1370 kg m^{-3}). The resulting mass was 1031690.6 tonnes.

3.3 Fallout radionuclide (FRN) results

The ^{137}Cs inventory for the pasture reference core (site JP17) was 219.8 Bq m^{-2}. The mean inventory of all soil sites was 248.9 Bq m^{-2} and for all pasture sites correspondingly 269.0 Bq m^{-2}. The mean ^{137}Cs inventory for the pasture sites amounted to 256.3 Bq m^{-2}, and the mean value for all shrubland sites was 292.3 Bq m^{-2}. The mean ^{137}Cs inventory for the measured lake sediment sites was 4801.8 Bq m^{-2}, while the median inventory amounted to 240.1 Bq m^{-2}.

3.3.1 Profile distribution model output

The mean erosion rate for all eroding sites calculated by the profile distribution model by ^{137}Cs corresponded to 0.82 kg m^{-2} $year^{-1}$, or 8.2 tonnes ha^{-1} $year^{-1}$. The mean erosion rate for the shrubland site was 0.85 kg m^{-2} $year^{-1}$ and the mean erosion rate for the pasture site was 0.79 kg m^{-2} $year^{-1}$.

3.3.2 Diffusion and migration model output for ^{137}Cs and $^{210}Pb_{ex}$

Diffusion and migration model (DMM) output suggests that erosion rates based on DMM-^{137}Cs range between 4.95–6.01 kg m^{-2} $year^{-1}$ for shrubland sites and 3.95–6.94 kg m^{-2} $year^{-1}$ for pasture sites, with a mean of 5.71 kg m^{-2} $year^{-1}$ for all sites, corresponding to 57.1 tonnes ha^{-1} $year^{-1}$. For $^{210}Pb_{ex}$ data, erosion rates obtained by DMM range between 1.61–2.03 kg m^{-2} $year^{-1}$ for shrubland sites, and between 1.00–1.98 kg m^{-2} $year^{-1}$ for pasture sites, with an overall mean of 1.63 kg m^{-2} $year^{-1}$ which corresponds to 16.3 tonnes ha^{-1} $year^{-1}$. These erosion rates were closer to PDM output for ^{137}Cs. The ^{137}Cs-DMM results did not agree with the other conversion model results, which appeared to be an effect of the irregular fallout giving inaccurate migration and diffusion coefficients.

3.3.3 Sediment accumulation rates

The average sediment depth (N=15) in João Penido reservoir was 0.25 m. Calculated SAR (cm $year^{-1}$) and accumulation of POC (g m^{-2} $year^{-1}$) from OC

data for sediment core samples in João Penido reservoir are summarized in Table 42, Figure 119. From field observations the sedimentation rate was calculated by dividing the thickness (cm) of the accumulated post-flooding sediment layer by the age of the reservoir (82–83 years depending on the year of sampling: 2016 or 2017), which gave SAR values between 0.07–0.44 cm year^{-1} in the reservoir. The POC accumulation rates were calculated by quantifying the inventory of POC (g) in the post-flooding sediment divided by the area of the sample corer (0.0028 m^2) and the age of the reservoir (years).

Average POC mass per volume (kg m^{-3}) was calculated by:

$$POC_{density} = \frac{POC_{tot}}{V}$$

Where POC_{tot} is the mean total mass of POC in the sediment cores (0.00986 kg) and V is the post-flooding volume of the core, derived from the core area (0.0028 m^2) and mean post-flooding sediment thickness (0.254 m). The average $POC_{density}$ was 13.86 kg m^{-3}.

An estimate of the total POC (kg) in the reservoir was then calculated as a product between the average POC mass per volume (13.86 kg m^{-3}) and calculated total reservoir sediment volume (753058.8 m^3). Based on these input factors the result gave a total POC inventory of 10196.41 tonnes in the reservoir post-flooding sediment. This would on average require a yearly net POC input of c. 127.29 tonnes year^{-1} into the reservoir storage since the year the dam was built (1934).

3.4 POC pathways and budget

A summary of POC pathways and budgets are presented in Table 42. Depending on which method that was used to calculate POC pathways and budget, slightly different results were achieved.

POC pathways and budgets

Erosion rates	Mean value	Unit
RUSLE (database)	37.8	tonnes ha^{-1} year^{-1}
RUSLE (observations of *C* and *K*, complete watershed)	10.9	tonnes ha^{-1} year^{-1}
RUSLE (observations of *C* and *K*, point samples of pasture and shrubland sites A and B only)	9.1	tonnes ha^{-1} year^{-1}

PDM-^{137}Cs	4.5	tonnes ha^{-1} year^{-1}
DMM-^{210}Pb$_{ex}$	16.1	tonnes ha^{-1} year^{-1}

POC erosion	**Mean value**	**Unit**
Calculated from RUSLE (database)	1.1	tonnes ha^{-1} year^{-1}
Calculated from RUSLE (database and observed *C* and *K*)	0.3	tonnes ha^{-1} year^{-1}
Calculated from RUSLE (database and observed *C* and *K*, of soil sites)	0.3	tonnes ha^{-1} year^{-1}
Calculated from PDM-Cs	0.1	tonnes ha^{-1} year^{-1}
Calculated from DMM-Pb	0.5	tonnes ha^{-1} year^{-1}

Catchment properties	**Value**	**Unit**
Catchment area	72140000	m^2
Area deforested grassland	52297821	m^2
% area deforested grassland in catchment	72	%
Reservoir area	3720000	m^2
Reservoir perimeter	22584	m

Total soil sediment remobilised in catchment deforested grasslands	**Mean value**	**Unit**
Calculated from RUSLE (database)	197686	tonnes year^{-1}
Calculated from RUSLE (database and observed C & K)	56743	tonnes year^{-1}
Calculated from RUSLE (database and observed C & K, of soil sites)	47486	tonnes year^{-1}
Calculated from PDM-^{137}Cs	42884	tonnes year^{-1}
Calculated from DMM-^{210}Pb$_{ex}$	84200	tonnes year^{-1}

Total soil POC remobilised in catchment deforested grasslands	**Mean value**	**Unit**
Calculated from RUSLE (database)	5535	tonnes year^{-1}
Calculated from RUSLE (database and observed C & K)	1589	tonnes year^{-1}
Calculated from RUSLE (database and observed C & K, of soil sites)	1330	tonnes year^{-1}
Calculated from PDM-^{137}Cs	1201	tonnes year^{-1}
Calculated from DMM-^{210}Pb$_{ex}$	2358	tonnes year^{-1}

Reservoir sediment	**Value**	**Unit**
Calculated total volume of sediment	753059	m3
Calculated total mass of sediment	1031691	tonnes
Average sediment density	1370	kg m^{-3}
Age reservoir postflooding sediment	82	years
Average accumulation of sediment in dam since 1934	12582	tonnes year^{-1}
Accumulation of sediment in dam since 1934 for each m^2	3.4	kg m^{-2} year^{-1}

Reservoir POC	**Value**	**Unit**
Average total mass of POC in all sediment cores (post-flooding)	9.86	g
Average core volume	0.0007112	m^3
Average total POC in sediment cores	13.86	kg m^{-3}

POC mass calculated from mean POC inventory	10440	tonnes
Calculated POC mass of sediment	1.4	%

Sedimentation rates	Mean value	Unit
Core observations	0.27	cm year^{-1}
CRS-^{210}Pb$_{ex}$ for SED5	0.5	cm year^{-1}
SAR based on ^{137}Cs peak in sediment core SED5 at 32 cm depth	0.6	cm year^{-1}
Calculated average SAR (QGIS) for the reservoir	0.3	cm year^{-1}
Accumulation of POC in dam since 1934	127	tonnes year^{-1}
Accumulation of POC in dam since 1934 for each m^2	105	kg m^{-2} year^{-1}
Calculated sediment yield	20.3	%

Table 37 Table of erosion rates, sedimentation rates and inventories of POC.

Figure 114 Sediment and POC transport in João Penido catchment and reservoir.

273

4 Conclusions

Soil erosion in the catchment of João Penido reservoir was modelled and measured by RUSLE and fallout radionuclides, and sediment volume and sedimentation rates were calculated from sediment cores from the reservoir. RUSLE output based partly on database data (R and LS) and partly on field observations (C and K) was considered the result closest to reality and averaged 10.9 tonnes ha^{-1} year^{-1}, which compared to other studies of similar systems in Brazil was deemed acceptable. RUSLE output based on database data only showed erosion rates up to 4 times higher than for partly field based output, indicating that field observations are important for validation of modelled results. Even though RUSLE results partly based on field observations indicate that erosion rates are lower than what would be achieved with available databases, the results still highlight that erosion is more extensive in perturbed deforested areas than in forested areas. 72% of the total catchment area comprised deforested grazing land which showed the highest erosion potential in the catchment. Erosion rates based on fallout radionuclide data were on the same order of magnitude as the model results and averaged 16.1 tonnes ha^{-1} year^{-1} for DMM-^{210}Pb$_{ex}$ and 8.2 tonnes ha^{-1} year^{-1} for PDM-^{137}Cs. These radionuclide erosion rates from field observations showed that the application of RUSLE was satisfactory as a method of soil erosion assessment in this type of impacted landscape.

The study catchment in this work is representative of a typical deforested Atlantic forest biome in Brazil and composes a representative study site to validate calculated soil erosion rates derived from the RUSLE model by field observations of fallout radionuclide inventories. Promising results provide confidence in the RUSLE model for upscaling and use of the model in other catchments with similar terrain, soils, climate and vegetation where the need to quantify soil erosion for ecosystem services and functioning are becoming increasingly necessary, for instance to motivate and mitigate restoration projects that reintroduce and preserve the precious biome of Atlantic Forest.

Disclosure statement

No potential conflict of interest has been recognised by the authors.

Manuscript 2: Importance of terrestrial particulate organic carbon (POC) for organic carbon accumulation in a tropical reservoir, Brazil

J.T.C. Snöälv[1], R. Mendonça[2,3], T.A. Quine[1] and S. Sobek[2]

[1]Department of Geography, University of Exeter, Exeter, UK
[2]Department of Limnology, Uppsala University, Uppsala, Sweden
[3]Department of Biology, Federal University of Juiz de Fora, Juiz de Fora, Brazil

Corresponding author: Jo Snöälv (j.snoalv@gmail.com)

Key Points:

- Soil organic carbon (SOC) composes an important contributor of POC to C burial and limnic storage in this Brazilian reservoir.
- Sources of sediment C indicate that soil erosion due to land use change (LUC) has contributed with significant input of soil organic matter during the presence of the reservoir since 1934.

Abstract

Particulate organic carbon (POC), commonly defined as the organic carbon (OC) fraction >0.45 μm, is a component of the carbon cycle that contributes to limnic storage of carbon in local to regional sediment traps in the landscape, e.g. wetlands, deltas, lakes and manmade reservoirs. POC originates from allochthonous sources, e.g. inputted by soil erosion and litterfall, and from autochthonous sources, e.g. in-stream growing macrophytes, biofilm and algae. Deposited POC can be buried or mineralized and emitted as greenhouse gases such as carbon dioxide (CO_2) and methane (CH_4) into the atmosphere. In the land-ocean aquatic continuum (LOAC), physical and chemical protection of organo-mineral aggregates and flocs determine the fate of catchment-derived POC. This study investigated whether allochthonous POC derived from terrestrial soils is more important than autochthonous POC from watershed sources for limnic storage in post-flooding sediments of a tropical reservoir. The input and sedimentation of allochthonous POC in the studied reservoir was estimated from

results of the Revised Universal Soil Loss Equation (RUSLE) soil erosion model, GIS analysis and from soil and sediment core observations. POC was calculated from C inventories of reservoir sediment cores collected along the delta–reservoir gradient and linked to organic matter content by loss on ignition (LOI). POC sources were determined by carbon-nitrogen ratio (C/N) analysis. Finally a POC budget was calculated for the post-flooding reservoir sediments. The results showed that soil derived allochthonous POC sources contributed with OM is an important source for limnic storage of organic carbon in this Brazilian reservoir.

Plain Language Summary

Particulate organic carbon (POC) content of post-flooding sediments was quantified for a small tropical reservoir in Brazil. The relative net input of allochthonous and autochthonous organic matter was assessed through soil erosion studies and field observations and C:N analysis. The post-flooding sediments composed on average

1 Introduction

About 25% of the land area in Brazil is used for agriculture and total soil erosion rates from these cultivated soils (including pasture) amount to c. 800 million tonnes year^{-1} (Merten and Minella, 2013). Clear cutting of forested land with subsequent conversion into cultivated fields or pasture not only increases land degradation, but also reduces natural ecosystem function and diversity. A highly impacted biome in South America is the Atlantic forest, which composes a biodiversity hotspot that mainly over the past c. 500 years has been reduced to less than 12% of its original extent of almost 1.5 million km^2 on the South American continent (Ribeiro et al, 2011). Similarly, in Brazil, deforestation practices have reduced corresponding Brazilian Atlantic forest (Mata Atlântica) to c. 8% of its original extent (Colombo & Joly, 2010). Atlantic forest contains exceptional biodiversity from a wide range of altitudes over coastal to inland areas that stretch from tropical to subtropical regions over the continent, but is threatened by severe habitat loss and increased fragmentation due to land use change (Ribeiro et al, 2009) and the increased land degradation which typically follows deforestation.

Manmade dams and reservoirs are effective sediment traps in the landscape that contribute to the acreage of semi-permanent water bodies which may act as emission hotspots of greenhouse gases such as carbon dioxide (CO_2) and methane (CH_4) (Barros et al, 2011; Maeck et al, 2013). Reservoirs also act as containers holding limnic storage of eroded soil and organic matter. While human impact has increased global soil erosion input into the aquatic continuum with about 2.3 ± 0.6 Giga-tonnes year^{-1}, there has been a reduction in sediment loads reaching the coastal oceans by 1.4 ± 0.3 Giga-tonnes year^{-1} due to entrapment within reservoirs and dams (Syvitski et al, 2005). When accounting for the effect of sediment trapping modelled global average input of sediments from the continents to coastal oceans amount to about 19 Pg year^{-1} (Beusen et al, 2005) and globally over 100 Giga-tonnes of sediment is estimated to be retained within reservoir storage, containing 1–3 Giga-tonnes of carbon (Syvitski et al, 2005). Moreover, about 75% of the organic carbon (OC) that is deposited in reservoir sediments is derived from allochthonous sources (Maavara et al, 2017). Eroded soil particles that end up in reservoir storage remove organic carbon from terrestrial soils and contribute with soil organic matter (SOM) to either fuel mineralisation or add input of POC to semi-permanent reservoir storage. Human perturbation on the natural landscape that leads to this increased flux of soil particles into the aquatic continuum and reservoir storage results not only in geomorphic disturbance but also degradation of terrestrial soil carbon deposits which previously were stabilized by the original forested ecosystem.

The objective of this work was to quantify the relative inputs of allochthonous and autochthonous organic matter into limnic storage and determine the fate of organic carbon in post-flooding sediments of a tropical reservoir

2 Materials and Methods

2.1 Field site

João Penido reservoir (LAT: –21.675459, LONG: –43.394960) is a drinking water reservoir built in 1934 for the city Juiz de Fora in state Minas Gerais, Brazil. The lithology of the catchment comprises metamorphic rocks, such as

Neoproterozoic schist and Rhyacian orthogneiss (CPRM 1:1M, 2018)[32]. The dominating soil type in the area is mapped as orthic ferralsol/ultisol (CPRM, 2016), characterized by highly weathered soil. The regional landscape is dominated by an undulating topography with mean slope values of 16% (Bacchi et al, 2003). The catchment which drains into João Penido reservoir has slope values ranging between 0–27 degrees (DEM analysis). The terrain of the João Penido reservoir catchment ranges between 684–1061 m.a.s.l. (DEM analysis) while the main water body is located at ca 457 m.a.s.l. The Köppen classification system categorizes the region as Cwa, which composes a sub-tropical climate with two distinct seasons composed of dry winters in May–September and rainy hot summers in October–April (Bucci et al, 2015), with the hottest months having mean temperatures >22°C. The annual rainfall on a regional scale for south-eastern Brazil range between 1200–1600 mm year^{-1} (da Silva, 2004), and for Juiz de Fora, the city located closest to the study site at c. 3.8 km distance, the mean annual rainfall amounted to 1949 mm year^{-1} between 1979–2013, with a minimum and maximum ranging between 1347–2949 mm year^{-1} (Global Weather Data for SWAT). The vegetation of the watershed is mapped as semi-deciduous forest belonging to the Atlantic forest biome[33], however most of the catchment area comprises deforested grasslands used for pasture. The local land use in the catchment compose mainly pasture and more sparse agriculture. Main parts of the land in direct connection to the reservoir compose deforested shrubland owned by the reservoir owner or local residence. The catchment of João Penido was and adequate site to study the effect of human perturbation where LUC in the form of deforestation and agricultural practices have taken place over the past century, and in addition, a manmade hydrological barrier built in 1934 to establish a drinking water reservoir, affect the natural inventories and redistribution of POC.

2.2 Soil erosion modelling with RUSLE

The upgraded empirical soil loss model Revised Universal Soil Loss equation (RUSLE) is based on the original Universal Soil Loss equation (USLE) model,

---

[32] URL: http://portal.onegeology.org/OnegeologyGlobal/
[33] Mapa de Vegetacão do Brasil (1992) http://mapas.mma.gov.br/mostratema.php?temas=vegetacao

initially developed by United States Department of Agriculture (USDA). It composes a product of the following six factors:

$$A = RKLSCP$$

where A is the calculated yearly mean soil erosion (metric tonnes ha^{-1} year^{-1}), R composes the yearly rainfall erosivity factor, K is the soil erodibility factor, S and L compose the slope steepness and slope length factors respectively, C is the vegetation and crop management factor, and P represents specific erosion control practices. The RUSLE model was used to quantify soil erosion in the catchment of João Penido and is described in previous work.

2.3 Field sampling

Sampling sites of soil and sediment were prepared by DEM analysis of the catchment with *QGIS 2.14 Essen*, using random allocation (*Random Points inside Polygon tool*).

2.3.1 Sampling

The soil sampling was conducted in dry conditions in May–June 2016, with additional sediment sampling in 2017. Soil samples from hand-dug pits were collected from the surface down to a maximum of 80 cm depth. Custom-made samplers were used to obtain a vertical soil profile in 20 cm segments from which increments were extracted with a spatula from every 2 cm sections in the top soils (<20 cm) and for subsoils (>20 cm) by 5 cm increments. Samples were stored in plastic zip-bags, after removal of larger particulates (e.g. stones, pebbles, roots). The samples were initially weighed, air dried and stored in room temperature before transport to University of Exeter, UK. Sediment samples were collected by a gravity corer from a boat within the main water body and in some of the reservoir arms (Figure 121). The cores were transported on the sampling day from the field to the laboratories at Federal University of Juiz de Fora and subdivided into 2 cm increments before being air dried. The samples were stored in sealed plastic zip-bags, before analysis at University of Exeter, UK.

2.4 Analytical methods

2.4.1 Bulk density and loss on ignition

The previously air-dried soil and sediment samples were oven-dried at 40°C for 24–48 hours, and weighed, ground, and sieved by hand to <2 mm fraction. 182 sediment and 219 soil samples from the João Penido reservoir were analysed for loss on ignition (LOI). Previously oven-dried (40°C) were subsampled and oven-dried at 100°C in pre-weighed crucibles overnight, before initial sample weighing and combustion at 550°C for 4 hours, before re-weighing.

2.4.2 C/N ratio

100 sediment samples and 50 soil samples were subsampled (15–20 mg) into silver capsules and pre-treated by acid fumigation with HCl (37% HCl, Sigma-Aldrich) using 10 mL per 50 samples for 24 hours in a desiccator to remove carbonates. The samples were stored in a desiccator, before encapsulated into larger tin capsules and analysed by a Flash 2000 Organic Elemental analyzer (CE Instruments Ltd). 90 subsamples fractionated by size and density were also analysed for C/N. Ethylenediaminetetraacetic acid (EDTA) standard (BDH AnalaR, assay 99.0%) was used as an internal standard and the percent error of the instrument was calculated to 0.65%.

2.4.3 Size and density fractionation

To understand the geochemical imprint of the aggregate-bound soil derived organic matter with respect to other sources in the sediments, density fractionation was done on 8 soil samples and 7 sediment samples. These samples were selected from four soil cores and four sediment cores, where 2 samples from the top layer (appropriate sample from the top 10 cm) and sub layers (appropriate samples from between 20–30 cm depth) were selected from each core respectively. Additionally, two samples from two sediment cores were selected from pre-flooding material. Two of the soil sites were from land used as pasture and two sites from non-managed shrubland. The sediment sites were located in deepest part of the reservoir (accumulation site) and from a site in the central part of the main water body. The previously dry-sieved samples (<2 mm)

were wet-sieved into 3 fractions each: >250 µm, 250>53 µm, and <53 µm. The samples were flushed with deionized water until a clear solution was visible, indicating sufficient loss of the finest fraction from the two coarser fractions. In samples where a floating fraction occurred, this material was separated from the 2000>250 µm fraction to remove inter-aggregate organic material, which is not considered SOM, e.g. roots. In samples where the <53 µm fraction appeared to be superfluous, a sample was retrieved from a maximum of 200 mL sieved solution, however to make sure the larger fractions were free of excess fine fractions the flushing continued until the sieving solution was clear. The solution with the <53 µm fraction was centrifuged (Thermo Scientific Multifuge 4KR) for 20 minutes at 1200 rpm before decantation and sampling. The samples were then oven-dried for 24 hours in aluminium beakers at 50 degrees C. Density separation of particles was then done with aqueous sodium polytungstate (SPT) liquid (CAS#12141-67-2) diluted with deionized water to achieve a density of 1.85 g cm^{-1}, to separate the inter-aggregate and intra-aggregate OM fractions respectively, following the method by Six et al (2002). Subsamples of up to 2 mL volume (where sufficient material had been obtained from wet-sieving) were added to centrifuge tubes containing 3 mL of the SPT solution. The samples were thoroughly mixed by a Vortex Mixer, and then centrifuged at 1200 rpm (Thermo Scientific SL 16, acceleration 9, deceleration 6), for 20 minutes, which separated the samples into a light fraction (LF) and a heavy fraction (HF). The light fraction was retrieved by either careful decanting of the surface solution or by using a spatula to scoop up the floating LF, and the clear solution between LF and HF was reclaimed before the heavy fraction could be recovered. The sample fractions were then freeze-dried at –42 degrees C for 36 hours, and prepared for C/N analysis (see above).

2.4.4 Sediment thickness

The sediment thickness was determined by the presence of pre-flooding material with depth, sediment accumulation rate (SAR) (cm year^{-1}) was simply calculated by the following:

$$SAR = \frac{d}{t_r}$$

Where *d* is the depth of the pre-flooding material and t_r is the reservoir age, which was 82 years for the 2016 sampling campaign and 83 years for the additional 2017 sediment core collection.

2.4.5 Data interpretation

The statistical software used for data interpretation was Microsoft Excel (2013) and RStudio version 1.1.453 (2016).

3 Results and discussion

3.1 Bulk density

The mean bulk density of soils from João Penido was 1.03 g cm^{-3}. For top soils down to 20 cm depth, the mean bulk density amounted to 1.00 and 1.05 g cm^{-3} for shrubland soils and pasture soils respectively. This low soil bulk density is likely due to high porosity and compared to sediment relatively coarse grain size. For sediment the average bulk density amounts to 1.37 g cm^{-3} (which indicates high porosity and organic matter content), and for observed pre-flooding material the average density is 1.61 g cm^{-3} (Table 43).

3.2 Loss on ignition

The highest concentrations of organic matter were present in samples from delta (30.76%) and reservoir post-flooding sediments (22.51%), while samples from soils (13.99%), colluvium (9.29%) and pre-flood soils (11.46%) exhibited low mean concentrations (Table 44, Figure 122). The low mean organic matter content in the post-flooding sediments showed that the minerogenic fraction was dominating. This minerogenic fraction originates from a terrestrial soil source and represents various inputs of soil erosion over the lifetime of the reservoir.

3.3 C/N ratios

The delta sediment cores showed C/N values of 8.07–29.56, with a mean of 15.34 (Table 45), indicating that most of the organic matter in the delta sediments (profiles 4A and 4B) in general contained organic matter of more allochthonous origin. Lake sediments in the deeper parts of the reservoir showed C/N ratios ranging between 3.42–65.37 with a mean of 13.56, while in soil samples displayed the highest C/N ratios of the catchment samples, ranging 2.53–386.36 with a mean of 48.08. The mean C/N ratio of post-flooding sediments (excluding pre-flood material) from 5 cores was 13.49 ($N=5$, $sd=1.65$). Samples of soil profiles (JP02, JP06, JP14, JP17, and JP28) typically showed C/N ratios above 20. The top sediments of delta samples from profiles SED4A and SED4B showed mixed towards slightly more terrestrial C/N ratios, while the deeper sediments of SED4B indicated mixed source to a more aquatic origin with lower C/N values. The sediment sites showed mainly low C/N values typical of lake sediments with aquatic origin, although a few outliers of SED2A and SED3C appear to have sediment layers indicative of terrestrial input. Non-fumigated samples show somewhat different C/N ratios, with less extreme values. Especially for sediments these samples showed less variation.

The relationship of C/N and concentrations of POC% (OC%) showed positive correlation in reservoir sediment, and negative correlation with the much higher ratios in soils, and weakly negative relationship with samples of delta sediments. The differences in C/N signatures are distinct for the terrestrial and aquatic samples.

3.4 Size and density fractionation

Samples separated by wet-sieving into fractions >250 μm, 250>53 μm and <53 μm showed maximum C/N values (17.22–126.15) in fine fraction soil samples from pasture sites (Figure 51). All fractions from samples of pasture soils showed more enriched OC% and N% content compared to shrubland, while the highest concentrations occurred in reservoir sediments (Figure 52).

3.5 Postflooding volume

Sediment volume was interpolated from sediment pre-flood depth observations ($N=15$) by IDW. The resulting interpolated map (Figure 75) showed sediment

thickness ranging between 0.06–0.52 m across the reservoir reach. The interpolated average sediment thickness equalled 0.27 m. Total post-flooding sediment volume was then calculated with the SAGA tool *Raster volume,* resulting in 753058.8 m^3. This equalled roughly an average sediment accumulation of 9183 m^3 $year^{-1}$ in the reservoir since it was built in 1934, with an average linear sediment accumulation rates of 0.3 cm $year^{-1}$. The average sediment density was assumed to be 1.37 g cm^{-3} and the mass of sediment in the reservoir was then calculated to 1031690.56 tonnes.

3.6 Sediment accumulation rates (SAR)

The average sediment depth (*N*=15) in João Penido reservoir was 0.254 m. Calculated SAR (cm $year^{-1}$) and accumulation of POC (g m^{-2} $year^{-1}$) from OC data for sediment core samples in João Penido reservoir are summarized in Table 46. From field observations the sedimentation rate was calculated by dividing the thickness (cm) of the accumulated post-flooding sediment layer by the age of the reservoir (82–83 years depending on the year of sampling: 2016 or 2017), which gave SAR values between 0.07–0.44 cm $year^{-1}$ in the reservoir. The POC accumulation rates were calculated by estimating the inventory of POC (g) in the post-flooding sediment divided by the area of the sample corer (0.0028 m^2) and the age of the reservoir (years). Figure 126 shows calculated SAR in the reservoir by inverse distance weighting interpolation.

While SAR vary across the reservoir gradient, the OC data showed OC accumulation with a minimum and maximum rate of 5.99 and 93.46 g OC m^{-2} $year^{-1}$, respectively. Average POC mass per volume (kg m^{-3}) was calculated by:

$$POC_{density} = \frac{POC_{tot}}{V}$$

Where *POC$_{tot}$* is the mean total mass of POC in the sediment cores (0.00986 kg) and *V* is the post-flooding volume of the core, derived from the core area (0.0028 m^2) and mean post-flooding sediment thickness (0.254 m). The average *POC$_{density}$* was 13.86 kg m^{-3}.

285

An estimate of the total POC (kg) in the reservoir was then calculated as a product between the average POC mass per volume (13.86 kg m^{-3}) and calculated total reservoir sediment volume (753059 m^3). Based on these input factors the result gave a total POC inventory of 10440 tonnes in the reservoir post-flooding sediment. This would on average require a yearly net POC input of c. 127 tonnes year^{-1} into the reservoir storage since the year the dam was built (1934).

3.7 POC concentrations in soils and sediment

POC inventories POC_{inv} (g m^{-3}) for soil are summarized in Table 47. The POC% soil profiles showed that many of the shrubland sites had low variability in POC content with depth, compared to pasture sites which were more enriched in top soils.

The sediment profiles presented in Figure 128 showed that POC concentrations tend to be lower in pre-flood material beneath the post-flooding sediment. As expected, POC% also tends to be higher in sediment profiles of reservoir arms and at the deltaic site (SED4, SEDJP01, SEDJP05, SEDJP07, SEDJP08, SEDJP09, SEDJP10, SEDJP13, SEDJP16), due to the shallower waters being abundant in growing macrophytes and algae in these parts of the reservoir. Most of the deeper open water sites of the main reservoir body (SED1, SED2, SED3) lack the declining POC% profile typical of the shallow reservoir arm sites, although the accumulation sites at SED5C and SEDJP17 showed a distinct difference in POC% of post-flooding sediment and sub-bottom pre-flooding material. The IDW interpolated POC distribution in the reservoir is presented in Figure 84.

3.7.1 POC redistribution in the catchment soils and sediments

The soil samples in this study were retrieved from pasture and shrubland, which represents ca 70% of the catchment. Although these soils can be considered relatively poor in organic matter and carbon, the redistribution of existing SOC may be mineralised and released as inorganic C species when exposed to the atmosphere or enter the aquatic system to contribute to buried organic matter in the reservoir. Compared to SOC stocks from national surveys such as Batjes

et al (2005) who summarized SOC distribution in different soil groups of Brazil and reported mean concentrations of 5.2 kg C m^{-2} for the upper 30 cm and 9.6 kg C m^{-2} for the upper 100 cm of ferralsols of Brazil, the soil carbon inventories (with its low content of inorganic carbon) found in this study are within the same comparable range with an average of 5.8 kg C m^{-2} in the upper 20 cm of catchment top soil. The resulting POC erosion map derived from RUSLE model output and average POC inventory in catchment grassland soils, indicated that a mean of 0.3 tonnes ha^{-1} year^{-1} is mobilized annually in the surface soil layer. This assumes negligible erosion in land use classes such as built up areas and broadleaf woods of the catchment.

The reservoir sediment characteristics showed that the average organic matter concentration in top sediments (2 cm) was 28.3%, while the remaining mass composed inorganic material (Figure 109) and that at 30 cm depth the average concentration was 10.7% lower. This low concentration (c. 17%) was maintained with depth. As pre-flood material have OM concentrations similar to terrestrial soils, it is likely that overlying layers of post-flooding sediment with low concentrations compose mainly terrestrial aggregate-bound SOC, and that surface sediments compose partly terrestrial allochthonous matter (equivalent of average soil OM%, c. 13.99%) and additional autochthonous OM. Simplified, the autochthonous part would compose the difference between total OM% and assumed allochthonous OM%, which when using the average concentrations amount to an average of 8.53% (22.55–13.99%). If these assumptions are valid the dominant source of OM in the reservoir sediments is terrestrial. These estimations only consider matter-dry weight and therefore do not represent dissolved OM in e.g. pore space solution of these fluffy post-flooding sediments. Post-flooding sediment bulk density was calculated to 1370 kg m^{-3} and this relatively low bulk density suggests that the porosity and water content are high in the post-flooding surface sediment, in which the concentrations of DOM become important, however this parameter was not specifically measured in this work.

In João Penido reservoir, POC contributions from allochthonous and autochthonous sources might be dependent on seasonal variation due to the local climate. In a study of reservoir Kentucky Lake, USA, by Yurista et al (2001), it was found that autochthonous POC was mainly inputted into the

reservoir during the summer months while allochthonous POC dominated during winter. In contrast, a study on POC sedimentation in oligotrophic Loch Ness in Scotland, Jones et al (1997) showed that allochthonous sources composed the dominant form of POC, with peak inputs in late winter to spring explained by higher riverine discharge. Upstream allochthonous POC mainly consist of litter and soil organic carbon, and primarily rainfall erosion events control these terrestrial inputs. In summer autochthonous POC sources such as growing macrophytes, algae and microbes are likely more important for POC production and sedimentation. For the eutrophic João Penido reservoir, POC mass of post-flooding sediments were estimated and the seasonal variability could not be determined from the samples collected and analysed, but it is probable that both growing biota and rainfed soil erosion contribute with POC into this reservoir.

C/N ratio of sediment POC showed the typical mixed source limnic signature of organic matter composition in João Penido reservoir, while pre-flood material had more terrestrial like signatures, which appears to confirm the boundary of post- and pre-flood material. Although the C/N data showed mixed terrestrial and aquatic signatures in post-flooding sediments, peaks in C/N indicate high input of terrestrial organic matter. These peak sediment layers are likely related to events of high erosion input.

Particle size appears more varied with depth in sediment cores compared to soil cores, which likely is connected to varying particle size input from soil erosion into the reservoir due to high-energy runoff during rainfall events in the catchment, where higher energy has mobilized coarser grain fractions.

3.7.2 Concentrations of organic matter and OC quality

Comparison between the OC data obtained from C/N analysis and calculated from OM data obtained by LOI analysis, revealed that the commonly used conversion factor of 0.58 (Pribyl et al, 2010) is too high for soils of João Penido watershed, when converting OM concentrations obtained from LOI analysis to OC concentrations. Soils showed varying OM% content with respect to land use, and soil samples from pasture in general displayed a wider range of OM%

than samples from non-managed shrubland. For terrestrial soils the lowest C% values appeared in colluvium, mainly in subsoils at depths >15 cm. In general, POC% decreased with depth in most pasture and colluvium profiles, while shrubland soils often showed lower content in the surface layer with mostly consistent POC content with depth. An explanation for this is that pasture is being continuously fertilized which promotes plant growth and organic matter input, while shrubland soils remain nutrient poor and often compose sandy texture in the top layer. Soil organic matter inventories appeared to be of consistent concentrations for all the eroding soil sites, but lower for seasonally dry colluvium. Soil to sediment transects revealed that colluvium was depleted in organic matter compared to eroding soils. This OM has likely been washed out and accumulated in reservoir sediments together with autochthonous OM. In sediments the density separated samples showed that the C/N signature of post-flooding sediment showed increasingly more terrestrial like signatures with depth, suggesting that this SOC is preferentially preserved with depth.

For the aquatic sediment sites, sites in the delta and shallow reservoir arms (depth c. 1 m) showed the highest POC content, while they were depleted further out in deeper (c. 8–10 m) reservoir sediments. C/N ratios were typically lower in reservoir sediments compared to deltaic sediment and soils and the C/N data also showed that deeper sediments were characterized by lower concentrations of carbon and nitrogen compared to the surface sediments. A higher C/N ratio is associated with terrestrial soil organic matter, which agreed with the distribution in the João Penido sediments.

3.7.3 OC accumulation in sediments

The calculated OC accumulation rates appear to be sensible for João Penido catchment. The average POC content of terrestrial soils from LOI data (2.8%) in the João Penido catchment and pre-flood material (2.9%) beneath post-flooding sediment in the reservoir suggest that the mineral aggregate associated POC content is general for soil particles in the catchment. If it is assumed that the mean soil POC value of 2.8% in this study is recalcitrant both in terrestrial soils and in eroded soils that have entered and been redeposited in the reservoir, while the average reservoir sediment POC value is 4.5%, this

would suggest that the excess POC in the sediment is of aquatic origin. Most of the sediment cores in the shallower water profiles showed POC profiles with declining POC concentrations with depth, indicating that there had been vertical loss of organic carbon from the surface sediment to the pre-flood material. The similar POC content of terrestrial soil and pre-flood matter suggest that mineral aggregate bound POC is physically protected from processes which transform organic carbon (e.g. microbial respiration), and that the organic matter loss mainly affects autochthonous organic matter. If it is assumed that the average difference (2.1%) of the total POC and in the reservoir is of aquatic origin, this would be an equivalent of autochthonous POC amounting to c. 4883 tonnes of the total POC mass (10440 tonnes) in the reservoir post-flooding sediment, or almost 47% of the total POC in post-flooding sediment is autochthonous.

The estimated quantity of the allochthonous component of terrestrial POC in post-flooding sediments is based on many assumptions about the average SOC content in the catchment soils, the quantity of inputted soil mass into the reservoir over the years since the dam was built, and recalcitrance of the mineral-associated organic carbon fraction. Because of all these assumptions, this output can only provide a simplified picture of the actual carbon transport and fate in this catchment, however the results appear to be within a plausible order of magnitude for such a system.

The results indicated that soil-derived aggregate-bound POC was an important source of organic carbon in the reservoir sediments of João Penido, but sample numbers from density fractionated C/N samples were insufficient to determine whether OC storage is controlled by allochthonous or autochthonous POC. Further analysis of a higher sample number, would statistically increase the confidence of the results. An overview of the OM and OC budget in the calculated mass of the reservoir sediments suggested that with depth heavy aggregate-bound and therefore physically protected OM increased in relation to free light organic matter.

Some extreme values of soil C/N were observed in the results. Average C/N ratios of world soils range between 9.9–25.8 (Batjes et al, 2014) and in this study the average SOC value amounted to 48.08, which was likely skewed by outliers in the dataset. Five samples had C/N ratio >100, mainly samples from the deeper layers of the soil profiles. Either the nitrogen content was depleted

for these outlier samples, or something happened during the analytical processing. Other analyses of qualitative properties were not measured in this study, but would have contributed to the interpretation when discriminating between allochthonous and autochthonous POC in the post-flooding sediments.

Figure 115 Sediment and POC transport in João Penido catchment and reservoir.

In summary, the study in João Penido catchment showed that
- POC erosion from surface soils calculated by RUSLE and SOC inventories amounted to an average rate of 0.02–0.11 kg m^{-2} year^{-1},

- A large component of the POC in post-flooding sediments was autochthonous, but that in deeper layers organic carbon bound to soil-aggregates from allochthonous sources composed a major component of POC,

- Soil erosion measured in the field by empirical methods utilizing fallout radionuclides revealed that ^{137}Cs was less useful, whilst ^{210}Pb$_{ex}$ showed more potential as a soil erosion tracer,

- The RUSLE model worked adequately in this deforested environment, however the results varied greatly depending on which input factors were used. It was demonstrated that the RUSLE model was a useful tool to calculate average erosion rates in the catchment (validated by field observations) and that the accuracy of the modelled results increased with improved detail in input factors.

4 Conclusions

POC erosion from soils in the catchment were calculated and compared with the total mass of POC input during the lifetime of the reservoir determined for reservoir sediments. The sediment data suggested that c. 12581.6 tonnes year^{-1} has accumulated in the reservoir since the dam was built 1934.

The results showed that the redistribution of particulate SOC from terrestrial soils into the reservoir contributed to semi-permanent limnic storage of carbon, while it seems that mostly autochthonous aquatic-produced carbon is subject to mineralisation processes in the sediments. The results indicate that not all autochthonous organic matter is mineralised, but that some is present in limnic storage at sediment depth, mixed with terrestrially sourced POC. This relocation of terrestrial organic carbon is in this catchment likely a result of land use change (LUC) such as deforestation and damming, and serves as an example of how effects of human perturbation of the natural ecosystem change the pathways of carbon. Future problems of such a landscape include for instance degradation in soil and land quality, along with increased greenhouse gas emissions from artificial reservoirs in which eroded soils are trapped as sediments together with autochthonous POC.

Disclosure statement

No potential conflict of interest has been recognised by the authors.

Appendix 2

Exmoor project

Descriptive tables

Descriptive Statistics: pH, EC (mS), T$_{water}$ (°C) of Exmoor streams

Variable	Site	N	N*	Mean	SE Mean	StDev	Min	Q1	Median	Q3	Max
pH	A	9	0	7.48	0.21	0.62	6.38	6.86	7.7	7.96	8.15
	B	9	0	7.29	0.18	0.54	6.31	6.77	7.52	7.69	7.85
	C	9	0	7.33	0.15	0.46	6.47	6.91	7.5	7.67	7.77
	D	9	0	7.25	0.13	0.39	6.48	6.94	7.42	7.52	7.65
	E	9	0	6.7	0.15	0.44	6.16	6.39	6.58	6.93	7.62
	F	9	0	6.79	0.13	0.39	6.4	6.5	6.65	7.06	7.63
	G	9	0	7	0.16	0.47	6.42	6.61	6.88	7.36	7.87
	H	9	0	7.16	0.14	0.42	6.49	6.8	7.14	7.5	7.81
	I	8	0	4.94	0.1	0.29	4.3	4.83	5.07	5.1	5.22
EC (mS)	A	9	0	0.06	0	0.01	0.04	0.05	0.05	0.07	0.07
	B	9	0	0.06	0	0.01	0.05	0.05	0.06	0.07	0.08
	C	9	0	0.03	0.01	0.02	0	0.02	0.03	0.05	0.06
	D	9	0	0.05	0	0.01	0.04	0.04	0.05	0.07	0.07
	E	9	0	0.06	0	0.01	0.04	0.05	0.06	0.07	0.07
	F	9	0	0.04	0.01	0.02	0.02	0.02	0.05	0.06	0.07
	G	9	0	0.05	0	0.01	0.03	0.05	0.05	0.07	0.07
	H	9	0	0.09	0.01	0.03	0.01	0.09	0.09	0.1	0.11
	I	8	0	0	0	0	0	0	0	0.01	0.01
Temperature stream water (Celsius)	A	9	0	8.42	0.85	2.55	5.7	6.85	7.7	9.85	14
	B	9	0	8.16	0.73	2.19	5.6	6.7	7.8	9.25	12.9
	C	9	0	7.77	0.83	2.49	5.1	6.05	7.2	9.1	13.2
	D	9	0	9.03	0.68	2.05	6.2	7.7	8.7	10.1	13.3
	E	9	0	8.85	0.73	2.18	6.66	7	8.5	10.1	13.5
	F	9	0	8.73	0.86	2.57	5.3	6.85	8.6	10.4	13.9
	G	9	0	9.33	0.86	2.59	6.3	7.05	9.1	11.15	14.4
	H	9	0	9.6	0.72	2.16	7.1	7.85	9.1	11.15	13.9
	I	8	0	7.35	1.13	3.2	4.2	4.85	6.5	9.52	13.7

Table 38 Bimonthly-monthly stream water data from 9 sampling campaigns between 2017-04-24–2018-05-01.

Diagrams
pH, electrical conductivity (EC) and temperature

pH in Exmoor streams

EC in Exmoor streams
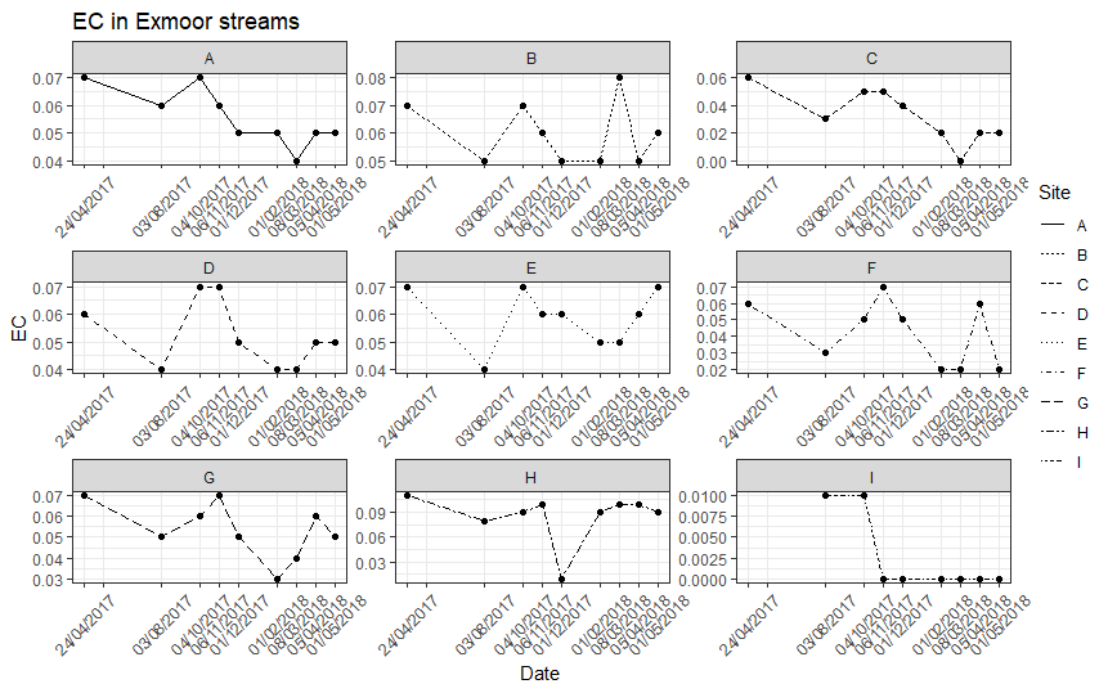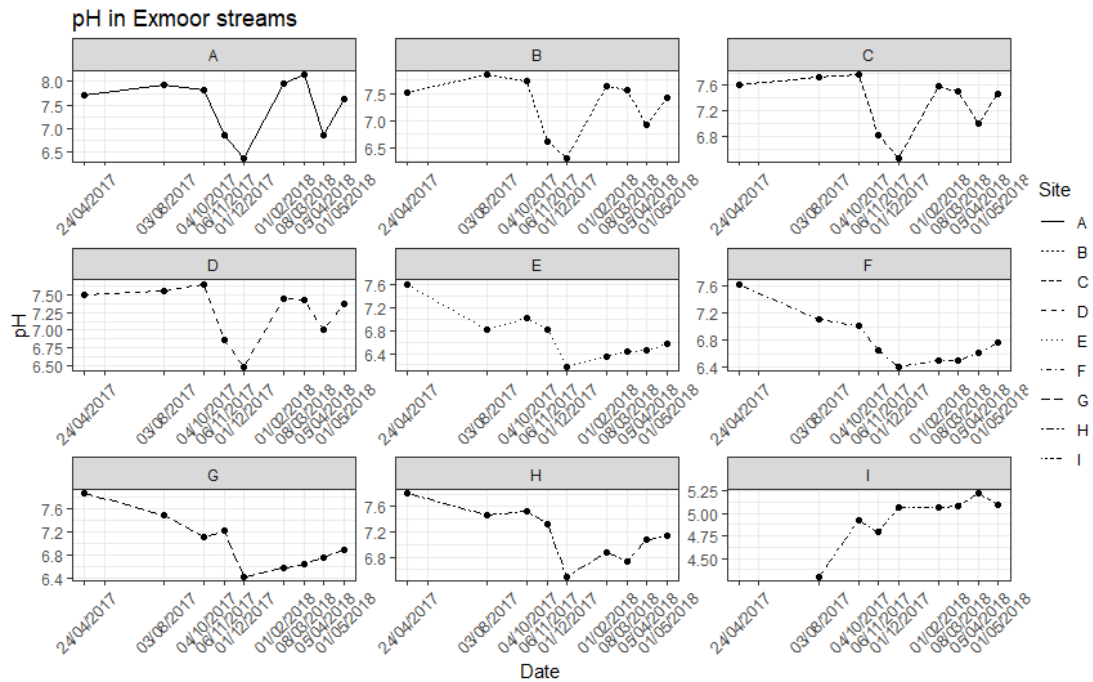
Descriptive Statistics: TSP mg L^{-1} & OM mg L^{-1}

Variable	Site	N	N*	Mean	SE Mean	StDev	Min	Q1	Median	Q3	Max
TSP mg L^{-1}	A	8	1	0.92	0.28	0.78	0.2	0.31	0.71	1.26	2.6
	B	8	1	1.3	0.31	0.87	0.35	0.77	1.15	1.49	3.25
	C	8	1	0.7	0.19	0.53	0	0.3	0.66	1.13	1.6
	D	8	1	1.15	0.25	0.7	0.43	0.6	0.97	1.63	2.5
	E	8	1	0.85	0.25	0.71	0.2	0.34	0.58	1.5	2.16
	F	7	2	0.46	0.13	0.34	0.2	0.25	0.31	0.6	1.18
	G	8	1	1.94	1.03	2.9	0.2	0.5	0.92	1.8	9
	H	8	1	1.67	0.48	1.37	N/A	0.85	1.45	2.66	4.15
	I	7	1	0.29	0.08	0.22	0.05	0.1	0.28	0.55	0.63
OM mg L^{-1}	A	5	4	0.03	0.01	0.03	0.01	0.01	0.03	0.06	0.09
	B	5	4	0.06	0.01	0.03	0.03	0.03	0.05	0.08	0.1
	C	5	4	0.02	0.01	0.01	0	0.01	0.02	0.03	0.04
	D	5	4	0.04	0.01	0.02	0.02	0.02	0.03	0.06	0.07
	E	5	4	0.02	0.01	0.02	0.01	0.01	0.01	0.04	0.05
	F	4	5	0.03	0.02	0.04	0.01	0.01	0.01	0.07	0.09
	G	5	4	0.1	0.07	0.16	0.02	0.02	0.03	0.22	0.38
	H	5	4	0.09	0.03	0.06	0.02	0.03	0.08	0.15	0.16
	I	4	4	0.01	0	0.01	0	0	0.01	0.02	0.02

Table 39 Descriptive statistics of TSP and OM (mg L^{-1}) of Exmoor streams.
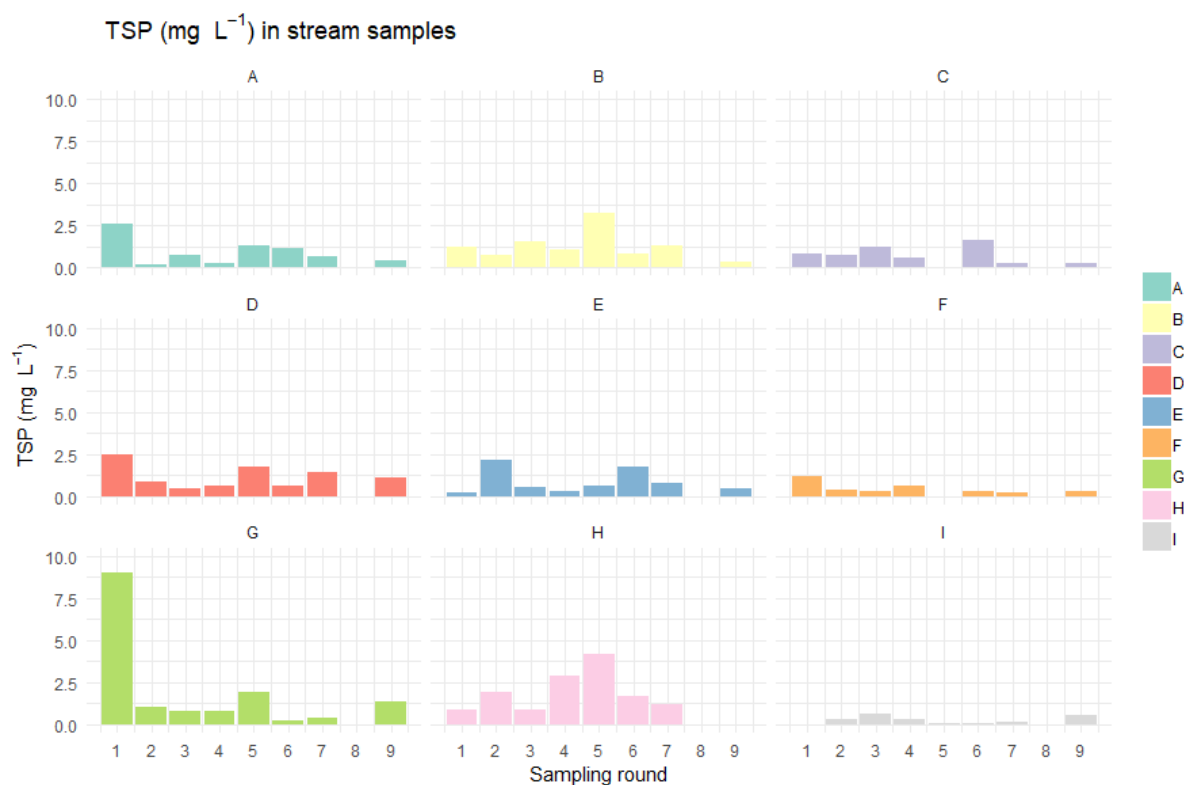
Figure 116 Total suspended particulates (TSP) of stream samples.

OM% of TSP in stream samples

Figure 117 POM% of TSP (mg L⁻¹) in stream samples.

POC (g L⁻¹) in Exmoor streams
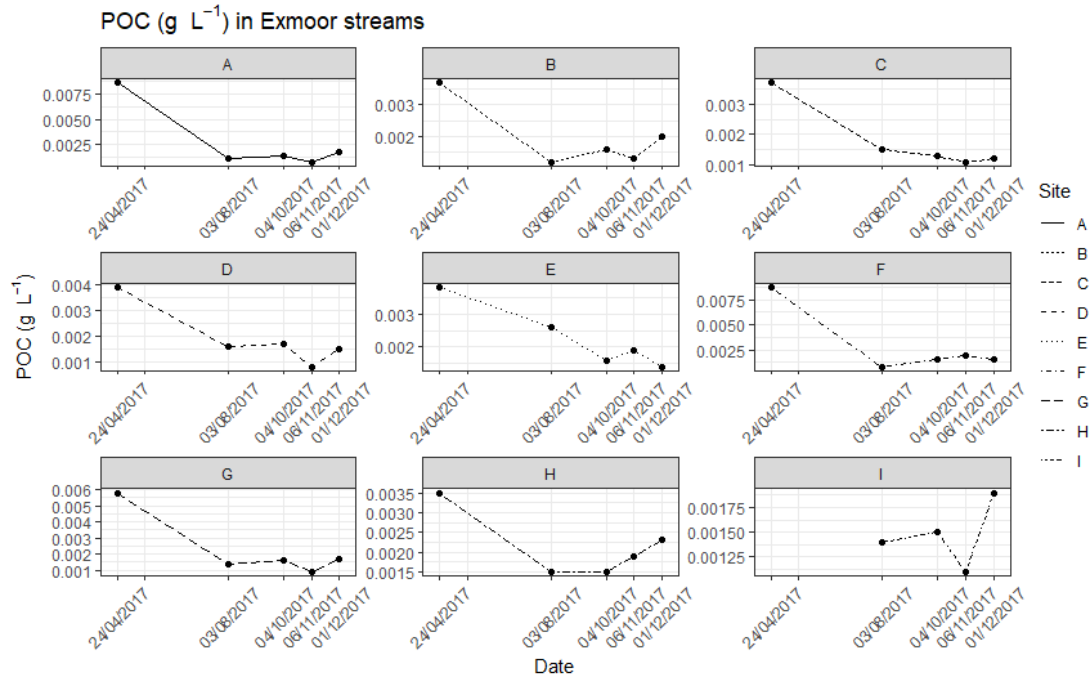
Fluorescence peaks A, B, C, M and T for experimental flocculation samples

Peak A for stream sites

Peak B for stream sites
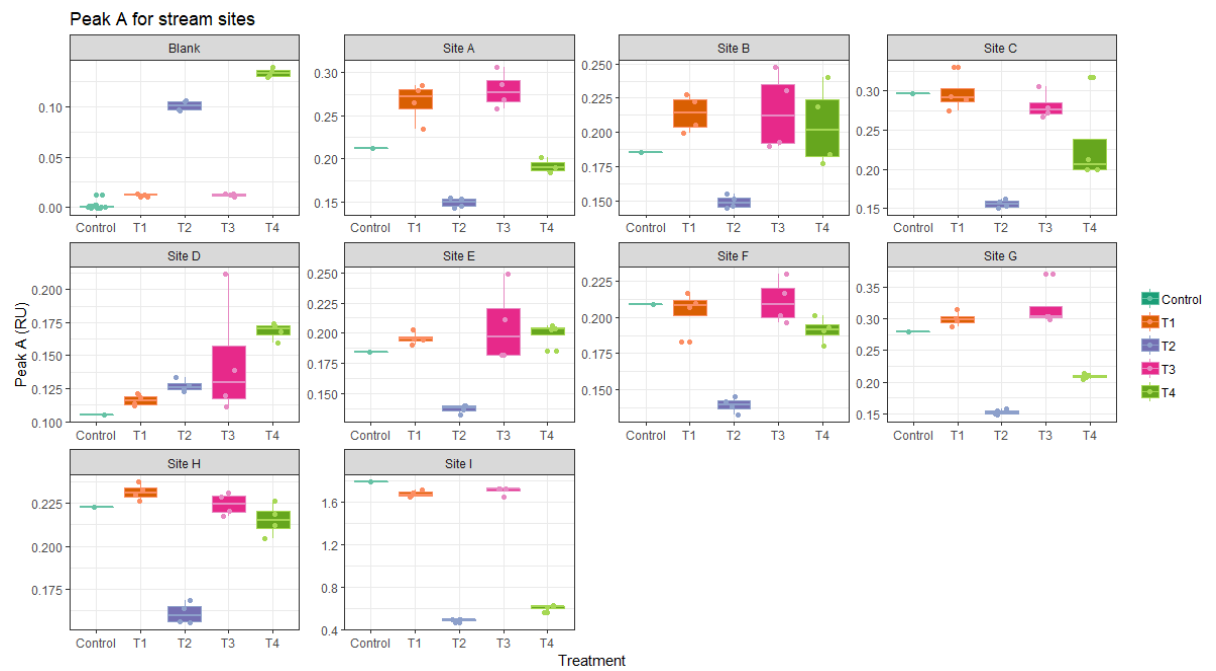
Peak C for stream sites

Peak M for stream sites

Peak T for stream sites

Method descriptions from Uppsala University (original M. Groeneveld, 2018)

Absorbance and fluorescence spectrometry

UV–Vis absorbance spectra (250 to 600 nm) of filtered water were measured in a 0.5 cm quartz cuvette using a Lambda35 UV–Vis Spectrometer (PerkinElmer Lambda 25, Perkin Elmer, Waltham, USA). Synchronous fluorescence scans were obtained using a FluoroMax-4 Spectrofluorometer (FluoroMax-4, Jobin Yvon, Horiba, Kyoto, Japan), with excitation-emission matrices (EEMs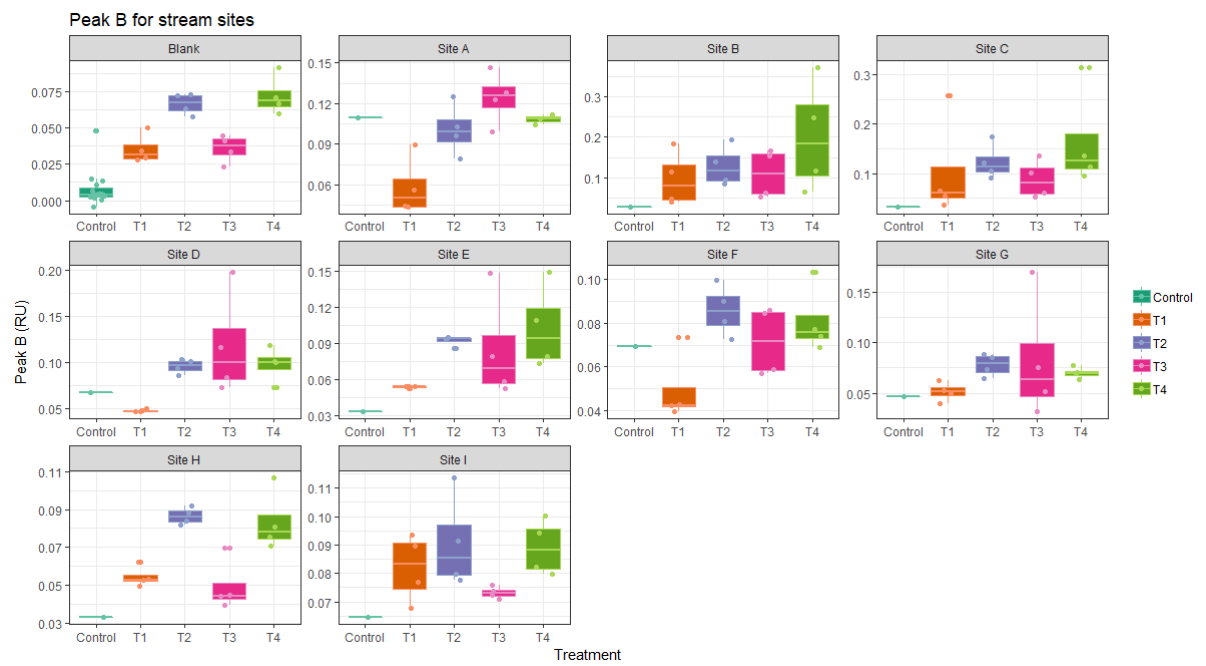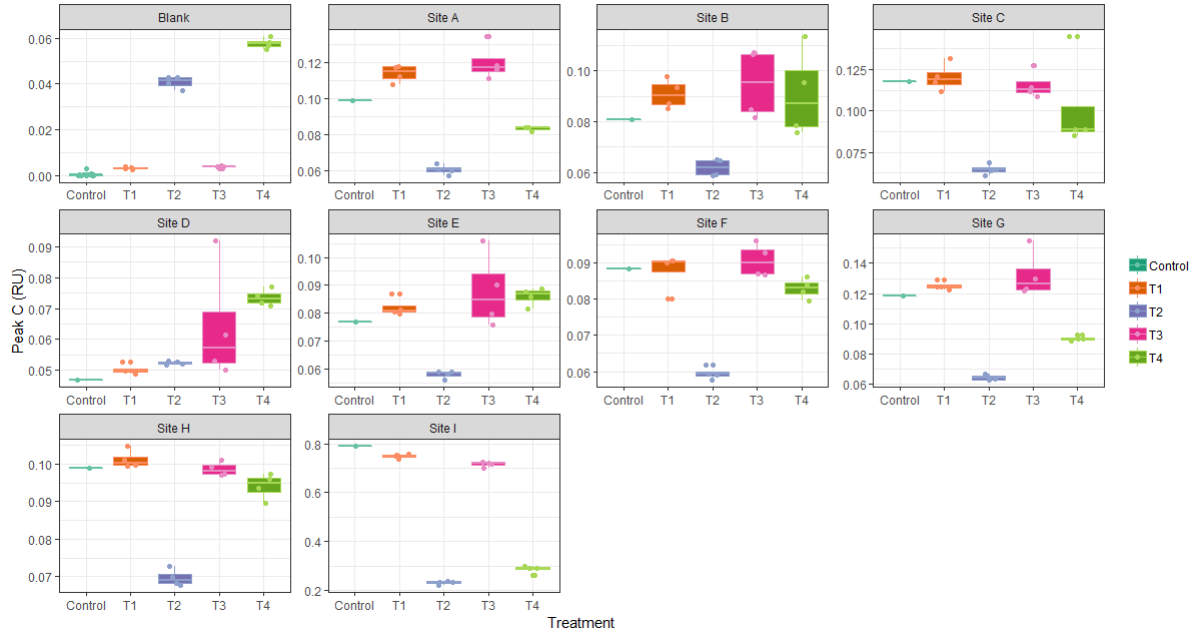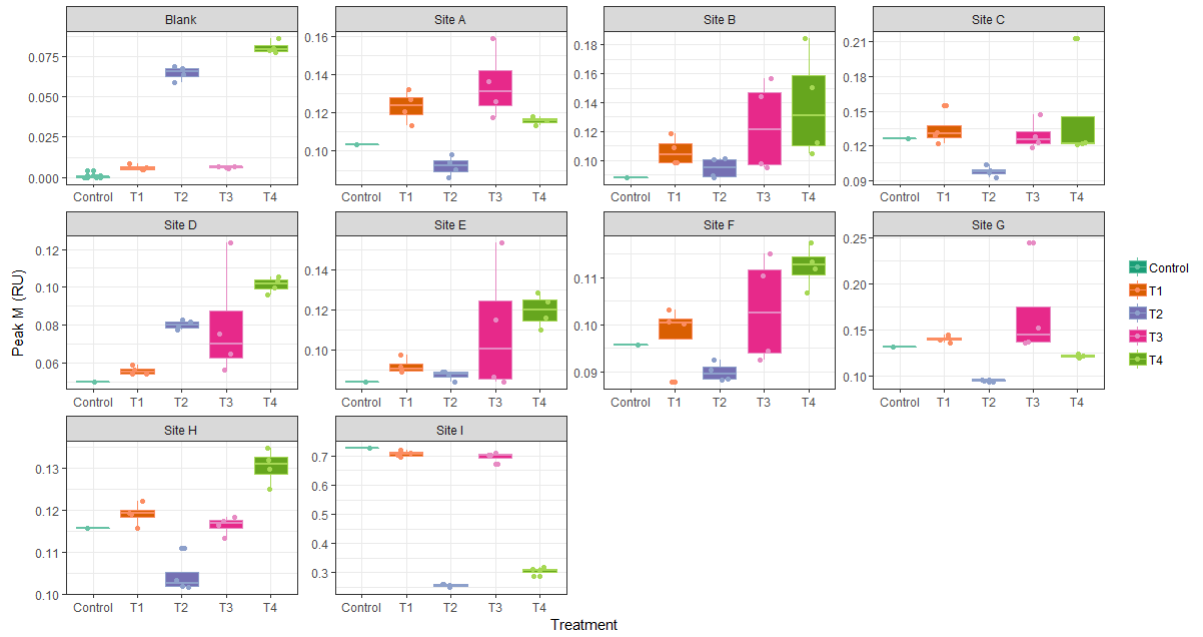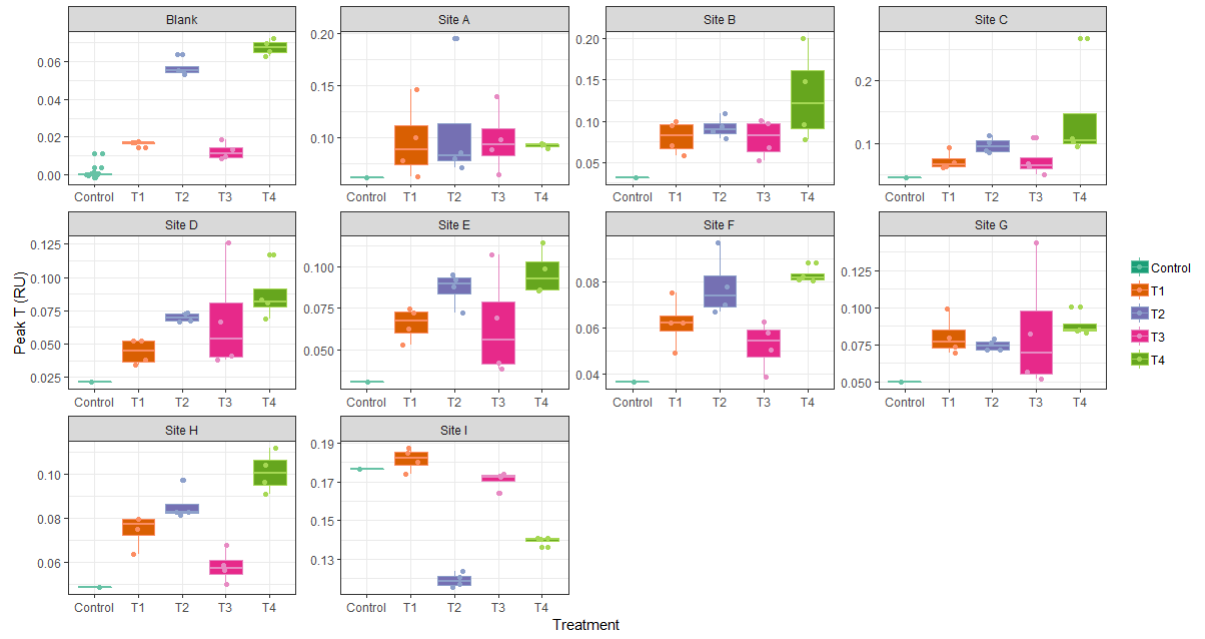) from excitation wavelengths 250 to 445 nm with 5 nm increments, and emission wavelengths 300 to 600 nm with 4 nm increments. The EEMs were blank subtracted using a sample of Milli-Q water run on the same day, corrected for instrument biases and normalised to Raman units (Lawaetz and Stedmon 2009). A shift in the location of the maximum intensity of peak A and peak C was observed across samples and as a result of treatment 2 (clay) and 4 (clay+salt). These locations were determined within Ex_{250}-$Em_{400-480}$ for peak A and $Ex_{300-360}$-$Em_{400-460}$ for peak C. Three commonly used indices were calculated at fixed excitation/emission wavelength pairs or regions: the fluorescence index (FI; Cory and McKnight, 2005), the humification index (HIX; Ohno et al. 2002), and the freshness index (FRESH; Parlanti et al. 2000). All fluorescence corrections were performed using the FDOMcorr toolbox (Murphy et al. 2010) for MATLAB (Mathworks, Inc., Natick, MA).

Parallel factor analysis (PARAFAC, Bro 1997) was used to identify the main fluorescence components of DOM present throughout the samples and to assess the effect of the treatments. The analysis was conducted on a set of 151 samples (four replicates and four treatments for nine sites and nine initial samples) using the drEEM toolbox for MATLAB (Mathworks, Inc., Natick, MA) following Murphy et al. (2013). EEMs were pre-processed as follows: 1) a faulty part of one EEM and one outlier were removed, 2) primary and secondary Rayleigh and Raman were removed and Em≤Ex was set to zero, and 3) the data were normalised to total fluorescence intensity of each sample. Non-negativity constraints were applied on all modes (excitation, emission and sample). The appropriate number of components was identified considering the effect of adding more components on the model fit (expressed as the sum of square errors), by visual inspection of the residuals and random initialization with 20 iterations with a convergence criterion of $1*10^{-08}$ to find a stable model. The model was validated using random split-half analysis.

Mass spectrometry

DOM composition was measured by direct infusion electrospray ionisation (ESI) Orbitrap mass spectrometry (Hawkes et al. 2016, Fleury et al. 2017). Solid phase extraction was performed with 100 mg Bond Elut PPL cartridges (Agilent Technologies). The cartridges were cleaned once with methanol, allowed to soak in fresh methanol overnight, and then rinsed with 0.1% formic acid. Due to the low DOC concentrations, all replicates were combined into one 160 ml sample. The samples were acidified to pH≈2 with 50% high purity HCl (Suprapure, VWR; 1 µL mL-1) and allowed to flow through the cartridges by gravity or slowly pushed through at a rate of a drop per second. The cartridges were flushed with 3 mL 0.1% formic acid to remove salts, and then dried using N2. The samples were then eluted with 2 mL methanol in pre-combusted 2 mL amber vials and stored at -20°C until analysis. (SPE was done 12-18/6, Orbitrap 11/7, if you want to how much time there was in between the experiment and the analysis) Samples were dried at 60°C, dissolved in 150 µl 50% methanol at a DOC concentration of approximately 50 ppm and loaded by autosampler (Agilent 1100) to the Orbitrap mass spectrometer (Velos Pro, Thermo Fisher). A mobile phase of 50% methanol (10 µL min-1) was used to transport the loaded organic material. The ESI source was operated in negative mode at 3kV and masses were calibrated using the lock mass setting on masses 269.06676, 369.08272 and 425.108935, which were present in every sample. 150 scans were acquired (4.5 minutes) for each sample after 3 minutes, after which lines were flushed for 4.5 minutes with methanol so that a baseline signal was achieved. Noise was removed and formulas assigned according to in-house routines (Hawkes et al. 2016), allowing up to C40H80O40N2S1 under the conditions 0.3≥H/C≤2, O/C≤1. Formulas were only assigned with a mass error <1ppm (1 x 106 x Δm/(m/z)). Isotopologues (13C peaks) and rare cases of double assignments were removed from consideration. Since many compounds were also identified in the treatment blanks, the samples were treatment blank-corrected as follows. Peaks were only considered if they were three times larger than the corresponding peak in the treatment blank, in which case the peak intensity for the treatment blank was subtracted from the peak intensity in the sample. The samples were then normalised to total sample intensity.

Weighted average H/C ratios (HCWA) were calculated for all samples and treatments as:

$$\sum_{i=1}^{n} \frac{H}{C} * I \ / \ \sum_{i=1}^{n} I$$

where *H* is the number of hydrogen atoms and *C* is the number of carbon atoms in molecular formula i, *I* is the intensity of formula *i*, and *n* is the total number of formulae in each sample. Weighted average O/C ratios (OCWA) were calculated in the same manner.

Formulae were assigned to compounds groups (black carbon, polyphenols, highly unsaturated, aliphatics, peptides, sugars) based on Seidel et al. (2014). (More specifically: "(1) polycyclic aromatics (PCAs, AImod > 0.66), which include condensed combustion-derived DBC if C > 15 (Dittmar and Koch, 2006), (2) highly aromatic compounds, which include polyphenols and PCAs with aliphatic chains (Koch

and Dittmar, 2006) (0.66 ≥ AImod > 0.50), (3) highly unsaturated compounds, which include phenols such as soil-derived products of lignin degradation (Stenson et al., 2003) (AImod ≤ 0.50 and H/C < 1.5), (4) unsaturated aliphatic compounds (2.0 > H/C ≥ 1.5), (5) saturated compounds, including fatty and sulfonic acids, and/or carbohydrates (H/C ≥ 2.0 or O/C ≥ 0.9), and (6) unsaturated aliphatic compounds containing N, which includes peptide molecular formulae (2.0 > H/C ≥ 1.5, N > 0)." – copied from Seidel et al. 2014, AImod is the modified aromaticity index defined by Koch and Dittmar, 2006)

In order to determine the effect of the treatment on DOM composition, we first performed a principal coordinate analysis (PCoA) on the Bray-Curtis dissimilarity matrix of the normalised molecular data and additional sample characteristics. When the variable 'treatment' approximately aligned with the one of the PCoA axes, this is axis was used a proxy for treatment. Univariate relationships between FT-Orbitrap-MS peak intensities and the principal coordinate representing the treatment were analysed using the *Spearman correlation* and plotted in *van Krevelen* space (H/C vs. O/C ratio). The correlation limit was set at 0.497 for a = 0.05 (N=16) and adjusted when outliers were removed (correlation limit = 0.514, N=15, correlation limit = 0.532, N=14) or when only T1 was considered (correlation limit=0.707, N=8). (taking principal coordinates as proxies for treatments is justified by the good correspondence between the effect shown by the correlations in *van Krevelen* space and the effect of treatment visible in the weighted average H/C and O/C plots).

References

Articles

Adams, J.L., Tipping, E., Bryant, C.L., Helliwell, R.C., Toberman, H., Quinton, J. (2015) Aged riverine particulate organic carbon in four UK catchments, *Science of the Total Environment 536*, 648–654

Alberto, M. C. R., Wassmann, R., Buresh, R. J., Quilty, J. R., Correa, T. Q., Sandro, J. M., & Centeno, C. A. R. (2014). Measuring methane flux from irrigated rice fields by eddy covariance method using open-path gas analyser, *Field Crops Research*, 160, 12–21. https://doi.org/10.1016/j.fcr.2014.02.008

Albuquerque, A.L.S. & Moseto, A.A. (1997). C:N:P ratios and stable carbon isotope compositions as indicators of organic matter sources in a riverine wetland system (Moji-Guaçu River, São Paulo-Brazil). *Wetlands*. 17. 1-9. http://dx.doi.org/10.1007/BF03160713.

Aldana Jague, E., Sommer, M., Saby, N.P.A., Cornelis, J-T., Van Wesemael, B., Van Oost, K. (2016) High resolution characterization of the soil organic carbon depth profile in a soil landscape affected by erosion. *Soil and Tillage Research*, 156, pp.185–193. Available at: http://dx.doi.org/10.1016/j.still.2015.05.014

Alonso, J., Audicio, P., Martínez, L., Scavone, M., Rezzano (2012). Comparison of measured Cs-137 data and USLE/RUSLE simulated long-term erosion rates. *Agrociencia*. 16. 261 -267.

Anderson, M. A., Pacheco, P. (2011) Characterization of bottom sediments in lakes using hydroacoustic methods and comparison with laboratory measurements, *Water Research 45,* 4399–4408

Anderson, M.A., Conkle, J.L., Pacheco, P., Gan, J. (2013) Use of hydroacoustic measurements to characterize bottom sediments and guide sampling and remediation of organic contaminants in lake sediments, *Science of the Total Environment 458–460*, 117–124

Andrews, S.S., Caron, S. & Zafiriou, O.C. (2000) Photochemical oxygen consumption in marine waters: A major sink for colored dissolved organic matter? *Limnology and Oceanography*, 45(2), pp.267–277.

Appleby, P. G. (2008). Three decades of dating recent sediments by fallout radionuclides: A review. *Holocene*, 18(1), 83–93. https://doi.org/10.1177/0959683607085598

Appleby, P.G. (1998) Dating recent sediment by ^{210}Pb: problems and solutions. *Stuk a-145*, pp.7–24.

303

Appleby, P.G. & Oldfield, F. (1983) The assessment of ^{210}Pb data from sites with varying sediment accumulation rates, *Hydrobiologica,* 103, 29–35.

Appleby, P. G. & Oldfield, F. (1978). The calculation of lead-210 dates assuming a constant rate of supply of unsupported ^{210}Pb to the sediment. *Catena*, 5(1), 1–8. https://doi.org/10.1016/S0341-8162(78)80002-2

Asmala, E., Bowers, D. G., Autio, R., Kaartokallio, H., Thomas, D.N. (2014) Qualitative changes of riverine dissolved organic matter at low salinities due to flocculation, *Journal of Geophysical Research: Biogeosciences, 119,* 1919–1933. https://doi.org/10.1002/2014JG002722

Atekwana, E.A., Krishnamurthy, R.V. (1998) Seasonal variations of dissolved inorganic carbon and δ^{13}C of surface waters: application of modified gas evolution technique, *Journal of Hydrology 205*, 265–278.

Atkinson M., Bingman C. (1998) Elemental composition of commercial seasalts. *Journal of Aquariculture and Aquatic Science*, 8: 39–43.

Aufdenkampe, A.K., Mayorga, E., Raymond, P.A., Melack, J.M., Doney, S.C., Alin, S.R., Aalto, R.E., Yoo, K. (2011) Riverine coupling of biogeochemical cycles between land, oceans, and atmosphere, *Frontiers in Ecology and the Environment.* 9(1) 53–60. doi: 10.1890/100014

Bacchi, O.O.S., Reichard, K., Sparovek, G., Ranieri, S. B. L. (2000) Soil erosion evaluation in a small watershed in Brazil through ^{137}Cs fallout redistribution analysis and conventional models. *Acta Geologica Hispanica*, 35(3–4), pp.251–259. Available at: http://www.geologica-acta.com/pdf/aghv3503a07.pdf.

Baker, A., Tipping, E., Thacker, S. A., & Gondar, D. (2008). Relating dissolved organic matter fluorescence and functional properties. *Chemosphere*, 73(11), 1765–1772. https://doi.org/10.1016/j.chemosphere.2008.09.018

Balakrishna, K., Kumar, I.A., Srinikethan, G., Mugaraya, G. (2006) Natural and anthropogenic factors controlling the dissolved organic carbon concentrations and fluxes in a large tropical river, India, *Environmental Monitoring and Assessment*, 122: 355. doi:10.1007/s10661-006-9188-7

Banaitis, M. R., Waldrip-Dail, H., Diehl, M. S., Holmes, B. C., Hunt, J. F., Lynch, R. P., & Ohno, T. (2006). Investigating sorption-driven dissolved organic matter fractionation by

multidimensional fluorescence spectroscopy and PARAFAC. *Journal of Colloid and Interface Science*, 304(1), 271–276. https://doi.org/10.1016/j.jcis.2006.07.035

Barros, N., Cole, J.J., Tranvik, L.J., Prairie, Y.T., Bastviken, D., Huszar. V.L.M., del Giorgio, P., Roland, F. (2011) Carbon emission from hydroelectric reservoirs linked to reservoir age and latitude, *Nature Geoscience 4*, 593–596. doi:10.1038/NGEO1211

Bastviken, D., Tranvik, L.J., Downing, J. A., Crill, M., P., & Enrich-Prast, A. (2011). Freshwater Methane Emissions Offset the Continental Carbon Sink. *Science*, 331, Issue 6013, pp. 50 DOI: 10.1126/science.1196808

Batjes, N. H. (2005) Organic carbon stocks in the soils of Brazil. *Soil Use and Management,* 21(1), 22–24. https://doi.org/10.1079/SUM2005286

Batjes, N. H. (2014) Total carbon and nitrogen in the soils of the world (EJSS Land Mark Paper No . 3). *European Journal of Soil Science*, 65(3), 4–21. https://doi.org/10.1111/ejss.12114

Battin, T. J., Kaplan, L.A., Findlay, S., Hopkinson, C. S., Marti, E., Packman, A.I., Newbold, J.D., Sabater, F. (2009) Biophysical controls on organic carbon fluxes in fluvial networks. *Nature Geoscience*, 2(8), 595–595. https://doi.org/10.1038/ngeo602

Beasley, D. B., Huggins, L. F. & Monke, E. J. (1980). ANSWERS: A Model for Watershed Planning. *Transactions of the ASAE*, 23(4), 0938–0944. https://doi.org/10.13031/2013.34692

Benmansour, M., Mabit, L., Nouira, A., Moussadek, R., Bouksirate, H., Duchemin, M., & Benkdad, A. (2013). Assessment of soil erosion and deposition rates in a Moroccan agricultural field using fallout ^{137}Cs and ^{210}Pb$_{ex}$. *Journal of Environmental Radioactivity*, 115, 97–106. https://doi.org/10.1016/j.jenvrad.2012.07.013

Berhe, A. A., Harden, J. W., Torn, M. S., & Harte, J. (2008). Linking soil organic matter dynamics and erosion-induced terrestrial carbon sequestration at different landforasm positions. *Journal of Geophysical Research: Biogeosciences,* 113(4), 1–12. https://doi.org/10.1029/2008JG000751

Beskow, S., Mello, C. R., Norton, L. D., Curi, N., Viola, M. R., Avanzi, J. C. (2009) Soil erosion prediction in the Grande River Basin, Brazil using distributed modeling. *Catena*, 79(1), pp.49–59. Available at: http://dx.doi.org/10.1016/j.catena.2009.05.010.

Beusen, A. H. W., Dekkers, A. L. M., Bouwman, A. F., Ludwig, W., & Harrison, J. (2005) Estimation of global river transport of sediments and associated particulate C, N, and P. *Global Biogeochemical Cycles*, *19* (4). https://doi.org/10.1029/2005GB002453

Bianchi, T.S. (2011), The role of terrestrially derived organic carbon in the coastal ocean: A changing paradigm and the priming effect, PNAS 108 (49), 19473-19481. doi:10.1073/pnas.1017982108

Bieroza, M., Baker, A., & Bridgeman, J. (2012). Exploratory analysis of excitation-emission matrix fluorescence spectra with self-organizing maps-A tutorial. *Education for Chemical Engineers*, 7(1), e22–e31. https://doi.org/10.1016/j.ece.2011.10.002

Bisutti, I., Hilke, I., Raessler, M. (2004) Determination of total organic carbon – an overview of current methods, *Trends in Analytical Chemistry* 23 (10–11), 716–726

Blair, N. E., & Aller, R. C. (2012). The Fate of Terrestrial Organic Carbon in the Marine Environment. *Annual Review of Marine Science*, 4(1), 401–423. https://doi.org/10.1146/annurev-marine-120709-142717

Bro, R. (1997) PARAFAC. Tutorial and applications, *Chemometrics and Intelligent Laboratory Systems* 38, 149-171. https://doi.org/10.1016/S0169-7439(97)00032-4

Bucci, M.M.H.S., da Fonseca Delgado, F.E. & de Oliveira, L.F.C. (2015) Water quality and trophic state of a tropical urban reservoir for drinking water supply (Juiz de Fora, Brazil), *Lake and Reservoir Management*, 31:2, 134–144. https://doi.org/10.1080/10402381.2015.1029151

Bujan, A., Santanatoglia, O.J., Chagas, C., Massobrio, M., Castiglioni, M., Yañez, M., Ciallella, H., Fernandez, J. (2003) Soil erosion evaluation in a small basin through the use of 137Cs technique, *Soil and Tillage Research*, Volume 69, Issues 1–2, Pages 127-137. https://doi.org/10.1016/S0167-1987(02)00134-4.

Callender, E. (2000) Geochemical effects of rapid sedimentation in aquatic systems: minimal diagenesis and the preservation of historical metal signatures, *Journal of Paleolimnology 23*, 243–260.

Carlson, T.N., Ripley, D.A. (1997) On the Relation between NDVI, Fractional Vegetation Cover, and Leaf Area Index, *Remote sensing of Environment*, 62:241–252. https://doi.org/10.1016/S0034-4257(97)00104-1

Carrasco-Letelier, L., Beretta-Blanco, A. (2017) Soil erosion by water estimated for 99 Uruguayan basins, *Ciencia e Investigación Agraria*, 44(2):184-194. https://doi.org/10.7764/rcia.v44i2.1717

Carvalhais, N., Forkel, M., Khomik, M., Bellarby, J., Jung, M., Migliavacca, M., Mu, M., Saatchi, S., Santoro, M., Thurner, M., Weber, U., Ahrens, B., Beer, C., Cescatti, A., Randerson, J.T. & Reichstein, M. (2014) Global covariation of carbon turnover times with climate in terrestrial ecosystems. *Nature,* 514(7521), 213–217. https://doi.org/10.1038/nature13731

Clark, J. M., Bottrell, S. H., Evans, C. D., Monteith, D. T., Bartlett, R., Rose, R., … Chapman, P. J. (2010). The importance of the relationship between scale and process in understanding long-term DOC dynamics. *Science of the Total Environment,* 408(13), 2768–2775. https://doi.org/10.1016/j.scitotenv.2010.02.046

Cole, J., Prairie, Y., Caraco, N., McDowell, W., Tranvik, L., Striegl, R., Duarte, C., Kortelainen, P., Downing, J., Middelburg, J. and Melack, J. (2007) Plumbing the Global Carbon Cycle: Integrating Inland Waters into the Terrestrial Carbon Budget. *Ecosystems. 10(1),* 172–185.

Collins, A.L., Walling, D.E., Webb, L. & King, P. (2009) Particulate organic carbon sources and delivery to river channels in the Somerset Levels ECSFDI priority catchment, southwest UK, *International Journal of River Basin Management*, 7:3, 277-291, https://doi.org/10.1080/15715124.2009.9635389

Colombo, A., & Joly, C. (2010). Brazilian Atlantic Forest lato sensu: the most ancient Brazilian forest, and a biodiversity hotspot, is highly threatened by climate change. Brazilian Journal of Biology, 70(3 suppl), 697–708. https://doi.org/10.1590/S1519-69842010000400002

Conrad, O., Bechtel, B., Bock, M., Dietrich, H., Fischer, E., Gerlitz, L., Wehberg, J., Wichmann, V., and Boehner, J. (2015) System for Automated Geoscientific Analyses (SAGA) v. 2.1.4. *Geosci. Model Dev.,* 8, 1991-2007, https://doi.org/10.5194/gmd-8-1991-2015

Cooper, M., Silveira Mendes, L.M., Costa Silva, W.L., Sparovek, G. (2005) A National Soil Profile Database for Brazil Available to International Scientists, *Soil Science Society of America.* 69:649–652. https://doi.org/10.2136/sssaj2004.0140

Cooper, R.J., Pedentchouk, N., Hiscock, K.M., Disdle, P., Krueger, T., Rawlins, B.G. (2015) Apportioning sources of organic matter in streambed sediments: An integrated molecular and compound-specific stable isotope approach, *Science of The Total Environment*, 520, 187-197, https://doi.org/10.1016/j.scitotenv.2015.03.058

307

Correchel, V., Bacchi, O. O. S., De Maria, I. C. Dechen, S. C. F., Reichardt, K. (2006) Erosion rates evaluated by the ^{137}Cs technique and direct measurements on long-term runoff plots under tropical conditions. *Soil and Tillage Research*, 86(2), pp.199–208.

Cory, R.M., Miller, M.P., McKnight, D.M., Guerard, J.J., Miller, P.L. (2010). Effect of instrument-specific response on the analysis of fulvic acid fluorescence spectra. *Limnology and Oceanography: Methods*, 8(2), 67–78. https://doi.org/10.4319/lom.2010.8.67

Cory, R.M., Harrold, K. H., Neilson, B. T., Kling, G. W. (2015) Controls on dissolved organic matter (DOM) degradation in a headwater stream: the influence of photochemical and hydrological conditions in determining light-limitation or substrate-limitation of photo-degradation, *Biogeosciences, 12,* 9793–9838. https://doi.org/10.5194/bg-12-6669-2015

da Cunha, E. R., Bacani, V. M., & Panachuki, E. (2017). Modeling soil erosion using RUSLE and GIS in a watershed occupied by rural settlement in the Brazilian Cerrado. *Natural Hazards*, 85(2), 851–868. https://doi.org/10.1007/s11069-016-2607-3

Da Silva, A.M. (2004) Rainfall erosivity map for Brazil. *Catena*, 57(3), pp.251–259.

de Carvalho, D. F., Durigon, V. L., Antunes, M. A. H., de Almeida, W. S., & de Oliveira, P. T. S. (2014) Predicting soil erosion using Rusle and NDVI time series from TM Landsat 5. *Pesquisa Agropecuaria Brasileira*, 49(3), 215–224. https://doi.org/10.1590/S0100-204X2014000300008

de Roo, A., Wesseling, C. G., Jetten, V. G., & Ritsema, C. J. (1996). LISEM : a physically-based hydrological and soil erosion model incorporated in a GIS. *HydroGIS 96: Application of Geographic Information Systems in Hydrology and Water Resources Management*, (235), 395–403. https://doi.org/10.1016/j.euromechflu.2013.06.011

de Vicente, Ortega-Retuerta, E., Romera, O., Morales-Baquero, R., Reche, I. (2009) Contribution of transparent exopolymer particles to carbon, sinking flux in an oligotrophic reservoir, I., *Biogeochemistry 96,* 13–23.

Delu, P., Qiong, L., Yan, B. (2013) Review and suggestions for estimating particulate organic carbon and dissolved organic carbon inventories in the ocean using remote sensing data, *Acta Oceanologica Sinica*, *33(1),* 1–10.

Depetris, P.J., Kempe, S. (1993), Carbon dynamics and sources in the Parani River, *Limnology and Oceanography*, 38, doi:10.4319/lo.1993.38.2.0382.

Dercon, G. Mabit, L., Hancock, G., Nguyen, M. L., Dornhofer, P., Bacchi, O. O. S., Benmansour, M., Bernard, C., Froehlich, W., Golosov, V. N., Haciyakupoglu, S., Hai, P. S., Klik, A., Li, Y., Lobb, D. A., Onda, Y., Popa, N., Rafiq, M., Ritchie, J. C., Schuller, P., Shakhashiro, A., Wallbrink, P., Walling, D. E., Zapata, F., Zhang, X. (2012) Fallout radionuclide-based techniques for assessing the impact of soil conservation measures on erosion control and soil quality: An overview of the main lessons learnt under an FAO/IAEA Coordinated Research Project. *Journal of Environmental Radioactivity*, 107, pp.78–85.

Desmet, P., & Govers, G. (1996) A GIS procedure for automatically calculating the USLE LS factor on topographically complex landscape units. *Journal of Soil and Water Conservation*, 51(5), 427–433.

Dhillon, G.S., Amichev, B.Y., de Freitas, R., Van Rees, K. (2015) Accurate and Precise Measurement of Organic Carbon Content in Carbonate-Rich Soils. *Communications in Soil Science and Plant Analysis,* 46(21), pp.2707–2720. Available at: http://www.tandfonline.com/doi/full/10.1080/00103624.2015.1089271.

Doetterl, S., Berhe, A.A., Nadeu, E.,Wang, Z., Sommer, M., Fiener, P. (2015) Erosion, deposition and soil carbon: A review of process-level controls, experimental tools and models to address C cycling in dynamic landscapes, *Earth Science Reviews 154*, 102–122. doi: 10.1016/j.earscirev.2015.12.005

Droppo, I.G. & Ongley, E.D. (1994) Flocculation of suspended sediment in rivers of southeastern Canada, *Water Research 28, 8,* 1799–1809

Droppo, I. G., Leppard, G. G., Flannigan, D. T., & Liss, S. N. (1997). The freshwater floc: A functional relationship of water and organic and inorganic floc constituents affecting suspended sediment properties. *Water, Air, and Soil Pollution*. https://doi.org/10.1023/A:1018359726978

Droppo, I. G., Jeffries, D., Jaskot, C., & Backus, S. (1998). The prevalence of freshwater flocculation in cold regions: A case study from the Mackenzie River Delta, Northwest Territories, Canada. *Arctic*, 51(2), 155–164. https://doi.org/10.14430/arctic1056

Du, P., & Walling, D. E. (2012). Using 210Pb measurements to estimate sedimentation rates on river floodplains. *Journal of Environmental Radioactivity*, 103(1), 59–75. https://doi.org/10.1016/j.jenvrad.2011.08.006

Durigon, V. L., Carvalho, D. F., Antunes, M. A. H., Oliveira, P. T. S., & Fernandes, M. M. (2014). NDVI time series for monitoring RUSLE cover management factor in a tropical watershed. *International Journal of Remote Sensing, 35*(2), 441–453. https://doi.org/10.1080/01431161.2013.871081

Edmondson, J.L., Stott, I., Potter, J., Lopez-Capel, E., Manning, D.A.C., Gaston, K.J., Leake, J.R. (2015) Black Carbon Contribution to Organic Carbon Stocks in Urban Soil, *Environ. Sci. Technol. 49,* 8339−8346. doi: 10.1021/acs.est.5b00313

Edzwald, J.K., Upchurch, J.B. & O'Melia, C.R. (1974) Coagulation in estuaries. Environmental Science and Technology, 8(1), pp.58–63.

Eisma, D. (1986) Flocculation and de-flocculation of suspended matter in estuaries, *Netherlands Journal of Sea Research 20 (2/3),* 183–199

Elderfield, H., Upstill-Goddard, R., Sholkovitz, E.R. (1990) The rare earth elements in rivers, estuaries, and coastal seas and their significance to the composition of ocean waters, *Geochimica et Cosmochimica Acta, 54*, 971–991

Estapa, M.L., Mayer, L.M. (2010) Photooxidation of particulate organic matter, carbon/oxygen stoichiometry, and related photoreactions, *Marine Chemistry 122*, 138–147

Fang, C., Moncrieff, J.B. (1999) A model for soil CO2 production and transport 1: Model development, *Agricultural and Forest Meteorology 95*, 225–236

Fellman, J. B., Hood, E., & Spencer, R. G. M. (2010). Fluorescence spectroscopy opens new windows into dissolved organic matter dynamics in freshwater ecosystems: A review. *Limnology and Oceanography*, 55(6), 2452–2462. https://doi.org/10.4319/lo.2010.55.6.2452

Feng, X., Simpson, A.J., Simpson, M.J. (2005) Chemical and mineralogical controls on humic acid sorption to clay mineral surfaces, *Organic Geochemistry 36*, 1553–1566

Fleury, G., Del Nero, M., & Barillon, R. (2017). Molecular fractionation of a soil fulvic acid (FA) and competitive sorption of trace metals (Cu, Zn, Cd, Pb) in hematite-solution systems: Effect of the FA-to-mineral ratio. *RSC Advances*, 7(68), 43090–43103. https://doi.org/10.1039/c7ra06838g

Fontaine, S., Barot, S., Barre, P., Bdioui, N., Mary, B., Rumpel, C. (2007) Stability of organic carbon in deep soil layers controlled by fresh carbon supply, *Nature 450,* 277–281. doi:10.1038/nature06275

310

Forsgren, G., Jansson, M., & Nilsson, P. (1996). Aggregation and sedimentation of iron, phosphorus and organic carbon in experimental mixtures of freshwater and estuarine water. *Estuarine Coastal and Shelf Science*, 43(2), 259–268. https://doi.org/10.1006/ecss.1996.0068

Foster, G. R., McCool, D. K., Renard, K. G., & Moldenhauer, W. C. (1981). Conversion of the universal soil loss equation to SI metric units. *Journal of Soil and Water Conservation*, 36(6), 335–359.

Galdino, S., Sano, E. E., Andrade, R. G., Grego, C. R., Nogueira, S. F., Bragantini, C., & Flosi, A. H. G. (2016) Large-scale Modeling of Soil Erosion with RUSLE for Conservationist Planning of Degraded Cultivated Brazilian Pastures. *Land Degradation and Development*, 27(3), 773–784. https://doi.org/10.1002/ldr.2414

Galy, V., France-Lanord, C., Beyssac, O., Faure, P., Kudrass, H., Palhol, F. (2007) Efficient organic carbon burial in the Bengal fan sustained by the Himalayan erosional system, Vol 450| 15 November 2007| doi:10.1038/nature06273

Gaspar, L. Navas, A., Walling, D. E., Machín, J., Gómez Arozamena, J. (2013) Using ^{137}Cs and [210]Pbex to assess soil redistribution on slopes at different temporal scales. *Catena*, 102, pp.46–54. Available at: http://dx.doi.org/10.1016/j.catena.2011.01.004.

Gessler, P. E., Moore, I. D., McKenzie, N. J., & Ryan, P. J. (1995). Soil-landscape modelling and spatial prediction of soil attributes. *International Journal of Geographical Information Systems*, 9(4), 421–432. https://doi.org/10.1080/02693799508902047

Glendell, M. & Brazier, R.E. (2014) Accelerated export of sediment and carbon from a landscape under intensive agriculture. *The Science of the Total Environment*, 476–477, pp.643–656. Available at: http://dx.doi.org/10.1016/j.scitotenv.2014.01.057.

Grand-Clement, E., Luscombe, D. J., Anderson, K., Gatis, N., Benaud, P., & Brazier, R. E. (2014). Antecedent conditions control carbon loss and downstream water quality from shallow, damaged peatlands. *Science of the Total Environment*, 493, 961–973. https://doi.org/10.1016/j.scitotenv.2014.06.091

Gregory, J. (1981) Flocculation in the laminar tube flow, *Chemical Engineering Science 36(11),* 1789–1794

Gudasz, C., Bastviken, D., Steger, K., Premke, K., Sobek, S., Tranvik, L.J. (2010) Temperature-controlled organic carbon mineralisation in lake sediments, *Nature 466*, 478–482. doi:10.1038/nature09186

Guggenberger, G., Kaiser, K. (2003), Dissolved organic matter in soil: challenging the paradigm of sorptive preservation, *Geoderma 113*, 293– 310

Guo, X., Meng, M., Zhang, J., & Chen, H. Y. H. (2016). Vegetation change impacts on soil organic carbon chemical composition in subtropical forests. Scientific Reports, 6(July), 1–9. https://doi.org/10.1038/srep29607

Guzmán, G. et al. (2013) Sediment tracers in water erosion studies: Current approaches and challenges. *Journal of Soils and Sediments*, 13(4), pp.816–833.

Hansen, A. M., Kraus, T. E. C., Pellerin, B. A., Fleck, J. A., Downing, B. D., & Bergamaschi, B. A. (2016). Optical properties of dissolved organic matter (DOM): Effects of biological and photolytic degradation. *Limnology and Oceanography*, 61(3), 1015–1032. https://doi.org/10.1002/lno.10270

Harris, D., Horwáth, W. R., van Kessel, C. (2001), Acid fumigation of soils to remove carbonates prior to total organic carbon or carbon-13 isotopic analysis, *Soil Sci. Soc. Am. J., 65*, 1853–1856.

He, Q. & Walling, D.E. (1996) Interpreting particle size effects in the adsorption of 137Cs and unsupported 210Pb by mineral soils and sediments. *Journal of Environmental Radioactivity*, 30(2), 117–137.

Helms, J. R., Mao, J., Schmidt-Rohr, K., Abdulla, H., & Mopper, K. (2013). Photochemical flocculation of terrestrial dissolved organic matter and iron. *Geochimica et Cosmochimica Acta*, 121, 398–413. https://doi.org/10.1016/j.gca.2013.07.025

Hoyle, J., Elderfield, H., Gledhill, A., Greaves, M. (1984) The behaviour of the rare earth elements during mixing of river and sea waters, *Geochemicia et Cosmochimica Acta, 48*, 143–149

Hu, F.S., Hedges, J.I., Gordon, E.S., Brubaker, L.B. (1999) Lignin biomarkers and pollen in postglacial sediments of an Alaskan lake, *Geochimica et Cosmochimica Acta*, Volume 63, Issue 9, 1421-1430, doi: 10.1016/S0016-7037(99)00100-3

IPCC (2013) Climate Change 2013: The Physical Science Basis. Contribution of Working Group I to the Fifth Assessment Report of the Intergovernmental Panel on Climate Change [Stocker, T.F., D. Qin, G.-K. Plattner, M. Tignor, S.K. Allen, J. Boschung, A. Nauels, Y. Xia, V. Bex andP.M. Midgley (eds.)]. Cambridge University Press, Cambridge, United Kingdom and New York, NY, USA, 1535 pp, doi:10.1017/CBO9781107415324

Jobbagy, E. G., & Jackson, R. B. (2000). The vertical distribution of soil organic carbon and its relation to climate and vegetation. *Ecological Applications*, ESA, 10(2), 423–436. https://doi.org/10.1890/1051-0761(2000)010[0423:TVDOSO]2.0.CO;2

Jones, R.I., J. Laybourn-Parry, M. C. Walton & J. M. Young (1997) The forms and distribution of carbon in a deep, oligotrophic lake (Loch Ness, Scotland). *Internationale Vereinigung für theoretische und angewandte Limnologie: Verhandlungen*, 26:2, 330-334. https://doi.org/10.1080/03680770.1995.11900728

Kaiser, K., Guggenberger, G. (2000), The role of DOM sorption to mineral surfaces in the preservation of organic matter in soils, *Organic Geochemistry 31,* 711–725

Kaiser, K., Kalbitz, K. (2012), Cycling downwards – dissolved organic matter in soils, *Soil Biology & Biochemistry 52,* 29–32

Kandasamy, S., & Nagender Nath, B. (2016). Perspectives on the Terrestrial Organic Matter Transport and Burial along the Land-Deep Sea Continuum: Caveats in Our Understanding of Biogeochemical Processes and Future Needs. *Frontiers in Marine Science*, 3, 1–18. https://doi.org/10.3389/fmars.2016.00259

Karydas, C.G., Panagos, P. & Gitas, I.Z., (2014). A classification of water erosion models according to their geospatial characteristics. *International Journal of Digital Earth*, 7(3), pp. 229–250.

Keeley, J.E. (2014), Aquatic CAM photosynthesis: A brief history of its discovery, *Aquatic Botany 118*, 38–44

Kieber, R.J., Whitehead, R.F., Skrabal, S.A. (2006), Photochemical production of dissolved organic carbon from resuspended sediments, *Limnol. Oceanogr., 51(5),* 2187–2195

Kim, J., Zell, C., Moreira-Turcq, P., Pérez, M. A.P., Abril, G., Mortillaro, J., Weijers, J.W.H., Meziane, T., Sinninghe Damsté, J.S. (2012) Tracing soil organic carbon in the lower Amazon River and its tributaries using GDGT distributions and bulk organic matter properties, *Geochimica et Cosmochimica Acta*, Volume 90, 163-180, doi: 10.1016/j.gca.2012.05.014.

313

Kim, S., Kramer, R. W., & Hatcher, P. G. (2003). Graphical Method for Analysis of Ultrahigh-Resolution Broadband Mass Spectra of Natural Organic Matter, the Van Krevelen Diagram. *Analytical Chemistry*, 75(20), 5336–5344. https://doi.org/10.1021/ac034415p

Kirschbaum, M. U. F., Zeng, G., Ximenes, F., Giltrap, D. L., & Zeldis, J. R. (2019). Towards a more complete quantification of the global carbon cycle. *Biogeosciences*, 16(3), 831–846. https://doi.org/10.5194/bg-16-831-2019

Koch, B. P., Witt, M., Engbrodt, R., Dittmar, T., & Kattner, G. (2005). Molecular formulae of marine and terrigenous dissolved organic matter detected by electrospray ionization Fourier transform ion cyclotron resonance mass spectrometry. Geochimica et Cosmochimica Acta, 69(13), 3299–3308. https://doi.org/10.1016/j.gca.2005.02.027

Koelmans, A.A., Prevo, L. (2003), Production of dissolved organic carbon in aquatic sediment Suspensions, *Water Research 37*, 2217–2222

Kouli, M., Soupios, P., & Vallianatos, F. (2008). Soil erosion prediction using the Revised Universal Soil Loss Equation (RUSLE) in a GIS framework, Chania, Northwestern Crete, Greece. *Environmental Geology*, 57(3), 483–497. https://doi.org/10.1007/s00254-008-1318-9

Köchy, M., Hiederer, R., & Freibauer, A. (2015). Global distribution of soil organic carbon – Part 1: Masses and frequency distributions of SOC stocks for the tropics, permafrost regions, wetlands, and the world. *Soil*, 1(1), 351–365. https://doi.org/10.5194/soil-1-351-2015

Lal, R. (2005) Soil erosion and carbon dynamics, *Soil and Tillage Research 81(2)*, 137–142.

Larsen, L. G., Harvey, J. W., & Crimaldi, J. P. (2009). Morphologic and transport properties of natural organic floc. *Water Resources Research,* 45(1), 1–13. https://doi.org/10.1029/2008WR006990

Le Guitton, M., Soetaert, K., Sinninghe Damsté, J.S., Middelburg, J.J. (2015), Biogeochemical consequences of vertical and lateral transport of particulate organic matter in the southern North Sea: A multiproxy approach, *Estuarine, Coastal and Shelf Science 165,* 117–127

Le Quéré, C., Peters, G. P., Andres, R. J., Andrew, R. M., Boden, T. A., Ciais, P., … Zaehle, S. (2014). Global carbon budget 2013. *Earth System Science* Data, 6(1), 235–263. https://doi.org/10.5194/essd-6-235-2014

Lev-Yadun, S., Gopher, A., & Abbo, S. (2000). The cradle of agriculture. *Science*, 288(5471), 1602–1603. https://doi.org/10.1126/science.288.5471.1602

Li, M., Peng, C., Wanga, M., Xuea, W., Zhang, K., Wang, K., Shi, G., Zhu, Q. (2017) The carbon flux of global rivers: A re-evaluation of amount and spatial patterns, *Ecological Indicators 80*, 40–51

Liebmann, B., & Allured, D. (2005) Daily precipitation grids for South America. *Bull. Amer. Meteor. Soc.,* 86, 1567-1570

Lindsay, J.B. & Creed, I.F. (2005) Removal of artifact depressions from digital elevation models: Towards a minimum impact approach. *Hydrological Processes,* 19(16), pp.3113–3126.

Lopes dos Santos, R.A., Vane, C.H. (2016) Signatures of tetraether lipids reveal anthropogenic overprinting of natural organic matter in sediments of the Thames Estuary, UK, *Organic Geochemistry*, Volume 93, 68-76, doi:10.1016/j.orggeochem.2016.01.003.
Lou, T. & Xie, H., 2006. Photochemical alteration of the molecular weight of dissolved organic matter. Chemosphere, 65(11), pp.2333–2342.

Lubis, A. A. (2006). Constant Rate of Supply (CRS) Model for Determining the Sediment Accumulation Rates in the Coastal Area Using 210 Pb. *Journal of Coastal Development*, 10(1), 1410–5217. https://doi.org/10.1.1.1032.3190

Maavara, T., Lauerwald, R., Regnier, P., & Cappellen, P. Van. (2017). Global perturbation of organic carbon cycling by river damming. *Nature Communications*, 8, 15347. https://doi.org/10.1038/ncomms15347

Mabit, L., Benmansour, M. & Walling, D.E. (2008) Comparative advantages and limitations of the fallout radionuclides ^{137}Cs, [210]Pbex and 7Be for assessing soil erosion and sedimentation. *Journal of Environmental Radioactivity*, 99(12), pp.1799–1807. Available at: http://dx.doi.org/10.1016/j.jenvrad.2008.08.009.

Maeck, A., DelSontro, T., McGinnis, D. F., Fischer, H., Flury, S., Schmidt, M., Fietzek, P., Lorke, A. (2013). Sediment trapping by dams creates methane emission hot spots. *Environmental Science and Technology*, 47(15), 8130–8137. https://doi.org/10.1021/es4003907

Maioli, O.L.G., Rossi de Oliveira, C., Dal Sasso, M.A., dos Santos Madureira, L.A., de Almeida Azevedo, D., de Aquino Neto, F.R. (2012) Evaluation of the organic matter sources

using the δ13C composition of individual n-alkanes in sediments from Brazilian estuarine systems by GC/C/IRMS, *Estuarine, Coastal and Shelf Science*, Volume 114, 140-147, doi: 10.1016/j.ecss.2012.09.001.

Martinez, C., Hancock, G. R., & Kalma, J. D. (2009). Comparison of fallout radionuclide (caesium-137) and modelling approaches for the assessment of soil erosion rates for an uncultivated site in south-eastern Australia. *Geoderma*, 151(3–4), 128–140. https://doi.org/10.1016/j.geoderma.2009.03.023

Martinez, C., Hancock, G. R., & Kalma, J. D. (2010). Relationships between 137Cs and soil organic carbon (SOC) in cultivated and never-cultivated soils: An Australian example. Geoderma, 158(3–4), 137–147. https://doi.org/10.1016/j.geoderma.2010.04.019

Marwick, T.R., Tamooh, F., Teodoru, C.R., Borges, A.V., Darchambeau, F., Bouillon, S. (2014) The age of river-transported carbon: A global perspective, *Global Biogeochemical Cycles,* 29, 122–137, doi:10.1002/2014GB004911.

Matilainen, A., Vepsäläinen, M., & Sillanpää, M. (2010). Natural organic matter removal by coagulation during drinking water treatment: A review. Advances in Colloid and Interface Science, 159(2), 189–197. https://doi.org/10.1016/j.cis.2010.06.007

Matisoff, G. (2014). 210Pb as a tracer of soil erosion, sediment source area identification and particle transport in the terrestrial environment. *Journal of Environmental Radioactivity*, 138, 343–354. https://doi.org/10.1016/j.jenvrad.2014.03.008

Mayer, L.M., Schick, L.L., Skorko, K. (2006), Photodissolution of particulate organic matter from sediments, *Limnol. Oceanogr., 51(2),* 1064–1071

Medeiros, G. de O. R., Giarolla, A., Sampaio, G., & Marinho, M. de A. (2016). Estimates of Annual Soil Loss Rates in the State of São Paulo, Brazil. *Revista Brasileira de Ciência Do Solo*, 40(0), 1–18. https://doi.org/10.1590/18069657rbcs20150497

Mendonca, R, Kosten, S., Sobek, S., Jaqueline Cardoso, S., Paulo Figueiredo-Barros, M., Henrique Duque Estrada, C., & Roland, F. (2016). Organic carbon burial efficiency in a subtropical hydroelectric reservoir. *Biogeosciences*, 13(11), 3331–3342. https://doi.org/10.5194/bg-13-3331-2016

Mendonça, R., Kosten, S., Sobek, S., Cole, J.J., Bastos, A. C., Albuquerque, A. L., Cardoso, S.J., Roland, F. (2014), Carbon Sequestration in a Large Hydroelectric Reservoir: An Integrative Seismic Approach, *Ecosystems, 17*, 430–441

Merten, G. H., & Minella, J. P. G. (2013). The expansion of Brazilian agriculture: Soil erosion scenarios. *International Soil and Water Conservation Research*, 1(3), 37–48. https://doi.org/10.1016/S2095-6339(15)30029-0

Mendonça, R., Kosten, S., Sobek, S., Barros, N., Cole, J.J., Tranvik, L., Roland, F. (2012), Hydroelectric carbon sequestration, *Nature Geoscience 5*, 838–840

Meybeck, M. (1982), Carbon, Nitrogen, And Phosphorous transport by world rivers*, American Journal of Science, 282,* 401–450

Meybeck, M., Helmer, R. (1989), The quality of rivers: from pristine stage to global pollution, *Palaeography, Palaeoclimatology, Palaeoecology (Global and Planetary Change Section), 75*, 283–309

Meyers, P. A., & Ishiwatari, R. (1993). Lacustrine organic geochemistry-an overview of indicators of organic matter sources and diagenesis in lake sediments. *Organic Geochemistry*, 20(7), 867–900. https://doi.org/10.1016/0146-6380(93)90100-P

Meyers, P.A. (1994), Preservation of elemental and isotopic source identification of sedimentary organic matter, *Chemical Geology 114,* 289–302

Millour, M., Gagné, J.P. (2013), Sorption Between Humic Substances and Marine Microalgae in Estuaries: Effects of Microalgae Species, pH and Salinity, J. Xu et al. (eds.), *Functions of Natural Organic Matter in Changing Environment*, Zhejiang University Press and Springer Science+Business Media Dordrecht. doi 10.1007/978-94-007-5634-2_149

Miklas Scholz, Chapter 7 - Coagulation and Flocculation, In Wetlands for Water Pollution Control (Second Edition), Elsevier, 2016, Pages 37-46, ISBN 9780444636072, https://doi.org/10.1016/B978-0-444-63607-2.00007-1.

Mikutta, R., Mikutta, R., Kalbitz, K., Scheel, T., Kaiser, K., Jahn, R. (2007), Biodegradation of forest floor organic matter bound to minerals via different binding mechanisms, *Geochimica et Cosmochimica Acta 71,* 2569–2590

Molot, L. A., Dillon, P.J. (1997), Photolytic regulation of dissolved organic carbon in northern lakes, *Global Biogeochemical Cycles 11(3),* 357-365

Monteiro, M. T. F., Oliveira, S. M., Luizão, F. J., Cândido, L. A., Ishida, F. Y., & Tomasella, J. (2014). Dissolved organic carbon concentration and its relationship to electrical conductivity in

317

the waters of a stream in a forested Amazonian blackwater catchment. *Plant Ecology and Diversity*, 7(1–2), 205–213. https://doi.org/10.1080/17550874.2013.820223

Monteith, D. T., Stoddard, J. L., Evans, C. D., De Wit, H. A., Forsius, M., Høgåsen, T., Wilander, A., Skjelkvåle, B.L., Jeffries, D.S., Vuorenmaa, J., Keller, B., Kopácek, J., Vesely, J. (2007). Dissolved organic carbon trends resulting from changes in atmospheric deposition chemistry. *Nature*, 450(7169), 537–540. https://doi.org/10.1038/nature06316

Morgan, R.P.C., Quinton, J.N., R.E., Smith, Gobers, G., Poesen, W.A., Auerswald, K., Chisci, G., Torri, D., Styczen, E. (1998). The European Soil Erosion Model (EUROSEM): A Dynamic Approach for Predicting Sediment Transport from Fields and Small Catchments, *Earth Surface Processes and Landforms,* 23, 527–544. https://doi.org/10.1002/(SICI)1096-9837(199806)23

Murphy, K. R., Stedmon, C. A., Graeber, D., & Bro, R. (2013). Fluorescence spectroscopy and multi-way techniques. PARAFAC. *Analytical Methods*, 5(23), 6557–6566. https://doi.org/10.1039/c3ay41160e

Nagao, S., Aramaki, T., Seki, O., Uchida, M., Shibata, Y. (2010) Carbon isotopes and lignin composition of POC in a small river in Bekanbeushi Moor, northern Japan, *Nuclear Instruments and Methods in Physics Research Section B: Beam Interactions with Materials and Atoms*, Volume 268, Issues 7–8, 1098-1101, doi: 10.1016/j.nimb.2009.10.108

Naipal, V., Reick, C., Pongratz, J., & Van Oost, K. (2015). Improving the global applicability of the RUSLE model - Adjustment of the topographical and rainfall erosivity factors. *Geoscientific Model Development*, 8(9), 2893–2913. https://doi.org/10.5194/gmd-8-2893-2015

Nearing, M. A., Foster, G. R., Lane, L. J. & Finkner, S. C. (1989). A Process-Based Soil Erosion Model for USDA-Water Erosion Prediction Project Technology. *Transactions of the ASAE*, 32(5), 1587–1593. https://doi.org/10.13031/2013.31195

Nerantzaki, S.D., Giannakis, G. V., Efstathiou, D., Nikolaidis, N. P., Sibetheros, I. A., Karatzas, G. P., Zacharias, I., 2015. Modeling suspended sediment transport and assessing the impacts of climate change in a karstic Mediterranean watershed. *Science of the Total Environment*, 538, pp.288–297. Available at: http://dx.doi.org/10.1016/j.scitotenv.2015.07.092.

Neto, R.R., Mead, R.N., Louda, J.W., Jaffe, R. (2006), Organic biogeochemistry of detrital flocculent material (floc) in a subtropical, coastal wetland, *Biogeochemistry 77,* 283–304

Neubecker, T. A., & Allen, H. E. (1983). The measurement of complexation capacity and conditional stability constants for ligands in natural waters. *Water Research*, 17(1), 1–14. https://doi.org/10.1016/0043-1354(83)90280-4

Niessner, G., Buchberger, W. & Bonn, G.K., (1998), Anion exchange solid phase extraction of humic substances for the determination of complexed heavy metals in natural waters with high dissolved organic contents. *Monatshefte für Chemie*, 129, pp.597–605.

Nouira, A., Sayouty, E.H. & Benmansour, M., 2003. Use of 137Cs technique for soil erosion study in the agricultural region of Casablanca in Morocco. *Journal of Environmental Radioactivity*, 68(1), pp.11–26.

Nystrand, M.I., Österholm, P., Nyberg, M.E., Gustafsson, J.P. (2012), Metal speciation in rivers affected by enhanced soil erosion and acidity, *Applied Geochemistry 27*, 906–916

Oliviera, P.T.S., Rodrigues, D.B.B., Sobrinho, T.A., Panachuki, E., Wendland, E. (2013), Use of SRTM data to calculate the (R)USLE topographic factor, *Acta Scientiarum. Technology 35(3),* 507–513

Oliveira, P.T.S., Wendland, E. & Nearing, M.A., 2013. Rainfall erosivity in Brazil: A review. *Catena*, 100, pp.139–147. Available at: http://dx.doi.org/10.1016/j.catena.2012.08.006.

O'Leary, M.H. (1981). Carbon isotope fractionations in plants, *Phytochemistry, 20(4)*, 553–567.

Oni, S. K., Futter, M. N., Bishop, K., Köhler, S. J., Ottosson-Löfvenius, M., & Laudon, H. (2013). Long-term patterns in dissolved organic carbon, major elements and trace metals in boreal headwater catchments: Trends, mechanisms and heterogeneity. *Biogeosciences*, 10(4), 2315–2330. https://doi.org/10.5194/bg-10-2315-2013

Owens, M., 1984. Severn Estuary - An appraisal of water quality. *Marine Pollution Bulletin*, 15(2), pp.41–47.

Owens, P.N. & Walling, D.E., 1996. Spatial variability of caesium–137 inventories at reference sites: An example from two contrasting sites in England and Zimbabwe. *Applied Radiation and Isotopes*, 47(7), pp.699–707.

Pacheco, F. S., Miranda, M., Pezzi, L. P., Assireu, A., Marinho, M. M., Malafaia, M., Reis, A., Sales, M., Correia, G., Domingos, P., Iwama, A., Rudorff, C., Oliva, P. & Ometto, J. P. (2017). Water quality longitudinal profile of the Paraíba do Sul River, Brazil during an extreme drought

319

event. *Limnology and Oceanography*, 62(October), S131–S146. https://doi.org/10.1002/lno.10586

Panagos, P., Borrelli, P., Meusburger, K., Alewell, C., Lugato, E., & Montanarella, L. (2015). Estimating the soil erosion cover-management factor at the European scale. *Land Use Policy*, 48, 38–50. https://doi.org/10.1016/j.landusepol.2015.05.021

Panagos, P., Borrelli, P., Meusburger, K. (2015), A New European Slope Length and Steepness Factor (LS-Factor) for Modeling Soil Erosion by Water, *Geosciences 5(2)*, 117–126. https://doi.org/10.3390/geosciences5020117

Pandey, A. Himanshu, S.K., Mishra, S.K., Singh, V.P. (2016) Physically based soil erosion and sediment yield models revisited. *Catena,* 147, pp.595–620. Available at: http://dx.doi.org/10.1016/j.catena.2016.08.002.

Paroissien, JB., Darboux, F., Couturier, A., Devillers, B., Mouillot, F., Raclot, D., Le Bissonnais, Y. (2015), A method for modeling the effects of climate and land use changes on erosion and sustainability of soil in a Mediterranean watershed (Languedoc, France), *Journal of Environmental Management, 150,* 57–68

Parsons, A.J. & Foster, I.D.L., (2011). What can we learn about soil erosion from the use of 137Cs? *Earth-Science Reviews*, 108 (1–2), pp.101–113. Available at: http://dx.doi.org/10.1016/j.earscirev.2011.06.004.

Passow, U. (2002) Transparent exopolymer particles (TEP) in aquatic environments, *Progress in Oceanography 55,* 287–333

Pawson, R. R., Evans, M. G. and Allott, T. E. (2012) Fluvial carbon flux from headwater peatland streams: significance of particulate carbon flux. *Earth Surface Processes and Landforms*, 37: 1203-1212. doi:10.1002/esp.3257

Petrone, K. C., Fellman, J. B., Hood, E., Donn, M. J., & Grierson, P. F. (2011). The origin and function of dissolved organic matter in agro-urban coastal streams. Journal of Geophysical Research: *Biogeosciences*, 116(1). https://doi.org/10.1029/2010JG001537

Pisani, O., Yamashita, Y., Jaffe, R. (2011), Photo-dissolution of flocculent, detrital material in aquatic environments: Contributions to the dissolved organic matter pool, *Water Research 45*, 3836–3844

Poirier, N. Sohi, S. P., Gaunt, J.L., Mahieu, N., Randall, E.W. Powlson, D.S. Evershed, R.P., (2005), The chemical composition of measurable soil organic matter pools. *Organic Geochemistry*, 36(8), pp.1174–1189.

Porcal, P., Molot, P.J., Dillon, L.A. (2015) Temperature Dependence of Photodegradation of Dissolved Organic Matter to Dissolved Inorganic Carbon and Particulate Organic Carbon, *PLOS ONE, 10(6)*, e0128884.

Porcal, P., Koprivnjak, J. F., Molot, L. A., & Dillon, P. J. (2009). Humic substances-part 7: The biogeochemistry of dissolved organic carbon and its interactions with climate change. *Environmental Science and Pollution Research*, 16(6), 714–726. https://doi.org/10.1007/s11356-009-0176-7

Porto, P. & Walling, D.E. (2012) Validating the use of ^{137}Cs and ^{210}Pb$_{ex}$ measurements to estimate rates of soil loss from cultivated land in southern Italy. Journal of Environmental Radioactivity, 106, pp.47–57. Available at: http://dx.doi.org/10.1016/j.jenvrad.2011.11.005.

Pourret, O., Davranche, M., Gruau, G., Dia, A. (2007), Rare earth elements complexation with humic acid, *Chemical Geology 243,* 128–141

Pribyl, D.W. (2010), A critical review of the conventional SOC to SOM conversion factor, *Geoderma* 156, 75–83

Pullin, M. J., Progess, C. A., & Maurice, P. A. (2004). Effects of photoirradiation on the adsorption of dissolved organic matter to goethite. *Geochimica et Cosmochimica Acta*, 68(18), 3643–3656. https://doi.org/10.1016/j.gca.2004.03.017

Quine, T.A. (1999), Use of caesium-137 data for validation of spatially distributed erosion models: the implications of tillage erosion, *Catena 37*, 415–430

Quine, T.A., Van Oost, K. (2007) Quantifying carbon sequestration as a result of soil erosion and deposition: retrospective assessment using caesium-137 and carbon inventories, *Global Change Biology*, 13, 2610–2625, doi: 10.1111/j.1365-2486.2007.01457.x

Quinton, J.N., Govers, G., Van Oost, K., Bardgett, R.D. (2010), The impact of agricultural soil erosion on biogeochemical cycling, *Nature Geoscience 3*. 311–314, doi: 10.1038/ngeo838

Raymond, P. A., Hartmann, J., Lauerwald, R., Sobek, S., McDonald, C., Hoover, M., Butman, D., Striegl, R., Mayorga, E., Humborg, C., Kortelainen, P., Dürr, H., Meybeck, M., Ciais, P. &

Guth, P. (2013). Global carbon dioxide emissions from inland waters. *Nature*, 503(7476), 355–359. https://doi.org/10.1038/nature12760

Raymond, P. A., Bauer, J. E., Caraco, N. F., Cole, J. J., Longworth, B., & Petsch, S. T. (2004). Controls on the variability of organic matter and dissolved inorganic carbon ages in northeast US rivers. Marine Chemistry, 92(1–4 SPEC. ISS.), 353–366. https://doi.org/10.1016/j.marchem.2004.06.036

Renard, K.G. & Freimund, J.R. (1994) Using monthly precipitation data to estimate the *R*-factor in the revised USLE, *Journal of Hydrology,* 157, 287–306

Regnier, P., Friedlingstein, P., Ciais, P., Mackenzie, F.T., Gruber, N., Janssens, I.A., Laruelle, G.G., Lauerwald, R., Luyssaert, S., Andersson, A.J., Arndt, S., Arnosti, C., Borges, A.V., Dale, A.W., Gallego-Sala, A., Goddéris, Y., Goossens, N., Hartmann, J., Heinze, C., Ilyina, T., Joos, F., LaRowe, D.E., Leifeld, J., Meysman, F.J.R., Munhoven, G., Raymond, P.A., Spahni, R., Suntharalingam, P., Thullner, M. (2013), Anthropogenic perturbation of the carbon fluxes from land to ocean, *Nature Geoscience 6*, 597–607. doi: 10.1038/ngeo1830

Repeta, D. J., Quan, T. M., Aluwihare, L. I., & Accardi, A. (2002). Chemical characterization of high molecular weight dissolved organic matter in fresh and marine waters. *Geochimica et Cosmochimica Acta,* 66(6), 955–962. https://doi.org/10.1016/S0016-7037(01)00830-4

Ribeiro, M. C., Metzger, J. P., Martensen, A. C., Ponzoni, F. J., & Hirota, M. M. (2009) The Brazilian Atlantic Forest: How much is left, and how is the remaining forest distributed? *Implications for conservation. Biological Conservation*, 142(6), 1141–1153. https://doi.org/10.1016/j.biocon.2009.02.021

Richey, J.E., Melack, J.M., Aufdenkempe, A.K., Ballester, V.M., Hess, L.L. (2002) Outgassing from Amazonian rivers and wetlands as a large tropical source of atmospheric CO_2, *Nature,* 416*,* 617–619

Ritchie, J.C. & McHenry, J.R. (1990) Application of Radioactive Fallout Cesium-137 for Measuring Soil Erosion and Sediment Accumulation Rates and Patterns: A Review. *Journal of Environmental Quality*, 19, pp.215–233. http://dx.doi.org/10.2134/jeq1990.00472425001900020006x

Ritson, J. P., Croft, J. K., Clark, J. M., Brazier, R. E., Templeton, M. R., Smith, D., & Graham, N. J. D. (2019). Sources of dissolved organic carbon (DOC) in a mixed land use catchment (Exe, UK). *Science of the Total Environment*, 666, 165–175. https://doi.org/https://doi.org/10.1016/j.scitotenv.2019.02.228

Rodway-Dyer, S.J. & Walling, D.E. (2010) The use of 137Cs to establish longer-term soil erosion rates on footpaths in the UK. *Journal of Environmental Management*, 91(10), pp.1952–1962. Available at: http://dx.doi.org/10.1016/j.jenvman.2010.04.014.

Rumpel, C., Kögel-Knabner, I. (2011), Deep soil organic matter—a key but poorly understood component of terrestrial C cycle, *Plant Soil 338,* 143–158

Saidy, A.R., Smernik, R.J., Baldock, J.A., Kaiser, K., Sanderman, J., Macdonald, L.M. (2012), Effects of clay mineralogy and hydrous iron oxides on labile organic carbon stabilisation, *Geoderma 173–174,* 104–110

Salomé, C., Nunan, N., Pouteau, V., Lerch, T.Z., Chenu, C. (2010), Carbon dynamics in topsoil and in subsoil may be controlled by different regulatory mechanisms, *Global Change Biology 16,* 416–426. doi:10.1111/j.1365-2486.2009.01884.x

Sanchez, N. P., Skeriotis, A. T., & Miller, C. M. (2014). A PARAFAC-based long-term assessment of DOM in a multi-coagulant drinking water treatment scheme. *Environmental Science and Technology*, 48(3), 1582–1591. https://doi.org/10.1021/es4049384

Sand-Jensen, K., Pedersen, M.F., Nielsen, S.L. (1992), Photosynthetic use of inorganic carbon among primary and secondary water plants in streams, *Freshwater Biology 27,* 283–293

Scharlemann, J. P. W., Tanner, E. V. J., Hiederer, R., & Kapos, V. (2014). Global soil carbon: Understanding and managing the largest terrestrial carbon pool. *Carbon Management*, 5(1), 81–91. https://doi.org/10.4155/cmt.13.77

Schindler Wildhaber, Y., Liechti, R., and Alewell, C. (2012) Organic matter dynamics and stable isotope signature as tracers of the sources of suspended sediment, *Biogeosciences*, 9, 1985–1996, doi: 10.5194/bg-9-1985-2012.

Schlesinger, W.H., Melack, J.M. (1981), Transport of organic carbon in world rivers, *Tellus 33,* 172–187

Schlesinger, W.H., Chapter 4 Soil organic matter: a source of atmospheric CO_2, The Role of Terrestrial Vegetation in the Global Carbon Cycle: Measurement by Remote Sensing, Edited by G.M. Woodwell, 1984 SCOPE, Published by John Wiley & Sons Ltd

Schäfer, A. I., Schwicker, U., Fischer, M.M., Fane, A.G., Waite, T.D. (2000). Microfiltration of colloids and natural organic matter. *Journal of Membrane Science*, 171, 151–172.

Segura, C., Sun, G., McNulty, S., & Zhang, Y. (2014). Potential impacts of climate change on soil erosion vulnerability across the conterminous United States. Journal of Soil and Water Conservation, 69(2), 171–181. https://doi.org/10.2489/jswc.69.2.171

Seidel, M., Beck, M., Riedel, T., Waska, H., Suryaputra, I. G. N. A., Schnetger, B., Niggemann, J., Meinhard, S., Dittmar, T. (2014). Biogeochemistry of dissolved organic matter in an anoxic intertidal creek bank. *Geochimica et Cosmochimica Acta*, 140, 418–434. https://doi.org/10.1016/j.gca.2014.05.038

Silva, L. H. S., Huszar, V. L. M., Marinho, M. M., Rangel, L. M., Brasil, J., Domingues, C. D., Branco, C. C., Roland, F. (2014). Drivers of phytoplankton, bacterioplankton, and zooplankton carbon biomass in tropical hydroelectric reservoirs. Limnologica, 48, 1–10. https://doi.org/10.1016/j.limno.2014.04.

Silveria, M.L., Comerford, N.B., Reddy, K.R., Cooper, W.T., El-Rifai, H. (2008), Characterization of soil organic carbon pools by acid hydrolysis, *Geoderma 144,* 405–414

Sinninghe Damsté, J.S., Rijpstra, W.I.C., Hopmans, E.C., Weijers, J.W.H., Foesel, B.U., Overmann, J., Dedysh, S.N. (2011) 13,16-Dimethyl Octacosanedioic Acid (iso-Diabolic Acid), a Common Membrane-Spanning Lipid of Acidobacteria Subdivisions 1 and 3, *Applied and Environmental Microbiology*, Vol. 77, No. 12, 4147-4154.

Six, J., Elliott, E.T., Paustian, K., Doran, J.W. (1998), Aggregation and Soil Organic Matter Accumulation in Cultivated and Native Grassland Soils, *Soil Sci. Soc. Am. J. 62,* 1367-1377

Sleighter, R. L., & Hatcher, P. G. (2008). Molecular characterization of dissolved organic matter (DOM) along a river to ocean transect of the lower Chesapeake Bay by ultrahigh resolution electrospray ionization Fourier transform ion cyclotron resonance mass spectrometry. *Marine Chemistry*, 110(3–4), 140–152. https://doi.org/10.1016/j.marchem.2008.04.008

Sonke, J.E., Salters, V.J.M. (2006), Lanthanide–humic substances complexation. I. Experimental evidence for a lanthanide contraction effect, *Geochimica et Cosmochimica Acta 70*, 1495–1506

Stallard, R.F. (1998), Terrestrial sedimentation and the carbon cycle: Coupling weathering and erosion to carbon burial, Global Biogeochemical Cycles 12(2), 231–257

Starr, G. C., Malone, R., Hothem, D., Owens, L., & Kimble, J. (2000). Modeling Soil Carbon Transported By Water Erosion Processes, *Land Degradation and Development* 91, 83–91.

Staunton, S., Roubaud, M. (1997), Adsorption of ^{137}Cs on Montmorillonite and Illite: effect of charge compensating cation, ionic strength, concentration of Cs, K and fulvic acid, *Clays and Clay Minerals, 45*, 2, 251–260.

Stechemesser, HJ., 2005, Coagulation and Flocculation, Second Edition, CRC Press, ISBN: 1-57444-455-7.

Stedmon, C. a., & Bro, R. (2008). Characterizing dissolved organic matter fluorescence with parallel factor analysis: a tutorial. *Limnology and Oceanography: Methods*, 6, 572–579. https://doi.org/10.4319/lom.2008.6.572

Stedmon, C. A., Markager, S., & Bro, R. (2003). Tracing dissolved organic matter in aquatic environments using a new approach to fluorescence spectroscopy. *Marine Chemistry*, 82(3–4), 239–254. https://doi.org/10.1016/S0304-4203(03)00072-0

Stockmann, U., Adams, M.A., Crawford, J.W., Field, D.J., Henakaarchchi, N., Jenkins, M., Minasny, B., McBratney, A.B., de Remy de Courcelles, V., Singh, K., Wheeler, I., Abbott, L., Angers, D.A., Baldock, J., Bird, M., Brookes, P.C., Chenu, C., Jastrow, J.D., Lal, R., Lehmann, J., O'Donnellk, A.G., Parton, W.J., Whitehead, D., Zimmermann, M. (2013), The knowns, known unknowns and unknowns of sequestration of soil organic carbon, *Agriculture, Ecosystems and Environment 164*, 80– 99

Strohmeier, S., Knorr, K.H., Reichert, M., Frei, S., Fleckenstein, J. H., Peiffer, S., E. Matzner (2013) Concentrations and fluxes of dissolved organic carbon in runoff from a forested catchment: insights from high frequency measurements, Biogeosciences, 10, 905–916, 2013

Strosser, E. (2010), Methods for determination of labile soil organic matter: An overview, *Journal of Agrobiology 27(2)*, 49–60

Sun, H., Han, J., Zhang, S., Lu, X. (2015), Carbon isotopic evidence for transformation of DIC to POC in the lower Xijiang River, SE China, *Quaternary International 380-381*, 288–296

Sørensen, R., Zinko, U., Seibert, J. (2006), On the calculation of the topographic wetness index: evaluation of different methods based on field observations. *Hydrology and Earth System Sciences Discussions*, European Geosciences Union, 10 (1), pp.101-112.

Syvitski, J.P.M., Vörösmarty, C.J., Kettner, A.J., Green, P. (2005), Impact of Humans on the Flux of Terrestrial Sediment to the Global Coastal Ocean, *Science*, 308 (5720), 376-380. https://doi.org/10.1126/science.1109454

Søndergaard, M., Stedmon, C. A., & Borch, N. H. (2003), Fate of terrigenous dissolved organic matter (DOM) in estuaries: Aggregation and bioavailability. *Ophelia*, 57(3), 161–176. https://doi.org/10.1080/00785236.2003.10409512

Tang, X. Y., Yang, H., Du, M. Y., Zhao, Q. G., Li, R. Y. (2006), Identification of ^{137}Cs reference sites in southeastern China. *Pedosphere*, 16(4), pp.468–476.

Taylor, M., Elliott, H. A., & Navitsky, L. O. (2018), Relationship between total dissolved solids and electrical conductivity in Marcellus hydraulic fracturing fluids. *Water Science and Technology*, 77(8), 1998–2004. https://doi.org/10.2166/wst.2018.092

Yasunari, T. J., Stohl, A., Hayano, R. S., Burkhart, J. F., Eckhardt, S., & Yasunari, T. (2011), Cesium-137 deposition and contamination of Japanese soils due to the Fukushima nuclear accident. *Proceedings of the National Academy of Sciences*, 108(49), 19530–19534. https://doi.org/10.1073/pnas.1112058108

Terranova, O. Antronico, L., Coscarelli, R., Iaquinta, P. (2009), Soil erosion risk scenarios in the Mediterranean environment using RUSLE and GIS: An application model for Calabria (southern Italy). Geomorphology, 112(3–4), pp.228–245. DOI: http://dx.doi.org/10.1016/j.geomorph.2009.06.009.

Tipping, E., Somerville, C.J., Luster, J. (2016), The C/N:P:S stoichiometry of soil organic matter, *Biogeochemistry*, 130:117-131. DOI: 10.1007/s10533-016-0247-z

Thurman, E.M., Wershaw, R.L., Malcolm, R.L., Pinckney, D.J. (1982), Molecular size of aquatic humic substances, *Organic Geochemistry 4*, 27–35

Tisdall, J.M., Oades, J.M. (1982), Organic matter and water-stable aggregates in soils, *Journal of Soil Science 33*, 141-163

Tranvik, L.J., Downing, J.A., Cotner, J.B., Loiselle, S.A., Striegl, R.G., Ballatore, T.J., Dillon, P., Finlay, K., Fortino, K., Knoll, L.B., Kortelainen, P.L., Kutser, T., Larsen, S., Laurion, I., Leech, D.M., McCallister, S.L., McKnight, D.M., Melack, J.M., Overholt, E., Porter, J.A., Prairie, Y., Renwick, W.H., Roland, F., Sherman, B.S., Schindler, D.W., Sobek, S., Tremblay, A., Vanni, M.J., Verschoor, A.M., von Wachenfeldt, E., Weyhenmeyer, G.A. (2009), Lakes

and reservoirs as regulators of carbon cycling and climate, *Limnology and Oceanography, 54(6,2)*, 2298–2314

Trumbore, S.E., Schiff, S.L., Aravena, R., Elgood, R. (1992), Sources and transformation of dissolved organic carbon in the Harp Lake forested catchment: the role of soils, *Radiocarbon,* VOL. 34(3), 626–635

Tsai, C., Iacobellis, S., Lick, W.J. (1987), Flocculation of fine-grained lake sediments due to a uniform shear stress, *Great Lakes Res. 13(2),* 135–146

van Dongen, B. E., Semiletov, I., Weijers, J. W. H., and Gustafsson, Ö. (2008), Contrasting lipid biomarker composition of terrestrial organic matter exported from across the Eurasian Arctic by the five great Russian Arctic rivers, *Global Biogeochemical Cycles*, 22, GB1011, doi:10.1029/2007GB002974

van Hemelryck, H., Govers, G., Van Oost, K., Merckx, R. (2011), Evaluating the impact of soil redistribution on the *in situ* mineralisation of soil organic carbon, *Earth Surf. Process. Landforms 36,* 427–438

van Olphen, H. (1964), Internal mutual flocculation in clay suspensions, *Journal of colloid science 19,* 313–322

Van Oost, K., Quine, T. A., Govers, G., De Gryze, S., Six, J., Harden, J.W., Ritchie, J. C., McCarty, G.W., Heckrath, G., Kosmas, C., Giraldez, J. V., Marques da Silva, J. R., & Merckx, R. (2007), The Impact of Agricultural Soil Erosion on the Global Carbon Cycle, *Science 318,* 626–629

Van Remortel, R., M. Hamilton & R. Hickey (2001) Estimating the LS factor for RUSLE through iterative slope length processing of digital elevation data. *Cartography,* v. 30, no. 1, pp. 27-35.

Vázquez-Ortega, A., Perdrial, J., Harpold, A., Zapata-Ríos, X., Rasmussen, C., McIntosh, J., Schaap, M., Pelletier, J.D., Brooks, P.D., Amistadi, M.K., Chorover, J. (2015) Rare earth elements as reactive tracers of biogeochemical weathering in forested rhyolitic terrain, *Chemical Geology 391*, 19–32¨

Verney, R., Lafite, R., & Brun-Cottan, J. C. (2009) Flocculation potential of estuarine particles: The importance of environmental factors and of the spatial and seasonal variability of suspended particulate matter. *Estuaries and Coasts*, 32(4), 678–693. https://doi.org/10.1007/s12237-009-9160-1

Vähätalo, A.V., Wetzel, R.G. (2008) Long-term photochemical and microbial decomposition of wetland-derived dissolved organic matter with alteration of 13C:12C mass ratio, *Limnology and Oceanography, 53(4),* 1387–1392

von Wachenfeldt, E., Tranvik, L.J. (2008), Sedimentation in Boreal Lakes—The Role of Flocculation of Allochthonous Dissolved Organic Matter in the Water Column, *Ecosystems 11,* 803–814. doi: 10.1007/s10021-008-9162-z

von Wachenfeldt, E., Sobek, S., Bastviken, D., Tranvik, L. (2008), Linking allochthonous dissolved organic matter and boreal lake sediment carbon sequestration: The role of light-mediated flocculation, *Limnology and Oceanography, 53(6),* 2416–2426

Wallin, M. B., G. A. Weyhenmeyer, D. Bastviken, H. E. Chmiel, S. Peter, S. Sobek, L. Klemedtsson (2015) Temporal control on concentration, character, and export of dissolved organic carbon in two hemiboreal headwater streams draining contrasting catchments, *Journal of Geophysical Research: Biogeosciences*, 120, 832–846, doi:10.1002/2014JG002814.

Walling, D.E., Russell, M.A., Webb, B.W. (2001) Controls on the nutrient content of suspended sediment transported by British rivers, *The Science of the Total Environment* 266, 113]123

Walling, D.E. (1998) Use of ^{137}Cs and other fallout radionuclides in soil erosion investigations: progress, problems and prospects, In *Use of ^{137}Cs in the Study of Soil Erosion and Sedimentation*, IAEA-TECDOC-1028, IAEA, Vienna 39-62.

Walling, D. E., He, Q., & Quine, T. A. (1995) Use of caesium-137 and lead-210 as tracers in soil erosion investigations. *Tracer Technologies for Hydrological Systems (Proceedings of a Boulder Symposium, July 1995)*, IAHS Publication No. 229, (229), 163–172.

Walling, D.E. & Quine, T.A. (1991) Use of Cs measurements to investigate soil erosion on arable fields in the UK: potential applications and limitations, *Journal of Soil Science*, 42,147-I65

Walling, D.E., Webb, B.W. (1985) Estimating the discharge of contaminants to coastal waters by rivers: some cautionary comments, *Marine Pollution Bulletin*. Vol. 16, No. 12, pp. 488-492

Walton, N. R. G. (1989). Electrical Conductivity and Total Dissolved Solids—What is Their Precise Relationship? *Desalination*, 72(3), 275–292. https://doi.org/10.1016/0011-9164(89)80012-8

Wang, B., Zheng, F., Guan, Y. (2016) Improved USLE-K factor prediction: A case study on water erosion areas in China, *International Soil and Water Conservation Research*, Volume 4, Issue 3, 168–176.

Wang, Z., Van Oost, K., Lang, A., Quine, T.A., Clymans, W., Merckx, R., Notebaert, B., Govers, G. (2014) The fate of buried organic carbon in colluvial soils: a long-term perspective, *Biogeosciences 11,* 873–883

Watanabe, K., & Kuwae, T. (2015) How organic carbon derived from multiple sources contributes to carbon sequestration processes in a shallow coastal system? *Global Change Biology*, 21(7), 2612–2623. https://doi.org/10.1111/gcb.12924

WCD World Commission on Dams (2000) Dams and development: a framework for decision making. London, UK: Earthscan.

Wei Guo, Feng Ye, Shendong Xu, Guodong Ji (2015) Seasonal variation in sources and processing of particulate organic carbon in the Pearl River estuary, South China, *Estuarine, Coastal and Shelf Science 167*, 540–548

Weishaar, J.L., Aiken, G.R., Bergmaschi, B.A., Fram, M.S., Fujii, R., Mopper, K. (2003) Evaluation of Specific Ultraviolet Absorbance as an Indicator of the Chemical Composition and Reactivity of Dissolved Organic Carbon, *Environ. Sci. Technol., 37*, 4702–4708

Wetzel, R.G. (1984) Detrital dissolved and particulate organic carbon functions in aquatic ecosystems. *Bulletin of Marine Science*, 35(3), pp.503–509.

Whittaker, A. & Leveridge, B.E. (2011) The North Devon Basin: A Devonian passive margin shelf succession. *Proceedings of the Geologists' Association*, 122(4), pp.718–744. Available at: http://dx.doi.org/10.1016/j.pgeola.2011.03.006.

Wilken, R.D., Moreira, I., Rebello, A., (1986) ^{210}Pb and ^{137}Cs fluxes in a sediment core from Guanabara Bay, Brazil, *The Science of the Total Environment*, 58, p. 195–198

Worrall, F., & Burt, T. P. (2007) Trends in DOC concentration in Great Britain. *Journal of Hydrology*, 346(3–4), 81–92. https://doi.org/10.1016/j.jhydrol.2007.08.021

Wren, D. G., Rigby, J. R., Davidson, G. R., & Locke, M. A. (2016) Determination of lake sediment accumulation rates in an agricultural watershed using lead-210 and cesium-137. *Journal of Soil and Water Conservation*, 71(2), 137–147. https://doi.org/10.2489/jswc.71.2.137

Yang, D., Kanae, S., Oki, T., Koike, T., & Musiake, K. (2003) Global potential soil erosion with reference to land use and climate changes. *Hydrological Processes*, 17(14), 2913–2928. https://doi.org/10.1002/hyp.1441

Yurista, P. M., Johnston, K., Rice, G., Kipphut, G. W. & White, D. S. (2001) Particulate Organic Carbon Patterns in a Mainstem Reservoir, Kentucky Lake, USA. *Lake and Reservoir Management*, 17:4, 330-340. https://doi.org/10.1080/07438140109354139

Zapata, F. (2003) The use of environmental radionuclides as tracers in soil erosion and sedimentation investigations: recent advances and future developments. *Soil & Tillage Research*, 69(1–2), pp.3–13.

Zech, W., Senesi, N., Guggenberger, G., Kaiser, K., Lehmann, J., Miano, T.M., Miltner, A., Schroth, G. (1997) Factors controlling humification and mineralisation of soil organic matter in the tropics, *Geoderma 79*, 117-161

Zhang X., Higgitt, D. L., Walling D. E. (1990) A preliminary assessment of the potential for using caesium-137 to estimate rates of soil erosion in the Loess Plateau of China, *Hydrological Sciences Journal*, 35:3, 243-252. https://doi.org/10.1080/02626669009492427

Zhang, X.C., Zhang, G.H., Wei, X. (2015), How to make ^{137}Cs erosion estimation more useful: An uncertainty perspective, *Geoderma 239–240*, 186–194

Zheng, J. J., He, X. Bin, Walling, D., Zhang, X. B., Flanagan, D., & Qi, Y. Q. (2007). Assessing soil erosion rates on manually-tilled hillslopes in the Sichuan Hilly Basin using ^{137}Cs and [210]Pb$_{ex}$ measurements. *Pedosphere*, 17(3), 273–283. https://doi.org/10.1016/S1002-0160(07)60034-4

Zou, X.M., Ruan, H.H., Fu, Y., Yang, X.D., Sha, L.Q. (2005), Estimating soil labile organic carbon and potential turnover rates using a sequential fumigation-incubation procedure, *Soil Biology & Biochemistry 37,* 1923–1928

Books

Anke, M., Ihnat, M., & Stoeppler, M. (2004). *Elements and their compounds in the environment.* Environmental Science and Pollution Research (Vol. 11). https://doi.org/10.1007/BF02979677

Atkins, P. & de Paula, J. (2005) *Elements of physical chemistry,* 4th edition, United States, W.H. Freeman and Company, pg. 473.

Bagotsky, V.S. (2006). *Fundamentals of Electrochemistry*, 2nd Edition, Hoboken, John Wiley & Sons, p. 22.

Blanco, H. & Lal, R. (2008) *Principles of Soil Conservation and Management*, Springer, Dordrecht, Springer Science+Business Media B.V. doi: https://doi.org/10.1007/978-1-4020-8709-7

Bratby, J. (2006) *Coagulation and Flocculation in Water and Wastewater Treatment*, IWA publishing, 2nd edition

Chesworth, W. (2008) *Encyclopaedia of Soil Science,* Springer, Dordrecht, Berlin, p. 7.

Engel, M.H., Macko, S.A. (1993), *Organic Geochemistry Principles and Applications,* Springer Science + Business Media LLC, New York, ISBN 978-1-4613-6252-4

Enghag, P. (2004), *Encyclopedia of the Elements*, WILEY-VCH Verlag GmbH & Co. KGaA: Weinheim.

Findlay, S.E.G., Sinsabaugh R.L. (2003) *Aquatic Ecosystems Interactivity of Dissolved Organic Matter,* ed by Findlay, S.E.G., Sinsabaugh R.L., pp–, Elsevier Science (USA)

Koopal, L.K. & Science, C. (2005) *Ion Adsorption on Homogeneous and Heterogeneous Surfaces.* In *Coagulation and Flocculation: Theory and Applications*, ed by B. Dobiáš, pp.43–69. New York: Marcel Dekker. 1993

Schlesinger, W.H. (2013), *Biogeochemistry: An Analysis of Global Change*, Third Edition, Academic Press, Elsevier Inc.

Stechemesser, H.J., 2005, *Coagulation and Flocculation*, 2nd Edition, CRC Press, ISBN: 1-57444-455-7, pg. 808.

Vaýsek, P., (1994). *Principles of Electrochemistry*, 2nd edition J. Koryta, J. Dvořák and L. Kavan, Wiley, Chichester, pp.107–108.
Available at: http://linkinghub.elsevier.com/retrieve/pii/030245989487042X.

Zanello, P. (2011). *Inorganic Electrochemistry Theory, Practice and Application*, 2nd Edition, Padstow, UK: TJ International, p. 11-12.

Chapters

Bauer, J. E., & Bianchi, T. S. (2012). Dissolved Organic Carbon Cycling and Transformation. *Treatise on Estuarine and Coastal Science* (Vol. 5). Elsevier Inc. https://doi.org/10.1016/B978-0-12-374711-2.00502-7

Bertilsson, S. & Jones, J.B. (2003) Supply of dissolved organic matter to aquatic ecosystems: autochthonous sources, *Aquatic Ecosystems Interactivity of Dissolved Organic Matter,* ed by Findlay, S.E.G., Sinsabaugh R.L., pp–, Elsevier Science (USA), p. 4–5

Dukhin, S.S., Sjöblom, J., Sæther, Ø., *An Experimental and Theorethical Approach to the Dynamic Behaviour of Emulsions*. In: Hubbard, A.T., ed., (2006). *Emulsions and Emulsion Stability* 2nd Edition, Boca Raton: CRC Press, p. 6–7.

Ertel, J. R., Alberts, J. J., & Price, M. T. (1991). Transformation of riverine organic matter in estuaries, *Proceedings of the 1991 Georgia Water Resources Conference*, held March 19 and 20, 1991, at The University of Georgia, Kathryn J. Hatcher, Editor, Institute of Natural Resources, The University of Georgia, Athens, Georgia.309–312.

Fischer, H. (2003) The Role of Biofilms in the Uptake and Transformation of Dissolved Organic Matter, *Aquatic Ecosystems Interactivity of Dissolved Organic Matter,* ed by Findlay, S.E.G., Sinsabaugh R.L., pp–, Elsevier Science (USA), p. 285

Goldberg, S. (2004) Surface complexation modelling, *Encyclopedia of Soils in the Environment*, ed Hillel, D., 1st Edition, Academic Press. Pg. 97,

Heinirchs, S.M. (1993) *Early Diagenesis of Organic Matter: The Dynamics (Rates) of Cycling of Organic Compounds.* Edited by Engel, M.H., Macko, S.A. (1993) *Organic Geochemistry Principles and Applications,* Springer Science + Business Media LLC, New York, ISBN 978-1-4613-6252-4

Meyers, P.A., Ishiwatari, R., (2003) *The Early Diagenesis of Organic Matter in*

Lacustrine Sediments. Edited by Engel, M.H., Macko, S.A. (1993) *Organic Geochemistry Principles and Applications,* Springer Science + Business Media LLC, New York, ISBN 978-1-4613-6252-4

Ittekot, V., Laane, R.W.P.M. (1991) Fate of Riverine Particulate Organic Matter. In: Degens, E.T., Kempe, S., Richey, J.E. (Eds.), *Biogeochemistry of Major World Rivers*, Scope 42. Wiley, Chichester

Miklas Scholz*, Coagulation and Flocculation*, In: *Wetlands for Water Pollution Control* (2nd Edition), Elsevier, 2016, Pages 37–46, ISBN 9780444636072. https://doi.org/10.1016/B978-0-444-63607-2.00007-1.

Mulholland, P.J. (2003) Large-Scale Patterns in Dissolved Organic Carbon Concentration, Flux, and Sources, *Aquatic Ecosystems Interactivity of Dissolved Organic Matter,* ed by Findlay, S.E.G., Sinsabaugh R.L. (eds), Elsevier Science (USA), p. 140

Murphy, K. R., Bro, R. and Stedmon, C. A. (2014) Chemometric Analysis of Organic Matter Fluorescence, in Coble, P. G., Lead, J., Baker, A., Reynolds, D. M., and Spencer, R. G. M. (eds) *Aquatic Organic Matter Fluorescence.* Cambridge: Cambridge University Press (Cambridge Environmental Chemistry Series), pp. 339–375. https://doi.org/10.1017/CBO9781139045452.016

Ribeiro, M.C., Martensen, A.C., Metzger, J.P., Tabarelli, M., Scarano, F., Fortin, M.J. (2011) The Brazilian Atlantic Forest: A Shrinking Biodiversity Hotspot. *Biodiversity Hotspots: Distribution and Protection of Conservation Priority Areas.* Springer-Verlag Berlin Heidelberg 2011. Ch. 21. Doi: https://doi.org/10.1007/978-3-642-20992-5_21

Seyler, P., Coynel, A., Moreira-Turcq, P., Etcheber, H., Colas, C. & Orange, D., Bricquet, J., Laraque, A., Guyot, J.L., Olivry, J.C., Meybeck, M. (2006) Organic carbon transported by the equatorial rivers: example of Zaire-Congo and Amazon basins. In *Soil Erosion and Carbon Dynamics*, CRC Press, Ch.17, 255–274.

Thurman E.M. (1985) Transport, Origin and Source of Dissolved Organic Carbon. In: *Organic Geochemistry of Natural Waters.* Developments in Biogeochemistry, vol 2. Springer, Dordrecht.

Vaýsek, P., 1994. Principles of Electrochemistry, In: *Bioelectrochemistry and Bioenergetics*, 33, pp.107–108. 2nd edition J. Koryta, J. Dvořák and L. Kavan, Wiley, Chichester. Available at: http://linkinghub.elsevier.com/retrieve/pii/030245989487042X

Walling D.E., He Q., Appleby P.G. (2002) Conversion Models for Use in Soil-Erosion, Soil-Redistribution and Sedimentation Investigations. In: Zapata F. (eds) *Handbook for the Assessment of Soil Erosion and Sedimentation Using Environmental Radionuclides*. Springer, Dordrecht. Doi: https://doi.org/10.1007/0-306-48054-9_7

Databases and Datasets

Kottek, M., J. Grieser, C. Beck, B. Rudolf, and F. Rubel, 2006: World Map of the Köppen-Geiger climate classification updated. *Meteorol. Z.*, 15, 259-263. DOI: 10.1127/0941-2948/2006/0130.

Liebmann, B. & Allured, D., 2005: Daily precipitation grids for South America. *Bull. Amer. Meteor. Soc.*, 86, 1567-1570.
South American Precipitation data provided by the NOAA/OAR/ESRL PSD, Boulder, Colorado, USA, from their Web site at https://www.esrl.noaa.gov/psd/

https://earthexplorer.usgs.gov/, SRTM DEM 30m, s22 1-arc-sec, downloaded in 2016.

http://webarchive.iiasa.ac.at/Research/LUC/External-World-soil-database/HTML/index.html?sb=1 FAO/IIASA/ISRIC/ISSCAS/JRC, 2012. *Harmonized World Soil Database (version 1.2)*. FAO, Rome, Italy and IIASA, Laxenburg, Austria

Lehner, B., Grill G. (2013): Global river hydrography and network routing: baseline data and new approaches to study the world's large river systems. *Hydrological Processes*, 27(15): 2171–2186. HydroBASIN http://www.hydrosheds.org/page/hydrobasins

Mapa de Vegetacão do Brasil (1992) Instituto Brasileiro de Geografica e Estatistica, publication date: 1992-12-22 (downloaded: 2017-08-01).
http://mapas.mma.gov.br/mostratema.php?temas=vegetacao

Muniz Benedetti, M., Curi, N., Sparovek, G., de Carvalho Filho, A. and Silva S.H.G. (2011). Updated Brazilian's Georeferenced Soil Database – An Improvement for International Scientific Information Exchanging, Principles, Application and Assessment in Soil Science, Dr. Burcu E. Ozkaraova Gungor (Ed.), ISBN: 978-953-307-740-6, InTech, Available from: http://www.intechopen.com/books/principles-application-and-assessment-in-soil-science/updated-brazilian-sgeoreferenced-soil-database-an-improvement-for-international-scientific-informat

Land Cover Map 2015 [TIFF geospatial data], Scale 1:250000, Tiles: GB, Updated: 24 March 2017, CEH, Using: EDINA Environment Digimap Service, https://digimap.edina.ac.uk. Downloaded: 2018-09-08 22:15:08.665

Land Cover Map 2015 [FileGeoDatabase geospatial data], Scale 1:2500, Tiles: GB, Updated: 26 May 2017, CEH, Using: EDINA Environment Digimap Service, https://digimap.edina.ac.uk. Downloaded: 2018-09-08 22:15:08.671

National River Flow Archive, https://nrfa.ceh.ac.uk/data/station/info/51002 (data downloaded on 24th September 2018)

Rowland, C.S., Morton, R.D., Carrasco, L., McShane, G., O'Neil, A.W., Wood, C.M. (2017) Land Cover Map 2015 (vector, GB). NERC Environmental Information Data Centre. DOI: https://doi.org/10.5285/60764028-adeb-4316-987a-14b3b21a8f9a

Rowland, C.S., Morton, R.D., Carrasco, L., McShane, G., O'Neil, A.W., Wood, C.M. (2017) Land Cover Map 2015 (25m raster, GB). NERC Environmental Information Data Centre. DOI: https://doi.org/10.5285/bb15e200-9349-403c-bda9-b430093807c7

Soil Parent Material Model [SHAPE geospatial data], Scale 1:50000, Tiles: ew277,ew278,eew293,ew294, Updated: 1 June 2011, BGS, Using: EDINA Geology Digimap Service, http://digimap.edina.ac.uk, Downloaded: 2016-03-19 14:21:11.431

DiGMapGB-50 [SHAPE geospatial data], Scale 1:50000, Tiles: ew277,ew278,ew293,ew294, Updated: 1 October 2013, BGS, Using: EDINA Geology Digimap Service, http://digimap.edina.ac.uk, Downloaded: 2016-03-21 10:02:27.135

The digital soil map of the world, food and agriculture organization of the United Nations, version 3.6, completed January 2003, ©FAO/UNESCO, 1995. All rights reserved worldwide. Source: Land and Water Development Division, FAO, Rome.

Reports

Boehner, J., Koethe, R., Conrad, O., Gross, J., Ringeler, A., & Selige, T. (2002). *Soil Regionalisation by Means of Terrain Analysis and Process Parameterisation*. Status and Prospect of Soil Information in South - Eastern Europe: Soil Databases, Projects and Applications. 1–4. https://doi.org/ISBN : 978-92-79-04972-9

Food and Agriculture Organization of the United Nations (FAO). *The State of the World's Landand Water Resources for Food and Agriculture (SOLAW)—Managing Systems at Risk*; Earthscan: New York, NY, UK, 2011.

IPCC, 2013: *Climate Change 2013: The Physical Science Basis. Contribution of Working Group I to the Fifth Assessment Report of the Intergovernmental Panel on Climate Change*

[Stocker, T.F., D. Qin, G.-K. Plattner, M. Tignor, S.K. Allen, J. Boschung, A. Nauels, Y. Xia, V. Bex and P.M. Midgley (eds.)]. Cambridge University Press, Cambridge, United Kingdom and New York, NY, USA, 1535 pp.

Mabit, F. (2014) *Guidelines for Using Fallout Radionuclides to Assess Erosion and Effectiveness of Soil Conservation Strategies*. IAEA-TECDOC-1741.Vienna: IAEA. p. 14-56.

Miller, G.R., Miles, J. (1984) *Moorland Management: A study of Exmoor*, Natural Environment Research Council (NERC), 68 Hills Road, Cambridge, United Kingdom.

Porto, P., & Walling, D. E. (2014). Using ^{137}Cs and ^{210}Pb$_{ex}$ measurements to document erosion rates for different time windows in a small catchment in southern Italy, *Hydrology in a Changing World: Environmental and Human Dimensions*, Proceedings of FRIEND-Water 2014, Montpellier, France, October 2014 (IAHS Publ. 363, 2014). 297–302.

Renard, K.G., et al. (1997) Predicting Soil Erosion by Water: A Guide to Conservation Planning with the Revised Universal Soil Loss Equation (RUSLE) (Agricultural Handbook 703). US Department of Agriculture, Washington, DC, 404.

Walling, D., Zhang, Y., He, Q. (2014) *Conversion models and related software. Guidelines for Using Fallout Radionuclides to Assess Erosion and Effectiveness of Soil Conservation Strategies.* IAEA-TECDOC-1741. Vienna: IAEA. p. 125-148.

Walling, D.E., Zhang, Y., He, Q. (2008) *Models for Converting Measurements of Environmental Radionuclide Inventories (^{137}Cs, excess ^{210}Pb and ^{7}Be) to Estimates of Soil Erosion and Deposition Rates*. School of Geography, University of Exeter, UK.

Wischmeier, W.H., Smith, D.D., 1978. Predicting Rainfall Erosion Losses. Agric. Hbk 537. U.S.D.A.-Sci. and Educ. Admin., Washington, DC.

Waste Development Plan Documents, Strategic Flood Risk Assessment, Devon City Council, Minerals and Waste Development Framework, October 2011.